Mathematical Modeling and Simulation of Water-Alternating-Gas (WAG) Injection

By

©Shokufe Afzali

A thesis submitted to the school of Graduate Studies in partial fulfilment of the requirements for the degree of

Doctor of Philosophy

Faculty of Engineering and Applied Science

Memorial University of Newfoundland

May 2021

St. John’s, Newfoundland and Labrador

Canada

ABSTRACT

Water-alternating-gas (WAG) injection is a relatively mature oil recovery technique in hydrocarbon reservoirs that has attracted the interest of the oil and gas industry due to its successful performance. The main goal of a WAG process is to control the mobility and to decrease the problem of viscous fingering, leading to improved oil recovery by combining the benefits of gas injection (GI) and waterflooding (WF). Mathematical modeling and simulation of three-phase flow in porous media involve complexities related to the three-phase relative permeability, capillary pressure, and hysteresis effects that are cycle-dependent. Extensive theoretical studies are available in the literature, simulating immiscible and miscible WAG processes; however, the simulation study on near-miscible WAG is overlooked. Also, the majority of WAG simulation studies lack the cycle-dependent three-phase hysteresis that appears in the relative permeability and capillary pressure models. Production from naturally fractured reservoirs (NFRs) is more complicated (compared to homogeneous reservoirs) due to the flow communication between the matrix and fracture in fractured porous media. The implementation of water-alternating-gas (WAG) injection in NFRs also features inherent complexities related to the three-phase flow, the saturation history, and cycle-dependent hysteresis of the individual phases. Moreover, the experimental evaluation of WAG injection in a fractured system is expensive and time-consuming, if not impractical.

In this research work, the three-phase flow modeling of near-miscible WAG process for enhanced oil recovery (EOR) implication is studied, using implicit pressure explicit saturation (IMPES) method. The mathematical model simulates a WAG case study in a strongly water-wet Berea core, using synthetic oil and brine at 38 ˚C and 12.7 MPa. The recovery data from the mathematical model is in excellent agreement with the experimental data of near-miscible WAG process. For instance, the absolute relative error is less than 1.7% while estimating the ultimate recovery factor of the oil in WF and GI stages of all three cycles. The effects of main variables such as injection rate, WAG ratio, slug size (PV) injection, crude oil viscosity, and core absolute permeability on the WAG performance are also studied. The findings from this study can help for better understanding of WAG injection at near-miscible condition for various scenarios under various conditions in terms of operational condition and rock and fluid's characteristics.

This work is also intended to simulate WAG injection in a fractured system through a computational fluid dynamics (CFD) approach. We evaluate the impacts of hysteresis, fracture characteristics (aperture, orientation, and fracture density in the network), and the three-phase

relative permeability of phases during the WAG injection using COMSOL Multiphysics®. The model simulates an immiscible WAG injection, and the modeling results are compared to the experimental data in a strong water-wet sand-pack. Similar to the experiments, we simulate Maroon crude as the oil phase, synthetic brine, and pure CO_2 at 100 ^oC and atmospheric pressure. The results from our model are in excellent agreement with the experimental data. The absolute relative error is less than 12 % while predicting the ultimate recovery factors (*RF*) of the oil in water flooding (WF) and gas injection (GI) cycles. Including three-phase hysteresis significantly increases the accuracy of a WAG process simulation. Excluding the hysteresis remarkably decreases the instantaneous *RFs* at each cycle (especially GI cycles) and also the ultimate *RF* by 4%. The simulation results can help to manage and design the optimum operation of immiscible WAG in fractured reservoirs. In the fourth phase of the work, a total number of 1457 data points to predict three sets of two-phase relative permeabilities involved in the WAG injection process, and in a strongly water-wet sandstone core where smart tools such as least squares-support vector machine (LSSVM) and adaptive network-based fuzzy inference system (ANFIS) are employed. The statistical parameters including coefficient of determination, root mean square error, mean error, and standard deviation are used to examine the predictive models. The LSSVM shows a better performance compared to ANFIS in estimating relative permeabilities. The analysis based on relative importance of parameters shows that for the LSSVM model, water saturation is the most influencing input for gas-water and oil-water systems, while gas saturation is the most important input parameter in the gas-oil system. Final RF of WAG process after three cycles of water-and gas injection is 93.6%.

Forecasting WAG flooding performance using fast and robust models is of great importance to obtain a better understanding of the process future, optimize the operational design procedure, and avoid high-cost blind tests in laboratory or pilot scales. In the last phase of this work, a novel correlation to predict the performance of near-miscible WAG injection is presented in strongly water-wet sandstones. An analytical correlation using gene expression programming (GEP) technique is developed. Dimensional analysis technique is applied and generated dimensionless numbers using eight key parameters with the aid of the Buckingham's π theorem. Based on the error analysis, the newly developed GEP-based correlation leads to the predictions, which are in a good match with the target data so that R^2= 92.85 % and *MSE*=1.38e-3 are obtained for the training phase; and the testing phase results in R^2= 91.93 % and *MSE*=4.30e-3. The correlation proposed

in this phase can be used to forecast the RF of a WAG injection process before committing to expensive and time-consuming laboratory and pilot tests.

ACKNOWLEDGMENTS

I would like to express my sincere gratitude and appreciation to my supervisor, Dr. Sohrab Zendehboudi, for his continued support and guidance as I undertook this study. Without your support, continuous engagement, and prompt and thoughtful feedback, this dissertation would not be completed.

I owe endless thanks to Dr. Nima Rezaei, thank you for your tireless support, mentorship, and expertise. I learnt a lot from you.

I would also like to thank my friends for providing me with their experience and unfailing and continuous support throughout my years of study: Ali Ghamartale, Dr. Hamideh Hamedi, Dr. Mohammad Mohammadi-Baghmolaei, and Dr. Omid Mohammadzadeh. Finally, I would like to express my profound gratitude to my family (especially to my sister Azi, who lived a year with a ghost (me!)) for all their endless love and support and continuous encouragements through all these years.

"This dissertation is dedicated to my mother who I am grateful for being her daughter every single day of my life"

TABLE OF CONTENTS:

LIST OF TABLES

LIST OF FIGURES

CHAPTER ONE

Introduction and Overview

Water-Alternating-Gas (WAG) injection is a relatively mature oil recovery technique in hydrocarbon reservoirs that has attracted the interest of oil and gas industry due to its successful performance. Currently, WAG injection is recognized as a common technology to enhance the total oil recovery through re-injection of produced gas in water injection wells in mature petroleum fields [1]. The main goal of the WAG projects is to control the mobility and to decrease the problem of viscous fingering, leading to improved oil recovery by combining the benefits of gas injection (GI) and waterflooding (WF). Initially, WAG injection as an enhanced oil recovery (EOR) technique was introduced to enhance the macroscopic sweep efficiency in gas injection processes [2]. This technique was firstly implemented in 1957 in Alberta, Canada in a sandstone reservoir by Mobil as a combination of two conventional approaches; namely, gas injection and water flooding [3-4]. Due to the low gas viscosity and considerable density difference between gas and reservoir crude oil, gas injection processes exhibit poor microscopic sweep efficiency which results in bypassing of a part of oil, fluids front instability, viscous fingering, and early breakthrough in the swept zone/area of a reservoir [1-2, 5]. In the case of alternating injection of water after gas, water (because of its higher density) will sweep the bottom part of the reservoir and stabilize the displacing front through creating a more favorable mobility ratio [6]. This technique is also profitable in terms of economic prospective by lowering the gas volume required to be injected into the reservoir [7]. It was reported that 80 % of USA WAG field projects were fruitful[8]. Skauge et al. reviewed 59 WAG fields. Their study revealed that the average oil recovery increases by 5 % to 10 % originally oil in place (OOIP) for all WAG cases [9]. WAG processes have been successfully applied (mostly by down dip injection) in the North Sea fields such as: Gullfaks, Stafjord, South Brae, Snorre, and Oseberg Ost [10]. Weak performance of WAG in some projects can be related to inappropriate WAG parameters such as the number of cycles, volume of each cycle, and the injection rates of the gas and water phases. Hence, WAG optimization is a proper scheme to control the gas mobility to increase the oil recovery [11-12]. These optimal parameters can vary with the reservoir rock and fluids characteristics [13]. The optimal design of WAG process needs strategic planning, which includes a milestone for the equipment installation, maintenance, and operation activities over the life of project.

According to the 2020 oil and gas resource assessment results of the Newfoundland and Labrador (NL), an addition of 11.1 billion barrels of oil and 24.5 trillion cubic feet of gas potential were identified in offshore NL. In total, reports show the combined resource potential of 63.6 billion barrels of oil and 224.1 trillion cubic feet of gas in only 10 % of the NL offshore [14]. The oil and gas industry plays an important role in growth and development of Newfoundland and Labrador's economy. For instance, from 2010-2017, the total (direct, indirect, and induced) economic benefits related to the oil and gas

industry in NL accounted for approximately 30 % of the province gross domestic product (GDP), 13 % of labour compensation, and 10 % of all employment [14]. Therefore, the application of reliable, efficient, and low-cost techniques for producing the hydrocarbon benefits the province in various ways. WAG injection is a great candidate to be applied in NL field which has been proved to be successful in several similar fields; in addition, this recovery technique can use the available resources (ocean water) and CO_2, resulting in low capital costs.

Modeling and simulations of the WAG process have been investigated in the literature by studying variables such as WAG ratio, the number of WAG injection cycles [15-22], wettability [20, 23-25], and relative permeability and hysteresis [17, 20, 22-23, 25-32]. The main difficulties in the modeling and optimizing of a WAG process are to find realistic correlations between rock/fluid properties and the amount of residual phases in the reservoir [33]. The cyclic nature of the WAG process and the mobility of the three-phase flow in porous media add to the complexity of modeling of three-phase flow in porous media. There are considerable research investigations in the literature with a focus on the analytical solution of the three-phase flow and three-phase relative permeability during WAG flooding [34-35].

Despite the worldwide applications of the WAG injection process in the fields [4], researchers still need to obtain comprehensive knowledge of the underlying mechanisms of this recovery technique. One of the overlooked aspects is the near-miscible-gas WAG condition. The near-miscible-gas injection relates to a process where the injected gas is close to the complete miscibility state [36]. The near-miscible gas injection processes seem interesting from both operational and economic perspectives. In the case of high oil-gas interfacial tension (IFT) (immiscible), in spite of the connectivity of the oil to the main flow of the system, if there are no other driving forces such as gravity forces, the recovery achieved by the film flow is very small. On the other hand, during the miscible GI, there is no interface between the gas and oil. Thus, the flow is similar to the single-phase condition where the oil is recovered through molecular diffusion and dispersion mechanisms [36]. Sohrabi et al. [36] conducted a series of pore-scale micromodel WAG experiments under the near-miscible condition. A substantial portion of the oil in micromodel that had been completely saturated with oil was recovered during low-IFT gas flooding. Some of the oil was bypassed by the main gas front. The recovery of the by-passed oil bank was continued behind the main gas front, and almost complete oil recovery was attained due to near-miscible gas injection.

It has been claimed in some studies that WAG injection is not beneficial to be implemented in natural fractured reservoirs (NFRs) [37]. However, there are some successful examples of the application of the WAG injection in fractured reservoirs [4, 10, 38-39]. Reservoir heterogeneity is among vital parameters that

strongly affects the WAG efficiency. Many failed EOR projects (in general) have been resulted from the reservoir heterogeneity or the lack of understanding of the reservoirs' general structure [40]. In highly fractured or stratified reservoirs, the operation of GI is not economical due to high recycle rate and early breakthrough of the injected gas [7]. In some NFRs, during a WAG process, water and gas displace each other and bypass the trapped oil in the matrix media. Therefore, the use of appropriate relative permeability and capillary pressure correlations significantly affects predictions of fluid flow between matrix and facture in a porous medium [41]. Although WAG injection in fractured reservoirs in field, pilot, or lab scale might be difficult and not economical, it would be helpful to investigate important aspects (transport phenomena and thermodynamics behaviors) of WAG in fractured media for better practical implementation. There are a few studies on mathematical modeling or simulation of this EOR process in heterogeneous porous systems.

Smart tools such as artificial neural network (ANN) models enable us to predict the target parameters with high accuracy, though there are non-linear, and multidimensional relationships between input parameters. However, the application of smart models in petroleum industry particularly in EOR processes is still in its infancy. There are not also adequate number of research works about dimensional analysis of WAG processes in the open sources.

Most of the WAG injection research studies in the literature are the experimental and/or modeling investigations with some limitations in terms of dimensions and process conditions where the porous media are homogeneous. WAG flooding in heterogeneous/fractured reservoirs is a common process, while has been overlooked in available research works. Most of the studies on this subject are experimental runs which have been conducted at environment condition; and no mathematical model under reservoir conditions has been provided so far. Among investigations in heterogeneous/fractured systems, there are limited research studies in the literature of WAG injection with focus on empirical and pore-network modeling. Also, there are a few research studies in the open sources that discuss about the important aspects such as the effect of gravity and capillary forces in the matrix-fracture transfer system [41], WAG injection in systems with different fracture patterns at various fracture intensities and with the effect of shape factor [43], upscaling the flow model from fine scale single porosity to dual porosity for a WAG injection process [19], WAG injection in a micromodel system with fracture elements [44], and the effects of non-wetting phase trapping and the miscible and immiscible WAG injection in a heterogeneous reservoir[23].

Three-phase relative permeability data are necessary to model the distribution and transport of oil, water, and gas in porous media [45]. Obtaining two-phase relative permeability data is more straightforward than those of the three-phase, as the lower number of phases decreases the available saturation paths. However, a three-phase flow system has infinite number of saturation paths that makes it difficult to estimate the three-phase relative permeability values. Hence, the evaluation of the three-phase relative permeability data has been the subject of numerous studies [42]. Two of the most known smart tools, namely LSSVM and ANFIS can be applied for predicting the two-phase relative permeability data. These models have been employed in oil and gas industry for different purposes such as the application of LSSVM for predicting natural gas viscosity [46], the effect of temperature on two-phase oil-water relative permeability data [47], phase equilibrium conditions of clathrate hydrate, modelling freezing point depression of electrolyte solutions, calculating minimum miscibility pressure for CO_2-oil systems, and estimating dew point pressure for a gas condensate system [48-50].

Despite the extensive success of WAG flooding technique, the process has not been well-developed. One of the overlooked areas of studying this process is the development of predictive tools prior to establishing full field operation and running pilot tests [51]. The gene expression programming (GEP) mathematical approach was introduced to overcome some application limitations involved with the GA and GP algorithms [52]. Generally, GEP as an extended and modified form of the GP method [53], performs an algorithm to obtain a solution for regression problems. GEP method has been extensively used in various fields of oil and gas engineering including: estimating mixture viscosity in solvent-assisted oil recovery process [54], CO_2 solubility in crude oil [55], minimum miscibility pressure (MMP) of live oil systems [56], petroleum emulsions' viscosity [57], surfactant retention in porous media [58], residual gas saturation during spontaneous and forced imbibition processes [59], and oil price [60]. However, the application of this technique has not been reported in the literature for forecasting the oil recovery of near miscible-WAG injection process.

The main contributions/phases of this research project are given below:

- In the review section, the effects of important variables on WAG performance (fluid properties, reservoir properties and operating conditions) are extensively studied and summarized.
- The pore-scale and field scale implementations are studied, and important technical challenges are given.
- A dynamic three-phase flow mathematical model (IMPES) of near-miscible water-alternating-gas (WAG) injection process with enhanced oil recovery application is developed.

- The recovery data from our mathematical model is in excellent agreement with the experimental data of near-miscible WAG process.
- The effects of various variables such as WAG ratio and injection rate on the WAG performance are studied.
- A simulation of immiscible water-alternating-gas (WAG) injection into porous media with fractures, using CO_2 as the gas phase; the model is implemented in COMSOL Multiphysics®.
- The impact of including hysteresis effects in the model is discussed and it was found that the hysteresis effects are mostly due to the gas trapping in the larger pores (such as fractures).
- Different parameters such as core alignment, fracture aperture, permeability contrast between fracture and matrix, and fracture inclination during WAG injection process are also examined.
- We use a total number of 1,457 training data points to develop three sets of two-phase relative permeability data using the LSSVM-CSA and ANFIS models that are applied in the WAG injection processes.
- Among the proposed hybrid models, the LSSVM-EM-FPM model significantly removes the non-linearity of the two-phase relative permeabilities.
- We develop an accurate correlation for predicting the WAG RF with the aid of gene expression programming (GEP) technique and the Buckingham's π theorem where all terms in the correlation are dimensionless.
- According to the error analysis, the newly developed GEP-based correlation is able to generate the target values with high precision. For instance, R^2= 92.85 % and *MSE*=1.38e-3 are obtained for the training phase, and R^2= 91.93 % and *MSE*=4.30e-3 are attained for the testing phase.

This thesis consists of a series of manuscripts either published or under review for publication, as listed below:

Chapter two has been published in the Journal of Fuel. The manuscript provides a systematic literature review on the conducted WAG injection processes at different scales. The review briefly discusses various aspects of WAG injection process including: active mechanisms during WAG injection, and WAG variations. The effects of petrophysical properties on WAG, such as reservoir heterogeneity and stratification, relative permeability and hysteresis, and wettability are studied. We also investigate the effects of fluid properties, such as type of the injected gas, brine salinity, and fluids miscibility on the recovery performance. The impacts of operational conditions on the WAG performance are explored. The literature review phase also covers the field and pilot applications, simulation/ modeling and

optimization of WAG processes, research challenges and problems, and economical and practical challenges involved during implication of a WAG process.

Chapter three has been published in the Journal of Fuel. In this chapter, we study the three-phase flow modeling of near-miscible WAG process for EOR implication, using implicit pressure explicit saturation (IMPES) method. The mathematical model simulates a WAG case study in a strongly water-wet Berea core, using synthetic oil and brine at 38 ˚C and 12.7 MPa. Three cycles of water and gas injections are used in the WAG operation. The recovery data from our mathematical model is in excellent agreement with the experimental data of near-miscible WAG process. The absolute relative error is less than 1.7% while estimating the ultimate recovery factor of the oil in WF and GI stages of all three cycles. We also study the effects of main variables such as injection rate, WAG ratio, slug size (PV) injection, crude oil viscosity, and core absolute permeability on the WAG performance.

Chapter four is submitted (under review) to the Journal of Hydrology. This chapter provides details on the CFD simulation of WAG injection in a fractured system. We evaluate the impacts of hysteresis, fracture characteristics (aperture, orientation, and fracture density in the network), and the three-phase relative permeability of phases during the WAG injection using a computational fluid dynamic (CFD) modeling approach. The model simulates an immiscible WAG injection, and the modeling results are compared to the experimental data in a strong water-wet sand-pack at 100^{o}C and atmospheric pressure. Chapter five has been presented in the 70th Canadian Society of Chemical Engineering Conference (CSChE) and also submitted to the Journal of Natural Gas Science and Engineering. In this chapter, a hybrid mathematical model is proposed for the near-immiscible WAG process. We use data-driven sub-models, including least square support vector machine (LSSVM) and adaptive neuro-fuzzy inference system (ANFIS) in series with an empirical model (EM) and a first principle model (FPM) to study three-phase flow in porous media. The LSSVM and ANFIS sub-models predict the two-phase water-oil, gas-oil, and gas-water relative permeabilities. The outputs from these models are supplied to the empirical models (EMs) to estimate the three-phase relative permeabilities for oil, gas, and water phases. We examine the accuracy of oil recovery estimates from each model and compare it with experimental data for a WAG injection process involving three water- and gas-injection cycles.

Chapter six has been submitted to the Natural Resources Research Journal. In this chapter, we develop a new correlation using gene expression programming (GEP) technique. We use dimensional analysis technique and generated dimensionless numbers using eight key parameters with the aid of the Buckingham's π theorem. Seven dimensionless numbers are generated and employed as the input

variables of the desired correlation for predicting the recovery factor of a near-miscible WAG injection. A statistical error analysis is conducted and some graphical illustrations are provided to evaluate the efficiency of the proposed model. Based on the statistical measures, the developed model is in a good match with the target RF values. In this chapter, we also determine the relative importance of each input variable to the newly developed model. A sensitivity analysis on the capillary number and viscosity ratio (as input variables) is also performed.

Chapter seven contains a summary, conclusions, and recommendations for future work.

References

1. Hustad, O. S.; Holt, T. In Gravity stable displacement of oil by hydrocarbon gas after waterflooding, *SPE/DOE Enhanced Oil Recovery Symposium, Society of Petroleum Engineers*: **1992**.

2. Touray, S., Effect of water alternating gas injection on ultimate oil recovery. *Master thesis, Dalhousie University*. **2013**.

3. Surguchev, L.; Korbol, R.; Haugen, S.; Krakstad, O. In Screening of WAG injection strategies for heterogeneous reservoirs, *European Petroleum Conference, Society of Petroleum Engineers* **1992**.

4. Christensen, J. R.; Stenby, E. H.; Skauge, A. In Review of WAG field experience, *International petroleum conference and exhibition of Mexico, Society of Petroleum Engineers*: **1998**.

5. Shpak, R. Modeling of Miscible WAG Injection Using Real Geological Field Data. *Institutt for petroleumsteknologi og anvendt geofysikk*, **2013**.

6. Knappskog, O. A. Evaluation of WAG injection at Ekofisk. *University of Stavanger, Norway*, **2012**.

7. Pariani, G.; McColloch, K.; Warden, S.; Edens, D., An approach to optimize economics in a West Texas CO_2 flood. *Journal of Petroleum Technology* **1992,** *44* (09), 984-1,025.

8. Sanchez, N. L. In Management of water alternating gas (WAG) injection projects, *Latin American and Caribbean petroleum engineering conference, Society of Petroleum Engineers*: **1999**.

9. Skauge, A.; Stensen, J. Å. In Review of WAG field experience, *1st International Conference and Exhibition, Modern Challenges in Oil Recovery*, **2003**; pp 19-23.

10. Awan, A. R.; Teigland, R.; Kleppe, J., A survey of North Sea enhanced-oil-recovery projects initiated during the years 1975 to 2005. *SPE Reservoir Evaluation & Engineering* **2008,** *11* (03), 497-512.

11. Bahagio, D., Ensemble Optimization of CO_2 WAG EOR. **2013**.

12. Chen, S.; Li, H.; Yang, D.; Tontiwachwuthikul, P., Optimal parametric design for water-alternating-gas (WAG) process in a CO2-miscible flooding reservoir. *Journal of Canadian petroleum technology* **2010,** *49* (10), 75-82.

13. Rogers, J. D.; Grigg, R. B., A literature analysis of the WAG injectivity abnormalities in the CO_2 process. *SPE Reservoir Evaluation & Engineering* **2001,** *4* (05), 375-386.

14. Findings of the 2020 Independent Resource Assessment Released, N. a. L., https://www.gov.nl.ca/releases/2020/iet/0929n02/. **2020**.

15. Al-Mamari, F.; Al-Shuraiqi, H.; Al-Wahaibi, Y. M. In Numerical simulation and experimental studies of oil recovery via first-contact miscible water alternating gas injection within shaley porous media, *SPE/EAGE Reservoir Characterization and Simulation Conference, Society of Petroleum Engineers* **2007**.

16. Bequette, B. W., Nonlinear control of chemical processes: A review. *Industrial & Engineering Chemistry Research* **1991,** *30* (7), 1391-1413.

17. Duchenne, S.; de Loubens, R.; Petitfrere, M.; Joubert, T. In Modeling and simultaneous history-matching of multiple WAG coreflood experiments at reservoir conditions, *Abu Dhabi international petroleum exhibition and conference, Society of Petroleum Engineers*: **2015**.

18. Haajizadeh, M.; Narayanan, R.; Waldren, D. In Modeling miscible WAG injection EOR in the Magnus field, *SPE reservoir simulation symposium, Society of Petroleum Engineers*: **2001**.

19. Heeremans, J. C.; Esmaiel, T. E.; Van Kruijsdijk, C. P. In Feasibility study of WAG injection in naturally fractured reservoirs, *SPE/DOE symposium on improved oil recovery, Society of Petroleum Engineers*: **2006**.

20. Larsen, J. A.; Skauge, A. In Simulation of the immiscible WAG process using cycle-dependent three-phase relative permeabilities, *SPE Annual Technical Conference and Exhibition, Society of Petroleum Engineers*: **1999**.

21. Rahmawati, S. D.; Whitson, C. H.; Foss, B., A mixed-integer non-linear problem formulation for miscible WAG injection. *Journal of Petroleum Science and Engineering* **2013,** *109*, 164-176.

22. Zuo, L.; Chen, Y.; Dengen, Z.; Kamath, J., Three-phase relative permeability modeling in the simulation of WAG injection. *SPE Reservoir Evaluation & Engineering* **2014,** *17* (03), 326-339.

23. Agada, S.; Geiger, S. In Wettability, trapping and fracture-matrix interaction during WAG injection in fractured carbonate reservoirs, *SPE Improved Oil Recovery Symposium, Society of Petroleum Engineers*: **2014**.

24. Agada, S.; Geiger, S.; Elsheikh, A.; Oladyshkin, S., Data-driven surrogates for rapid simulation and optimization of WAG injection in fractured carbonate reservoirs. *Petroleum Geoscience* **2017,** *23* (2), 270-283.

25. Kløv, T.; Øren, P.; Stensen, J.; Lerdahl, T.; Berge, L.; Bakke, S.; Boassen, T.; Virnovsky, G. In Pore-to-field scale modeling of WAG, *SPE Annual Technical Conference and Exhibition, Society of Petroleum Engineers* **2003**.

26. Egermann, P.; Vizika, O.; Dallet, L.; Requin, C.; Sonier, F. In Hysteresis in three-phase flow: experiments, modeling and reservoir simulations, *SPE European petroleum conference, Society of Petroleum Engineers* **2000**.

27. Hustad, O. S.; Browning, D. J. In A fully coupled three-phase model for capillary pressure and relative permeability for implicit compositional reservoir simulation, *SPE/EAGE Reservoir Characterization & Simulation Conference*, **2009**.

28. Jerauld, G., General three-phase relative permeability model for Prudhoe Bay. *SPE reservoir Engineering* **1997,** *12* (04), 255-263.

29. Larsen, J.; Skauge, A., Methodology for numerical simulation with cycle-dependent relative permeabilities. *SPE Journal* **1998,** *3* (02), 163-173.

30. Shahverdi, H.; Sohrabi, M., An improved three-phase relative permeability and hysteresis model for the simulation of a water-alternating-gas injection. *Spe Journal* **2013,** *18* (05), 841-850.

31. Sherafati, M.; Jessen, K. In Modeling and simulation of WAG injection processes-the role of counter-current flow, *SPE Western Regional Meeting, Society of Petroleum Engineers* **2015**.

32. Skauge, A.; Dale, E. I. In Progress in immiscible WAG modelling, *SPE/EAGE Reservoir Characterization and Simulation Conference, Society of Petroleum Engineers* **2007**.

33. Skauge, A.; Dale, E. In Fluid Flow Properties of WAG Injection Processes, *IOR 2005-13th European Symposium on Improved Oil Recovery*, **2005**.

34. Juanes, R.; Patzek, T. W., Analytical solution to the Riemann problem of three-phase flow in porous media. *Transport in Porous Media* **2004,** *55* (1), 47-70.

35. Stone, H., Probability model for estimating three-phase relative permeability. *Journal of Petroleum Technology* **1970,** *22* (02), 214-218.

36. Sohrabi, M.; Danesh, A.; Tehrani, D. H.; Jamiolahmady, M., Microscopic mechanisms of oil recovery by near-miscible gas injection. *Transport in Porous Media* **2008,** *72* (3), 351-367.

37. Haghighat, S. WAG Modeling in Fractured Reservoirs. *Thesis Report MTA/PW/04-15 TU Delft* **2004**.

38. Afzali, S.; Rezaei, N.; Zendehboudi, S., A comprehensive review on enhanced oil recovery by water alternating gas (WAG) injection. *Fuel* **2018,** *227*, 218-246.

39. Brodie, J. A.; Jhaveri, B. S.; Moulds, T. P.; Mellemstrand Hetland, S. In Review of gas injection projects in BP, *SPE Improved Oil Recovery Symposium, Society of Petroleum Engineers* **2012**.

40. Donaldson, E. C.; Chilingarian, G. V.; Yen, T. F., Enhanced oil recovery, II: Processes and operations. *Elsevier* **1989**.

41. Elfeel, M. A.; Al-Dhahli, A.; Geiger, S.; van Dijke, M. I., Fracture-matrix interactions during immiscible three-phase flow. *Journal of Petroleum Science and Engineering* **2016,** *143*, 171-186.

42. Corey, A. T.; Rathjens, C.; Henderson, J.; Wyllie, M., Three-phase relative permeability. *Journal of Petroleum Technology* **1956,** *8* (11), 63-65.

43. Al Eidan, A. A.; Mamora, D. D.; Schechter, D. S. In Experimental and Numerical Simulation Studies of Different Modes of CO2 Injection in Fractured Carbonate Cores, S*PE Enhanced Oil Recovery Conference, Society of Petroleum Engineers* **2011**.

44. Dehghan, A.; Ghorbanizadeh, S.; Ayatollahi, S., Investigating the fracture network effects on sweep efficiency during WAG injection process. *Transport in porous media* **2012,** *93* (3), 577-595.

45. Aziz, K.; Settari, A., Petroleum reservoir simulation: Applied science publ. *Ltd., London* **1979**.

46. Fayazi, A.; Arabloo, M.; Shokrollahi, A.; Zargari, M. H.; Ghazanfari, M. H., State-of-the-art least square support vector machine application for accurate determination of natural gas viscosity. *Industrial & Engineering Chemistry Research* **2014,** *53* (2), 945-958.

47. Esmaeili, S.; Sarma, H.; Harding, T.; Maini, B., A data-driven model for predicting the effect of temperature on oil-water relative permeability. *Fuel* **2019,** *236*, 264-277.

48. Shokrollahi, A.; Arabloo, M.; Gharagheizi, F.; Mohammadi, A. H., Intelligent model for prediction of CO2–reservoir oil minimum miscibility pressure. *Fuel* **2013,** *112*, 375-384.

49. Sinehbaghizadeh, S.; Roosta, A.; Rezaei, N.; Ghiasi, M. M.; Javanmardi, J.; Zendehboudi, S., Evaluation of phase equilibrium conditions of clathrate hydrates using connectionist modeling strategies. *Fuel* **2019,** *255*, 115649.

50. Yarveicy, H.; Moghaddam, A. K.; Ghiasi, M. M., Practical use of statistical learning theory for modeling freezing point depression of electrolyte solutions: LSSVM model. *Journal of Natural Gas Science and Engineering* **2014,** *20*, 414-421.

51. Belazreg, L.; Mahmood, S. M., Water alternating gas incremental recovery factor prediction and WAG pilot lessons learned. *Journal of Petroleum Exploration and Production Technology* **2020,** *10* (2), 249-269.

52. Ferreira, C., Gene expression programming: a new adaptive algorithm for solving problems. *arXiv preprint cs/0102027* **2001**.

53. Koza, J. R.; Koza, J. R., Genetic programming: on the programming of computers by means of natural selection. *MIT press* **1992**; Vol. 1.

54. Rostami, A.; Hemmati-Sarapardeh, A.; Mohammadi, A. H., Estimating n-tetradecane/bitumen mixture viscosity in solvent-assisted oil recovery process using gep and gmdh modeling approaches. *Petroleum Science and Technology* **2019,** *37* (14), 1640-1647.

55. Rostami, A.; Arabloo, M.; Kamari, A.; Mohammadi, A. H., Modeling of CO2 solubility in crude oil during carbon dioxide enhanced oil recovery using gene expression programming. *Fuel* **2017,** *210*, 768-782.

56. Kamari, A.; Arabloo, M.; Shokrollahi, A.; Gharagheizi, F.; Mohammadi, A. H., Rapid method to estimate the minimum miscibility pressure (MMP) in live reservoir oil systems during CO2 flooding. *Fuel* **2015,** *153*, 310-319.

57. Umar, A. A.; Saaid, I. M.; Sulaimon, A. A.; Pilus, R. M., Predicting the Viscosity of Petroleum Emulsions Using Gene Expression Programming (GEP) and Response Surface Methodology (RSM). *Journal of Applied Mathematics* **2020,** *2020*.

58. Kamari, A.; Sattari, M.; Mohammadi, A. H.; Ramjugernath, D., Reliable method for the determination of surfactant retention in porous media during chemical flooding oil recovery. *Fuel* **2015,** *158*, 122-128.

59. Rostami, A.; Raef, A.; Kamari, A.; Totten, M. W.; Abdelwahhab, M.; Panacharoensawad, E., Rigorous framework determining residual gas saturations during spontaneous and forced imbibition using gene expression programming. *Journal of Natural Gas Science and Engineering* **2020,** *84*, 103644.

60. Mostafa, M. M.; El-Masry, A. A., Oil price forecasting using gene expression programming and artificial neural networks. *Economic Modelling* **2016,** *54*, 40-53.

CHAPTER TWO

Literature Review (A Comprehensive Review on Enhanced Oil Recovery by Water Alternating Gas (WAG) injection, (Published)

Preface

A version of this manuscript has been published in the Journal of Fuel 227 (2018): 218-246. I am the primary author of this paper. Along with the co-authors, Nima Rezaei, Sohrab Zendehboudi, I carried out most of the literature review, data collection, and discussions on experimental and modeling studies on WAG process. I prepared the first draft of the manuscript and subsequently revised the manuscript based on the co-authors' feedback as well as the comments received from the peer review process. The co-author, Nima Rezaei, helped in reviewing, revising, criticizing the technical points of the manuscript. The co-author, Sohrab Zendehboudi, contributed through providing the manuscript's outlines, comments on various parts of the manuscript, and technical points/critiques on previous works in the related field. Sohrab Zendehboudi also assisted in reviewing and revising the manuscript.

ABSTRACT

Water-Alternating-Gas (WAG) injection is a relatively mature oil recovery technique in hydrocarbon reservoirs that has long attracted the interest of oil and gas industry due to its successful performance. The main goal of the WAG projects is to control the mobility and to decrease the problem of viscous fingering, leading to improved oil recovery by combining the benefits of gas injection (GI) and waterflooding (WF). Implementation of a new EOR/IOR project requires a comprehensive knowledge of previous successful and failed experiences, and adequate understanding of the technical and non-technical aspects of this recovery process. This knowledge may be derived from reviewing similar projects that were reported in the literature. Despite great applications of WAG injection in hydrocarbon reservoirs and extensive studies, the last comprehensive review goes back to 1998, focusing on the field applications only. There are a few review papers that are more updated; however, they are either dedicated to a particular aspect of WAG (such as CO_2 abnormalities), or applications in a specific geographical region (such as North Sea). An updated comprehensive study, covering recent experiences and lessons that are learnt from previous studies seems to be imperative. This chapter reviews the WAG theory, applications, governing mechanisms of fluid displacement and oil production from pore to field scale, and the most common challenges and operational problems along with the remedies during WAG projects. The effect of important variables such as reservoir properties, fluid properties, and operating conditions on the performance of WAG is studied from experimental, simulation and modeling, and pore-scale investigations.

Keywords: Water Alternating Gas (WAG), Water Injection, Gas Injection, Enhanced Oil Recovery (EOR), Mobility, Displacement Mechanisms, Review

2.1 INTRODUCTION

For a typical oilfield, the average recovery factor is approximately 40 %, highlighting that a huge portion of oil left behind after primary oil recovery despite the extensive production infrastructures. The need to improve recovery factor and to accelerate the associated production rate is the main motivation/goal behind many EOR schemes in practice around the world [1]. Due to the low gas viscosity and considerable density difference between gas and reservoir crude oil, gas injection processes exhibit poor microscopic sweep efficiency which results in bypassing of a part of oil, fluids front instability, viscous fingering, and early breakthrough in the swept zone/area of a reservoir [2-4]. Initially, Water-Alternating-Gas (WAG) injection as an EOR technique was introduced to enhance the macroscopic sweep efficiency in gas injection processes [3]. This technique was firstly implemented in 1957 in Alberta, Canada in a sandstone

reservoir by Mobil as a combination of two conventional approaches; namely, gas injection and water flooding [5-6]. Currently, WAG injection is recognized as a common technology to enhance the total oil recovery through re-injection of produced gas in water injection wells in mature petroleum fields [2]. However, WAG is a difficult process and in most cases is an impractical technique in terms of reducing the fluids front instabilities due to high completion costs, complexity of operational conditions, and gravity segregation problems in injection wells associated with simultaneous injection of water and gas [7]. Thus, the sequential injection of water and gas slugs-WAG injection was proposed. Generally, a WAG process combines the advantages of two conventional methods, water flooding and gas injection, i.e., enhancement of macroscopic sweep efficiency in water flooding operation and high displacement efficiency in gas injection process to improve the incremental oil production [8]. In the case of alternating injection of water after gas, water (because of its higher density) will sweep the bottom part of the reservoir and stabilize the displacing front through creating a more favorable mobility ratio [9]. This technique is also profitable in terms of economic prospective by lowering the gas volume required to be injected into the reservoir [10]. It was reported that 80 % of USA WAG field projects were fruitful [11]. Skauge et al. reviewed 59 WAG fields. Their study revealed that the average oil recovery increases by 5 % to 10 % Originally Oil In Place (OOIP) for all WAG cases [12]. WAG processes have been successfully applied (mostly by down dip injection) in the North Sea fields such as: Gullfaks, Stafjord, South Brae, Snorre, and Oseberg Ost [13]. Because of gravity segregation, a majority of the attic oil is displaced by the gas phase and that of the bottom oil by the water. The down dip injection scheme results in dispersed flow zones as the attic oil is being produced [13]. In 1991, the technical potentials of surfactant flooding and WAG injection were evaluated by the Norwegian Petroleum Directorate (NPD) and three Norwegian oil companies [14]. Since then, WAG injection has been extensively applied in the Norwegian Shelf; chemical EOR techniques were also used in a few pilot studies [14]. The WAG performance is highly affected by the injection strategies (e.g., injection well pattern, WAG ratio, number of WAG cycles, volume of each cycle, and injection rate and pressure) and different optimal strategies were found in the literature. Simulation results reported in the open sources show that multiple WAG cycles with high Voidage Replacement Ratio (VRR) in the gas cycles at a WAG ratio of 1 result in the optimum oil recovery [15]. Different WAG scenarios have been studied. For instance, Kulkarni and Rao performed a set of tertiary immiscible and miscible core flood experiments to compare WAG and Gas Injection (GI) processes [16] in which WAG injection was found to be superior to GI [16]. WAG is also effective in heterogeneous reservoirs. In low permeability heterogeneous reservoirs, waterflooding features include poor injectability, low production rate, high WOR, and low oil recovery factor [17]. Through numerical

simulations, Liao et al. investigated three different technologies to implement WAG injection: 1) Allocation Of Injection Rates (AOIR), 2) Tapered Water Alternate Gas (TWAG), and 3) AOIR-TWAG. All of these methods provided higher recovery factor, compared to the conventional WAG injection [17].

Experimental and modeling studies demonstrate that a high recovery of up to 90 % is achievable in simultaneous water and gas injection using the five-spot pattern, while gas injection alone usually results in residual oil saturation of 20-50 % [18]. One of the best WAG strategies was applied in the Brent reservoir of the Stafjord field [19] in which WAG injection horizontal wells were practiced; the injection well was deeply perforated while the production well was sidetracked [19]. Panda et al. proposed an optimal design strategy through applying WAG injection in Eileen West End (EWE) reservoir, Prudhoe Bay field [15].

The WAG injection process combines the imbibition and drainage mechanisms during successive injections of gas and water cycles in a three-phase regime in the reservoir [5, 20]. Designing an optimal WAG process requires fine-tuning of the critical parameters, affecting the optimum conditions and ultimate recovery factor. Weak performance of WAG in some projects can be related to inappropriate WAG parameters such as the number of cycles, volume of each cycle, and the injection rates of the gas and water phases. Hence, WAG optimization is a proper scheme to control the gas mobility to increase the oil recovery [21-22]. These optimal parameters can vary with the reservoir rock and fluids characteristics [7]. The optimal design of WAG process needs strategic planning which includes a milestone for the equipment installation, maintenance, and operation activities over the life of project. To the best of our knowledge, no systematic reviews were found in the literature on WAG processes.

This comprehensive review chapter covers a wide range of research studies related to WAG processes in the open sources. It is structured as follows: first a brief description of process mechanisms along with the governing equations related to the three-phase flow in porous media will be provided. Based on the shortcomings of conventional WAG processes, different WAG configurations have been suggested by researchers which will be reviewed. Then, we will study the effects of different variables on the performance of WAG including, petrophysical properties, fluid properties, and the operating conditions. After that, a review of the pore-scale of WAG including experimental and theoretical studies will be summarized. Following the pore-scale observations, the large-scale implementations of WAG technology (pilot and field cases) will be discussed. Then, the mathematical modeling of WAG process from classical works to modern studies with the three-phase relative permeability, capillary pressure, and hysteresis models will be briefly explained. The technical and non-technical WAG challenges and conclusions will be addressed at the end.

2.2 WAG PROCESS DESCRIPTION: THEORY AND MECHANISMS

According to the 2016 British Petroleum (BP) statistical review of the world energy [23], 1.2 trillion barrels are the total proved oil reserved of the world. While, in most discovered reservoirs 377 million barrels of oil are still trapped in porous systems after primary and secondary stages of recovery [8]. Knowing this large amount of trapped oil which is a huge energy potential for current and future demands, many research and engineering projects have focused (and are focusing) on Enhancing Oil Recovery (EOR) techniques. However, many of these proposed techniques have failed or attained low success. The main goal of EOR methods is to achieve the best performance in terms of economic and recovery factor prospects.

EOR techniques aim to create a more effective movement of displacing and displaced fluids in the reservoir by maintaining a favorable mobility ratio (M<1.0) and increasing the capillary number (N_{ca}). The mobility ratio is defined as follows:

$$M = \frac{\lambda_{ing}}{\lambda_{ed}} \tag{2-1}$$

where λ_{ing} is the mobility of the displacing fluid (injected water/gas) and λ_{ed} stands for the mobility of the displaced fluid (e.g., oil). The mobility ratio affects both the micro-sweep (areal and pore scale) and macro-sweep (volumetric) displacement efficiencies. The capillary number (N_{ca}) is given by [24]:

$$N_{ca} = \frac{v\,\mu}{\sigma} \tag{2-2}$$

in which, σ is the interfacial tension, *IFT* (N/m), μ refers to the viscosity of the displacing fluid (Pa.s), and v is the Darcy velocity (m/s). One of the strategies to increase the capillary number is reduction of the interfacial tension through using a surfactant or heat to increase the temperature of system. Increasing the capillary number by three orders of magnitude, the residual oil saturation will decrease by 50 % [24]. In a miscible displacement, the capillary number becomes infinite and the residual oil saturation in the swept region may approach zero (if the mobility ratio is favorable) [25]. The efficiency of any flooding process such as water, gas, and WAG injection is highly dependent on macroscopic (volumetric) and microscopic (displacement) efficiencies [24]. Displacement efficiency is related to the produced oil from the pore spaces by injecting fluid, while the volumetric sweep efficiency corresponds to the amount of produced oil which has been in contact with the injected fluid [26]. The total oil recovery efficiency is resulted from combination of both displacement efficiency (E_d) and volumetric efficiency (E_v) [27], as given below:

$$E = E_d \times E_v \tag{2-3}$$

where E is the total recovery efficiency (%).

In the case of gas injection, an unfavorable mobility ratio leads to gas fingering phenomenon which reduces the sweep efficiency. This problem has been reported in several field cases [28-30]. Gas fingering and consequently, early gas breakthrough might be resulted from reservoir heterogeneities such as fracture and high permeable layers [31-32]. The injection of water slugs along with gas injection can appreciably lower the gas effective permeability in the reservoir. Thereby, the fluids' front will be stabilized, leading to an improvement in overall sweeping efficiency. Another important mechanism during the WAG injection processes is gravity segregation caused by the density difference between the phases. The gravity segregation improves the vertical sweep efficiency by displacing the oil, especially the attic oil in the bottom of the reservoir which might be bypassed due to gas migration to the upper part of the reservoir. Viscous and gravity forces control the vertical sweep efficiency as expressed by a variation of the dimensionless gravity number ($N_{gr} = \frac{k \Delta \rho g}{\mu_o \upsilon}$, [33]):

$$R_{v/g} = (\frac{\upsilon \mu_o}{kg \Delta \rho})(\frac{L}{h}) \tag{2-4}$$

where v is the Darcy velocity, μ_o is the oil viscosity, L refers to the distance between the wells, k is the oil permeability, g denotes the acceleration due to the gravity, $\Delta\rho$ is the density difference between fluids, and h represents the height of displacement zone. There are other reservoir characteristics influencing the vertical sweep efficiency such as permeability variation, porosity, and reservoir dip angle [25]. For example, with an increase in the porosity (or/and an increase in the permeability), the fluid flow will be stabilized, resulting in a greater displacement efficiency [6, 34]. Furthermore, a lower IFT between the gas-oil phases provides better conditions for the gas to displace the oil from small pores which have been untouched by the water phase [3]. Figure 2-1 depicts a simple schematic of miscible WAG injection expected to happen in a reservoir.

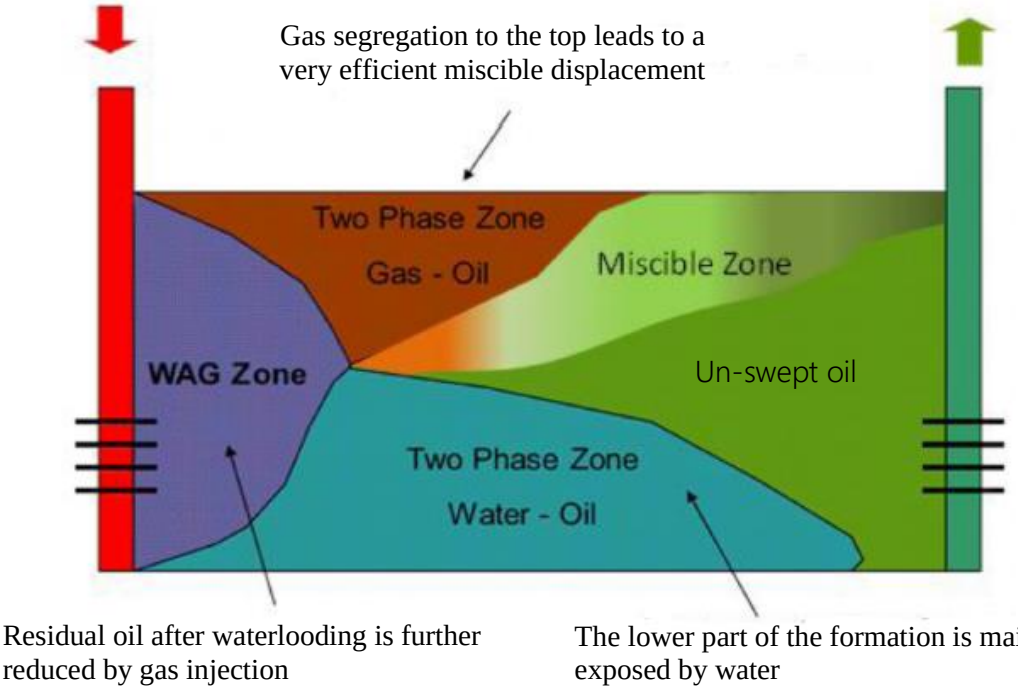

Figure 2-1: Schematic representation of WAG injection in a reservoir (modified after Luis et al. [35]).

The governing equations for immiscible three-phase flow in porous media (with application to the WAG process) uses the classical formulation of Muskat's extension [36] for the Darcy's equation. The continuity and auxiliary equations are given in this section.

Continuity equation for phase α is as follows [37]:

$$\frac{\partial(\varphi\rho_\alpha \mathrm{S}_\alpha)}{\partial t} + \nabla.(\rho_\alpha \mathrm{u}_\alpha) = \mathrm{q}_\alpha \qquad \alpha = w, o, g \tag{2-5}$$

where t is the time; ϕ signifies the porosity; ρ_α is the density of phase α (which can be water, oil or gas); S_α is the saturation of phase α; u_α is the velocity of phase α; and q_α denotes the sink or source term. The velocity of phase α can be obtained from the extended Darcy's equation for the multiphase flow systems as given below [37]:

$$u_\alpha = -\frac{Kk_{r\alpha}}{\mu_\alpha}(\nabla \mathrm{p}_\alpha - \rho_\alpha \mathrm{g}) \qquad \alpha = \mathrm{w}, \mathrm{o}, \mathrm{g} \tag{2-6}$$

in which, K is the intrinsic permeability of porous medium; $k_{r\alpha}$ represents the relative permeability to phase α; p_α is the pressure of phase α; μ_α stands for the viscosity of phase α; and g denotes the acceleration vector due to the gravity.

The auxiliary relationships are shown below:

$$k_{ra} = k_{ra}\left(S_w, S_o, S_g\right) \tag{2-7}$$

$$P_{cow}(S_w, S_o, S_g) = p_o - p_w \tag{2-8}$$

$$P_{cgo}(S_w, S_o, S_g) = p_g - p_o \tag{2-9}$$

$$P_{cwg}(S_w, S_o, S_g) = p_g - p_w \tag{2-10}$$

The summation of saturation of three phases holds one as follows:

$$S_w + S_o + S_g = 1 \tag{2-11}$$

Only two of the three saturation terms are independent. Three -phase relative permeability and capillary pressure models are functions of the phase saturation. Due to the cyclic nature of the WAG, researchers have suggested to use three-phase relative permeability and capillary pressure models with hysteresis effects [38].

2.3 WAG Variations

Different variations of WAG were found in the literature based on different attributes of this EOR process as shown in Figure 2-2. These variations were proposed to enhance the efficiency of process and to compensate some of the shortcomings of conventional WAG. With regard to the process scheme, conventional water-alternating-gas (WAG), simultaneous water and gas injection (SWAG) and hybrid-WAG (HWAG, also called Denver Unit WAG or DUWAG) were introduced. In the hybrid-WAG, the conventional WAG process is hybridized with cycles of CO_2 injection only. In the simultaneous water and gas injection (SWAG), gas and water are mixed at the surface and injected to the reservoir. Although SWAG does not philosophically belong to the category of WAG (water-alternating-gas) process, it is often classified under this process. Hence, we do not consider this classification (SWAG) to be unambiguous. Modifications were also applied on the fluids (gas or aqueous phases) to improve the sweeping efficiency. The gas phase modifications include the following alternatives for the gas phase: 1) foam (in foam-assisted WAG or FAWAG), 2) miscible gas, 3) CO_2, and 4) steam (water-alternating-steam process or WASP). The liquid phase modifications include the following alternatives for water: 1) low salinity water (LSW), 2) water soluble polymer additives (polymer WAG or PWAG or PAG), 3) surfactant additives, 4) o/w emulsions (emulsions WAG or EWAG). Arguably, the most important classification of WAG is based on the miscibility condition in the gas cycles (miscible WAG versus

immiscible WAG). The miscibility or immiscibility nature of the injection scheme is a strong function of reservoir conditions (temperature, pressure, and depth) and the properties of the displaced phase (oil) and injected fluids (water and gas) [39]. The miscible and immiscible injection processes are comprehensively described later in this chapter. Other categories of WAG processes, which are less common in terms of practical implications, are composed of HWAG (also called DUWAG), Simultaneous Water-Alternating-Gas injection (SWAG), Water-Alternating-Steam Process (WASP), Foam Assistant WAG injection (FAWAG), and Polymer-Alternating-Gas injection (PWAG or PAG), as listed in Figure 2-2.

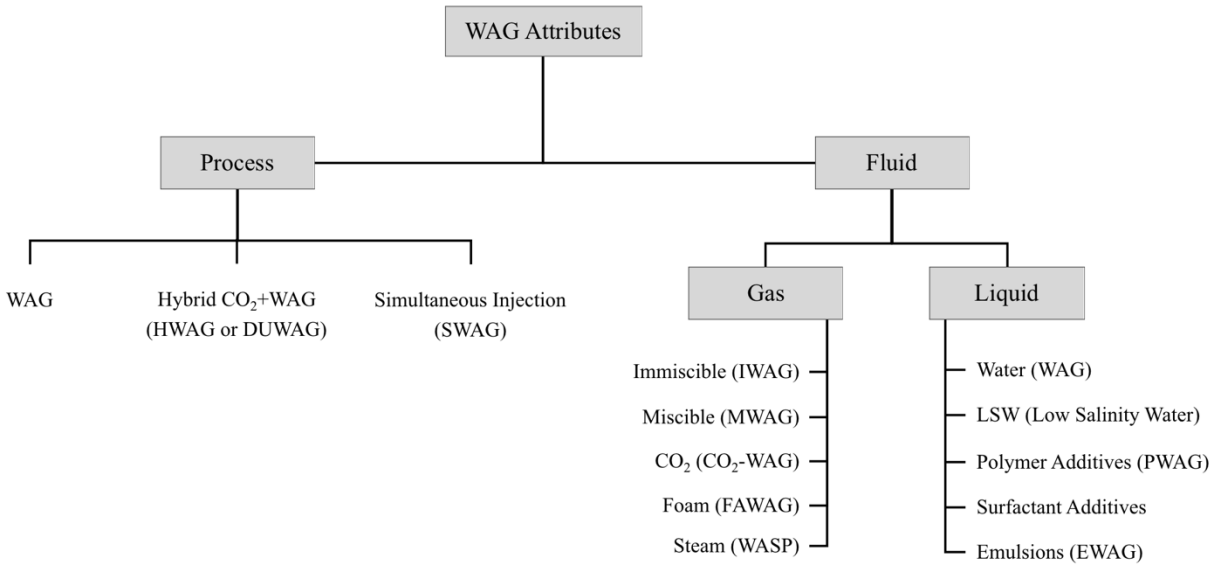

Figure 2-2: Variations of WAG processes based on different attributes.

In the following, some of the important variations of WAG processes will be discussed in more details.

2.3.1 Hybrid-WAG and DUWAG

Union Oil Company of California (UNOCAL) introduced hybridization of CO_2 injection and WAG injection for the first time. In this technique, a considerable fraction (pore volume) of CO_2 is injected and followed by a number of WAG cycles with the ratio of 1:1 [40]. Lin and Pool [41] numerically evaluated the recovery performance for different strategies such as single-slug CO_2, WAG, and hybrid CO_2 flooding processes with application to Dollarhide Devonian field. Their results indicated that both single-slug and hybrid processes speed up the oil production during the early CO_2 injection. It was also concluded that the overall incremental recovery of the hybrid process is 0.7 % OOIP higher than the case of single-slug CO_2 injection. It was interesting that the hybrid injection outperformed the WAG injection case, while the overall recovery of the hybrid case was 1.2 % OOIP lower than the WAG injection [41]. In

1992, Shell developed an empirical model to obtain the optimized recovery of gas injection. Similar to the hybrid-WAG process, four to six years of continuous CO_2 injection were followed by 1:1 WAG injection to take the advantages of both conventional WAG injection and continuous CO_2 injection [42]. The early EOR response, fine injection performance, an increase in hydrocarbon GOR as well as an instant decrease in CO_2 production, all were the main prospects of the project. Due to the ongoing process, the quantitative data/info were not reported.

2.3.2 Simultaneous Water-Alternating-Gas injection (SWAG)

In 1963, Humble Oil and Refining Co. first applied the simultaneous injection of water and enriched gas in the Seeligson Field Kleberg Country, Texas [43]. They used the low injection rates and high pressures during the process. Although this process lacks a cyclic nature, it is often classified as a variation of WAG in the literature. In 1964, water alternating enriched gas was also implemented. Despite having higher injection rates in the first cycle, the wells received a little gas and the saturation of water around the wellbore was increased in the next cycles. Based on the literature studies, SWAG provides a higher mobility control than WAG injection. It also enhances the gas displacement efficiency due to the creation of more stable gas production and eventually ultimate oil recovery [44-45]. In Joffre Viking Tertiary Oil Unit (JVTU) pilot study, various injection strategies such as continuous CO_2 injection, Water Alternating CO_2 (CO_2-WAG) injection, and simultaneous injection of CO_2 and water were tested. The dual tubing strings for the SWAG operation were installed in the pilot study. The results showed that the simultaneous injection of water and CO_2 at the ratio of 1:1 yields a higher improvement in the sweep efficiency than the conventional CO_2-WAG and continuous CO_2 injection [46]. Experimental results [18] have also revealed a higher sweep efficiency in SWAG; the simultaneous injection of water and gas resulted in 90 % sweep efficiency in a five-spot flooding pattern, while the gas injection alone led to 60 % ultimate sweep efficiency [18]. In some cases, the simultaneous injection of water and gas is referred to the processes that a solution of water and dissolved CO_2 is injected into the reservoir—a process which is often called carbonated water flooding (or injection) or “fizz flood” [47]. Compared to the WAG-EOR processes or full-scale miscible gas flooding strategy, the carbonated water injection might not offer remarkable economic benefits. Based on the literature, fizz flooding has been proved to be applicable in naturally fractured reservoirs and low permeable reserves (e.g., Austin chalks) [48-51]. Despite the advantages of the SWAG injection, there are several drawbacks to this process such as higher costs for well completion, equipment and operation; design complexities; gravity segregation; and gas-front instabilities [7].

2.3.3 Water Alternating Steam Process (WASP)

Water Alternating Steam Process (WASP) was originally developed to overcome the problems associated with steam injection such as steam gravity, steam channeling, and occasional surface breakouts. This process can be considered as a variation of WAG strategy that leads to improving the reservoir vertical conformance/displacement. The main difference between the conventional WAG injection and WASP is that in WASP the vapor phase is condensable while the gas phase in the conventional WAG process is commonly non-condensable [52]. The steam also carries thermal energy that can lower the viscosity of oil and help productivity and also sweeping efficiency (by improving the mobility ratio). Upon vapor condensation, the gravity over-ride process will decrease. In general, comparing with continuous steam injection, the advantages of WASP include enhancing areal conformance, lowering the chance of channeling, lessening fuel waster, decreasing wellbore heat loss, facilitating the oil production, improving the incremental oil recovery, and specifying the best time to inject the continuous water if water injection after the steam process is considered [52-53]. WASP was applied in West Coalinga Field at the pilot scale and resolved the steam breakthrough problem of steam injection processes[52]. It was also implemented at the Cymric field [54]. The project started with two cycles of steam injection over a 4-month period. The subsurface temperature data indicated that the WASP can effectively control the steam channeling in the down-dip producers; but no considerable breakthrough control was noticed in the up-dip reservoirs. WASP was also efficient in terms of reservoir pressure maintenance, oil production pattern, thermal efficiency, and economic prospective [54]. In 1999, with the minimum capital costs, four (4) Petrotrin's steam flooding projects were converted to WASP. It was reported that 18 % oil production reduction in 1988 turns to 12 % increase in production in 1999 through applying the WASP technique. This incremental increase in the oil production could be potentially greater if there was no water supply shortage for the water cycles. It was also economically successful, as the direct operating expenditure per barrel of oil was reduced by 33 % which was mainly due to a decrease in the steam and workover costs. [55].

2.3.4 Foam Assistant WAG injection (FAWAG)

Generally, the main application of foam in EOR processes is to control the mobility of gas phase which leads to improving the sweep efficiency and postponing the breakthrough time [56-57]. The idea of using foam to control the fluid front mobility was first introduced by Bond and Holbrook in 1958 [58]. Since then, in a number of oil recovery processes (e.g., CO_2 injection and water flooding), CO_2 foams including surfactants have been used as an effective mobility reduction approach. The stability and properties of

the foam are the main factors which influence the performance of FAWAG processes [56]. In a series of core-flood experiments, the performances of SWAG and FWAG were evaluated [59], showing a promising performance of the SWAG processes in reducing the problems with adverse mobility, gravity segregation, and viscous fingering; a higher recovery factor was however attained in the FAWAG processes so that it increased to 61 % first, and then a significant increase up to 92 % was achieved after the FAWAG application, as illustrated in Figure 2-3[59].

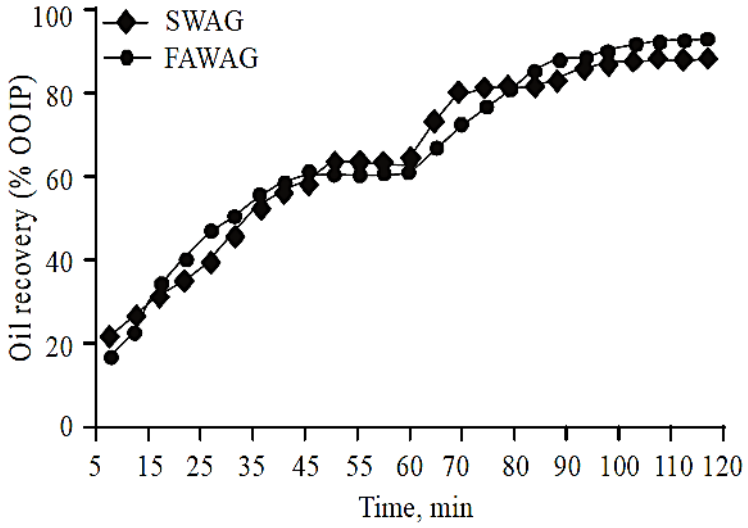

Figure 2-3: Comparison between SWAG and FAWAG recoveries in a series of coreflood experiments [59].

Foam injections were used in the EOR projects in the North Sea field for the purposes of mobility control and production well treatment (to reduce produced GOR) [60-62]. Foams can be generated in situ, mostly in high-permeable layers due to a higher chance of fluids to flow. The foam generation from a given surfactant is highly dependent on time, oil saturation, and capillary pressure [63]. Figure 2-4 shows a schematic of the challenges and advantages associated with the continuous gas injection (CO_2 injection in Figure 2-4 (a)), conventional WAG injection (in Figure 2-4 (b)), and FAWAG (in Figure 2-4 (c)).

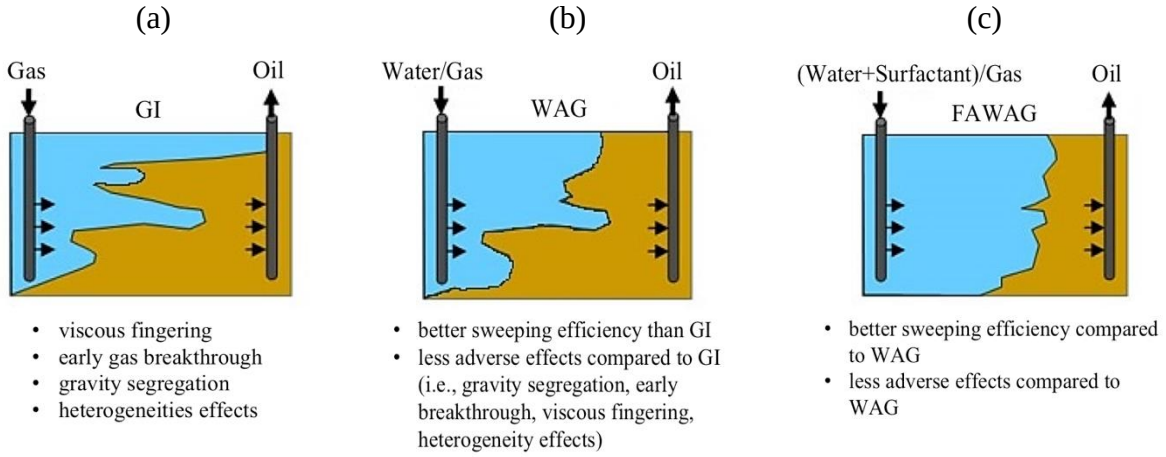

Figure 2-4: Schematic of challenges and benefits of (a): continuous gas injection, (b): conventional WAG injection, and (c): FAWAG injection in a reservoir [64].

In 1997, a large-scale FAWAG injection was applied in the Central Fault Block (CFB) of the Snorre field where 2000 tons of the commercial grade surfactant were injected into the reservoir to conduct two injectivity tests and two full-scale treatments [62, 65]. Due to the gas leakage in one of the wells, the process of FAWAG injection was stopped in CFB and the project was moved to Western Fault Block (WFB) in the Snorre filed. The main objective of the FAWAG process in WFB was to increase the gas sweep efficiency, which leads to an increase in the gas storage and a decrease in the GOR at the production well [56]. In a series of FAWAG coreflood tests [66], the foam generation was found to decrease with an increase in the gas density. At a constant density, a CO_2-rich foam exhibited a better mobility control than CO_2-lean foam. The foam enables to benefit from three-phase flow (microscopic-scale sweep efficiency); the foam lamellas help to control the gas mobility [66]. The stability and mobility of foams (as the main parameter, affecting the foam propagation and stability) were investigated by a series of laboratory tests at different injection rates [67]. It was concluded that the Mobility Reduction Factor (MRF) increases by increasing the flow rate. The MRF is defined as follows [67]:

$$MRF = \frac{\Delta p_{with-foam}}{\Delta p_{without-foam}} \tag{2-12}$$

in which, $\Delta p_{with-foam}$ and $\Delta p_{without-foam}$ are the pressure difference across the porous medium with and without foam, respectively. The effect of injection rate on the stability of foams was investigated in Surfactant Alternating Gas (SAG) injection tests [67]. At low flow rates, SAG showed a poor efficiency in

generating foam, resulting in a low MRF. In addition, SAG caused high MRFs at various flow rates due to the frequent contact and mixing between the gas and surfactant phases [67].

2.3.5 Polymer Alternating Gas (PAG) injection

Another modification of the WAG process to overcome the early gas breakthrough and gravity segregation was proposed through Polymer-WAG (PWAG) or Polymer Alternating Gas (PAG) injection [68]. A hybridized CO_2 and polymer injection WAG (CO_2-WAG) was applied to Saskatchewan heavy oilfield. The hybrid strategy resulted in a higher recovery factor, compared to the sole polymer flooding. In these coreflood experiments, the immiscible CO_2-WAG injection recovered 15.3 % OOIP, using 6.16 MSCF/STB. The sole polymer flooding led to 12.93 % OOIP. The highest recovery efficiency was attained at the hybridized CO_2-polymer (or PAG) flooding with 18.7 % OOIP by consuming only 2.0 MSCF/STB injected gas (one-third of CO_2 were consumed in the first run), as demonstrated in Figure 2-5[68].

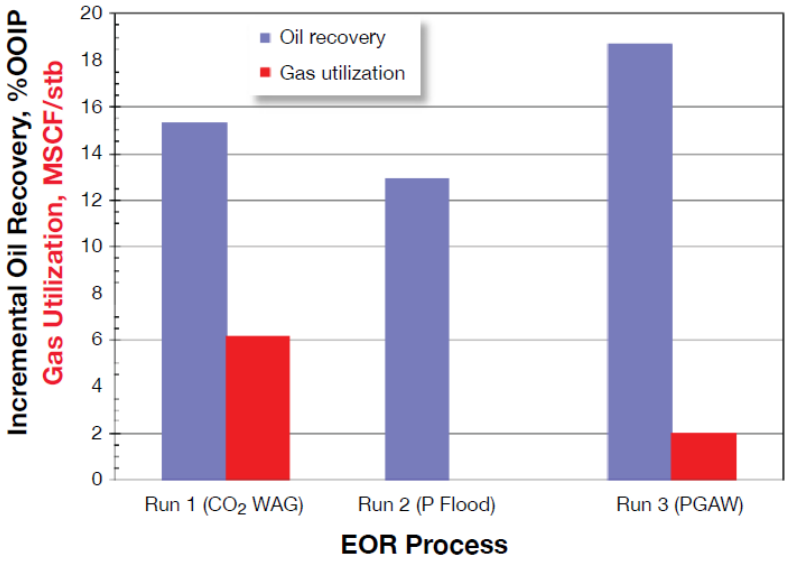

Figure 2-5: Comparison of EOR recoveries and gas utilization at three runs of coreflood experiments [68].

A more general term, known as Chemically enhanced Water-Alternating-Gas (CWAG), is also used in the literature [69] which refers to the use of any chemical slug such as alkaline, surfactant, and polymer during the WAG process to control the mobility and to reduce the IFT [69]. A higher efficiency was attained in CWAG, compared to the conventional WAG injection. According to the simulation results It was estimated that PAG increases the oil recovery up to 14.3 %, which is 7.0 % higher than WAG injection in TR78 section of the North Burbank Unit [70]. The simulation results [70] also show a remarkable GOR

reduction (at production well), a noticeable delay in the gas breakthrough, and an improvement in the gas and water sweep efficiencies during the PAG processes. Figure 2-6 illustrates the simulation results in terms of oil production rate versus time for the injection of CGI, WAG, PAG, and polymer flooding [70]. In 2014, Li and Schechter studied the effects of polymer concentration and adsorption on the efficiency of PAG where CO_2 was used as a gas phase [71]. It was found that the PAG performance strongly depends on the polymer adsorption and a higher oil recovery is expected at a lower polymer adsorption. In homogeneous reservoirs with a permeability higher than 500 mD, the PAG processes give 7-15 % higher oil recovery than the WAG injection [71].

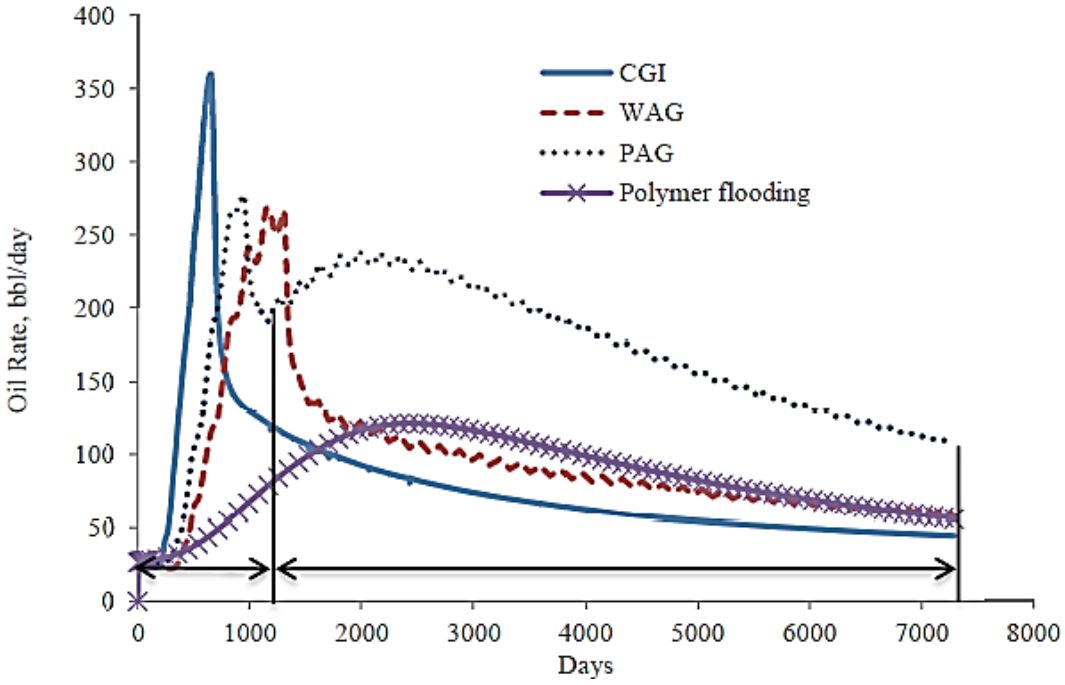

Figure 2-6: Simulation results of oil production rate for different injection operations [70].

PAG exhibits an acceptable performance in both low and high permeable heterogeneous reservoirs with the heterogeneity coefficient (V_{DP}), ranging from 0.5 to 0.9. It was also estimated that 2.1 lb/STB polymer are needed to increase the oil recovery by 20 % (which is 12 % higher than the recovery for the WAG injection) where the economic feasibility is met [71]. The coreflood experiments indicate that the use of polymer in WAG is only efficient when the process is miscible displacement. In the absence of miscibility condition, PWAG does not offer any significant improvement to oil recovery, compared to conventional WAG injection [72]. However, during miscible WAG process in a homogeneous reservoir, the addition of polymer to the water cycle (in a conventional WAG process) reinforces the oil trapping phenomena (in which water shield oil droplets) which leads to higher residual oil saturation (S_{or}=25.34

%) than both WAG injection (S_{orWAG}=15.95 %) and continuous CO_2 injection ($S_{or\ CO2}$=6.35 %). However, in heterogeneous reservoir at the same miscible condition, no residual oil saturation gap between these two methods was observed which is mainly due to inactivity of dispersion viscous fingering in such a type of reservoirs.

2.4 EFFECTS OF PETROPHYSICAL PROPERTIES ON WAG

The success of a WAG injection process depends on a variety of factors/parameters such as petrophysical properties of the reservoir, fluid characteristics, field scale considerations, and economic aspects [73]. Among the petrophysical properties, we study the impacts of reservoir heterogeneity, relative permeability, hysteresis, and wettability on the performance of WAG, according to the materials available in the literature.

2.4.1 Reservoir Heterogeneity and Stratification

The production performance of reservoirs in a WAG process is highly affected by the reservoir heterogeneities. The failure of EOR projects (in general) has been attributed to the reservoir heterogeneity in many cases [74]. In highly stratified reservoirs, economical gas injection is not possible, due to the early breakthrough and high gas recycle rates. In such reservoirs, the WAG scheme is the most cost effective technique to delay the gas breakthrough and to decrease the gas-to-water ratio (GWR) which will result in economical oil recovery [10]. In reservoirs with high stratifications, the displacement front tends to move along the highly permeable layers which leads to bypassing a considerable residual oil in the layers with less permeability [74]. A higher vertical permeability results in perpendicular crossflow to the bulk flow which is influenced by other forces such as gravity, capillary, viscous, and dispersion [75]. The vertical conformance/displacement of the WAG processes in terms of performance is strongly affected by anisotropy, stratification, the flow connectivity between the reservoir layers, and the ratio of viscous-to-gravity forces [5]. Due to the decrease in fluid flow velocity in reservoir and gravity segregation problems, the cross flow adversely affects the reservoir, which results in restriction of frontal advancement in the low permeable layers, while it may improve the vertical sweep efficiency [76]. Previous studies demonstrated that the crossflow created by capillary imbibition can assist the vertical sweep efficiency in an immiscible displacement if the mobility ratio is favorable in heterogeneous systems [77-79]. Their results also confirmed the previous studies that gas first occupies the high permeability strata and bypass the low permeability zones (as a result of channeling), while the water phase due to its favorable mobility flows into all layers that the gas has not been able to sweep [80]

Claridge conducted different simulation runs for CO_2 flooding at various vertical transmissibility factors where CO_2 injection and WAG injection processes (with different ratios of CO_2 and water) were utilized [81]. He found that the WAG injection leads to a higher oil recovery (and a lower residual oil saturation) at the end of the process in the case of zero vertical transmissibility (e.g., $K_v/K_h=0$). It was concluded that as the vertical transmissibility increases, the recovery of the WAG process decreases. In fact, the WAG injection mitigates the extent of crossflow and consequently lowers the adverse effects which are observed in the continuous CO_2 injection strategy [81]. Gorell et al. compared the results of continuous injection of CO_2 with different WAG approaches through simulating a 3D, five-spot elements of a symmetrical pattern [82]. They reported that the vertical displacement during the WAG injection is highly influenced by the flow communications between the zones. In a non-communicating medium, the permeability contrast controls the vertical distribution of the gas phase. Normally, the flowrate in each layer is directly proportional to the flow capacity (K_h) of that layer, which is independent of the WAG ratio. At high WAG ratios, the gas tends to quickly enter the high permeable zones. Thus, high permeable layers will be quickly filled and they may contain more fluids than their capacity (K_h) during the WAG cycles. As the water cycle is injected (in WAG), it sweeps most of the gas from the zones and improves/modifies the mobility ratio close to its initial value [82]. The most efficient displacement of the WAG injection will be attained when both the water and gas phases move in the reservoir at equal pore velocities [83-84]. The simulation results revealed that the WAG injection in heterogeneous reservoirs not only reduces the mobility in high permeable layers, but also in less permeable layers, since it leads to migration of a large portion of the gas into the highest permeable layers during the WAG injection [82]. In gas condensate reservoirs, due to a greater viscosity difference between the water and gas condensate, the water partially blocks the thief layers (layers with higher permeability). Depending on the crossflow effects and fluids density and viscosity, K_h differences between the layers and relative permeabilities result in gas diverting into a superior sweep of the matrix and reducing gas channeling. Several simulation runs performed by Jones et al. showed that the improvement in oil recovery is a strong function of the permeability ratio of the thief zone to matrix and also their fluids viscosity ratio [85]. In the condensate gas reservoirs, the magnitude of permeability in various directions has a remarkable impact on both continuous GI and WAG processes in highly stratified reservoirs. In the case where the top layers have the highest permeability, the gas overrides will intensify and water will prefer to move to the lower strata; however, if the layer placed at the bottom has the highest permeability, the water phase underrides and diverts the gas to the upper zones [86].

2.4.2 Relative Permeability and Hysteresis

Simultaneous flow of three phases (oil, water, and gas) in WAG demands accurate knowledge of relative permeability (through experimental and modeling investigations) to obtain the mobility and velocity of the individual phases [87]. It is clear that the miscibility nature of the phases and the time required to attain the miscibility condition have considerable effects on the displacement mechanisms and oil recovery in WAG. Three phase relative permeability data are required for reservoir simulator packages to model the transport phenomena in porous systems, to understand the interactions between the phases, and to determine the saturation, pressure distributions, and the velocities of all phases [88]. Several studies reported that the classical techniques to obtain the relative permeability of each phase might not be accurately applicable in WAG due the cyclic hysteresis nature [89-90]. Owing to the technical challenges in obtaining laboratory measurement of three-phase relative permeability data, they are usually inferred from two-phase relative permeability data and a three-phase relative permeability models [91-92].

Relative permeability is a lumped variable that considers the impacts of heterogeneity, wetting properties, porosity, pore size distribution, Interfacial Tension (IFT), and fluid saturations [7]. As discussed previously, one of the main mechanisms during the WAG injection is the IFT reduction so that gas-oil IFT is lower than water-oil IFT, resulting in more oil displaced from the pore spaces compared to waterflooding [3]. IFT affects the relative permeability curvatures. For instance, in a completely miscible process, the IFT value is zero and the relative permeability is a linear function of saturation with a slope of one [93]. There are many research works in the open sources, discussing about IFT impacts on the relative permeability in gas condensate reservoirs. This discussion can be extended to other miscible or near miscible EOR projects such as WAG injection processes [93-95]. Harbert performed coreflood tests using alcohol, brine, and oil samples. It was concluded from the results that as the IFT decreases, two phases have less inference with each other and the relative permeability curves are shifted upward [94].

Skauge and Larsen designed a set of WAG injection experiments at different rock wettability states under unsteady state conditions [96]. They measured the three-phase relative permeability at various stages of gas and water cycles. In each cycle, the relative permeability for all phases showed irreversible hysteresis effects during the process. It was also found that the gas phase exhibits the strong hysteresis effects regardless of the wetting state of the rock. The relative permeability of non-wetting (gas) phase was more affected by the hysteresis and at similar saturation level, the relative permeability to the non-wetting phase (k_{rg}) was lower when decreasing the gas saturation (imbibition cycle), compared to the increasing saturation path (drainage cycle) [96].

In another work, Larsen and Skauge presented a relative permeability model that is applicable for local hysteresis effects. Their hysteresis model accounts for both wetting and non-wetting phases. The model also considers the reduced mobility and irreversible hysteresis loops during the three- phase flow of the WAG injection processes. Their proposed approach takes the initial saturation and relative permeability values of the wetting and non-wetting phases as the input data to the model [38]. Egermann et al. implemented successive drainage and imbibition experiments (WAG injection) for various initial saturations and proposed a three- phase model (including the hysteresis) which was validated by the experimental data. They found that the hysteresis not only depends on the saturation history, but it also is a function of the displacement history. They observed two types of hysteresis: mechanism (imbibition/drainage) and cycle (history) hysteresis. At the large scale of WAG injection, the ratio of vertical permeability to horizontal permeability (K_v/K_h) has a significant influence on the overall production efficiency [97]. Based on the experimental data, Element et al. validated the hysteresis models [98]. They designed a series of experimental tests to investigate the secondary and tertiary immiscible in WAG injection in water-wet and intermediate-wet Berea cores. They concluded that the hysteresis cycles are irreversible; the gas trapping by water leads to a reduction in the residual oil saturation; and both water and gas permeability values reduce. Thus, the fractional flow varies with trapped gas saturation and the land trapping factor (C) changes between the hysteresis cycles as shown below.

$$C = \frac{1}{S_{gt}} - \frac{1}{S_{gi}} \tag{2-13}$$

where the C represents the land trapping factor, S_{gt} is the trapped gas saturation, and S_{gi} refers to the initial gas saturation [99-100]. They also concluded that Carlson and Killough's two-phase hysteresis models cannot describe the secondary and tertiary WAG processes [98]. Spiteri and Juanes studied the impact of the relative permeability hysteresis on the efficiency of WAG processes at the field scale in which the three-phase relative permeability was inferred from two-phase data. They applied history-depending saturation function in the simulation runs. The validity of existing models was also investigated and the model parameters that created the most uncertainty were also identified. Their analysis showed that the models introduced by the experimental observation of hysteresis behavior cannot be generalized for cyclic nature of gas and water injection during the WAG processes. To illustrate the effects of relative permeability model (considering hysteresis) on the output of the reservoir simulation runs, they used a five-spot pattern model in both homogeneous and heterogeneous reservoirs, which is a modified version of PUNQ-S3 model. This model is a reservoir model originally suggested (as a test case) for production prediction under uncertainty. They designed their models with and without hysteresis and noticed great

differences in simulation results. They concluded that the relative permeability models involving hysteresis are required to forecast the performance of the immiscible WAG injection processes, though the current hysteresis relative permeability models still need modifications for the sake of further accuracy and generalization [101].

The effect of rock wettability on the relative permeability during the WAG injection is also important. Shahverdi et al. investigated the relative permeability and hysteresis in the WAG process with various rock wettability conditions where a series of two-phase coreflooding experiments were carried out at unsteady state conditions [102]. Their results exhibited a significant reduction in three-phase relative permeability and consequently a reduction in the gas mobility and injectivity at different wettability conditions. They observed different hysteresis effects for all three phases (oil, gas, and water) at various wettability states during the WAG injection. It was found that the relative permeability of each phase is a function of two independent saturations [102].

2.4.3 Wettability

Wettability is one of the main factors controlling the fluids flow and distribution in a porous medium [103]. The wettability of a reservoir influences the vital variables such as capillary pressure, relative permeability, dispersion, and electrical properties [103]. It has been proven that the wettability plays an important role in tertiary oil recovery processes such as hot water, surfactant, miscible, and caustic flooding [103]. It has been also claimed that the reservoirs' cross beds are initially in contact with water. As a result, they were initially water-wet. After oil migration to the water-wet reservoir rock, the oil phase was able to invade the large pores and the water remained in the small pores. However, fluid phases became detached as an interplay between the capillarity and gravity forces which might lead to alteration of wetting properties of the rock surface. The polar components of the crude oil such as asphaltene and resin might adsorb onto the pore surface and alter the wettability to oil-wet or mixed-wet [104-107].

The experimental and modeling results show that more oil trapping occurs in the water-wet rocks, compared to the oil-wet rocks during WAG injection [40]. In the WAG injection, other aspects such as recovery, injectivity, optimum WAG ratio, and three-phase relative permeability are affected by the wettability condition. For instance, an experimental study carried out by Jackson et al. suggested that an optimum WAG ratio of 0:1 (continuous slug injection) is attained in the water-wet reservoirs, while this optimal ratio is 1:1 in the oil-wet rocks. In tertiary floods of water- wet cores, the gravity override is the main factor, controlling the enhanced oil recovery factor.

Both oil-wet and water-wet tertiary floods have the same gravity-to-viscous ratios, but the first one is controlled by viscous forces, while in the other one the gravity forces is the dominant force. Stern conducted a series of tertiary multi-contact CO_2 coreflooding tests and investigated the impacts of wettability and WAG ratio on the displacement mechanisms and recovery factor. He reported lower oil recovery due to less extraction of bypassed oil at high WAG ratios in water-wet rock samples. However, in mixed-wet rocks, the WAG ratio became less important and the most portion of the recovery was obtained due to the extraction regardless of amount of the WAG ratio. That might had to do with the wall-coating on mixed-wet surfaces that enhances the interaction among oil and solvent [108].

Wettability also influences the three-phase relative permeability and displacement hysteresis during the WAG processes. Reliable measurements of relative permeability need careful and complicated methodologies in the WAG processes. Shahrokhi et al. examined different three-phase relative permeability models (e.g., Stone I, Stone II, IKU, Carlson, Killough, and Jargon) and compared the results for various rock wettability. They concluded that none of the available methods can accurately predict the experimental WAG injection data in mixed-wet reservoirs [109]. There are other studies in the literature that report micro-model experiments under various wettability conditions. For example, a set of capillary dominant WAG injection tests were conducted by Sohrabi et al. in glass micromodels [110]. They concluded that the WAG injection process has a higher oil recovery factor than waterflooding or gas injection alone regardless of the type of wettability. The pore-scale observations revealed that the fluids in the WAG injection process find new flow pathways in the porous medium (in each cycle) which are different from the previous paths. It was reported that the WAG injection in the oil-wet and mixed-wet systems is more efficient than that in the water-wet models. Having additional injection cycles in the mixed-wet models leads to a gradual increase in the oil recovery, while the additional oil recovery is reduced in the oil-wet and water-wet systems, after first two cycles [111]. It is important to note that wettability is not the sole parameter governing the recovery mechanisms [108, 112-113].

2.5 EFFECT OF FLUID PROPERTIES ON WAG

2.5.1 Gas Type

As mentioned earlier, WAG injection improves the recovery through enhancing the microscopic efficiency of gas injection and enhancing the macroscopic efficiency of waterflooding. Due to the cyclic nature of WAG, the slugs of water and gas invade the porous media and reduce the oil viscosity due to the gas dissolution in the oil phase [114]. The type of injected gas in the WAG process may be categorized into three classes: 1) non-hydrocarbons (CO_2 excluded), 2) CO_2, and 3) hydrocarbons [6]. Nitrogen and flue gas are two examples of the non-hydrocarbons and non-CO_2 gases which have been used in a few

fields due to their economic prospects and resources availability [115-118]. Nitrogen is not as common as the other gases for EOR by the WAG process, nitrogen can be still used in both miscible and immiscible processes [119]. In an experimental study, Salehi et al. used nitrogen at a constant injection rate in WAG, Surfactant-Alternating-Gas (SAG) and gas injection and compared the production results with those of waterflooding [119]. They reported the ultimate recovery factors of 87 %, 70 %, 66 %, and 50 % for SAG, WAG, waterflooding, and gas injection, respectively, as depicted in Figure 2-7[119].

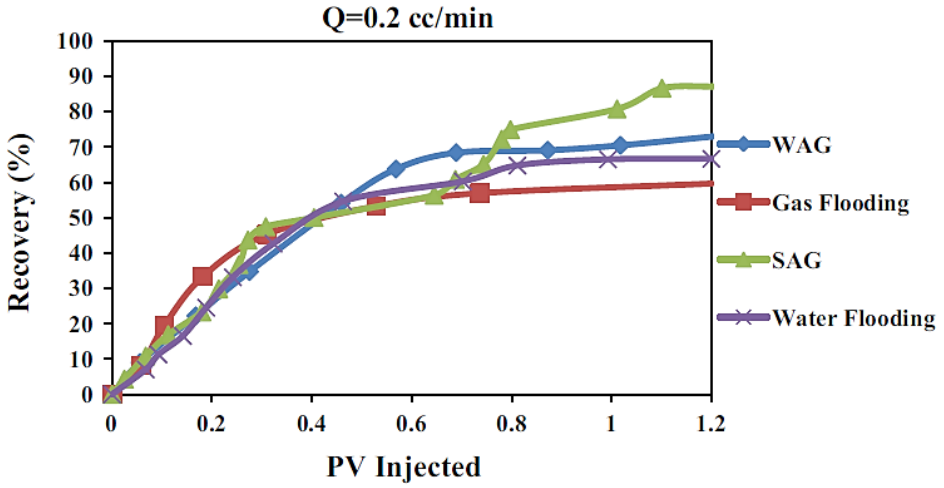

Figure 2-7: Comparison of oil recovery for SAG, WAG, gas flooding, and water flooding [119].

There are some advantages using nitrogen in the WAG processes, compared to CO_2. For instance, CO_2 is a highly corrosive gas, while nitrogen is an inert gas in many cases [120]. Ghafoori et al. experimentally investigated the performance of the WAG injection and continuous gas injection (CGI) processes using two types of gases: nitrogen and CO_2 in a carbonate porous sample. According to their results, the WAG injection with both gases exhibited a higher performance, compared to the CGI process. The ultimate oil recovery was not sensitive to the size of nitrogen slugs in the WAG injection. However, it was found that the miscible CO_2 WAG injection attains about 13 % more oil than the immiscible nitrogen WAG injection [121]. Although CO_2 is a relatively expensive gas, it has been utilized for many miscible injection EOR operations. Among 60 WAG field applications reviewed by Christian et al., 28 WAG injection cases employed CO_2 as the injected gas [6]. Initially, there were some concerns regarding the CO_2 flooding (e.g., in CO_2-WAG) such as water blocking, corrosion, injectivity loss, low oil production, and production concerns. However, most of these problems have been resolved through engineering experience, efficient management, and optimal process design [7]. For example, it has been reported that

an average of 20 % water injectivity loss occurs in the WAG operations [122]. There are some suggestions to compensate this drawback by adding more injection wells, creating fractures, increasing the injection pressure, and decreasing the WAG ratio. One of the main concerns regarding the CO_2 WAG injection is the injectivity loss. For more details on injectivity loss issues during WAG injection, technical readers may refer to the Rogers et al. review [7]. An analysis on Wilmington field test in Tar zone block V CO_2 injection project indicated that the high oil recovery in immiscible CO_2 injection is attributed to two major mechanisms: first, an instant response resulted from moving the portion of the oil left untouched over water movement by gas; and the second one is related to the relative permeability alteration, swelling, and viscosity reduction which have a long term impact on the project performance [123]. Another advantage of using CO_2 is that it creates higher gravity segregation in zones with a greater water saturation, compared to the areas with a higher percentage of oil saturation. This phenomenon is helpful in recovering oil from bypassed or target pocket zones through improvement of sweep efficiency [7]. The design criteria for CO_2 injection include some limitations such as minimum depth, oil viscosity range, and value of oil specific gravity [76]. Moritis' EOR survey showed that the number of CO_2 miscible projects is increasing while the application of other injecting gases such as nitrogen and flue gases is decreasing over time [76]. Despite the environmental benefits of using CO_2, most of offshore WAG projects inject hydrocarbon gases due to the availability in the production site. In a review study, 24 fields out of 60 reviewed fields used hydrocarbon gases in dry or enriched forms [6]. In a study which focused on the feasibility of WAG injection in Ekofisk field, the slim tube simulation results recommended the immiscible WAG injection by dry hydrocarbon gases due to the high minimum miscible enrichment and minimum miscibility pressure [9]. The WAG injection experiments conducted on the GS-5C sand of a mature light oil field showed that CO_2 with 5 cycles of WAG injection yields an incremental recovery of 40.18 % Hydrocarbon Pore Volume (HCPV), which is much higher than the recovery of 19.3 % HCPV for the same number of cycles, in the WAG injection using hydrocarbon gases [124]. Another technique, named Water Alternating High Pressure Air Injection (WAHPAI), was recently proposed by Batenburg et al. in which a high pressure air was used [125]. The main advantage of WAHPAI is the availability and low cost of air, compared to other injecting gases. The man goal of WAHPAI implementation is to enhance the oil sweeping efficiency.

2.5.2 Brine Salinity

Water salinity is an influential parameter in WAG. This has been confirmed by several numerical and experimental investigations in waterflooding [126]. According to the coreflooding experiments conducted by Sharma et al., the imbibition relative permeability curves strongly depend on the salinity. It was also

concluded that high oil recovery can be achieved at low salinity level of connate water [127]. A significant reduction in the water/oil ratio and an increase in the oil recovery factor were observed in an Alaskan reservoir by injecting low salinity water. A double increase in oil production rate was also reported by continuing the production for nearly 12 months [128]. Therefore, the effect of salinity is expected to be considerable in WAG or SWAG injection processes. Comparing Simultaneous Water And Gas injection (SWAG) and WAG injection using brines with various salinities, at seawater (SW) and twenty times dilution of seawater (SW/20) brine salinities, SWAG exhibited a higher oil recovery compared to WAG injection an continuous gas injection due to more efficient mobility control during gas cycles even in the microscopic level [129]. Figure 2-8 shows the simulation results of ultimate oil recovery in various tertiary injection modes including miscible CGI, SWAG, and WAG [129].

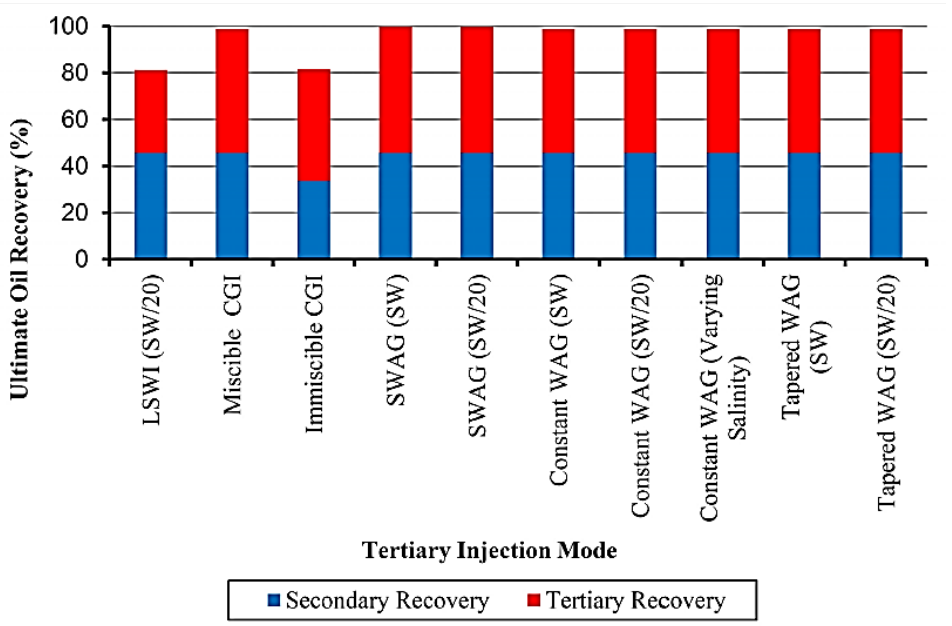

Figure 2-8: Ultimate oil recovery for different tertiary injection modes [129].

In a research study, a synthetic brine with NaCl salinity in the range 1,000 to 32,000 ppm, and a synthetic brine containing 4000 ppm NaCl and 4000 ppm $CaCl_2$ were used to examine the performance of the WAG injection process [126]. Tertiary oil recovery from the coreflooding experiments showed a slight increase in the oil recovery factor with increasing the brine salinity (see Figure 2-9). This is due to a decrease in the solubility of CO_2 in the brine phase with increasing salinity [126].

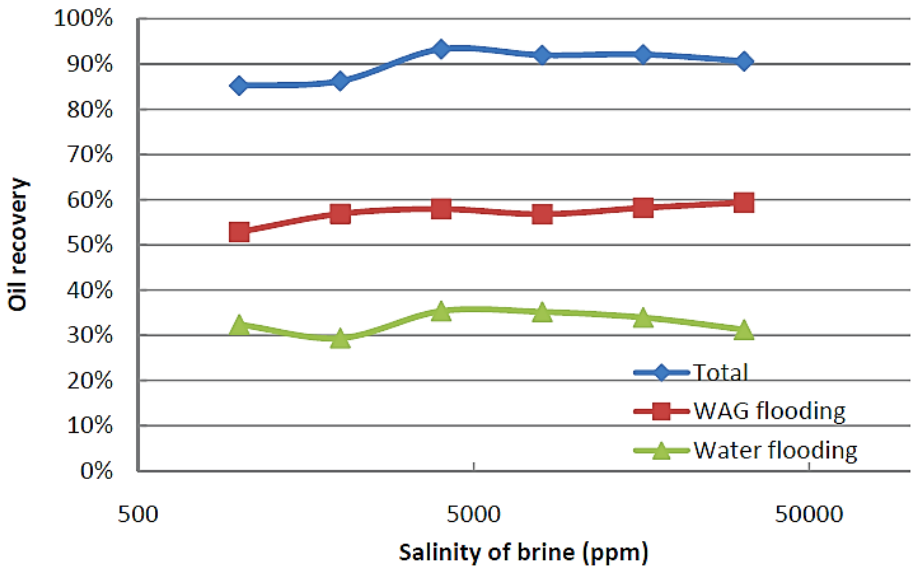

Figure 2-9: The effect of brine salinity on oil recovery [126].

This phenomenon was also observed in a series of Low Salinity Water Flooding (LSWF) and seawater coreflooding experiments for both CO_2 WAG injection and stand-alone waterflooding tests. The seawater case showed a greater oil recovery, compared to the LSWF, during the CO_2 WAG injection process because of the same reason addressed above. Another reason might be the fine migration that occurs in the LSWF-CO_2 WAG injection [130]. Figure 2-10 shows the influence of various water salinities on the dynamic contact angle during CO_2-WAG injection [130].

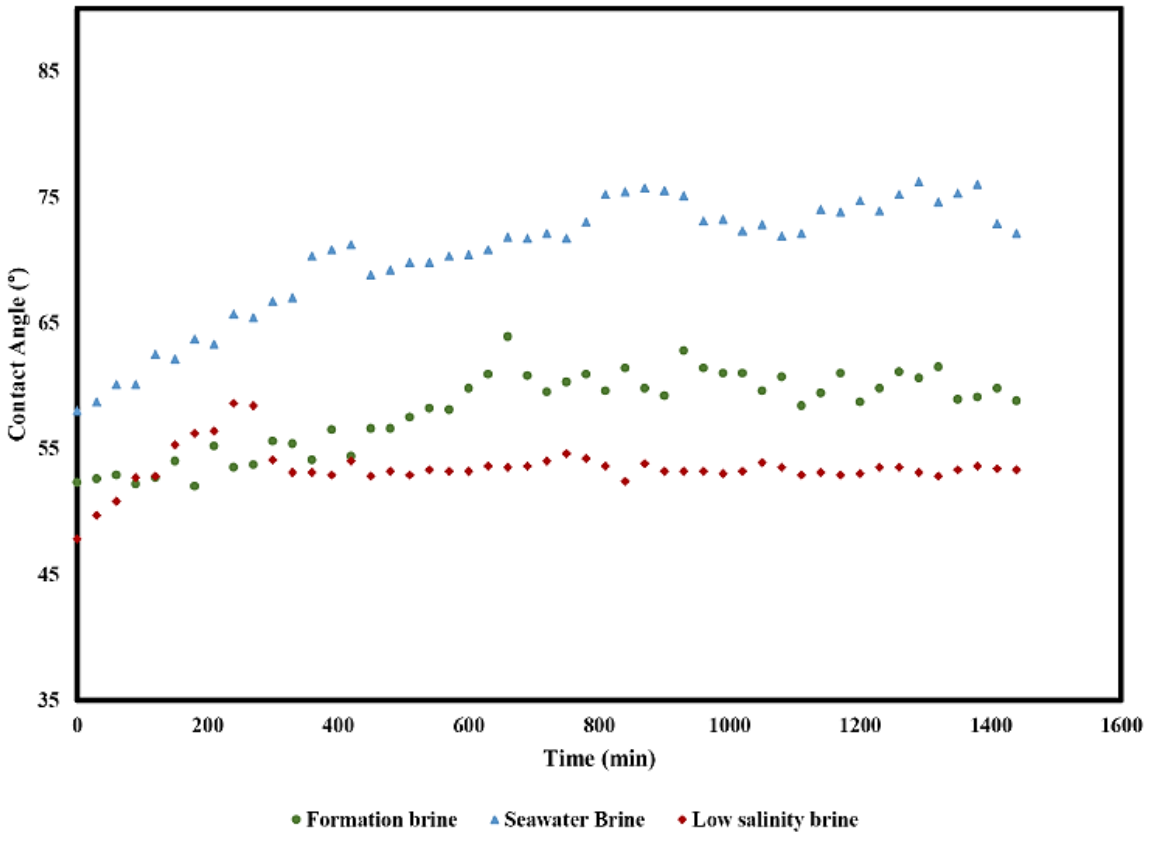

Figure 2-10: Dynamic contact angle of unaged Grey Brea sandstone at 500 psi and 149° F with different salinities during the CO_2-WAG process [130].

In another research study, Kulkarni and Rao designed a series of coreflooding experiments under both Continuous Gas Injection (CGI) and WAG injection conditions where the salinity varied from 5 wt % NaCl to 0.926 wt % multivalent salinity in Yates reservoir [8]. Although the recovery factor increases from 96.7 % to 97.6 % through changing the brine salinity from 5 % NaCl to Yates formation brine, CGI showed a negligible dependency to the salinity in the tested range. However, in the miscible WAG injection, a notable dependency of oil recovery to the brine composition and salinity percentage was observed [8]. Using the modified brine composition (which is sometimes referred to smart waterflooding) during CO_2-WAG injection leads to a decrease in the relative permeability of both water and oil phases. In another words, utilizing smart water in the WAG cycles lowers the oil recovery factor and water cut. The slight shift of the intersection point between the relative permeability of water and oil curves highlights that the smart water injection during CO_2-WAG injection alters the wettability state of the system towards more water-wet. The impact of divalent ions such as Mg^{2+} and Ca^{2+} in the composition of the smart water CO_2-WAG injection was also investigated. It was found that an increase in the

concentration of these ions improves the oil recovery due to a decrease in the ion binding at the interface of carboxylic oil components and the rock surface [131]. Hence, modifying the brine chemistry during the WAG injection is clearly demonstrated by determining the variation of the relative permeability of phases which needs further experimental and simulation research works. Cuong et al. studied the mechanisms and advantages of CO_2 Low Salinity WAG (CO_2-LSWAG) injection through coupling an ion exchange model with geochemical mechanisms in the coreflooding tests [132]. Their modeling results highlighted the promising aspects of CO_2-LSWAG mechanisms (in terms of recovery performance) such as chemical reactions, ion exchange process, and wettability alteration. They showed that the CO_2-LSWAG eliminates the late production problems that usually occur during the WAG injection projects. Comparing the CO_2 High Salinity WAG (CO_2-HSWAG) with CO_2-LSWAG, the low salinity case improved the incremental oil recovery up to 9.0 % OOIP [132]. The success of the CO_2-LSWAG injection approach depends on various factors such as the amount of clay and its type, initial wettability condition, formation heterogeneity, type of minerals, compositions of injected water and formation brine, and reservoir pressure and temperature.

2.5.3 Fluids Miscibility

In recent decades, gas injection has become one of the most applicable and environmentally friendly techniques in several oilfields. This technique is more efficient when the injected gas is at nearly or completely miscible condition with reservoir oil [133]. Miscible or near miscible WAG injection (nMWAG) processes generally feature a higher recovery factor (9.7 % OOIP), compared to immiscible WAG (IWAG) injection (6.4 % OOIP) [6]. A number of factors such as injectivity loss and pressure maintenance failure can negatively affect the life-span and performance of miscible and immiscible gas injection processes [76]. There are no certain screening criteria to decide between the miscible or immiscible injection strategies. Thomas et al. inquired the importance of miscible gas injection [134]. Based on their study, as long as the desired recovery is achieved at reduced interfacial tension, the condition for miscibility is not required. The success of such processes depends on a compromise between the mobility, IFT and a safety factor to account for problems such as gravity overriding [134]. Miscible flooding is normally implemented by increasing the reservoir pressure above the Minimum Miscibility Pressure (MMP). It is conducted with or without WAG injection to lower the IFT between the gas and oil phases and to control viscous fingering. In the case of nearly miscible processes (nMWAG), the injected gas slugs displace the oil bank which is also referred to multi-contact WAG injection. The main role of the water slugs is to achieve a better volumetric sweep efficiency in the nMWAG process due to lower residual oil saturation after near miscible gas front. MWAG processes in very early cases were

commonly performed in onshore fields using solvents such as propane which is not currently economical [135]. Production history analysis of the oilfields under MWAG shows that a close well-spacing is used in the majority of projects. However, recent offshore MWAG projects have been conducted using large well-spacing [135]. Although mass transfer between the gas and oil phases might happen during the IWAG injection (which can enhance the oil recovery), IWAG injection is strictly referred to the injection of gas slugs that cannot develop miscibility with the oil phase. Skauge and Sorbie studied both miscible and immiscible mechanisms through analyzing WAG injection at pore scale, core scale, and field scale. The results of pore scale (micro-model) experiments showed an additional oil recovery in the IWAG process, compared to the miscible WAG process [136]. This enhancement is resulted from the gas spreading to the larger pores due to the microscopic dispersion during gas cycles. In nMWAG processes, less gas trapping occurs, resulting in expansion of the gas clusters within the continuous oil phase in the system and eventually sweeping almost all of the contacted oil [137-138].

2.6 EFFECT OF OPERATIONAL PARAMETERS ON WAG

2.6.1 Injection Pattern

Selection of an optimum injection pattern is an important stage in designing a WAG injection project. This refers to the best injection pattern that involves more contact of the displacing fluids (water and gas) with the reservoir fluid (oil) [26]. Several vital factors that should be taken into account in designing optimal injection pattern include reservoir heterogeneity, directional permeability, fracture directions, the nature of the injected fluids, well intervals, and performance of injection and production wells [139]. A review of WAG field cases reports that the five-spot injection pattern is the most common configuration in onshore fields [6]. Although five-spot patterns with close well-spacing dictate higher costs to the project, compared to other patterns, due to requiring more careful control on pressure of miscible processes, they are still the favorite injection patterns especially in miscible operations in Texas, USA [6]. Other criteria such as geological characteristics and operating and capital costs also control the well placement and injection pattern (such as the North Sea field) [13]. Pritchard et al. concluded that as the injection pattern size reduces, the oil recovery factor by tertiary EOR improves. In Judy Creek oilfield, the five-spot configurations with 40 acre pattern size attain the highest oil recovery [140]. For port Neches field, using WAG injection and modifying the injection pattern were reported among the main reasons for an oil production improvement [141].

Extensive upward gas migration in the formations flooded by WAG causes a low volumetric sweep efficiency for the gas phase [142]. For this case, reservoir simulations suggest the horizontal WAG injection

to achieve a higher gas volumetric sweep efficiency, compared to vertical injectors [142]. For instance, a compositional simulator model was employed to simulate the WAG process in the Alpine field. The results showed that the horizontal wells have higher performance (with 59 % oil recovery factor), compared to vertical wells (with 50 % oil recovery factor) [142]. The WAG injection strategy using horizontal wells is more suitable for reservoirs that are thin and contain low permeable layers with high continuity between the vertical layers [142].

2.6.2 WAG Ratio

The WAG ratio is one of the most important operating variables in the design of WAG injection projects. For SWAG injection in a homogeneous formation, the optimum WAG ratio is achieved based on the displacement front of advanced water-oil rates and oil-solvent displacement front [143]. Stalkup proposed a graphical methodology using the water-solvent fractional flow to determine the optimum WAG ratio [144]. There are two main criticisms on this method: 1) it considers the same relative permeability for the water-solvent and water-oil systems, and 2) it overlooks the effect of capillary pressure on the efficiency of small scale displacement processes [144]. In some research studies, wettability is considered as the main factor affecting the WAG performance especially at high WAG ratios [108]. At high WAG ratios due to less oil extractions, a lower amount of oil would be recovered. This effect is even more severe in water-wet reservoirs at high WAG ratios where no extraction occurs; while the WAG ratio has less impact in mixed (or/and oil)-wet media and a substantial amount of oil is recovered by extraction [145]. Elmond et al. showed through a simulation study that the optimum WAG ratio is affected by the shape of water-blocking curve, which represents the residual oil saturation versus water saturation [145]. The WAG ratio of 1:1 was reported as the optimum value [145]. Moreover, Stalkup investigated the influence of wetting condition on the water blocking. It was noticed that more oil trapping occurs in the water-wet samples than the oil-wet cases [146]. Raimondi and Torcaso observed that a portion of the oil phase that was trapped after water injection, can be mobilized by the solvent injection [147]; the rest of oil remains blocked in the pore throats. They suggested an empirical equation based on the water blocking data in strongly water-wet reservoirs as follows [147]:

$$\frac{S_{ot}}{S_{orw}} = \frac{1.0}{[1.0 + \frac{k_{ro}}{k_{rw}}]} \tag{2-14}$$

where S_{ot} is the transverse oil saturation; S_{orw} represents the water flood residual oil saturation; K_{ro} and K_{rw} are the oil and water relative permeability, respectively. Tiffin and Yellig investigated the impacts of both WAG ratio and reservoir wettability on the oil recovery, using linear coreflooding experiments

[113]. They reported an optimum WAG ratio of 0:1, representing the continuous slug injection in either water-wet or oil-wet rock samples [113]. Kootiani et al. designed a series of WAG injection experiments using glass-bead packs to visually investigate the impacts of miscibility and WAG ratio on the performance of WAG [148]. The experiments were performed at three different WAG ratios of 1:1, 4:1, and 1:4. The results implied that the optimum WAG ratio is 1:1. Comparing this optimum ratio to that obtained by Stalkup's method, it reveals that the optimum WAG ratio based on the Stalkup approach offers a higher oil recovery, but it fails to suppress the viscous fingering at an acceptable level [149].

A number of simulation studies suggested an optimum WAG ratio of 4:1 which is much greater than the optimal WAG ratio of 1:1 proposed by the experimental studies [148]. The differences between predictions of optimal WAG ratio from theoretical and experimental studies might have various reasons such as neglecting gravity force and reservoir heterogeneity. In addition, the relative permeability and capillary pressure curves may also cause error [143]. Gorell showed that over a limited range of WAG ratios (the optimum WAG ratio in which the solvent-water and oil bank move at equal velocities), the displacement efficiency is insensitive to the amount of water injection [150]. In most field studies, a WAG ratio of 1:1 is used due to higher recovery efficiency, although other WAG ratios are also applied. Injection below or above the equal velocity is unfavorable, since it causes viscous instabilities and higher residual oil [6].

2.6.3 Tapering

When the WAG injection is progressing in a porous system, the tapering phenomenon occurs due to an increase or a decrease in the water/gas ratio [6]. The relative volume of the water compared to gas can be increased at the later stages of the WAG injection to control the flow problems such as gas breakthrough and channeling [151]. Tapering becomes important when the injected gas is expensive; in such a case, fluid recycling is needed [152]. Tapering during the CO_2-WAG injection is implemented to optimize the oil recovery and to attain a better use of CO_2 gas. It is better to initially inject the gas at high flow rates and to decrease the flow rate in the later cycles [75]. Tapering was found to be useful in reducing the CO_2 production and in improving the CO_2 injectivity. Chevron applied a tapered WAG injection through increasing the ratio of water-to-gas in a step-wise process at predesigned quantities of solvent bank to alleviate the CO_2 production [122]. Khan et al. investigated the optimization of miscible WAG injection using tapering technique by varying duration of the gas injection cycles in which the time interval of gas injection was decreased with injection time [153]. They concluded that tapered WAG is more efficient than the uniform WAG injection when the duration of both gas and water cycles are the same and fixed [153]. Tapered WAG also reduces the response time through shortening the arrival time of the oil bank at the

production wells. Thus, this strategy can offer an efficient usage of gas, which leads to a greater oil recovery per unit of injected gas [153]. Srivastava observed an improvement in the displacement efficiency in the WAG injection process using gas tapering [124]. The gas tapering resulted in an incremental efficiency of 20.73 % HCPV by increasing the WAG ratio and 23.84 % HCPV through decreasing the ratio [124].

2.7 PORE-SCALE INVESTIGATIONS ON WAG

The majority of WAG research studies have focused on the field applications, pilot tests, coreflooding experiments, and simulation studies. The WAG injection process represents a complex phenomenon that involves inter-phase mass transfer, multiphase momentum transfer, swelling, oil trapping, and water blocking by injected gas slugs. The complicated nature of WAG creates strong motivation to discover the interactions between the phases and transport phenomena mechanisms in the porous medium at various process and fluids conditions during WAG injection through conducting pore-scale experiments. The pore-scale tests are also useful to verify numerical modeling results and simulation outputs that assist to track the phase movement, saturation distribution, and phase hysteresis. Dong et al. investigated the displacement mechanisms of gas, oil, and water during IWAG injection in a water-wet micro-model [154]. A stable oil layer was formed between the gas and water phases. Due to the blockage effect of gas bubbles, the oil/water blobs could not be displaced. After the first water injection cycle, additional oil was recovered in next water cycles mainly due to two mechanisms: water displacing the oil that was trapped in water injected pores in the previous gas injection cycles, and water displacing oil that was trapped in other zones when the gas refilled the water channels. A significant decrease in the oil recovery was observed due to high water saturation and less oil discontinuity. In further cycles, fingering in long oil channels occurred due to unfavorable high gas mobility [154]. Sohrabi et al. conducted a series of WAG injection tests in a water-wet micro-model where a capillary dominant flow regime was maintained [155]. Their results indicated that the corner filament flow controls the oil snap-off during the initial water cycle injection. Hence, the process became more filament flow than piston like displacement at the pore-scale as seen in Figure 2-11.

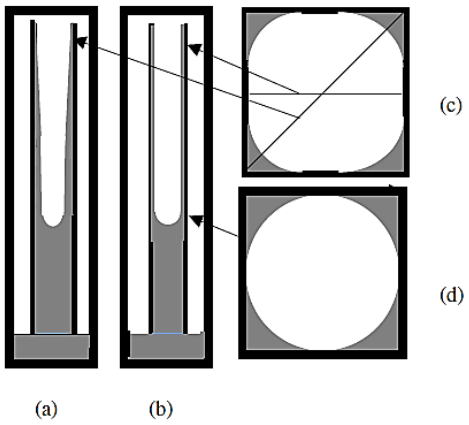

Figure 2-11: Corner filament flow in a square water-wet tube: (a) profile along the diagonal line, (b) profile along the middle of the tube parallel with sides, (c) water in the corners on top of the tube and (d) water in the corners on top of the water column [155].

During the gas injection cycles, the gas invades the oil trapped (after the first water cycle) in the pores due to the lower gas/oil IFT, resulting in more oil production (or recovery). In the next water cycles, the gas bubbles may snap off at the pore throats and become discontinuous due to the interplay of capillary forces and local gas pressure fluctuations [155]. Generally, the main improvement in the oil recovery was achieved after a few cycles of WAG injection in the pore-scale experiments. Sohrabi and Jamiolahmady carried out pore-scale visualization study at high pressures to further understand the WAG injection mechanisms at different wettability conditions where a strongly water-wet glass micro-model was utilized (see Figure 2-12) [156]. The experiments showed that the relative permeability reduction and injectivity loss take place due to the gas trapping [156]. In fact, the subsequent injections of water and gas cycles lead to fragmentation and trapping of the gas in pores that limit the available area for water to flow and consequently reduce the relative permeabilities [156].

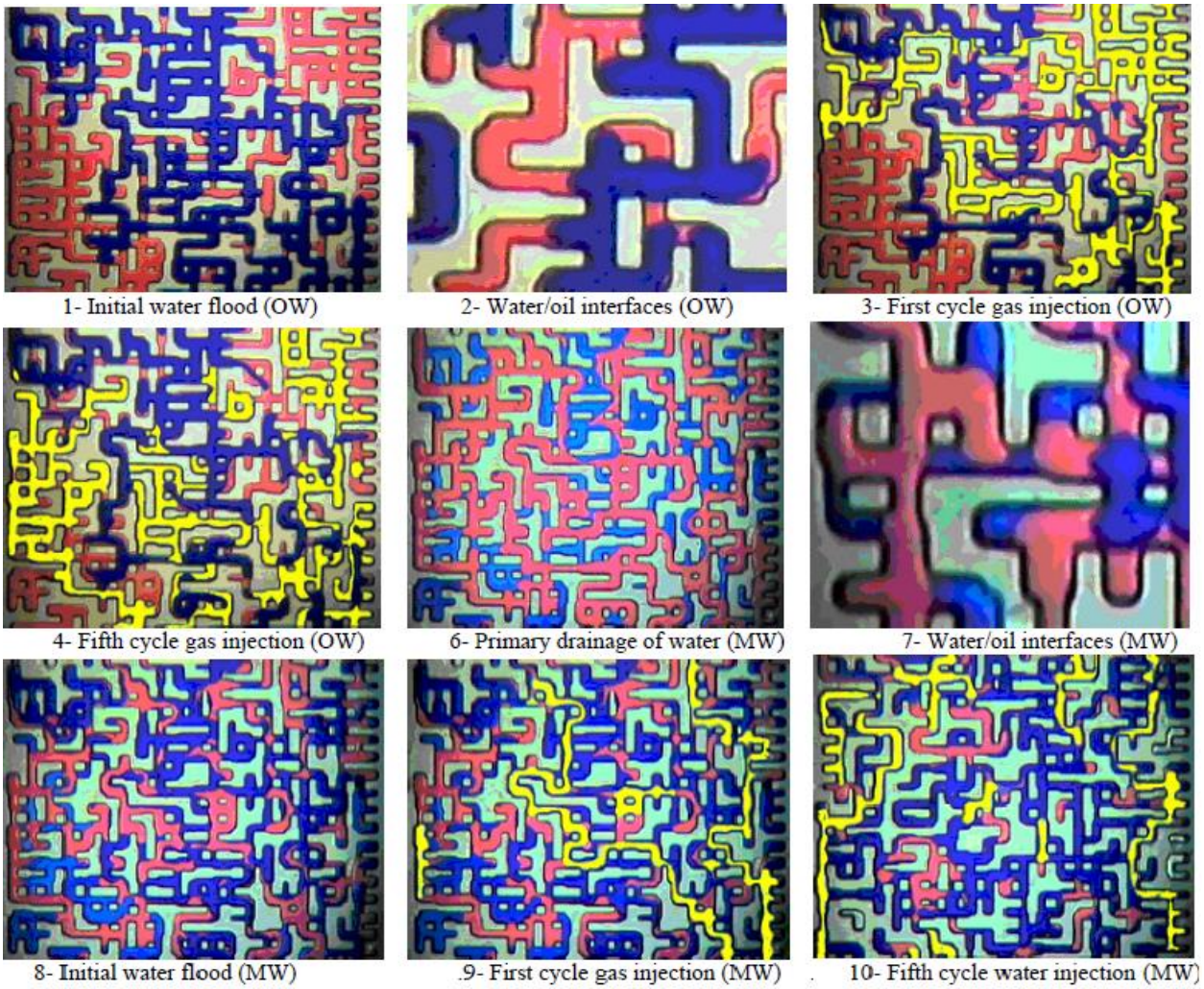

Figure 2-12: WAG injection in a micro-model at different cycles and wettability conditions [156].

The amount of trapped gas is a strong function of the IFT between the oil and gas which highlights the importance of further investigation on IFT impacts on gas trapping during WAG injection processes. Sohrabi et al. repeated the tests for strongly oil-wet micro-model systems in another research study [157]. In the oil-wet micro-model, the flow was piston like displacement, and the residual oil appeared in the form of pore surface films and corner filaments in the pores surrounded by throats [157]. Suicmez et al. employed a 3-D network model for Berea sandstone to predict the production rate and relative permeabilities and to specify the displacement pathways during WAG injection [158]. Over the waterflooding cycles (in the presence of gas), the relative permeability of water is lower than that of the gas in the gas flooding cycle as the oil/water capillary pressure increases, resulting in the conduction/continuity of the wetting layer. However, the relative permeability of gas is higher in the cycles after the first gas slug injection at high gas saturation due to the collective pore filling [158]. In the oil-wet pore medium, the relative permeability of water remains low until water fills the pores in the

entire porous system. It then increases rapidly. In the presence of water, the gas relative permeability has lower values, compared to the case where oil and gas are present since it is no longer the most wetting phase. Suicmez et al. demonstrated the application of pore network modeling to estimate the three-phase relative permeabilities [158]. It was indicated that the relative permeabilities are almost independent of the saturation path in the plot of relative permeability as a function of flowing saturation. The flowing saturation is defined as the phase saturation minus the saturation of the phase that is trapped [158]. Van Dijke et al. used a network model to simulate the WAG injection in a water-wet micro- system where the WAG operation was conducted after the primary drainage and waterflooding [159]. A good agreement between their simulation results and experimental data was attained. A multiple displacement chain was predicted by the pore network modeling at higher numbers of WAG cycles as observed in the micro-models (even water-wet media). Network model was also able to forecast the qualitative behavior of the phases in future WAG cycles such as the gas clusters break-up and redistribution of the oil and gas phases that yield a minor improvement in the oil recovery [159]. Al-Dhahli et al. developed a three-phase network model of WAG to determine the relative permeability and capillary pressure functions where the effects of single and multiple-displacements on the residual oil saturation were investigated [160]. According to the pore network modeling results, a higher residual oil saturation was obtained in a single displacement process, compared to multiple-displacement process. This is mainly because of the disconnected oil, water, and gas clusters that can be mobilized in multiple-displacement (WAG), while most of the clusters are trapped and immobile during single displacement [160].

A summary of the experimental investigations of WAG process in cores, packed columns or micromodels is presented in Table 2-1.

Table 2-1**:** Summary of experimental studies on WAG.

Year	WAG Process							WAG Fluids			Porous Medium			WAG Performance		Ref
	Type	Mode[1]	Cycles	Slug (PV)	Ratio	T (°C)	P (MPa)	Oil	Brine	Gas	Porous Medium	K (mD)	ϕ (%)	RF_{Tot} (%PV)	Remarks	
1983	SWAG	s,t	NA	NA	4:1	93.3	26.5	Crude (Prudhoe Bay)	Synthetic (20.93 g/l)	HC (mix)	Core (D=3.81 cm, L=45.72 cm, 53.34 cm)	123-178	22.6 - 25.8	90.7-95.5	• For gravity-stabilized enriched gas flooding and SWAG, S_{or} were similar with an average of 2.26 %STPV. • In water-wet Berea, high residual oil obtained at S_{or}=19.4%STPV.	161
1985	MWAG	s,t	NA	0.05	0:1 1:1 1:3 3:1 7:1	NA	NA	Refine oil	Water + glycyrin	Naphta	Packed (38 cm×38 cm×2.54 cm)	8000	30	4-8 (secondary) 3-11 (tertiary)	• slug size is more effective in secondary rather than tertiary recovery. • In oil-wet packing, WAG ratio of 1:1 gave the maximum incremental recovery. • Max incremental RF_{WAG} =11-12% obtained in oil-wet packing, compared to 3-8% in water-wet packing.	162
1991	CO_2-MWAG	s,t	NA	NA	0:1 1:1 3:1	37.8	23.4	Crude (Means and, Fullerton, TX)	Synthetic (3.5 wt%)	CO_2	Berea sandstone (D=2.54 cm, L=25.4-203 cm) Carbonate (2.54 square, 30.5, 203 cm long)	240-650 (Berea) 110-234 (carbonate)	NA	69-92	• The effect of wettability on RF_{MWAG} was more pronounced at high WAG ratios. • Less RF obtained at high WAG ratio, especially in water-wet Berea core; however, in mixed-wet, the effect was insignificant. • The effect of core length on RF_{MWAG} was minimal; miscibility condition is met even in the shortest cores (1 ft long).	108
1992	MWAG	t	4-10	0.0375-0.24	1:1 1:2 2:1	68.7, 82.2	15.3 - 18.2	Crude (Libyan)	Formation	CO_2 HC mix	Core (sandstone, limestone, D=2.5,3.8,10.2 inch, L=91.4 cm)	1.356-573	20.5 - 22.5	77.5-82.9	• Tertiary RF was in the range 18.4-26.3% and total RF in the range 77.5-82.9%. • Total RF_{MWAG} and GOR were not affected by the solvent-to-water ratio when the solvent slug size was fixed.	163
1993	WAG	t	NA	0.05	1:1	65.6	10.3	Gas Condens. (nC_3)	Synthetic (5% wt)	nC_2, nC_4	Layered Texas and Indiana limestone	10 (Texas) 0.3 (Indiana)	26 11.3	74, 85	• RF= 74% (more permeable layer at top) and 85% (10 mD layer bottom). • The RF of gas injection was ~58% regardless of the layers' arrangement.	86

[1] In the recovery mode column, s=secondary and t=tertiary modes.

1998	IWAG	t	10	0.2	4:1	23	1	Crude (Aberfeldy HO)	Synthetic	CO_2 + N_2	Packing (45.7 cm ×45.7 cm×2.2 cm)	11.1-13	37.2 - 42.1	41.6-51.3	• Increasing the concentration of N_2 contamination (in N_2+ CO_2 mixture) from 0 to 30% decreased total RF from 51.3% to 41.6%.	164
2004	WAG	t	5	NA	1:1	37.8	3.4	C_1+nC_4	Water+C_1	C_1 + nC_4	Glass micromodel (6 mm by 38 mm, Pores: 35 μm deep and 30-300 μm channel width)	NA	NA	58-78	• The min RF (58%) obtained in ww model; ow and mw models had similar ultimate recovery. • In ww and ow models, no significant production observed after two WAG cycles; considerable production obtained in the mw model after two cycles.	111
2005	IWAG MWAG	s,t	3.5	0.7	1:1	27.8 27.8	3.5 17.2	nC_{10}	5% NaCl, Reservoir (Yates, TX)	CO_2	Berea (L=30.48 cm)	136.1, 450.0	NA	23-84.5	• RF_{WAG} increased from 23 to 84.5% after miscibility condition achieved. • RF_{MWAG} was 12% higher in 5% NaCl.	8
2006	CO_2-IWAG FWAG	t	NA	0.2, 0.8	4:1	29	2.5	Crude (HO)	Synthetic, 0.5% foaming agent in brine	CO_2 N_2 Flue gas	Sandpack (D=5 cm, L=30 cm)	1074-1692	39.1	37.5-42.2	• N_2 decreased WAG recovery (tertiary) by 18% compared to CO_2. • Maximum tertiary recovery and total recovery were 6.24 and 42.2% both in FWAG from which 36% was achieved in WF alone. • RF_{WAG} increased with concentration of CO_2 in gas mixture.	165
2007	MWAG	s,t	5	0.5 0.05	1:1 1:4 4:1	NA	NA	Synthetic (Isopar V)	Water	NA	Packing glass beads (23 cm×10 cm×0.6 cm)	29000	38	85-98	• Larger water slug resulted in more fingering of solvent (paraffin). • Max and min RF were obtained at WAG ratios of 1:1 and 4:1.	166
2010	CO_2-MWAG	s,t	6	0.5	1:1	60	11.5	Synthetic (C_{10}+C_{16}) Crude (Cottonwood Creek)	Synthetic (1-32 g/l NaCl+ $CaCl_2$)	CO_2	Berea (D=2.54 cm, L=26.7 cm)	60.7-96.5	19.6 - 20.3	70-90	• RF_{WAG} 50% and 35% more than RF_{WF} with synthetic oil and crude. • RF_{WF} affected by salinity; RF_{WAG} changed only slightly (RF=37 to 40% for salinity 1-32 g/l).	126
2010	CO_2-IWAG PWAG	t	4	0.5 0.2, 0.8	1:1 , 4:1	24	5	Crude (SK heavy)	Synthetic (2, 4 g/l), 0.2% polymer in brine	CO_2	Sandpack (D=5.1 cm, L=30 cm)	1256-3394	32.8 - 35.0	65.3, 71.9	• The incremental RF_{IWAG} =15.3% and RF_{PWAG} =18.7%. • The incremental RF of IWAG and PWAG were 44.6% and 18.3% higher than that of polymer flooding. • The maximum ultimate RF of 71.89% was obtained in PWAG.	68

2011	CO_2-nMWAG	t	4	NA	NA	37.8	12.8	C_1+nC_4	Synthetic (1 g/l)	CO_2	NA	65, 1000	NA	95-99	• nMWAG has superior performance compared to WF and GI. This is especially true for low permeability and mw cores. • WF performs better in mw and GI performs better in the ww cores. • For nMWAG, it is better to start with WF cycle in mixed-wet and with GI cycle in the ww medium.	167
2012	FAWAG SWAG	s	NA	NA	NA	65	5.5	Crude	Synthetic (3 g/l), 2% surf. (in FWAG)	CO_2	NA	NA	NA	88-92	• SWAG: 62% RF after WF cycle, and 88% RF at the end of SWAG. • FA-WAG: 61% RF after WF cycle and 92% RF at the end of FWAG.	59
2012	CO_2-MWAG IWAG	s	1,5	0.05, 0.15 0.25	1:1	30	15.2	Crude (Binak)	Reservoir	CO_2 N_2	Carbonate core (D=3.8 cm, L=15.84 cm)	0.36	12.15	71.8-86.2	• The effect of gas slug size on IWAG using N_2 was not significant. Max RF was obtained for slug=0.15 PV. • $RF_{CO2\text{-}MWAG}$=86.2% highest compared to RF_{HWAG}=81.4% and F_{IWAG}=73.7%. • Gas injection alone gave RF_{CO2}=73.5% and RF_{N2}=45.6%.	121
2012	CO_2-WAG IWAG	t	1-5	NA	NA	128	22.5	Crude	Reservoir	CO_2 HC (mix)	Sandstone core (D=3.8 cm, L=7 cm)	323.3	21	64.6-97.9	• Using HC gas mix, 43% increase in IWAG recovery observed when #cycles increased from 1 to 5. • Incremental RF in CO_2-MWAG had 120% increase compared to HC-IWAG (5 cycles). • Tapering (increasing) WAG ratio improved incremental recovery but did not changed total recovery much.	124
2012	IWAG MWAG	t	10	0.1	1:1	57	8.5, 20.4	Crude (South Slattery, WY)	Synthetic (16 g/l)	CO_2 + O_2	Berea core (D=3.8 cm, L=25.4 cm)	64.7-76.9	19.3 - 19.7	20-73	• Increasing O_2 contamination from 0 to 10% (by mole) decreased the RF_{WAG} from 12 to 10% in immiscible and from 33 to 27% in miscible mode. • Total RF decreased from 28 to 20% in IWAG and from 73 to 57% in MWAG.	168
2012	CO_2-WAG	s	11	0.2	1:1	25	0.34	Crude (Heavy oil)	Synthetic (10 g/l NaCl)	CO_2	Sand pack	12600-43000	36.1 - 40.6	25.4-47.3	• The effect of oil viscosity on RF_{WAG} was more than that of permeability. • For viscous oil, CO_2-WAG was more efficient than CO_2 flooding and less efficient than WF.	169

2013	CO_2-WAG	s	5	0.16	1:1	50	5.5	Crude (Stock HO)	Synthetic (1-50 g/l)	CO_2	Sandstone (D=3.8 cm, L=7.5 cm)	333-357	29-32	74, 92	• RF_{WAG} were 92% in low salinity and 74% in high salinity brines.	[170]
2014	CO_2-MWAG	s	3	0.4		48.9	17.2	Crude (Devonian), Refined (nC_{10}+nC_{14+} mineral oil)	Formation (60.2 g/l)	CO_2	Berea (ww,mw,ow) Devonian (mw), Tensleep (ow)	547-725 381-446	18.7-20.2 23-30	66.1-88.6	• In ww Berea, CO_2 injection was better than WAG. • Oil trapping in ww, mw, and ow Berea after 1 PV were 45%, 15-20% and 5%, respectively.	[40]
2014	IWAG SAG	s	NA	NA	1:1 2:1 3:1	70	14.5	Crude	Synthetic (7.3%), 1.5 g/l surf.	N_2	Sand pack (D=5 cm, L=15 cm)	350	29	70, 87	• RF_{WF}= 66%. • RF_{max}=87% obtained in SAG (1:1) compared to $RF_{N2\text{-}WAG}$ =70%. • RF SAG orders: 3:1<2:1<1:1.	[119]
2014	IWAG	s	NA	NA	1:1	93.3	23.4	Crude (Iran)	NA	CH_4	Carbonate core (OD=3.8 cm, L=31.5 cm)	8	12.5	51.9	• At optimum injection rate, the RF_{WAG}>RF_{WF}>RF_{GI} (e.g., 51.9%>46.2%>42%). • At other injection rates, the performances of WAG, WF, and GI were similar.	[171]
2015	CO_2-IWAG	s	5	2.5-8.2	1:1	65	3.5	Crude	NaCl (5 g/l), Formation (174.2 g/l), Sea water (54.7 g/l)	CO_2	Grey Berea (D=3.8 cm, L=50.8 cm)	62.1-79.2	17.6-19.1	61.6-64.6	• Aging changed wettability towards oil-wet and increased RF_{WF} from 22.7% to 51.6%. • Only with aging, LSW was beneficial. • RF_{WAG} using LSW was 61.7% which was less than that with sea water.	[130]
2015	SAG	s,t	2-5	0.4-4	1:1	NA	NA	Crude	Sea water (15.8, 30.8 g/l), 0.5% surf. sea water	CO_2	Berea (D=3.92 cm, L=14.96 cm) Reservoir (D=3.74 cm, L=9.01 cm)	113-120	19.8, 32.5	NA	• The stability of foam was more stable at higher injection rate and in small, but more frequent cycles.	[67]
2015	CO_2-WAG CO_2-PWAG	s,t	NA	0.2-3.5	NA	50	9, 12.8	Crude (North Burbank Unit)	Synthetic (183.8 g/l)	CO_2	Bernheimer (D=5.08 cm, L=15.24 cm)	13-1300	22-25	43.3-78.6	• Pressure affected RF more in immiscible condition. • Immiscible: RF_{PWAG} (60.4%) > RF_{WAG} (53.1%). • Miscible: RF_{PWAG} (63.0%) < RF_{WAG} (75.9%). • The effect of polymer additive was more in a highly heterogeneous core.	[72]
2015	CO_2-WAG WAG	t	NA	NA	NA	96	31	Crude (Azadegan)	Reservoir (200 g/l)	CO_2 N_2 APG	Core (D=3.8 cm, L=10 cm)	13.5-14	13-25	74-88.5	• RF_{WF}=52%. Four WAG scenarios: 1) RF_{N2}=74%, 2) RF_{CO2}=80%, 3) RF_{APG}=83%, 4) Hot water and APG (RF=88.5%)	[120]

In Table 2-1, the performance of WAG process is assessed through recovery factor or residual oil saturation and is compared to baselines such as stand-alone gas injection (GI) or waterflooding (WF) processes. Different attributes of the experimental works such as WAG process (type, recovery mode, number of cycles, slug size, water-to-gas ratio, temperature and pressure), WAG fluids (oil, gas, and brine), porous medium used (type of porous medium and its permeability and porosity ranges), and the WAG performance (recovery range and major conclusion remarks) are chronologically summarized.

2.8 FIELD AND PILOT APPLICATIONS OF WAG PROCESS

Prior to conducting a WAG project, it would be vital to have a comprehensive literature survey on its field application studies. In general, WAG injection is a mature EOR technology; so, there are numerous successful WAG projects in the North Sea, US, and Canada. The field and pilot studies of the WAG injection processes are summarized in Table 2-2. This section provides details on the realistic large-scale WAG projects across the world.

Table 2-2: WAG injection projects across the world.

Project/field	Year	Scale	Process	Objective	Ref.
Statfjord	1997	Field	WAG	Increased incremental oil recovery	19
Mangus	2002	Field	MWAG	Improved Areal and vertical sweep efficiency	172
Siri	1999	Field	SWAG	Increased oil recovery	173
Snorre	1997	Field	FAWAG	Improved gas sweep efficiency	56
Petrotrin	1999	Pilot	WASP	Increased oil recovery and reducing the capital cost	55
Dulang	2002	Pilot	IWAG	Increased oil recovery	174
Ivanic	2001	Pilot	MWAG	Increased oil recovery	175-176
Abu Dhabi	2005	Field	MWAG	Enhanced oil production	35
Cranfield	2015	Pilot	PAG	Improved water sweep efficiency	177
West Africa	2009	Pilot	WAG	Reduced gas flaring and improve oil recovery	178
Lagocinco	2000	Pilot	IWAG	Increased oil production	179
Abu Dhabi	2007	Pilot	IWAG	Increased sweep efficiency and optimize oil recovery	180

Christensen et al. reviewed WAG field projects from 1957 to 1996 where the main process and reservoir characteristics influencing the performance of successful and unsuccessful projects are systematically discussed [6]. USA with 37 WAG field projects (in the period 1957 to 1996) has the highest number of executed WAG injection projects [6]. Many other WAG projects with various injection strategies are performed after 1996. Offshore (such as in North Sea) WAG injection has different prospects in terms of equipment requirement, and drilling and operating expenses. Awan et al. reviewed EOR projects (including WAG) in the North Sea fields during the period 1975 to 2005 [13]. In 1997, Statfjord field experienced a pilot scale WAG injection in Brent reservoir in the North Sea [13]. Achieving successful

results, the project was extended to the entire oilfield. At the beginning, the recovery factor was 56 % and the water cut was 70 % in the Statfjord field. Over five years of WAG injection, the water cut was reduced (from 90 % to 20 % in some wells), and increase of the oil recovery rate and GOR were experienced [13]. In 2002, a field-scale immiscible WAG injection was implemented in an isolated sub-block part of the Dulang field for the first time [174]. The main objectives of this pilot test were to verify the contribution of IWAG in improved sweep efficiency, to obtain optimal conditions for the design and operation of WAG processes, and to determine the magnitudes or/and typical ranges of recovery factor and capital and operating costs. The results obtained from the water and gas tracers' injection tests indicated the possibility of high flow transmissibility between the wells, and a reasonable increase in the oil recovery factor (by 7 %) and production rate. The Dulang field was recognized as a good potential to experience the WAG injection approach after these promising results [174]. In 2003, the first WAG cycle in the sandstone Ivanic pilot at Croatia oilfield was examined where the CO_2 injection rate was 50000 m^3/day and the injection rate of water was 160 m^3/day after six months of continuous CO_2 injection [175-176]. The pilot study was run to evaluate the oil recovery after five cycles (6 months of CO_2 injection and 6 months of water injection) over 19.5 years. Due to the financial problems, the pilot test was stopped after two WAG cycles; however a decision was made to establish a full-field project [175-176]. In 2005, an enriched hydrocarbon WAG injection was implemented in a heterogeneous, low dipping, and tight carbonate oil reservoir in Abu-Dhabi onshore oilfield, in UAE [35]. The tests and observations did not show early gas breakthrough, asphaltene deposition, and corrosion while operating the project. The only main problem was the injectivity loss during the waterflooding which was compensated through increasing the injection pressure. Although, no recovery factor was reported for this project, an increase in the oil recovery by 10 % was expected [35]. Kong et al. conducted pilot tests of Polymer Assistant Gas (PAG) and WAG injection in Cranfield reservoir located in Mississippi, USA, featuring a gas cap, an oil ring, and a water leg at various depths [177]. They employed a commercial chemical flooding simulator (e.g., CMG-STARS) to simulate polymer and CO_2 flooding. Hybrid approaches of WAG and PAG injection were applied by injecting water (or polymer) and CO_2 with the ratio of 1:1 where the duration of each cycle was three months. According to their results, PAG with recovery factor of 74 % outperformed the WAG injection with 68 % recovery factor and CO_2 flooding with 59 % recovery factor. The higher recovery factor of PAG was attributed to the reduction of the reservoir pressure that leads to less injection volumes of water and CO_2 fluids [177]. A WAG pilot was established in a down-dip injector located in offshore West Africa to decrease the flare gas release (to environment) and to enhance the oil recovery [178]. Through alteration of a water injection well to WAG injector, the WAG process

successfully attained the project goals in which the water cut and oil recovery curves were monitored over the project. After successful implementation of this pilot test, the down-dip water injectors were changed to WAG injectors and this change caused promising recovery performance [178]. Based on a study conducted by Hinderaker and Njaa, the ultimate recovery factor of the Norwegian WAG/gas injection projects was in the range of 53 % to 66 %; a total oil production of 2012 to 2026 MMSTB was achieved through utilizing WAG technique [181]. A pilot N_2-WAG injection was conducted in Lake Maracaibo field with a light oil and an increase of 4.4 % STOOIP was achieved compared to the waterflooding. It was also concluded that hydrocarbon-WAG (75 % of methane) operation has a greater performance due to stronger swelling effects and higher solubility in oil, compared to the N_2-WAG strategy. The project caused a 2-3 % improvement in oil recovery at the field scale [179]. In 2007, a gas injection process in a carbonate reservoir in an onshore Abu-Dhabi oilfield was converted to a WAG pilot test with 3-month cycles [180]. With the aid of extensive monitoring programs (e.g., BHCIP, PBU, and PFO), the simulation results demonstrated a significant improvement (up to approximately 68 % in some wells)in the sweep efficiency through implementation of WAG approach over five years [180].

2.9 SIMULATION/MODELING AND OPTIMIZATION OF WAG

The theoretical aspect of WAG process has been studied through extensive modeling and optimization works, including analytical, numerical, empirical, stream-line, forecasting, data-driven, pore-scale simulation, and optimization of WAG processes. According to the literature, researchers investigated the effects of different variables such as cyclic injection configuration, [87, 166, 182-190] WAG ratio, cycle volume, wettability [182, 188, 191-192], hysteresis, relative permeability, capillary pressure [38, 87, 97, 185, 188, 190-196], gravity segregation [190], capillary instability [166, 197], petrophysical properties [97, 186, 192], heterogeneities [87, 166, 182, 187, 190-193, 198], miscibility [87, 185-186, 189, 193, 199-200], compositional effects [87, 194, 199, 201], operating conditions such as temperature, pressure and injection rate [87, 185, 187, 189, 192, 198-200, 202], well pattern [200], scaling [97, 192], initial water saturation [190], and asphaltene precipitation [202]. Pore scale simulations of the WAG process have also been investigated since 2002 [158, 192, 203-204]. In this review, we will discuss more about the macroscopic modeling of WAG. The macroscopic mathematical modeling of WAG is conventionally based on the Muskat extension [36] of Darcy's law in the context of Reimann's problem of three-phase flow in porous media. There has been a strong debate in the literature regarding the analytical solution of the three-phase flow using the Muskat method [205]. Some researchers suggested that the three-phase relative permeability models such as Stone 1[206] model will result in the loss of hyperbolicity in particular ranges of fluids saturation. Juans and Patzek [205] argue that a physically realistic three-phase flow in porous media should have hyperbolic nature. Therefore, such relative permeability models will

result in a mathematical model that does not capture the physics of three-phase flow in porous systems. A review on the comparison of various formulations of the three- phase flow in porous media is given by Chen and Ewing [37]. The mathematical modeling of a conventional WAG process is more challenging than continuous three-phase flow in porous media due to its cyclic nature. In the WAG simulation, the relative permeability to a specific phase depends on: 1) the saturation history of the displacement process (drainage or imbibition), and 2) the chronologic cycle history [97] in which each cycle has the scanning curves for the saturation-increasing and saturation-decreasing paths [201] .An excellent review of the three-phase relative permeability models that can be applied in WAG process has been recently provided by Beygi et al. [201].

Current WAG simulations with the three-phase hysteresis models of relative permeability and capillary pressure still suffer from mass transfer ignorance between phases (near miscible), especially when one phase disappears [195, 201] . The compositional effects also become important in determination of equilibrium parameters (such as end-point saturations in relative permeability models); dynamic tuning of the WAG simulation parameters may become inevitable when the oil phase evaporates or absorbs the injected gas [185, 207] . In a WAG simulation, the three- phase hysteresis is found to affect the relative permeability of the non-wetting phase more than that of the wetting and intermediate wetting phases [185] ; however, the three- phase hysteresis effects become less important in the MWAG injection (compared to IWAG) [87] . A comprehensive review of the experimental studies on three- phase flow relative permeability measurements is given by Alizadeh and Piri [208], which can be used as the input data/function for simulation studies on WAG.

In the following, we report a brief progress in the development of numerical simulation studies of WAG. Larsen and Skauage [38] proposed a methodology in the simulation of WAG, by integrating the three-phase hysteresis models with the three- phase flow model in porous media. They demonstrated that the two-phase hysteresis models are not able to explain some features such as irreversible hysteresis loops which are observed in the relative permeability behavior. New correlations for three- phase relative permeability were also introduced. They were able to correctly capture characteristics of the WAG processes such as increased oil recovery and decreased gas mobility due to the three- phase hysteresis effects. They found that the WAG models that utilize the three- phase relative permeability models (and three phase hysteresis) predict a higher oil recovery factor (and consequently more accurate values), compared to those models without a hysteresis model or with a two-phase hysteresis model. Egermann et al. [97] simulated the WAG process based on three- phase relative permeability hysteresis models. In agreement with their experiments, they found that the two- phase hysteresis models cannot capture the

performance of three- phase flow in a cyclic process such as WAG. They proposed a methodology to modify the relative permeability formulations proposed by Land [99], in which the hysteresis effect was attributed to the pore structure of the porous medium only without including the hysteresis effects of the process (imbibition/drainage). This modification was performed by using different constants in the Land model to account for the irreversibility of relative permeability scans. Using Implicit Pressure Explicit Saturation (IMPES) simulation of WAG, they concluded that the three- phase hysteresis influences the non-wetting phase more and it does not considerably affect the wetting phase. The ratio of vertical to horizontal permeability was found to significantly influence the WAG performance. Fayers et al. [209] suggested a procedure to calculate the three- phase relative permeability and capillary pressure models and they used it to simulate the three- phase flow with applications to WAG. They used Baker's [210] relative permeability model and modified it to include the saturation of all phases in the three- phase relative permeability model, considering the compositional effects. Hajizadeh et al. [186] simulated a field scale miscible WAG injection in Mangus field. They first simulated a fine grid block. After upscaling, they used the Todd and Longstaff formulation [211] to account for the miscibility condition in WAG. Klov et al. [192] conducted multi-scale modeling of WAG. They proposed a mathematical framework for pore-to-field scale modeling, and applied it to Etive formation in North Sea. The input parameters to the field-scale simulation (such as relative permeability and capillary pressure) were initially obtained through pore-scale modeling which was tested for 11 different rock types. Upon steady-state up-scaling, the properties of facies scale heterogeneities were obtained. They utilized the effective relative permeability and capillary pressure curves through standard saturation weighted model that relied on two- phase relative permeability models. This framework allowed them to avoid using history matching to obtain the parameters of the input models. The framework was successfully tested in the Etive formation. Heermans et al. [187] conducted mathematical modeling of WAG in fractured porous media. They performed 2D fine grid simulations using the dual porosity model and a transfer function to account for matrix-fracture flow communication in a proxy model. They found that the shape factor used in the transfer function is significantly affected by the reservoir properties and injection type. After conducting scaling analysis, they concluded that the effective permeability to phases, and matrix and fracture permeability values contribute the most to the recovery achieved by WAG. Skauge and Dale [196] reviewed the progress in the modeling of WAG, focusing on three- phase capillary pressure and three- phase hysteresis models. They proposed a methodology to obtain the three-phase capillary pressure model from two- phase capillary pressure data. A better match was attained (in the simulation of WAG) when the three- phase capillary pressure model was included. Moreover, the inclusion of capillary pressure

resulted in an increase in the oil relative permeability and a decrease in the relative permeability of the injected fluid. The simulation study was then able to predict the shape of recovery plot, breakthrough time, and injection pressure better. Hustad and Browning [193] conducted implicit compositional simulations of WAG where the three- phase hysteresis is included. The relative permeability and capillary pressure were allowed to correlate to all three saturations, and three sets of saturations in the hysteresis model were used. Both hysteresis and hydrocarbon miscibility were considered and the end-points in the models (relative permeability and capillary pressure) were allowed to change dynamically by capillary number scaling to account for the compositional effects. The model was tested in water-wet and mixed-wet media, and the proposed model was found to improve the recovery results. Shahverdi and Sohrabi [190] conducted IMPES simulations of WAG with focus on the effect of gravity segregation. When the gravity segregation was included in the simulations, it decreased the total mobility; it was more pronounced in WAG with a smaller volume of the injected fluids. Duchenne et al. [185] adopted the mathematical modeling framework of Larsen and Skuage [38] in simulation of WAG and developed an optimization algorithm to obtain the parameters of three- phase relative permeability models, based on two sets of experiments. They argued that the history matching should be conducted simultaneously for all experiments (at different conditions) and not for individual experiments. The simulation results were validated by the coreflood tests at near miscible conditions in sandstone cores. It was found that simultaneous optimization (history matching) tends to better results. Streamline (also called front-tracking) methods have also been used for the modeling of three - phase flow in porous media that in general combine analytical solution to Riemann problem [205] with a front tracking method [212]. Researchers have also implemented the streamline method for modeling of WAG processes [200, 213].

A summary of the studies that were found in the literature on experimental (in cores, sand-packs, and micromodels), and theoretical (macro- and pore-scale mathematical modeling, simulation) aspects of WAG is summarized in Table 2-3. This table is organized to chronologically show the focus of each study including the four categories of 1) fluid properties, 2) reservoir properties, 3) operating conditions and 4) pore-scale mechanisms. In the miscibility condition, M, I and nM are used for miscible, immiscible and near miscible conditions.

Table 2-3. Summary of literature works on WAG with their focus of study.

Effect	Year	Variable(s) studied	Process	Miscibility*			Porous Medium	Scale	Ref.
				M	I	nM			
Fluid properties	1993	Mobility control	CGI, WAG, SWAG	M	-	-	Sandstone	Pilot	45
	2005	Brine composition and miscibility	WAG, CGI	M	I	-	Berea sandstone	Experimental	8
	2006	Gas type (N_2, CO_2, enriched gas)	WAG	-	I	-	Sand pack	Experimental	165
	2010	Brine composition	WAG	M	-	-	Berea sandstone	Experimental	126
	2010	Salinity	WAG, PWAG	-	I	-	Sandstone	Experimental	68
	2012	Gas type (N_2, CO_2)	WAG, CGI	M	I	-	Carbonate	Experimental	121
	2013	Salinity	WAG	M	-	-	Sandstone	Experimental	170
	2014	Salinity	CGI, WAG, SWAG	M	I	-	Carbonate	Modeling	129
	2014	Salinity	WAG	M	-	-	Carbonate	Compositional Simulator	132
	2014	Gas type (N_2)	SAG, WAG, WF, CGI	-	I	-	Sand pack	Experimental	119
	2015	Salinity	WAG	-	I	-	Berea sandstone	Experimental	130
	2015	Salinity	WAG	M	-	-	-	Simulation (CMG-STAR)	131
	2015	Gas type (N_2, CO_2, associated gas)	WAG	M	-	-	Sandstone	Experimental	120
	2015	Gel treatment	WAG	-	I	-	-	Simulation	214
	2016	Salinity	WAG	M	-	-	Carbonate	Compositional Simulator	215
Petrophysical properties	1982	Heterogeneity	CGI, WAG	M	-	-	-	Simulation (Todd, Dietrich)	81
	1985	Wettability	WAG, CGI	M	-	-	Bead-pack	Experimental	162
	1988	Wettability	WAG, CGI	M	-	-	Sandstone	Experimental	40
	2000	k_r	WAG	M	-	-	Sandstone	Simulation	91
	2003	k_r	WAG	-	I	-	Berea Sandstone	Experimental	98
	2004	Vertical gas sweep	SWAG	M	I	-	-	Simulation (quasi steady-state)	216
	2005	k_r hysteresis	WAG	-	I	-	Berea sandstone	Simulation (ECLIPSE 100)	101
	2005	k_r, injection loss	WAG	-	I	-	Glass micromodel	Experimental	156
	2009	Optimal parametric design	WAG	M	-	-	-	Simulation	22
	2011	Wettability	WAG, CGI, WF	-	-	nM	Sandstone	Experimental	167
	2011	k_r hysteresis, P_c, wettability	WAG	-	I	-	-	Network modelling	217
	2013	k_r, Hysteresis, wettability	WAG	-	I	-	Sandstone	Experimental and simulation	102
	2013	k_r	WAG	M	I	-	-	Simulation	87
	2014	Heterogeneity, K	WAG, PAG, CGI	M	-	-	-	Simulation (ECLIPSE 100)	70
	2014	Relative permeability, wettability	WAG	M	-	-	-	Experimental	109
Operational parameters	1985	WAG ration, wettability	WAG, CGI	M	-	-	Bead-pack	Experimental	162
	1991	WAG ratio	WAG, CGI	M	-	-	Berea Sandstone	Experimental	108
	1992	WAG ratio	WAG, CGI	M	-	-	Berea Sandstone	Experimental	163
	1999	WAG ratio	WAG	M	-	-	Sandstone, carbonate	Experimental	163
	2001	WAG ratio and slug size	WAG	M	-	-	Sandstone	Simulation	186
	2003	WAG ratio, flow rate	WAG	M	-	-	Bead-pack	Experimental	143
	2003	WAG ratio and flow rate	WAG	M	-	-	Glass bead pack	Experimental	143
	2005	Injection pattern	WAG	M	-	-	Carbonate	Modelling	218
	2007	WAG ratio, viscous fingering	WAG	M	-	-	-	Experimental	219
	2010	Heated WAG	Heated WAG	-	I	-	Sand pack	Experimental	220
	2010	Slug ratio	WAG, CGI, WF	-	I	-	-	Experimental	169
	2011	Cycle time and slug size	WAG, CGI, WF	M	-	-	-	Simulation (E100, E300)	135
	2012	Tapering	WAG	-	I	-	-	Experimental	124
	2014	Injection rate	WAG, CGI, WF	-	I	-	Carbonate	Experimental	171
	2015	Injection pattern	WAG	-	I	-	Carbonate	Simulation (ECLIPSE)	139
	2015	Injection rate, WAG ratio, slug size	WAG	M	-	-	Berea sandstone	Simulation	221
	2016	Injection pattern, injection rate	WAG	M	-	-	Limestone	Field operation	222
	2016	Injection rate	WAG, SWAG	-	I	-	Carbonate	Simulation (ECLIPSE 100)	223
	2016	Tapering	WAG	-	I	-	-	Simulation	153
Pore-scale mechanisms	2005	Three phase flow mechanisms	WAG	M	-	-	Glass micromodel	Experimental	154
	2000	Visualization of three phase flow	WAG	-	I	-	Glass micromodel	Experimental	155
	2006	k_r, hysteresis, wettability	WAG	-	I	-	Berea sandstone	Pore Network modelling	158
	2002	Three phase flow processes	WAG	-	I	-	Glass micromodel	Network modelling, Experim.	159
	2011	Three phase flow processes	WAG	-	I	-	Berea Sandstone	Pore Network modelling	160
	2013	k_r, P_c	WAG	-	I	-	Berea Sandstone	Pore Network modelling	224
	2008	Pore scale fluid distribution	SWAG	-	-	nM	Glass micromodel	Experimental	110
	2005	Oil displacement mechanisms	WAG	-	I	-	Sandstone, micromodel	Simulation, Experimental	225
	2014	Recovery enhancement using nano-particles	WAG	-	I	-	Glass micromodel	Experimental	226
	2014	Miscibility, IFT, wettability	WAG	-	-	nM	Carbonate	Experimental	227

* M=Miscible, I=Immiscible and nM=near Miscible

2.10 THEORETICAL AND PRACTICAL CHALLENGES OF WAG IMPLEMENTATION

2.10.1 Field Challenges

Operating an EOR/IOR project in any scale (field, pilot or lab) is always associated with numerous limitations and challenges. In WAG injection processes, process and thermodynamic conditions of both water flooding and gas injection affect the production efficiency. Generally, the major practical challenges in most field applications of WAG can be classified as follows:

- Early breakthrough [228-230],
- Injectivity loss [6, 73, 75, 82, 122, 222, 230-231],
- Corrosion [232-234],
- Asphlatene and hydration formation [6, 13 235-236].

Awan et al. reviewed the EOR technologies including WAG projects that were conducted in North Sea fields [13]. They briefly discussed about the experimental, techniques, and global statistical aspects of the EOR projects [13]. The operational problems and reported limitations of the WAG projects in the North Sea fields were discussed. The main issues were related to equipment such as compressor specification (e.g., compression of enriched gas) in Gullfake field during miscible WAG injection or tubing malfunction due to heating and injected gas expansion in Brage field [229]. In the Brage field, the gas breakthrough occurred after three months of WAG initiation, and a low sweep efficiency was observed in the next gas cycles [229]. The main reason for this problem was a thin and high permeable layer that behaved as a thief layer which linked the production and injection wells.

The availability of gas for gas cycles is also a challenge, such as that in Gullfaks field [237]. Due to gas availability and market price, a majority of the North Sea fields experience more gas injection in summer, compared to winter [237]. In Snorre field, the leakage of tubing annulus imposed a high cost in compressors' maintenance due to corrosion. Early breakthrough occurred due to the channeling of gas in high permeable layers. The issues reported above are the main operational problems during the HC miscible WAG injection [6, 230]. In Ekofisk field, the pilot operation was failed during SWAG injection because of hydrate formation [238-239]. The same EOR process was implemented in Siri field and the main problems for this Iranian field were unfavorable field characteristics (low horizontal permeability and porosity) and the injectivity problems [238-239]. During FAWAG operation in Snorre field (SnA-CFB), the major concerns were the injectivity of gas below the fracture pressure and the vertical connectivity of the layers that prevented the foam propagation [6, 230]. Injectivity loss corresponding to the reduction in injection

rates of gas slugs and water slugs was an initial concern in this project in both continuous gas and WAG injection processes [82, 231]. It has been reported that about 20 % of the reported water injectivity loss happen in the WAG injection projects [122]. Rogers et al. reviewed CO_2-WAG injectivity abnormalities, and systematically discussed the hypothesis and theories that create this phenomenon during CO_2-WAG injection [7]. They concluded that the factors affecting the injectivity of CO_2-WAG are oil bank mobility, water salinity and pH, wettability, dissolution, precipitation and invasion of fluids, fluid trapping or bypassing, relative permeability, reservoir heterogeneity, and phase behavior [7]. Ghahfarokhi et al. observed two types of CO_2-WAG injection patterns; 1) WAG-sensitive which is a general form of injectivity loss that occurred during above 150 injection patterns, and 2) WAG-insensitive which includes injectivity loss characterized by differences in injectivity profiles, Dykstra-Parson (DP) coefficient, and injectivity indexes. The WAG flow is not able to notably redistribute the flow injection profiles in high permeable and low heterogeneous regions of the reservoir. There is a high chance of injectivity loss problem in wells with DP coefficient of 0.81 or more and injectivity indexes of 10 bbl/psi/day or less. A decrease in Dykstra-Parson coefficient, production of oil, gas and water for WAG sensitive-wells was also noticed, while a majority of patterns were WAG-insensitive for which no production decline was noticed. It was recommended to design a longer CO_2 and shorter water cycles (drier WAG cycles) over CO_2-WAG injection operation for the wells with injectivity values lower than 10 bbl/day/psi [222]. One of the common challenges with the WAG injection is that the oil recovery rate significantly decreases with more WAG cycle injections due to a significant increase in the water saturation and reduction in oil phase discontinuity [154, 159, 204]. Although WAG can effectively controls the gas mobility, highly heterogeneous reservoirs still challenge this recovery technology. Choi et al. suggested gel treatment during CO_2-WAG injection to overcome unfavorable sweep efficiency as a result of gravity override effect and the channeling problem caused by inappropriate mobility ratio between oil and CO_2 [214]. These unfavorable conditions decrease the sweep efficiency that leads to low recovery factor [214]. They simulated the hybrid gel treatment with CO_2-WAG injection, using dynamic gel viscosity in a heterogeneous heavy oil reservoir. To quantify the extent of permeability reduction by gel treatment, the following equation was introduced by Lake et al., which is called Residual Resistant Factor (RRF):

$$RRF_w = \frac{(\frac{k_w}{\mu_w})_{initial}}{(\frac{k_w}{\mu_w})_{final}} \quad (2\text{-}15)$$

The $(k_w / \mu_w)_{initial}$ and $(k_w / \mu_w)_{final}$ are the ratio of water permeability over water viscosity before and after gel treatment, respectively. Eq. (2-15) is an assessment tool to demonstrate the permanence of permeability reduction during polymer solution flooding [240]. The simulation results indicated 31 % improvement in the oil recovery by applying micro gel assisted WAG (considering dynamic gel viscosity), compared to traditional WAG injection because of better conformance (or displacement performance) and mobility control (e.g., reduction in oil viscosity) [214].

Another strategy to overcome unfavorable sweep efficiency and mobility ratio is Viscosity Reducing WAG (VR-WAG) injection which was developed to improve the recovery of viscos-oil reservoirs. This technique leads to mixing of heavy components of oil with produced lean gas to create Viscosity Reducing Injectant (VRI). This method reduces the oil viscosity up to 90% and improves the oil recovery factor by 15-20 % [241].

Generally, EOR techniques in fractured reservoirs are challenging for the petroleum industry. Due to early breakthrough and flow channeling in the fractures, the injected flow directly goes from the injection wells to the production wells. Chakravathy et al. suggested water viscosified with polymer to be injected directly into fractures in order to redirect the CO_2 flow to the matrix and to postpone the breakthrough [228]. They also recommended that a cross-linked gel can be used for the conformance control to overcome the water leak off to the matrix. The control and regulation of injection operational conditions in WAG are challenging, especially when CO_2 is injected in the gas cycles. Generally, the contact of CO_2 and water leads to corrosion of tubing, resulting in serious technical, environmental, and economic concerns [232].

2.10.2 Research Challenges and Problems

During WAG injection in a reservoir, two processes of imbibition and drainage are involved which take place sequentially; it results in complex saturation patterns as both gas and water saturations increase and decrease alternatively. Hence, a reliable modelling of WAG process requires a comprehensive knowledge on three-phase relative permeability and capillary pressure, including the saturation directions and cyclic hysteresis effects [151]. Several correlations for calculating the three-phase relative permeability are provided in the literature [8, 38]; however, they suffer in situations where the mass transfer between phases occurs and specially when one phase disappears. Dynamic effects due to the evaporation of residual oil and adsorption of injected gas in the residual oil also increase the complexities. Previous studies show a remarkable error in the performance of WAG obtained from simulations by applying inappropriate three- phase model parameters [90, 92, 101-102]. An accurate prediction of the three- phase

relative permeability data based on the rigorous and reliable models or experimental data is still remaining as a challenging issue. One of the challenges regarding the reservoir simulation of WAG injection at heterogeneous reservoirs is the sensitivity of the process to the K_v/K_h (vertical to horizontal permeability) ratio. For example, Jackson's simulation studies indicated that as the K_v/K_h ratio increases, the vertical displacement improves, while it adversely influences the overall oil recovery [162].

WAG simulation in the fractured carbonate reservoirs becomes computationally expensive due to the multiscale heterogeneities and matrix transfer mechanisms that should be involved through a detailed model with a large number of grid cells [182]. The connectivity of the fracture network and the variability in the matrix structure are two sources for uncertainties in fractured carbonate flow behavior in WAG injection [242-243]. For example, Agada used data-driven surrogate modelling technique which significantly lowers the computational cost for CO_2-WAG injection in a fractured carbonate reservoir through completing each model evaluation in 13.2 seconds, compared to 8.2 hour-time needed for numerical simulation runs, using the mathematical structure for three- phase flow in porous systems [182].

2.10.3 Economical and Practical Aspects

WAG injection was originally developed to control the mobility of gas phase in a porous medium during gas injection process; it is the second widely used EOR process with economic benefits [8]. Increased concerns over the greenhouse gas emissions lead to the evaluation and realization of CO_2 potential as a carbon storage technique. Previous studies on CO_2-EOR (WAG) projects suggest a promising feature because of low cost of CO_2 source, availability and high gas utilization efficiency (167-227 sm^3 CO_2/STB oil) [244]. With an increase in the global awareness about sustainability, global warming, and new environmental regulations, CO_2-EOR is receiving an increasing attention from energy industries [245].

It is believed that approximately two-third of the original oil is place is bypassed after primary and secondary recovery processes [246]. A recent report by the Department of Energy [247] suggests that the tertiary techniques of CO_2-EOR can recover an additional 20 % of the Initial Oil In Place (IOIP). If it is applied to all of the U.S reservoirs, this additional recovery is equivalent to 87.1 billion barrels. At an oil price of $70 per barrel and a CO_2 price of $45 per metric ton, 45 billion barrels oil can be potentially produced by the CO_2-EOR [247]. A sensitivity analysis on economic factors of the CO_2-WAG injection in a low permeable heterogeneous reservoir was conducted by Changlin-lin. Three configurations of WAG were suggested (allocation of injection rates, tapered Water-Alternate-Gas, and their combinations).

They investigated different cases for oil price varying between $50-$140 and found the peak in the Net Present Value (NPV) in the range of 2-4 years, depending on the oil price and CO_2 price [17].

2.11 CONCLUSIONS

WAG injection is a mature EOR/IOR technique with successful experiences in many projects from pore to field scales. Due to its proven performance, different variations of WAG were introduced by researchers to enhance its production characteristics through modifying the liquid phase, gas phase and operating conditions. This includes alternate processes such as Foam Assistant WAG (FAWAG), Simultaneous Water and Gas injection (SWAG), Polymer Alternating Gas (PAG) or Polymer Assistant WAG (PAWAG), and Water Alternating High Pressure Air Injection (WAHPAI). Despite extensive recent investigations on theoretical, experimental and mechanistic aspects of WAG, no comprehensive review is available in the literature. In this chapter, the effects of important variables on WAG performance (fluid properties, reservoir properties and operating conditions) are extensively studied and summarized. The pore-scale and field scale implementations are studied and important technical challenges are given. The following key conclusions are drawn based on this review.

- CO_2 is the most common gas used in the WAG operations and it has advantages over N_2 or O_2. The use of high-pressure air is also recently proposed due to its abundance.
- Brine composition and salinity are important parameters in WAG. Low salinity water injection has been recently proposed for the water cycles; although the performance of LSW in waterflooding is proven, its performance in WAG is controversial in the literature.
- Five-spot pattern is found the most common injection pattern employed in the WAG projects. However, it may result in poor volumetric sweep efficiency due to extensive upward gas migration. Horizontal wells may be alternatively used to overcome this problem.
- WAG injection at equal volumes of water and gas cycles (WAG ratio = 1:1) is preferred and results in optimal oil production. However, the WAG ratio does not influence the oil recovery performance in mixed-wet formations.
- The saturation history in individual drainage and imbibition processes, and the chronological cycle history of water and gas injection in the WAG will significantly affect the distribution of fluids in three-phase flow. Mathematical modeling of WAG demands the inclusion of these two types of three-phase hysteresis effects that if accounted, will increase the oil mobility and decrease the gas mobility, resulting in more realistic predictions.

- In both miscible and immiscible WAG recovery processes, an accurate relative permeability model is needed to determine reliable values of fluids distribution and production in the three phase flow in porous media. The relative permeability models become less accurate in near miscible conditions when mass transfer between the two phases occur. Due to the complexity of the WAG flow pattern, the classical techniques to obtain relative permeability may not be efficient.
- Wettability significantly controls the performance of WAG process. Optimal values of injection rate, WAG ratio, number of cycles, brine salinity and polymer additive concentration will be significantly affected by the wettability.
- Tapering (WAG ratio variation) is a potential strategy to control excessive gas production. It also reduces the response time and accelerates the oil bank, reaching the production wells.
- The most common challenges in WAG operation are early gas breakthrough, injectivity loss, corrosion, and the potential for asphaltene and hydration formation. Of potential solutions for those problems originated by the adverse mobility ratio include hybrid gel treatment, viscosity reduction WAG (VR-WAG), and polymer additives in water.

ACKNOLEDGEMENTS

The authors would like to acknowledge the financial support provided by Memorial University (NL, Canada), Natural Sciences and Engineering Research Council of Canada (NSERC), InnovateNL (formerly RDC), and Equinor Canada.

NOMENCLATURES

Acronyms

AOIR	Allocation Of Injection Rate
CGI	Continuous Gas Injection
CWAG	Chemically enhanced Water Alternating Gas
EOR	Enhanced Oil Recovery
FAWAG	Foam Assistant Water Alternating Gas
GI	Gas Injection
GWR	Gas Water Ratio
GOR	Gas Oil Ratios

HCPV	Hydrocarbon Pore Volume
IFT	Interfacial Tension
IOR	Improved Oil Recovery
IWAG	Immiscible WAG
LSWAG	Low Salinity WAG
LSWF	Low Salinity Water Flooding
MMP	Minimum Miscible Pressure
MRF	Mobility Reduction Factor
mw	Mixed-wet
NPV	Net Present Value
nMWAG	Near Miscible WAG
OOIP	Original Oil In Place
ow	Oil-wet
PWAG	Polymer WAG injection
PAG	Polymer Alternating Gas injection
RRF	Residual Resistant Factor
SAG	Surfactant alternating Gas injection
SWAG	Simultaneous Water And Gas
TWAG	Tapered WAG
VRR	Voidage Replacement Ratio
VRI	Viscosity Reduction Injectant
VDP	Dykstra-Parson permeability variation coefficient
WAG	Water Alternating Gas
WASP	Water Alternating Steam Process
ww	Water-wet

English letters

E	Total recovery efficiency
g	Gravity force
K	Permeability
L	Wells’ distance

M	Mobility ratio
N_{ca}	Capillary Number
$R_{v/g}$	Ratio of viscous force to gravity force
v	Darcy velocity
Greek letters	
μ	Viscosity
λ	Mobility
ρ	Density
σ	Interfacial tension

References

1. http://www.slb.com/services/technical_challenges/enhanced_oil_recovery.aspx.
2. Hustad, O. S.; Holt, T. In *Gravity stable displacement of oil by hydrocarbon gas after waterflooding*, SPE/DOE Enhanced Oil Recovery Symposium, Society of Petroleum Engineers: 1992.
3. Touray, S., EFFECT OF WATER ALTERNATING GAS INJECTION ON ULTIMATE OIL RECOVERY. **2013**.
4. Shpak, R. Modeling of Miscible WAG Injection Using Real Geological Field Data. Institutt for petroleumsteknologi og anvendt geofysikk, 2013.
5. Surguchev, L.; Korbol, R.; Haugen, S.; Krakstad, O. In *Screening of WAG injection strategies for heterogeneous reservoirs*, European Petroleum Conference, Society of Petroleum Engineers: 1992.
6. Christensen, J. R.; Stenby, E. H.; Skauge, A. In *Review of WAG field experience*, International Petroleum Conference and Exhibition of Mexico, Society of Petroleum Engineers: 1998.
7. Rogers, J. D.; Grigg, R. B., A literature analysis of the WAG injectivity abnormalities in the CO2 process. *SPE Reservoir Evaluation & Engineering* **2001,** *4* (05), 375-386.
8. Kulkarni, M. M.; Rao, D. N., Experimental investigation of miscible and immiscible Water-Alternating-Gas (WAG) process performance. *Journal of Petroleum Science and Engineering* **2005,** *48* (1), 1-20.
9. Knappskog, O. A. Evaluation of WAG injection at Ekofisk. University of Stavanger, Norway, 2012.
10. Pariani, G.; McColloch, K.; Warden, S.; Edens, D., An approach to optimize economics in a West Texas CO2 flood. *Journal of Petroleum Technology* **1992,** *44* (09), 984-1,025.
11. Sanchez, N. L. In *Management of water alternating gas (WAG) injection projects*, Latin American and Caribbean Petroleum Engineering Conference, Society of Petroleum Engineers: 1999.

12. Skauge, A.; Stensen, J. Å. In *Review of WAG field experience*, Oil Recovery–2003, 1st International Conference and Exhibition, Modern Challenges in Oil Recovery, 2003; pp 19-23.
13. Awan, A. R.; Teigland, R.; Kleppe, J., A survey of North Sea enhanced-oil-recovery projects initiated during the years 1975 to 2005. *SPE Reservoir Evaluation & Engineering* **2008,** *11* (03), 497-512.
14. Hinderaker, L.; Bygdevoll, J.; Bu, T.; Nybraten, G.; Krakstad, O. S. In *lOR Resource potential of Norwegian North Sea sandstone reservoirs*, IOR 1991-6th European Symposium on Improved Oil Recovery, 1991.
15. Panda, M.; Ambrose, J. G.; Beuhler, G.; McGguire, P. L., Optimized eor design for the Eileen west end area, Greater Prudhoe bay. *SPE Reservoir Evaluation & Engineering* **2009,** *12* (01), 25-32.
16. Kulkarni, M.; Rao, D. In *Experimental investigation of various methods of tertiary gas injection*, SPE annual technical conference and exhibition, Society of Petroleum Engineers: 2004.
17. Changlin-lin, L.; Xin-wei, L.; Xiao-liang, Z.; Ning, L.; Hong-na, D.; Huan, W.; Yong-ge, L. In *Study on Enhanced Oil Recovery Technology in Low Permeability Heterogeneous Reservoir by Water-Alternate-Gas of COFlooding*, SPE Asia Pacific Oil and Gas Conference and Exhibition, Society of Petroleum Engineers: 2013.
18. Caudle, B.; Dyes, A., Improving miscible displacement by gas-water injection. **1958**.
19. Crogh, N. A.; Eide, K.; Morterud, S. E. In *WAG injection at the statfjord field, a success story*, European Petroleum Conference, Society of Petroleum Engineers: 2002.
20. Tabatabaei Nezhad, S. A. R.; Rahimzadeh Mojarad, M.; Oskouei, P.; Javad, S.; Moghadas, J. S.; Farahmand, D. R. In *Experimental Study on Applicability of Water Alternating CO2 Injection in the Secondary and Tertiary Recovery*, International Oil Conference and Exhibition in Mexico, Society of Petroleum Engineers: 2006.
21. Bahagio, D., Ensemble Optimization of CO2 WAG EOR. **2013**.
22. Chen, S.; Li, H.; Yang, D.; Tontiwachwuthikul, P., Optimal parametric design for water-alternating-gas (WAG) process in a CO2-miscible flooding reservoir. *Journal of Canadian petroleum technology* **2010,** *49* (10), 75-82.
23. https://www.bp.com/content/dam/bp/pdf/energy-economics/statistical-review-2016/bp-statistical-review-of-world-energy-2016-full-report.pdf, **2016**.
24. Speight, J. G., *Enhanced recovery methods for heavy oil and tar sands*. Elsevier: 2013.
25. Shahverdi, H.; Sohrabi, M.; Fatemi, M.; Jamiolahmady, M., Three-phase relative permeability and hysteresis effect during WAG process in mixed wet and low IFT systems. *Journal of Petroleum Science and Engineering* **2011,** *78* (3), 732-739.
26. Ahmed, T., *Reservoir engineering handbook*. Gulf Professional Publishing: 2006.
27. Thakur, G. C.; Satter, A., *Integrated waterflood asset management*. PennWell Books: 1998.
28. Holm, L., Propane-Gas-Water Miscible Floods in Watered-out Areas of the Adena Field, Colorado. *Journal of Petroleum Technology* **1972,** *24* (10), 1,264-1,270.
29. Moffitt, P.; Zornes, D. In *Postmortem Analysis: Lick Creek Meakin Sand Unit Immiscible CO2 Waterflood Project*, SPE Annual Technical Conference and Exhibition, Society of Petroleum Engineers: 1992.

30. Watts, R. J.; Conner, W. D.; Wasson, J. A.; Yost, A. B. In *CO2 Injection for Tertiary Oil Recovery, Granny's Creek Field, Clay County, West Virginia*, SPE Enhanced Oil Recovery Symposium, Society of Petroleum Engineers: 1982.
31. Birarda, G. S.; Dilger, C. W.; McIntosh, I., Re-evaluation of the miscible WAG flood in the Caroline Field, Alberta. *SPE Reservoir Engineering* **1990,** *5* (04), 453-458.
32. Cuesta, J.; MERRITT, G. In *CAROLINE WAG PROJECT, INJECTIVITY AND INTERFERENCE TEST-A FIELD EXAMPLE*, JOURNAL OF CANADIAN PETROLEUM TECHNOLOGY, CANADIAN INST MINING METALLURGY PETROLEUM 101 6TH AVE SW, STE 320, CALGARY AB TZP 3P4, CANADA: 1982; pp 33-33.
33. Gharbi, R.; Peters, E.; Elkamel, A., Scaling miscible fluid displacements in porous media. *Energy & fuels* **1998,** *12* (4), 801-811.
34. Arogundade, O. A.; Shahverdi, H.-R.; Sohrabi, M. In *A study of three phase relative permeability and hysteresis in water alternating gas (WAG) injection*, SPE Enhanced Oil Recovery Conference, Society of Petroleum Engineers: 2013.
35. Figuera, L. A.; Al-Hammadi, K. E.; Amro, B.; Abdulla, A.; Aryani, A.; Mohamed, F. In *Performance Review and Field Measurements of an EOR-WAG Project in Tight Oil Carbonate Reservoir-Abu Dhabi Onshore Field Experience*, Abu Dhabi International Petroleum Exhibition and Conference, Society of Petroleum Engineers: 2014.
36. Muskat, M., Physical principles of oil production. **1981**.
37. Chen, Z.; Ewing, R. E., Comparison of various formulations of three-phase flow in porous media. *Journal of Computational Physics* **1997,** *132* (2), 362-373.
38. Larsen, J.; Skauge, A., Methodology for numerical simulation with cycle-dependent relative permeabilities. *SPE Journal* **1998,** *3* (02), 163-173.
39. Lyons, W. C.; Plisga, G. J., *Standard handbook of petroleum and natural gas engineering*. Gulf Professional Publishing: 2011.
40. Huang, E.; Holm, L., Effect of WAG injection and rock wettability on oil recovery during CO2 flooding. *SPE Reservoir Engineering* **1988,** *3* (01), 119-129.
41. Lin, E.; Poole, E., Numerical Evaluation of Single-Slug, WAG, and Hybrid CO2 Injection Processes, Dollarhide Devonian Unit, Andrews County, Texas. *SPE reservoir engineering* **1991,** *6* (04), 415-420.
42. Tanner, C.; Baxley, P.; Crump III, J.; Miller, W. In *Production performance of the Wasson Denver Unit CO2 flood*, SPE/DOE Enhanced Oil Recovery Symposium, Society of Petroleum Engineers: 1992.
43. Walker, J.; Turner, J., Performance of seeligson zone 20B-07 enriched-gas-drive project. *Journal of Petroleum Technology* **1968,** *20* (04), 369-373.
44. Attanucci, V.; Asbsen, K.; Wright, C., WAG process optimization in the rangely carbon dioxide miscible flood. *paper SPE* **1993,** *2662*.
45. Stephenson, D.; Graham, A.; Luhning, R. In *Mobility control experience in the Joffre Viking miscible carbon dioxide flood*, IOR 1991-6th European Symposium on Improved Oil Recovery, 1991.
46. Stephenson, D. J.; Graham, A. G.; Luhning, R. W., Mobility control experience in the Joffre Viking miscible CO2 flood. *SPE Reservoir Engineering* **1993,** *8* (03), 183-188.
47. Christensen, R. In *Carbonated waterflood results--Texas and Oklahoma*, Annual Meeting of Rocky Mountain Petroleum Engineers of AIME, Society of Petroleum Engineers: 1961.

48. Perez, J.; Poston, S.; Sharif, Q. In *Carbonated water imbibition flooding: an enhanced oil recovery process for fractured reservoirs*, SPE/DOE Enhanced Oil Recovery Symposium, Society of Petroleum Engineers: 1992.
49. Perez, J. M.; Poston, S.; Berg, R.; Friedman, M.; Gangi, A.; Nighswander, J. In *Improving the Potential to Produce Oil From Naturally Fractured Reservoirs*, International Petroleum Conference and Exhibition of Mexico, Society of Petroleum Engineers: 1994.
50. Shenawi, S.; Wu, C. In *Compositional Simulation of Carbonated Waterfloods in Naturally Fractured Reservoirs*, SPE/DOE Improved Oil Recovery Symposium, Society of Petroleum Engineers: 1994.
51. Shenawi, S.; Wu, C.; Jiang, C.; Luan, Z. In *A new iterative mathematical model for the analysis of imbibition carbonated waterflood in naturally fractured reservoirs*, Permian Basin Oil and Gas Recovery Conference, Society of Petroleum Engineers: 1994.
52. Hong, K.; Stevens, D. In *Water-alternating-steam process improves project economics at West Coalinga field*, Annual Technical Meeting, Petroleum Society of Canada: 1990.
53. DeFrancisco, S.; Sanford, S.; Hong, K. In *Utilizing WASP and Hot Waterflood to Maximize the Value of a Thermally Mature Steam Drive in the West Coalinga Field*, SPE Western Regional Meeting, Society of Petroleum Engineers: 1995.
54. Bautista, L.; Friedmann, F. In *Water-alternating-steam process (WASP) alleviates downdip steam migration in Cymric field*, SPE/DOE Improved Oil Recovery Symposium, Society of Petroleum Engineers: 1994.
55. Ramlal, V.; Singh, K. S., Success of Water-Alternating-Steam-Process for Heavy Oil Recovery at Petrotrin. **2000**.
56. Aarra, M.; Skauge, A.; Martinsen, H. In *FAWAG: A Breakthrough for EOR in the North Sea*, SPE Annual Technical Conference and Exhibition, Society of Petroleum Engineers: 2002.
57. Zuta, J.; Fjelde, I. In *Mechanistic modeling of CO2-foam processes in fractured chalk rock: effect of foam strength and gravity forces on oil recovery*, SPE enhanced oil recovery conference, Society of Petroleum Engineers: 2011.
58. Boud, D. C.; Holbrook, O. C., Gas drive oil recovery process. Google Patents: 1958.
59. Tunio, S. Q.; Chandio, T. A.; Memon, M. K., Comparative Study of FAWAG and SWAG as an Effective EOR Technique for a Malaysian Field. *Research Journal of Applied Sciences, Engineering and Technology* **2012,** *4* (6), 645-648.
60. Aarra, M.; Skauge, A., Status of Foam Applications in North Sea Reservoirs. *paper* **2000,** *22*, 19-22.
61. Hanssen, J.; Holt, T.; Surguchev, L. In *Foam processes: An assessment of their potential in North Sea reservoirs based on a critical evaluation of current field experience*, SPE/DOE Improved Oil Recovery Symposium, Society of Petroleum Engineers: 1994.
62. Skauge, A.; Aarra, M.; Surguchev, L.; Martinsen, H.; Rasmussen, L. In *Foam-assisted WAG: experience from the Snorre Field*, SPE/DOE Improved Oil Recovery Symposium, Society of Petroleum Engineers: 2002.
63. Skoreyko, F. A.; Villavicencio, A. P.; Rodriguez Prada, H.; Nguyen, Q. P. In *Understanding foam flow with a new foam EOR model developed from laboratory and field data of the naturally fractured cantarell field*, SPE Improved Oil Recovery Symposium, Society of Petroleum Engineers: 2012.
64. http://www.eor-alliance.com/solutions/foam/.

65. Aarra, M.; Skauge, A.; Sognesand, S.; Stenhaug, M., A foam pilot test aimed at reducing gas inflow in a production well at the Oseberg Field. *Petroleum Geoscience* **1996,** *2* (2), 125-132.
66. Batôt, G.; Delaplace, P.; Bourbiaux, B.; Pedroni, L.; Nabzar, L.; Douarche, F.; Chabert, M. In *WAG Management with Foams: Influence of Injected Gas Properties and Surfactant Adsorption*, Abu Dhabi International Petroleum Exhibition & Conference, Society of Petroleum Engineers: 2016.
67. Mohd Shafian, S.; Kamarul Bahrim, R.; Foo, Y.; Abdul Manap, A.; Tewari, R. In *Foam mobility control during WAG injection in a difficult reservoir with high temperature and high acid gas*, SPE Asia Pacific enhanced oil recovery conference, Society of Petroleum Engineers: 2015.
68. Zhang, Y.; Huang, S. S.; Luo, P., Coupling immiscible CO2 technology and polymer injection to maximize EOR performance for heavy oils. *Journal of Canadian Petroleum Technology* **2010,** *49* (05), 25-33.
69. Majidaie, S.; Khanifar, A.; Onur, M.; Tan, I. M. In *A simulation study of chemically enhanced water alternating gas (CWAG) injection*, SPE EOR Conference at Oil and Gas West Asia, Society of Petroleum Engineers: 2012.
70. Li, W.; Dong, Z.; Sun, J.; Schechter, D. S. In *Polymer-alternating-gas simulation: A Case Study*, SPE EOR Conference at Oil and Gas West Asia, Society of Petroleum Engineers: 2014.
71. Li, W.; Schechter, D. S. In *Using Polymer Alternating Gas to Maximize CO2 Flooding Performance*, SPE Energy Resources Conference, Society of Petroleum Engineers: 2014.
72. Tovar, F. D.; Barrufet, M. A.; Schechter, D. S. In *Experimental Investigation of Polymer Assisted WAG for Mobility Control in the Highly Heterogeneous North Burbank Unit in Oklahoma, Using Anthropogenic CO 2*, SPE Latin American and Caribbean Petroleum Engineering Conference, Society of Petroleum Engineers: 2015.
73. Latil, M., *Enhanced oil recovery*. Éditions Technip: 1980.
74. Donaldson, E. C.; Chilingarian, G. V.; Yen, T. F., *Enhanced oil recovery, II: Processes and operations*. Elsevier: 1989; Vol. 17.
75. Rogers, J. D.; Grigg, R. B. In *A literature analysis of the WAG injectivity abnormalities in the CO2 process*, SPE/DOE Improved Oil Recovery Symposium, Society of Petroleum Engineers: 2000.
76. Kulkarni, M. M. Immiscible and miscible gas-oil displacements in porous media. Citeseer, 2003.
77. Craig, F. F., *The reservoir engineering aspects of waterflooding*. HL Doherty Memorial Fund of AIME: 1971; Vol. 3.
78. Matthews, J.; Hawes, R.; Hawkyard, I.; Fishlock, T., Feasibility studies of waterflooding gas-condensate reservoirs. *Journal of petroleum technology* **1988,** *40* (08), 1,049-1,056.
79. Yokoyama, Y.; Lake, L. W. In *The effects of capillary pressure on immiscible displacements in stratified porous media*, SPE Annual Technical Conference and Exhibition, Society of Petroleum Engineers: 1981.
80. Sorbie, K.; Wat, R.; Rowe, T. In *Oil displacement experiments in heterogeneous cores: analysis of recovery mechanisms*, SPE Annual Technical Conference and Exhibition, Society of Petroleum Engineers: 1987.
81. Claridge, E. L., co2 Flooding Strategy in a Communicating Layered

Reservoir. *J. Pet. Tech* **Dec., 1982,** *2746-2756*.
82. Gorell, S. In *Implications of water-alternate-gas injection, for profile control and injectivity*, SPE/DOE Enhanced Oil Recovery Symposium, Society of Petroleum Engineers: 1990.
83. Fayers, F.; Blunt, M.; Christie, M. In *Accurate calibration of empirical viscous fingering models*, ECMOR II-2nd European Conference on the Mathematics of Oil Recovery, 1990.
84. Hanssen, J.; Norvik, H.; Card, J. In *Nitrogen Miscibility with North Sea Reservoir Fluids*, 4th Eur. Symp. on EOR, Hamburg, 1987; pp 1081-1092.
85. Jones, L.; Cullick, A.; Cohen, M. In *WAG Process Promises Improved Recovery in Cycling Gas Condensate Reservoirs: Part 1--Prototype Reservoir Simulation Studies*, SPE Gas Technology Symposium, Society of Petroleum Engineers: 1989.
86. Cullick, A.; Lu, H.; Jones, L.; Cohen, M.; Watson, J., WAG may improve gas-condensate recovery. *SPE reservoir engineering* **1993,** *8* (03), 207-213.
87. Zuo, L.; Chen, Y.; Dengen, Z.; Kamath, J., Three-Phase Relative Permeability Modeling in the Simulation of WAG Injection. *SPE Reservoir Evaluation & Engineering* **2014,** *17* (03), 326-339.
88. Aziz, K., and Settari, A., Petroleum Reservoir Simulation. *Elsevier, London.*
89. Dicarlo, D. A.; Sahni, A.; Blunt, M. J., The effect of wettability on three-phase relative permeability. *Transport in Porous Media* **2000,** *39* (3), 347-366.
90. Fenwick, D. H.; Blunt, M. J., Network modeling of three-phase flow in porous media. *SPE Journal* **1998,** *3* (01), 86-96.
91. Christensen, J.; Larsen, M.; Nicolaisen, H. In *Compositional simulation of water-alternating-gas processes*, SPE Annual Technical Conference and Exhibition, Society of Petroleum Engineers: 2000.
92. Delshad, M.; Pope, G. A., Comparison of the three-phase oil relative permeability models. *Transport in Porous Media* **1989,** *4* (1), 59-83.
93. Henderson, G.; Danesh, A.; Tehrani, D.; Al-Shaidi, S.; Peden, J., Measurement and correlation of gas condensate relative permeability by the steady-state method. *SPE Reservoir Evaluation & Engineering* **1998,** *1* (02), 134-140.
94. Harbert, L. In *Low interfacial tension relative permeability*, SPE Annual Technical Conference and Exhibition, Society of Petroleum Engineers: 1983.
95. Chen, H.; Wilson, S.; Monger-McClure, T. In *Determination of relative permeability and recovery for North Sea gas condensate reservoirs*, SPE Annual Technical Conference and Exhibition, Society of Petroleum Engineers: 1995.
96. Skauge, A.; Larsen, J. A. In *Three-phase relative permeabilities and trapped gas measurements related to WAG processes*, SCA 9421, proceedings of the International Symposium of the Society of Core Analysts, Stavanger, Norway, 1994.
97. Egermann, P.; Vizika, O.; Dallet, L.; Requin, C.; Sonier, F. In *Hysteresis in three-phase flow: experiments, modeling and reservoir simulations*, SPE European Petroleum Conference, Society of Petroleum Engineers: 2000.
98. Element, D.; Masters, J.; Sargent, N.; Jayasekera, A.; Goodyear, S. In *Assessment of three-phase relative permeability models using laboratory hysteresis data*, SPE International Improved Oil Recovery Conference in Asia Pacific, Society of Petroleum Engineers: 2003.

99. Land, C. S., Calculation of imbibition relative permeability for two-and three-phase flow from rock properties. *Society of Petroleum Engineers Journal* **1968,** *8* (02), 149-156.
100. Land, C. S. In *The optimum gas saturation for maximum oil recovery from displacement by water*, Fall Meeting of the Society of Petroleum Engineers of AIME, Society of Petroleum Engineers: 1968.
101. Spiteri, E. J.; Juanes, R., Impact of relative permeability hysteresis on the numerical simulation of WAG injection. *Journal of Petroleum Science and Engineering* **2006,** *50* (2), 115-139.
102. Shahverdi, H.; Sohrabi, M., Relative Permeability Characterization for Water-Alternating-Gas Injection in Oil Reservoirs. *SPE Journal* **2015**.
103. Anderson, W. G., Conoco Inc.,

Wettability Literature Survey- Part 1: Rock/Oil/Brine Interactions and the Effects of Core Handling on Wettability *13932-PA SPE Journal Paper* **1986**.
104. Basu, S.; Sharma, M. M. In *Defining the wettability state of mixed wet reservoirs: Measurement of critical capillary pressure for crude oils*, SPE Annual Technical Conference and Exhibition, Society of Petroleum Engineers: 1996.
105. Hirasaki, G., Wettability: fundamentals and surface forces. *SPE Formation Evaluation* **1991,** *6* (02), 217-226.
106. Morrow, N. R.; Lim, H. T.; Ward, J. S., Effect of crude-oil-induced wettability changes on oil recovery. *SPE Formation Evaluation* **1986,** *1* (01), 89-103.
107. Crocker, M.; Marchin, L., Wettability and adsorption characteristics of crude-oil asphaltene and polar fractions. *Journal of petroleum technology* **1988,** *40* (04), 470-474.
108. Stern, D. In *Mechanisms of miscible oil recovery: effects of pore-level fluid distribution*, SPE Annual Technical Conference and Exhibition, Society of Petroleum Engineers: 1991.
109. Shahrokhi, O.; Fatemi, M.; Sohrabi, M.; Ireland, S.; Ahmed, K. In *Assessment of three phase relative permeability and hysteresis models for simulation of water-alternating-gas (WAG) injection in water-wet and mixed-wet systems*, SPE Improved Oil Recovery Symposium, Society of Petroleum Engineers: 2014.
110. Sohrabi, M.; Danesh, A.; Jamiolahmady, M., Visualisation of residual oil recovery by near-miscible gas and SWAG injection using high-pressure micromodels. *Transport in Porous Media* **2008,** *74* (2), 239-257.
111. Sohrabi, M.; Tehrani, D.; Danesh, A.; Henderson, G., Visualization of oil recovery by water-alternating-gas injection using high-pressure micromodels. *SPE Journal* **2004,** *9* (03), 290-301.
112. Patel, P.; Christman, P.; Gardner, J., Investigation of unexpectedly low field-observed fluid mobilities during some CO2 tertiary floods. *SPE Reservoir Engineering* **1987,** *2* (04), 507-513.
113. Tiffin, D.; Yellig, W., Effects of mobile water on multiple-contact miscible gas displacements. *Society of Petroleum Engineers Journal* **1983,** *23* (03), 447-455.
114. Green, D.; Willhite, G., Enhanced oil Recovery, vol. 6. *SPE Textbook Series, TX, USA* **1998**.
115. Christian, L.; Shirer, J.; Kimbel, E.; Blackwell, R., Planning a Tertiary Oil-Recovery Project for Jay/LEC Fields Unit. *Journal of Petroleum Technology* **1981,** *33* (08), 1,535-1,544.

116. Greenwalt, W. A.; Vela, S.; Christian, L.; Shirer, J., A field test of nitrogen WAG injectivity. *Journal of Petroleum Technology* **1982,** *34* (02), 266-272.
117. Langston, E.; Shirer, J., Performance of Jay/LEC Fields Unit Under Mature Waterflood and Early Tertiary Operations. *Journal of petroleum technology* **1985,** *37* (02), 261-268.
118. Kirkpatrick, R.; Flanders, W.; DePauw, R. In *Performance of the Twofreds CO2 Injection Project*, SPE Annual Technical Conference and Exhibition, Society of Petroleum Engineers: 1985.
119. Salehi, M. M.; Safarzadeh, M. A.; Sahraei, E.; Nejad, S. A. T., Comparison of oil removal in surfactant alternating gas with water alternating gas, water flooding and gas flooding in secondary oil recovery process. *Journal of Petroleum Science and Engineering* **2014,** *120*, 86-93.
120. Ahmadi, Y.; Eshraghi, S. E.; Bahrami, P.; Hasanbeygi, M.; Kazemzadeh, Y.; Vahedian, A., Comprehensive Water–Alternating-Gas (WAG) injection study to evaluate the most effective method based on heavy oil recovery and asphaltene precipitation tests. *Journal of Petroleum Science and Engineering* **2015,** *133*, 123-129.
121. Ghafoori, A.; Shahbazi, K.; Darabi, A.; Soleymanzadeh, A.; Abedini, A., The experimental investigation of nitrogen and carbon dioxide water-alternating-gas injection in a carbonate reservoir. *Petroleum Science and Technology* **2012,** *30* (11), 1071-1081.
122. Hadlow, R. In *Update of industry experience with CO2 injection*, SPE annual technical conference and exhibition, Society of Petroleum Engineers: 1992.
123. Spivak, A.; Garrison, W. H.; Nguyen, J. P., Review of an immiscible CO2 project, tar zone, fault block V, Wilmington field, California. *SPE reservoir engineering* **1990,** *5* (02), 155-162.
124. Srivastava, J.; Mahli, L. In *Water alternating gas (WAG) injection a novel EOR technique for mature light oil fields a laboratory investigation for GS-5C sand of gandhar field*, A paper presented in biennial international conference and exposition in petroleum geophysics, Hyderabad, 2012.
125. van Batenburg, D. W.; De Zwart, A. H.; Doush, M. In *Water alternating high pressure air injection*, SPE Improved Oil Recovery Symposium, Society of Petroleum Engineers: 2010.
126. Jiang, H.; Nuryaningsih, L.; Adidharma, H. In *The effect of salinity of injection brine on water alternating gas performance in tertiary miscible carbon dioxide flooding: experimental study*, SPE Western Regional Meeting, Society of Petroleum Engineers: 2010.
127. Sharma, M.; Filoco, P., Effect of brine salinity and crude-oil properties on oil recovery and residual saturations. *SPE Journal* **2000,** *5* (03), 293-300.
128. Lager, A.; Webb, K. J.; Collins, I. R.; Richmond, D. M. In *LoSal enhanced oil recovery: Evidence of enhanced oil recovery at the reservoir scale*, SPE Symposium on Improved Oil Recovery, Society of Petroleum Engineers: 2008.
129. Al-Shalabi, E. W.; Sepehrnoori, K.; Pope, G. A. In *Modeling the combined effect of injecting low salinity water and carbon dioxide on oil recovery from carbonate cores*, International Petroleum Technology Conference, International Petroleum Technology Conference: 2014.
130. Ramanathan, R.; Shehata, A.; Nasr-El-Din, H. In *Water Alternating CO 2 Injection Process-Does Modifying the Salinity of Injected Brine Improve Oil Recovery?*, OTC Brasil, Offshore Technology Conference: 2015.

131. Yip, P. M.; Alta'ee, A. F., Simulation Study of the Effect of Smart Water on Relative Permeability During WAG-CO2 Injection for Light Oil Reservoir. In *ICIPEG 2014*, Springer: 2015; pp 109-120.
132. Dang, C. T.; Nghiem, L. X.; Chen, Z.; Nguyen, N. T.; Nguyen, Q. P. In *CO2 Low salinity water alternating gas: a new promising approach for enhanced oil recovery*, SPE Improved Oil Recovery Symposium, Society of Petroleum Engineers: 2014.
133. Jakupsstovu, S.; Zhou, D.; Kamath, J.; Durlofsky, L.; Stenby, E. H. In *Upscaling of miscible displacement processes*, Proceedings of the 6th Nordic Symposium on Petrophysics, 2001; pp 15-16.
134. Thomas, F.; Erian, A.; Chan, M.; Bennion, D.; Bennion, D.; Okazawa, T. In *Does miscibility matter in gas injection?*, Annual Technical Meeting, Petroleum Society of Canada: 1995.
135. Namani, M.; Kleppe, J. In *Investigation Of The Effect Of Some Parameters In Miscible WAG Process Using Black-Oil And Compositional Simulators*, SPE Enhanced Oil Recovery Conference, Society of Petroleum Engineers: 2011.
136. Skauge, A.; Sorbie, K. In *Status of Fluid Flow Mechanisms for Miscible and Immiscible WAG*, SPE EOR Conference at Oil and Gas West Asia, Society of Petroleum Engineers: 2014.
137. Sohrabi, M.; Danesh, A.; Tehrani, D. In *Oil recovery by near-miscible SWAG injection*, SPE Europec/EAGE Annual Conference, Society of Petroleum Engineers: 2005.
138. Sorbie, K.; van Dijke, M., Fundamentals of three-phase flow in porous media of heterogeneous wettability. *Institute of Petroleum Engineering, Heriot-Watt University, Edinburgh, Scotland* **2004**.
139. Barkhan, M. H.; Zargar, G.; Zakariyaei, S.; Jamal, S., STUDYING THE EFFECT OF INJECTION PATTERN ON WATER ALTERNATING GAS (WAG) INJECTION PROCESS USING ECLIPSE SIMULATOR SOFTWARE IN AN OIL RESERVOIR IN IRAN. *Petroleum & Coal* **2015,** *57* (3), 234-240.
140. Pritchard, D.; Georgi, D.; Hemingson, P.; Okazawa, T. In *Reservoir Surveillance Impacts Management, of the Judy Creek Hydrocarbon Miscible Flood*, SPE/DOE Enhanced Oil Recovery Symposium, Society of Petroleum Engineers: 1990.
141. Bou-Mikael, S. In *A New Analytical Method to Evaluate, Predict, and Improve CO2 Flood Performance in Sandstone Reservoirs*, SPE/DOE Improved Oil Recovery Symposium, Society of Petroleum Engineers: 1996.
142. Redman, R. S. In *Horizontal miscible water alternating gas development of the Alpine Field, Alaska*, SPE Western Regional/AAPG Pacific Section Joint Meeting, Society of Petroleum Engineers: 2002.
143. Al-Shuraiqi, H.; Muggeridge, A.; Grattoni, C. In *Laboratory investigations of first contact miscible WAG displacement: the effects of WAG ratio and flow rate*, SPE International Improved Oil Recovery Conference in Asia Pacific, Society of Petroleum Engineers: 2003.
144. Stalkup, F., Miscible Flooding Fundamentals. *Society of Petroleum Engineers Monograph Series* **1983,** *8*.
145. Bunge, A.; Radke, C., CO2 flooding strategy in a communicating layered reservoir. *Journal of Petroleum Technology* **1982,** *34* (12), 2,746-2,756.
146. Stalkup, F. I., Displacement of oil by solvent at high water saturation. *Society of Petroleum Engineers Journal* **1970,** *10* (04), 337-348.

147. Raimondi, P.; Torcaso, M. A., Distribution of the oil phase obtained upon imbibition of water. *Society of Petroleum Engineers Journal* **1964,** *4* (01), 49-55.
148. Christie, M.; Muggeridge, A.; Barley, J., 3D simulation of viscous fingering and WAG schemes. *SPE reservoir engineering* **1993,** *8* (01), 19-26.
149. Kootiani, R. C.; Samsuri, A. B., Analysis of First Contact Miscible WAG Displacement of the Effects of WAG Ratio and Flow Rate. *Am. J. Eng. Res* **2013,** *2* (12), 373-381.
150. Gorell, S. In *Modeling the effects of trapping and water alternate gas (WAG) injection on tertiary miscible displacements*, SPE Enhanced Oil Recovery Symposium, Society of Petroleum Engineers: 1988.
151. Shahverdi, H. Characterization of three-phase flow and WAG injection in oil reservoirs. Heriot-Watt University, 2012.
152. Masoner, L.; Abidi, H.; Hild, G. In *Diagnosing CO2 flood performance using actual performance data*, SPE/DOE Improved Oil Recovery Symposium, Society of Petroleum Engineers: 1996.
153. Khan, M. Y.; Kohata, A.; Patel, H.; Syed, F. I.; Al Sowaidi, A. K. In *Water Alternating Gas WAG Optimization Using Tapered WAG Technique for a Giant Offshore Middle East Oil Field*, Abu Dhabi International Petroleum Exhibition & Conference, Society of Petroleum Engineers: 2016.
154. Dong, M.; Foraie, J.; Huang, S.; Chatzis, I. In *Analysis of immiscible water-alternating-gas (WAG) injection using micromodel*, Canadian International Petroleum Conference, Petroleum Society of Canada: 2002.
155. Sohrabi, M.; Henderson, G.; Tehrani, D.; Danesh, A. In *Visualisation of oil recovery by water alternating gas (WAG) injection using high pressure micromodels-water-wet system*, SPE Annual Technical Conference and Exhibition, Society of Petroleum Engineers: 2000.
156. Sohrabi, M.; Jamiolahmady, M., Mechanism of Injectivity Loss During Water-Alternating-Gas (WAG) Injection. *Gas (C1+ nC10) 5* (7), 0.0209.
157. Sohrabi, M.; Tehrani, D.; Danesh, A.; Henderson, G. In *Visualisation of oil recovery by water alternating gas (WAG) injection using high pressure micromodels-oil-wet & mixed-wet systems*, SPE Annual Technical Conference and Exhibition, Society of Petroleum Engineers: 2001.
158. Suicmez, V. S.; Piri, M.; Blunt, M. J. In *Pore-scale modeling of three-phase WAG injection: Prediction of relative permeabilities and trapping for different displacement cycles*, SPE/DOE Symposium on Improved Oil Recovery, Society of Petroleum Engineers: 2006.
159. Van Dijke, M.; Sorbie, K.; Sohrabi, M.; Tehrani, D.; Danesh, A. In *Three-phase flow in WAG processes in mixed-wet porous media: pore-scale network simulations and comparison with micromodel experiments*, SPE/DOE Improved Oil Recovery Symposium, Society of Petroleum Engineers: 2002.
160. Al-dhahli, A.; Geiger, S.; van Dijke, M. I. In *Three-phase pore-network modelling for mixed-wet carbonate reservoirs*, SPE Reservoir Characterisation and Simulation Conference and Exhibition, Society of Petroleum Engineers: 2011.
161. Spence, A.; Ostrander, J. In *Comparison of WAG and Continuous Enriched-Gas Injection as Miscible Processes in Sadlerochit Core*, SPE Annual Technical Conference and Exhibition, Society of Petroleum Engineers: 1983.

162. Jackson, D.; Andrews, G.; Claridge, E. In *Optimum WAG ratio vs. Rock wettability in CO2 flooding*, SPE Annual Technical Conference and Exhibition, Society of Petroleum Engineers: 1985.
163. Zekri, A.; Natuh, A. In *Laboratory study of the effects of miscible WAG process on tertiary oil recovery*, Abu Dhabi Petroleum Conference, Society of Petroleum Engineers: 1992.
164. Nguyen, T.; Ali, S., Effect of nitrogen on the solubility and diffusivity of carbon dioxide into oil and oil recovery by the immiscible WAG process. *Journal of Canadian Petroleum Technology* **1998,** *37* (02).
165. Zhang, Y.; Sayegh, S.; Huang, S. In *Enhanced heavy oil recovery by immiscible WAG injection*, Canadian International Petroleum Conference, Petroleum Society of Canada: 2006.
166. Al-Mamari, F.; Al-Shuraiqi, H.; Al-Wahaibi, Y. M. In *Numerical simulation and experimental studies of oil recovery via first-contact miscible water alternating gas injection within shaley porous media*, SPE/EAGE Reservoir Characterization and Simulation Conference, Society of Petroleum Engineers: 2007.
167. Fatemi, S. M.; Sohrabi, M.; Jamiolahmady, M.; Ireland, S.; Robertson, G. In *Experimental investigation of near-miscible water-alternating-gas (WAG) injection performance in water-wet and mixed-wet systems*, Offshore Europe, Society of Petroleum Engineers: 2011.
168. Jiang, H.; Nuryaningsih, L.; Adidharma, H. In *The Influence of O2 Contamination on MMP and Core Flood Performance in Miscible and Immiscible CO2 WAG*, SPE Improved Oil Recovery Symposium, Society of Petroleum Engineers: 2012.
169. Torabi, F.; Jamaloei, B. Y.; Zarivnyy, O.; Paquin, B.; Rumpel, N., The evaluation of variable-injection rate waterflooding, immiscible CO2 flooding, and water-alternating-CO2 injection for heavy oil recovery. *Petroleum Science and Technology* **2012,** *30* (16), 1656-1669.
170. Zolfaghari, H.; Zebarjadi, A.; Shahrokhi, O.; Ghazanfari, M. H., An Experimental Study of CO2-low Salinity Water Alternating Gas Injection in Sandstone Heavy Oil Reservoirs. *Iranian Journal of Oil & Gas Science and Technology* **2013,** *2* (3), 37-47.
171. Jafari, M., Laboratory Study for Water, Gas and WAG Injection in Lab Scale and Core Condition. *Pet. Coal* **2014,** *56* (2), 175-181.
172. Erbas, D.; Dunning, M.; Nash, T. M.; Cox, D.; Stripe, J. A.; Duncan, E. In *Magnus WAG Pattern Optimization Through Data Integration*, SPE Improved Oil Recovery Symposium, Society of Petroleum Engineers: 2014.
173. Berge, L. I.; Stensen, J. Å.; Crapez, B.; Quale, E. A. In *SWAG injectivity behavior based on siri field data*, SPE/DOE Improved Oil Recovery Symposium, Society of Petroleum Engineers: 2002.
174. Nadeson, G.; Anua, N. A. B.; Singhal, A.; Ibrahim, R. B. In *Water-alternating-gas (WAG) pilot implementation, a first EOR development project in Dulang field, offshore Peninsular Malaysia*, SPE Asia Pacific Oil and Gas Conference and Exhibition, Society of Petroleum Engineers: 2004.
175. Novosel, D. In *Initial results of WAG CO2 IOR pilot project implementation in Croatia*, SPE International Improved Oil Recovery Conference in Asia Pacific, Society of Petroleum Engineers: 2005.

176. Novosel, D. In *Thermodynamic Criteria and Final Results of WAG CO2 Injection in a Pilot Project in Croatia*, SPE Middle East Oil and Gas Show and Conference, Society of Petroleum Engineers: 2009.
177. Kong, X.; Delshad, M.; Wheeler, M. F. In *A Numerical Study of Benefits of Adding Polymer to WAG Processes for a Pilot Case*, SPE Reservoir Simulation Symposium, Society of Petroleum Engineers: 2015.
178. Choudhary, M. K.; Parekh, B.; Dezabala, E.; Solis, H. A.; Pujiyono, P.; De Narvaez, Z.; Zambrano, J. In *Design, Implementation and Performance of a Down-Dip WAG Pilot*, International Petroleum Technology Conference, International Petroleum Technology Conference: 2011.
179. Alvarez, C.; Manrique, E.; Alvarado, V.; Saman, A.; Surguchev, L.; Eilertsen, T. In *WAG pilot at VLE field and IOR opportunities for mature fields at Maracaibo Lake*, SPE Asia Pacific Improved Oil Recovery Conference, Society of Petroleum Engineers: 2001.
180. Al Shamsi, H. A.; Al-Katheeri, A. B.; Al Ameri, A. F.; Abdulrahman, A. S.; Sajeel, K.; Al Yaaqoobi, A. In *Immiscible WAG Injection Pilots Performance and Lessons Learnt in Carbonate Reservoir. Onshore Abu Dhabi Oil Field, United Arab Emirates*, Abu Dhabi International Petroleum Conference and Exhibition, Society of Petroleum Engineers: 2012.
181. Hinderaker, L.; Njaa, S. In *Utilization of Associated Petroleum Gas (APG)-The Norwegian Experience*, SPE Russian Oil and Gas Conference and Exhibition, Society of Petroleum Engineers: 2010.
182. Agada, S.; Geiger, S.; Elsheikh, A.; Oladyshkin, S., Data-driven surrogates for rapid simulation and optimization of WAG injection in fractured carbonate reservoirs. *Petroleum Geoscience* **2017,** *23* (2), 270-283.
183. Bequette, B. W., Nonlinear control of chemical processes: A review. *Industrial & Engineering Chemistry Research* **1991,** *30* (7), 1391-1413.
184. Chen, B.; Reynolds, A. C. In *Ensemble-Based Optimization of the WAG Injection Process*, SPE Reservoir Simulation Symposium, Society of Petroleum Engineers: 2015.
185. Duchenne, S.; de Loubens, R.; Petitfrere, M.; Joubert, T. In *Modeling and Simultaneous History-Matching of Multiple WAG Coreflood Experiments at Reservoir Conditions*, Abu Dhabi International Petroleum Exhibition and Conference, Society of Petroleum Engineers: 2015.
186. Haajizadeh, M.; Narayanan, R.; Waldren, D. In *Modeling Miscible WAG Injection EOR in the Magnus Field*, SPE Reservoir Simulation Symposium, Society of Petroleum Engineers: 2001.
187. Heeremans, J. C.; Esmaiel, T. E.; Van Kruijsdijk, C. P. In *Feasibility study of WAG injection in naturally fractured reservoirs*, SPE/DOE Symposium on Improved Oil Recovery, Society of Petroleum Engineers: 2006.
188. Larsen, J. A.; Skauge, A. In *Simulation of the immiscible WAG process using cycle-dependent three-phase relative permeabilities*, SPE Annual Technical Conference and Exhibition, Society of Petroleum Engineers: 1999.
189. Rahmawati, S. D.; Whitson, C. H.; Foss, B., A mixed-integer non-linear problem formulation for miscible WAG injection. *Journal of Petroleum Science and Engineering* **2013,** *109*, 164-176.

190. Sherafati, M.; Jessen, K. In *Modeling and Simulation of WAG Injection Processes-The Role of Counter-Current Flow*, SPE Western Regional Meeting, Society of Petroleum Engineers: 2015.
191. Agada, S.; Geiger, S. In *Wettability, trapping and fracture-matrix interaction during WAG injection in fractured carbonate reservoirs*, SPE Improved Oil Recovery Symposium, Society of Petroleum Engineers: 2014.
192. Kløv, T.; Øren, P.; Stensen, J.; Lerdahl, T.; Berge, L.; Bakke, S.; Boassen, T.; Virnovsky, G. In *Pore-to-field scale modeling of WAG*, SPE Annual Technical Conference and Exhibition, Society of Petroleum Engineers: 2003.
193. Hustad, O. S. B., D. J. A Fully Coupled Three-Phase Model for Capillary Pressure and Relative Permeability for Implicit Compositional Reservoir Simulation. SPE Journal 15, 1003–1019 (2010).
194. Jerauld, G., General three-phase relative permeability model for Prudhoe Bay. *SPE reservoir Engineering* **1997,** *12* (04), 255-263.
195. Shahverdi, H.; Sohrabi, M., An improved three-phase relative permeability and hysteresis model for the simulation of a water-alternating-gas injection. *Spe Journal* **2013,** *18* (05), 841-850.
196. Skauge, A.; Dale, E. I. In *Progress in immiscible WAG modelling*, SPE/EAGE Reservoir Characterization and Simulation Conference, Society of Petroleum Engineers: 2007.
197. Marchesin, D.; Plohr, B. J. In *Wave structure in WAG recovery*, SPE Annual Technical Conference and Exhibition, Society of Petroleum Engineers: 1999.
198. Mollaei, A.; Delshad, M. In *A Novel Forecasting Tool for Water Alternating Gas (WAG) Floods*, SPE Eastern Regional Meeting, Society of Petroleum Engineers: 2011.
199. Haajizadeh, M.; Hafez, H. H.; Chaliha, P. R.; Al-Katheeri, A. B. In *Sub-miscible Gas-WAG Injection Piloting and Compositional Modeling in a Carbonate Reservoir*, International Petroleum Technology Conference, International Petroleum Technology Conference: 2007.
200. Ruan, F.; Carhart, S.; Giordano, R.; Grinestaff, G.; Bratvedt, F.; Olufsen, R. In *An overview of streamline tracer modeling of miscible/immiscible WAG injection IOR*, SPE/DOE Improved Oil Recovery Symposium, Society of Petroleum Engineers: 2002.
201. Beygi, M. R.; Delshad, M.; Pudugramam, V. S.; Pope, G. A.; Wheeler, M. F., Novel three-phase compositional relative permeability and three-phase hysteresis models. *SPE Journal* **2015,** *20* (01), 21-34.
202. Khanifar, A.; Demiral, B.; Darman, N. B. In *Modelling of Asphaltene Precipitation and Deposition during WAG Application*, International Petroleum Technology Conference, International Petroleum Technology Conference: 2011.
203. Van Dijke, M.; Sorbie, K., Pore-scale network model for three-phase flow in mixed-wet porous media. *Physical Review E* **2002,** *66* (4), 046302.
204. van Dijke, M. I.; Lorentzen, M.; Sohrabi, M.; Sorbie, K. S., Pore-scale simulation of wag floods in mixed-wet micromodels. *SPE Journal* **2010,** *15* (01), 238-247.
205. Juanes, R.; Patzek, T. W., Analytical solution to the Riemann problem of three-phase flow in porous media. *Transport in Porous Media* **2004,** *55* (1), 47-70.
206. Stone, H., Probability model for estimating three-phase relative permeability. *Journal of Petroleum Technology* **1970,** *22* (02), 214-218.

207. Patacchini, L.; Sebastien, D.; Bourgeois, M.; Moncorge, A.; Pallotta, Q., Simulation of Residual Oil Saturation in Near-Miscible Gasflooding Through Saturation-Dependent Tuning of the Equilibrium Constants. *SPE Reservoir Evaluation & Engineering* **2015,** *18* (03), 28-302.
208. Alizadeh, A.; Piri, M., Three-phase flow in porous media: A review of experimental studies on relative permeability. *Reviews of Geophysics* **2014,** *52* (3), 468-521.
209. Fayers, F.; Foakes, A.; Lin, C.; Puckett, D. In *An improved three phase flow model incorporating compositional variance*, SPE/DOE Improved Oil Recovery Symposium, Society of Petroleum Engineers: 2000.
210. Baker, L. In *Three-phase relative permeability correlations*, SPE Enhanced Oil Recovery Symposium, Society of Petroleum Engineers: 1988.
211. Todd, M.; Longstaff, W., The development, testing, and application of a numerical simulator for predicting miscible flood performance. *Journal of Petroleum Technology* **1972,** *24* (07), 874-882.
212. Lie, K.-A.; Juanes, R., A front-tracking method for the simulation of three-phase flow in porous media. *Computational Geosciences* **2005,** *9* (1), 29-59.
213. Venkatesan, R.; Östlund, J.-A.; Chawla, H.; Wattana, P.; Nydén, M.; Fogler, H. S., The effect of asphaltenes on the gelation of waxy oils. *Energy & Fuels* **2003,** *17* (6), 1630-1640.
214. Choi, J.; Jeong, M. S.; Park, K.; Lee, K. S. In *CO 2 WAG Process with Gel Treatment Considering Flowing Gel Viscosity in Heavy Oil Reservoir*, The Twenty-fifth International Ocean and Polar Engineering Conference, International Society of Offshore and Polar Engineers: 2015.
215. Dang, C.; Nghiem, L.; Nguyen, N.; Chen, Z.; Nguyen, Q., Evaluation of CO 2 Low Salinity Water-Alternating-Gas for enhanced oil recovery. *Journal of Natural Gas Science and Engineering* **2016,** *35*, 237-258.
216. Stone, H. L. In *A simultaneous water and gas flood design with extraordinary vertical gas sweep*, SPE international petroleum conference in Mexico, Society of Petroleum Engineers: 2004.
217. Be, A.; Skauge, A.; Delshad, M. In *Simulation of Three-phase Flow in Porous Media Including Capillary Pressure Representing Variation in Rock Wettability*, IOR 2011-16th European Symposium on Improved Oil Recovery, 2011.
218. Schneider, C. E.; Shi, W. In *A Miscible WAG Project Using Horizontal Wells in a Mature Offshore Carbonate Middle East Reservoir*, SPE Middle East Oil and Gas Show and Conference, Society of Petroleum Engineers: 2005.
219. Juanes, R.; Blunt, M. J. In *Impact of viscous fingering on the prediction of optimum WAG ratio*, SPE/DOE Symposium on Improved Oil Recovery, Society of Petroleum Engineers: 2006.
220. Gholamzadeh, M. A.; Hashemi, P.; Dorostkar, M. J. In *New improved oil recovery from heavy and semi-heavy oil reservoirs by implementing immiscible heated WAG injection*, Trinidad and Tobago Energy Resources Conference, Society of Petroleum Engineers: 2010.
221. Kim, G.; Jang, H.; Cho, M.; Lee, J. In *Optimizing the Design Parameters for Performance Evaluation of the CO 2-WAG Process in a Heterogeneous Reservoir*, The Twenty-fifth International Ocean and Polar Engineering Conference, International Society of Offshore and Polar Engineers: 2015.

222. Ghahfarokhi, R. B.; Pennell, S.; Matson, M.; Linroth, M. In *Overview of CO2 Injection and WAG Sensitivity in SACROC*, SPE Improved Oil Recovery Conference, Society of Petroleum Engineers: 2016.
223. Reza, H.; Arman, A.; Ghazal, H., Comparative Study on Oil Recovery Enhancement by WAG Injection Technique in a Fractured Oil Reservoir in the Southwest of Iran. *Journal of Petroleum & Environmental Biotechnology* **2016,** *7*, 263.
224. Ahmed Elfeel, M.; Al-Dhahli, A.; Geiger, S.; van Dijke, M. I. In *Multi-scale simulation of WAG flooding in naturally fractured reservoirs*, EAGE Annual Conference & Exhibition incorporating SPE Europec, Society of Petroleum Engineers: 2013.
225. Shandrygin, A.; Shelepov, V.; Ramazanov, R.; Andrianov, N.; Klemin, D.; Nadeev, A.; Yakimchuk, I. In *Mechanism of Oil Displacement During WAG in Porous Media with Micro-Inhomogeneities*, SPE Russian Petroleum Technology Conference, Society of Petroleum Engineers: 2015.
226. Khezrnejad, A.; James, L.; Johansen, T. In *Water enhancement using nanoparticles in water alternating gas (WAG) micromodel experiments*, SPE Annual Technical Conference and Exhibition, Society of Petroleum Engineers: 2014.
227. Gibrata, M. A.; Van Dijke, R.; Geiger, S. In *Pore Scale Modeling and Its Advantage for Enhanced Oil Recovery of Near Miscible Three-Phase Flow WAG Flooding in Carbonate Reservoir*, International Petroleum Technology Conference, International Petroleum Technology Conference: 2014.
228. Chakravarthy, D.; Muralidharan, V.; Putra, E.; Hidayati, D.; Schechter, D. S. In *Mitigating oil bypassed in fractured cores during CO2 flooding using WAG and polymer gel injections*, SPE/DOE symposium on improved oil recovery, Society of Petroleum Engineers: 2006.
229. Lien, S.; Lie, S.; Fjellbirkeland, H.; Larsen, S. In *Brage Field, lessons learned after 5 years of production*, European Petroleum Conference, Society of Petroleum Engineers: 1998.
230. Slotte, P.; Stenmark, H.; Aurdal, T., Snorre WAG pilot. *RUTH* **1992,** *1995*, 85-91.
231. Grigg, R. B.; Schechter, D. S. In *State of the Industry in CO2 Floods*, SPE annual technical conference and exhibition, Society of Petroleum Engineers: 1997.
232. Borling, D. In *Injection Conformance Control Case Histories Using Gels at the Wertz Field CO2 Tertiary Flood in Wyoming*, SPE/DOE Improved Oil Recovery Symposium, Society of Petroleum Engineers: 1994.
233. Newton Jr, L.; McClay, R. In *Corrosion and Operation Problems Caused by CO2 Injection for Enhanced Oil Recovery*, Proc. 5th Annual DOE Symposium, pp 22-24.
234. Kane, A., Performance review of a large-scale CO2-WAG enhanced recovery project, SACROC Unit Kelly-Snyder Field. *Journal of Petroleum Technology* **1979,** *31* (02), 217-231.
235. Khanifar, A.; Sheykh Alian, S.; Demiral, B.; Darman, N. B. In *Study of asphaltene precipitation and deposition phenomenon during WAG application*, SPE Enhanced Oil Recovery Conference, Society of Petroleum Engineers: 2011.
236. Nenniger, J.; Cutten, J.; Shields, S. In *Wax Deposition in a WAG Flood*, SPE Production Technology Symposium, Society of Petroleum Engineers: 1985.
237. Instefjord, R.; Todnem, A. C. In *10 years of WAG injection in Lower Brent at the Gullfaks Field*, European Petroleum Conference, Society of Petroleum Engineers: 2002.

238. Hermansen, H.; Thomas, L.; Sylte, J.; Aasboe, B. In *Twenty five years of Ekofisk reservoir management*, SPE Annual Technical Conference and Exhibition, Society of Petroleum Engineers: 1997.
239. Jakobsson, N.; Christian, T. In *Historical performance of gas injection of Ekofisk*, SPE Annual Technical Conference and Exhibition, Society of Petroleum Engineers: 1994.
240. Lake, L. W.; Johns, R. T.; Rossen, W. R.; Pope, G. A., Fundamentals of enhanced oil recovery. **2014**.
241. McGuire, P.; Redman, R.; Jhaveri, B.; Yancey, K.; Ning, S. In *Viscosity reduction WAG: an effective EOR process for north slope viscous oils*, SPE Western Regional Meeting, Society of Petroleum Engineers: 2005.
242. Mäkel, G., The modelling of fractured reservoirs: Constraints and potential for fracture network geometry and hydraulics analysis. *Geological Society, London, Special Publications* **2007,** *292* (1), 375-403.
243. Agada, S.; Geiger, S.; Doster, F., Wettability, hysteresis and fracture–matrix interaction during CO 2 EOR and storage in fractured carbonate reservoirs. *International Journal of Greenhouse Gas Control* **2016,** *46*, 57-75.
244. Gozalpour, F.; Ren, S.; Tohidi, B., CO2 EOR and storage in oil reservoir. *Oil & gas science and technology* **2005,** *60* (3), 537-546.
245. Griffin, J. M., *Smart Energy Policy: An Economist's Rx for Balancing Cheap, Clean, and Secure Energy*. Yale University Press: 2014.
246. Van't Veld, K.; Phillips, O. R., The Economics of Enhanced Oil Recovery: Estimating Incremental Oil Supply and CO_2 Demand in the Powder River Basin. *The Energy Journal* **2010**, 31-55.
247. Ferguson, R. C.; Nichols, C.; Van Leeuwen, T.; Kuuskraa, V. A., Storing CO2 with enhanced oil recovery. *Energy Procedia* **2009,** *1* (1), 1989-1996.

CHAPTER THREE

Mathematical modeling and simulation of water-alternating-gas (WAG) process by incorporating capillary pressure and hysteresis effects (Published)

Preface

A version of this manuscript has been published in Fuel 263 (2020)-116362. I am the primary author of this paper. With the help and advice of the co-authors, Ali Ghamartale, Nima Rezaei, and Sohrab Zendehboudi, I developed the conceptual mathematical model and designed the manuscript's structure. Most of the literature review, data collection, and the performance comparison of different methods and previous experimental works were done by me as the first author. I prepared the first draft of the manuscript and subsequently revised the manuscript based on the co-authors' feedback and comments received from journal reviewers. The co-author, Ali Ghamartale contributed to the developing the method and reviewing the manuscript. The co-author, Sohrab Zendehboudi, helped in developing the method, and considerably contributed to entirely correcting the text in terms of technical and editorial aspects. Nima Rezaei thoroughly reviewed and revised the manuscript and helped in results interpretation, and statistical analysis.

ABSTRACT
Mathematical modeling and simulation of three-phase flow in porous media involves complexities related to the three-phase relative permeability, capillary pressure, and hysteresis effects that are cycle-dependent. Extensive theoretical studies are available in the literature, simulating immiscible and miscible WAG processes; however, the simulation study on near-miscible WAG is overlooked. Also, the majority of WAG simulation studies lack the cycle-dependent three-phase hysteresis that appears in the relative permeability and capillary pressure models. In this chapter, we study the three-phase flow modeling of near-miscible WAG process for EOR implication, using implicit pressure explicit saturation (IMPES) method. The mathematical model simulates a WAG case study in a strongly water-wet Berea core, using synthetic oil and brine at 38 ˚C and 12.7 MPa. Three cycles of water and gas injections are used in the WAG operation. The recovery data from our mathematical model is in excellent agreement with the experimental data of near-miscible WAG process. The absolute relative error is less than 1.7% while estimating the ultimate recovery factor of the oil in WF and GI stages of all three cycles. We also study the effects of main variables such as injection rate, WAG ratio, slug size (PV) injection, crude oil viscosity, and core absolute permeability on the WAG performance. We find the WAG ratio of 1 to be better than 0.5 and 2 cases. Although the absolute permeability changes the breakthrough recovery performance of individual stages, it does not significantly affect the ultimate recovery of near miscible WAG. Increasing the injection rate decreased the recovery factor. The effect was more pronounced in the gas injection cycles. Also by increasing the viscosity of the in-situ oil, the ultimate recovery factor decreased by 20%. The finding from this study can help for better understanding of WAG injection on near-miscible condition for various scenarios and at different conditions in terms of operational condition and rock and fluid's characteristics.

Keywords: WAG injection; Mathematical modeling; Hysteresis effects; Three-phase capillary pressure; Three-phase relative permeability

3.1 Introduction

It has been proven that the low microscopic sweep efficiency in gas injection (GI) process is the result of both low density of the gas phase and/or a significant difference between the densities of the reservoir fluid and injected gas as well as the wettability of the rock which affects the capillarity of the system [1-3]. Gravity segregation, complexities in operational procedures and high completion costs have made the GI technique challenging and even in some cases, impractical [4]. Water-alternating-gas (WAG) injection

process provides an efficient method to recover hydrocarbons by combining the benefits of water flooding (WF) and GI [5]. In the oil and gas industry, the WAG injection is being considered as a matured and reliable enhanced oil recovery (EOR) for producing the trapped oil after the primary water flooding (WF) operation. In fact, the WAG approach has been introduced as an EOR technique to enhance the macroscopic sweep efficiency and to reduce the cost of the GI process [6]. During the WAG injection process, the mass transfer can also occur between the invading and in-situ fluids, that can affect the ultimate oil recovery and fluids' density and viscosity [7]. Through several decades of the field [6, 8-10], pilot [11-15], laboratory [16-19], and simulation [20-24] studies of WAG process, a variety of WAG aspects have been investigated. For instance, production mechanisms and optimal conditions have been studied from pore to field scales at various fluid and rock characteristics [19, 25-33]. Water flooding into a reservoir will cause a phenomenon called voidage replacement in which it intend to deliver pressure support to the reservoir. However, there are problems associated with this method including low recovery caused by the variable permeability of fluids in the reservoir, and unfavorable mobility ratio of the injected water. These drawbacks makes the application of WF inefficient especially facing a heavy oil reservoir [34-35].
In a recent study, Khezrnejad et al. [36] investigated the impact of silicon oxide (SiO_2) and aluminum oxide (Al_2O_3) nanoparticles added to the brine phase in WAG injection, that decreased the residual oil saturation by up to 20%. A systematic review by Afzali et al. [6] comprehensively covers previous experimental and modeling studies related to WAG injection process.

Modeling and simulations of the WAG process have been investigated in the literature by studying variables such as WAG ratios, the number of WAG injection cycles [37-44], wettability [42, 45-47], and relative permeability and hysteresis [39, 42, 44-45, 47-54]. The main difficulties in the modeling and optimizing of a WAG process are realistic correlations between rock/fluid properties and the amount of residual phases in the reservoir [55]. The cyclic nature of the WAG process and the mobility of the three-phase flow in porous media add to the complexity of modeling of three-phase flow in porous media. There are considerable research works in the literature with a focus on the analytical solution of the three-phase flow and three-phase relative permeability during WAG flooding [56-57]. Some researchers, including Juanes and Patzek [56] discussed the hyperbolic nature of the three-phase flow models in porous media and questioned the validity of previous models such as Stone I [57]. Beygi et al. [58] provided a comprehensive review of the three-phase relative permeability and hysteresis models in the literature with application to multiphase flow in porous media, including process WAG process [58]. Beygi et al. concluded that in a WAG process, the relative permeability of each phase is a function of saturation

history of drainage or imbibition displacement processes and the chronological scanning curves for saturation paths (decreasing/increasing saturation of phases) in each cycle [58].

According to the WAG simulation results, the three-phase hysteresis effects are less pronounced in miscible WAG (MWAG) cases compared to immiscible WAG process (IWAG) [44]. In addition, the three-phase hysteresis has a greater impact on the three-phase relative permeability of the non-wetting phase than the wetting and intermediate wetting phases [39]. According to Larsen and Skauge [51], two-phase hysteresis models may not adequately explain some aspects of the relative permeability behavior such as irreversible hysteresis loops [51]. Their model integrated three-phase hysteresis models with the three-phase flow equations to simulate the WAG process in porous media [51]. The obtained three-phase relative permeability models were able to properly capture an increase in oil recovery and a decrease in gas mobility as the result of the three-phase hysteresis effects in the WAG process. Models without hysteresis effects or with two-phase hysteresis models underestimated the oil production (recovery). By including the three-phase hysteresis, capillary pressure, and relative permeability models, a higher recovery factor was obtained, providing a better fit to the actual data [6]. Egerman et al. [48] demonstrated the same notion by comparing the experimental data with the simulation results of the WAG process where the two- and three-phase hysteresis models were used. They suggested a model that did not use the displacement direction like imbibition or drainage patterns, but it modified the Land's relative permeability model by including the effect of pore structure[48]. Fayes et al. [59] extended Baker's [60] relative permeability model through the compositional model and included the effect of all phases saturations in the three-phase relative permeability model. They also provided a framework to calculate the capillary pressure and relative permeability in the WAG injection process [59]. The simulation of MWAG injection in Mangus field was performed by Hajizadeh et al. [40], where the MWAG process was simulated at two scales: fine grids and field-scale. In the field-scale simulation, they applied the Todd and Longstaff mathematical formulations [61] to attain greater accuracy. The effect of reservoir wettability was also considered in WAG experimental and simulation studies. In general, a higher residual oil saturation was achieved in water-wet reservoirs, compared to oil-wet systems during WAG operation [6]. The wettability state of the reservoir rock has considerable impacts on injectivity, optimum WAG ratio, injection rate, three-phase relative permeability, and three-phase capillary pressure [28]. Stern [62] studied the effect of reservoir wettability and WAG ratio on the recovery factor by conducting a series of multi-contact tertiary CO_2 core flooding experiments. They reported a lower oil recovery in cases with a high WAG ratio in water-wet rocks due to the considerable amount of bypassed oil [28]. In the mixed-wet rock samples, the recovery factor was not appreciably affected by the WAG ratio due to the wall-coating surface of the rock by oil

films that improve the contact of the oil and solvents [62]. It was found that wettability has a profound impact on the hysteresis effects and the three-phase relative permeability. For instance, Shahrokhi et al. [63] employed different three-phase relative permeability models such as Stone I, Stone II, Carlson, Killough, and Jargon for WAG injection in mixed-wet rock samples. They showed that none of the examined models could accurately simulate the experimental data of WAG injection under the mixed-wet condition [63].

Klov et al. [47] provided a new multi-scale (pore-to-field) mathematical methodology based on the data of Etive formation in the North Sea field [47]. To obtain the input data, including the relative permeability and capillary pressure, they conducted experimental tests on 11 different types of rocks to attain reliable data for their pore-scale modeling. They also used a relative permeability model based on two-phase relative permeability models and capillary pressure curves using the standard saturation weighed model [47]. This methodology enabled them to avoid history matching for calculating the relative permeability and capillary pressure data calculations. The simulation of WAG injection in fractured porous media was conducted by Heermans et al. [41]. They simulated the process in a two-dimensional fine-grid system by applying a dual-porosity model, using a proxy model as a transfer function to model the flow between fracture and matrix media. After scaling analysis, they concluded the significance of the effective permeability to the phases and the fracture and matrix communication term in the WAG injection process. They also found the injection type and reservoir properties to significantly affect the shape factor parameter used in the transfer function [41]. Skauge and Dale studied the production history of WAG injection with focus on the three-phase relative permeability and three-phase hysteresis models. They proposed a new model for the three-phase capillary pressure, based on the two-phase capillary pressure data and three-phase relative permeability calculations [55]. A better match with real data was obtained, using the three-phase capillary pressure model, where they found higher oil relative permeability values and lower relative permeability for the injected fluid [55]. Sherafati et al. [53] studied the effect of gravity segregation, using an IMPES WAG simulation model. Their results highlighted the importance of the gravity segregation during the processes with a small injecting fluid volume; the segregation also decreased the total mobility of the fluid system, compared to the case without including the gravity segregation effect [52].

The mathematical modeling and simulation of the WAG injection process at near-miscible (very low oil-gas interfacial tension or IFT) condition is overlooked in the literature despite the considerable effort on modeling of IWAG or MWAG processes. In the near-miscible GI condition, the gas phase does not have complete miscibility condition with the oil phase [64-65]. This process is similar to condensing-

vaporizing gas driving at a pressure close to the minimum miscibility pressure (MMP) value. The process of the near-miscible WAG is efficient and practical from both the economic and operational perspectives [66]. In the near-miscible GI processes, the capillary forces are not as significant as those in the IWAG, due to low oil-gas IFT; thereby, a small value of gas-oil capillary entry pressure is expected for the leading interface to advance to the pores filled with the trapped oil. As a result, the gas phase can easily advance into the oil phase. This mechanism creates a driving force to recover the trapped oil from pores to the main flow stream; the oil flow would be even more improved through coupling with the flow of the gas phase [67]. Sohrabi et al. [65] showed that this mechanism is not active in the miscible gas injection and immiscible gas flooding processes. A significant portion of the research studies in the literature of WAG injection mostly focuses on the development of the relative permeability and hysteresis models for fluid flow in porous media based on the experimental data and in-house or commercial simulators.

None of the previous research works studied the WAG injection on near-miscibility condition, while this condition is very common in any field or reservoir. Most of studies were conducted at laboratory condition with numerous limitations on performing sensitivity analysis due to high cost and time consuming of the process. However, the conducted simulation studies were not comprehensive regarding the accuracy of data and reliability of the model.

In this study, a robust mathematical explicit finite-difference modeling system is implemented by considering the three-phase relative permeability, capillary pressure, and hysteresis models. This chapter is structured as follows. After the introduction, a brief description of the WAG process, including a schematic of the fluid flow direction during WAG injection in the porous media, is provided. After that, a mathematical framework is introduced that includes the governing and auxiliary equations. The model is applied to a case study with experimental core flooding test results to verify our model. In the results and discussion section, the effects of various rock and fluid properties are discussed. Finally, the main conclusions are listed.

3.2 WAG PROCESS: DESCRIPTION

In June 2018, British Petroleum (BP) statistical review [68] of the world's energy reported approximately 1.7 trillion barrels globally proven oil reserves by 2017. After producing 92.6 million barrels per day, a large quantity of the oil remains in the reservoirs [68]. A large portion of this trapped oil is because of capillary forces, unfavorable mobility ratio (between the displacing and displaced fluids), and unwanted bypassed oil resulted from reservoir heterogeneities [69]. Economical production of this trapped/residual oil is an ultimate target of all enhanced oil recovery (EOR) and improved oil recovery (IOR) projects. Among the EOR/IOR techniques, gas injection (GI) and water flooding (WF) are the most used and

mature methods of oil and gas production [70]. The effectiveness of these techniques dependents on the macroscopic volumetric sweep efficiency and microscopic displacement sweep efficiency (e.g., the amount of oil produced from pore spaces) [71].

The main drawbacks of the GI are gas fingering as a result of unfavorable mobility ratio and low volumetric sweep efficiency [69]. The occurrences of early gas breakthrough are reported in different field and pilot applications [72-74] as a result of the gas fingering and channeling through more permeable layers. The primary concerns of the GI efficiency are attributed to the fluid mobility and reservoir conformance [69]. Alternatively injecting water and gas (in WAG injection) lowers the gas effective permeability, leading to a higher stabilization of the fluids' interfaces and consequently, improving the overall sweep efficiency. Another governing mechanism during the WAG injection process is gravity segregation, which occurs due to the density difference between the acting phases [75]. This mechanism can improve the vertical sweep efficiency by recovering the oil left at the bottom of the reservoir (from the gas injection cycle) in the waterflooding cycle [75]. Figure 3-1 shows a schematic of the WAG injection and the fluid flow distributions for oil, gas, and water in a typical reservoir.

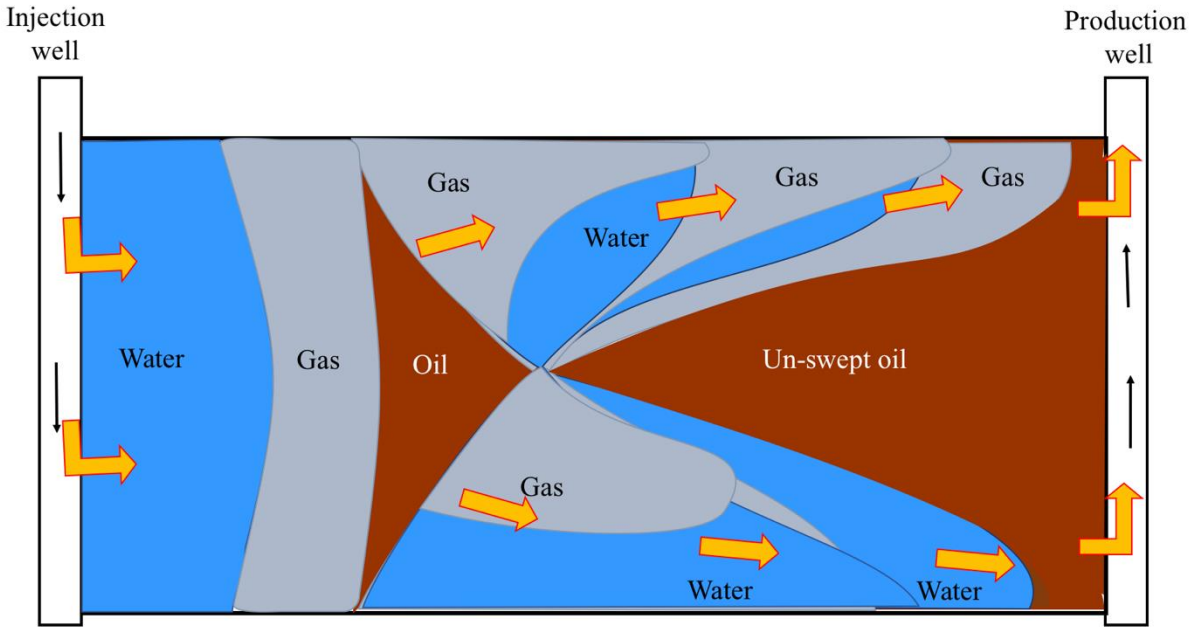

Figure 3-1: A schematic of WAG process in a hypothetical oil reservoir (Modified after Shahverdi et al.) [7].

Measurements of the three-phase relative permeability are difficult and are time-demanding; especially, when the steady-state method is used [51]. Numerous empirical models such as Stone-I, Stone-II, and Baker are introduced to estimate the three-phase relative permeability values from two-phase data [60,57,94]. Various theoretical and experimental studies confirm the dependency of the relative permeability to

parameters such as rock and fluid properties including fluid viscosity, interfacial tension, injection rate, wettability, immobile water saturation, pore size distribution, and especially the saturation history [100]. The dependency of relative permeability to fluid saturation history is described as relative permeability hysteresis, which becomes significant in three-phase flow systems [100]. Cyclic dependency of the three-phase hysteresis permeability becomes important in tertiary oil recovery processes such as WAG injection and cyclic steam stimulation (CSS) processes [67]. Simulation studies showed remarkable uncertainties associated with applying three-phase relative permeability models in gas and WAG injections at field scales [101]. The simulation results of oil recovery with and without including hysteresis revealed that a higher oil recovery is obtained by incorporating hysteresis effect in relative permeability correlations, compared to the no-hysteresis case [102]. In the case of involving hysteresis effects, a higher oil recovery is obtained over a longer period which is attributed to the effect of trapped gas, blocking the oil flow from high-permeability pore spaces.

Improving the macroscopic sweep efficiency during the gas injection was one of the main reasons to use cyclic injection scheme for water and gas [76]. This inherent cyclic nature makes the WAG injection as a complex process for the three-phase flow that contains sequential imbibition and drainage displacements as well as the hysteresis effects. Despite the worldwide applications of the WAG injection process in the fields [10], obtaining a comprehensive knowledge of the underlying mechanism of this recovery process is still ongoing research. One of the overlooked areas is the near-miscible-gas WAG condition. The near-miscible-gas injection relates to a process where the injected gas is close to the complete miscibility state [65]. The near-miscible gas injection processes seem interesting from both operational and economic perspectives. In the case of high oil-gas IFT (immiscible), in spite of the connectivity of the oil to the main flow of the system, if there are no other driving forces such as gravity forces, the recovery achieved by the film flow is very small. On the other hand, during the miscible GI, there is no interface between the gas and oil. Thus, the flow is similar to the single-phase condition where the oil is recovered through molecular diffusion and dispersion mechanisms [65]. Sohrabi et al. [65] conducted a series of pore-scale micromodel WAG experiments under the near-miscible condition. A substantial portion of the oil in micromodel that had been completely saturated with oil is recovered during low-IFT gas flooding. Some of the oil is bypassed by the main gas front. The recovery of the by-passed oil bank is continued behind the main gas front, and complete oil recovery is resulted due to near-miscible gas injection. So, more oil is recovered even after passing the gas front that are not reported in previous processes containing high oil-gas IFT systems [65].

3.3 MATHEMATICAL MODELING OF WAG

The process of WAG injection is a three-phase flow system, including both imbibition and drainage displacement schemes during the sequential injections of gas and water [77-78]. Because of the complexities of the three-phase flow and its cyclic nature, the numerical modeling of the oil recovery by WAG process remains as a challenge. In our work, we employ the implicit-pressure explicit-saturation (IMPES) method in a two-dimensional core system. In the following sections, first the mathematical framework of the model is presented, following the numerical formula, boundary and initial conditions, discretization, and numerical solution approach.

3.3.1. Governing Equations

The primary equations to be solved for an incompressible and three-phase flow system (gas, oil, and water) are the mass/molar balances for all involved phases. Neglecting the gravity effects and the dispersion between phases and applying Darcy's equation (as the momentum balance equation) for an immiscible three-phase system, the following relationships for all phases (oil, water, and gas) can be written:

$$\nabla.\left(\frac{\rho_o K k_{ro}}{\mu_o}\frac{\partial p_o}{\partial x}\right) + q_o = \frac{\partial}{\partial t}(\phi \rho_o s_o) \tag{3-1}$$

$$\nabla.\left(\frac{\rho_w K k_{rw}}{\mu_w}\frac{\partial p_w}{\partial x}\right) + q_w = \frac{\partial}{\partial t}(\phi \rho_w s_w) \tag{3-2}$$

$$\nabla.\left(\frac{\rho_g K k_{rg}}{\mu_g}\frac{\partial p_g}{\partial x}\right) + q_g = \frac{\partial}{\partial t}(\phi \rho_g s_g) \tag{3-3}$$

where the subscripts *o*, *w*, and *g* refer to the oil, water, and gas phases, respectively; *p* is the pressure; *s* denotes the saturation; ρ and μ are the density and viscosity, respectively; *q* represents the source/sink term, which can be the production or injection rate; ϕ and *K* are the rock porosity and absolute permeability, respectively; *t* is time; and *x* is spatial location.

3.3.2. Auxiliary Equations.

The following relationship exists between the phase saturations:

$$s_o + s_w + s_g = 1 \tag{3-4}$$

where s_o, s_w, and s_g resemble the saturation of oil, water, and gas, respectively.

Reliable three-phase relative permeability and three-phase capillary pressure models are needed to model the three-phase flow in WAG injection accurately. Measurements of the three-phase capillary pressure data from the coreflooding tests are time-consuming and practically challenging [79-80].

In general, the capillary pressure (p_c) is defined as the pressure difference of non-wetting phase and wetting phase (see Eq. (3-5)), which is a function of rock properties such as permeability and porosity as well as the saturation value and distribution.

$$p_c = p_{non-wet} - p_{wet} \tag{3-5}$$

in which, $p_{non\text{-}wet}$ and p_{wet} denote the pressure of the non-wetting, and wetting phases, respectively. In this study, we use a three-phase capillary pressure model proposed by Neshat et al. [81], which uses the Gibbs free energy; this model is an extended/modified version of Skjaveland et al.'s [82] two-phase capillary pressure model. This capillary pressure model applies to all types of cores in terms of wettability state. The generalized form of capillary pressure model follows:

$$p_{c,ow} = \sigma_{ow}\, cos\,(\theta_{ow}) \sqrt{\frac{\varphi}{K}} \left(\frac{c_o}{(\frac{s_o - s_{or}}{1 - s_{or}})^{ao}} + \frac{c_w}{(\frac{s_w - s_{wr}}{1 - s_{wr}})^{aw}} \right) \tag{3-6}$$

$$p_{c,og} = \sigma_{og}\, cos\,(\theta_{og}) \sqrt{\frac{\varphi}{K}} \left(\frac{c_o}{(\frac{s_o - s_{or}}{1 - s_{or}})^{ao}} + \frac{c_g}{(\frac{s_g - s_{gr}}{1 - s_{gr}})^{ag}} \right) \tag{3-7}$$

where $p_{c,ij}$ is the three-phase capillary pressure between phase *i* and *j*, where the subscripts *i* and *j* can be oil, water or oil gas phases.; σ_{ij} and θ_{ij} are the interfacial tension and contact angle between phase *i* and *j*, respectively; c_i and c_j are the capillary entry pressure for the phases *i* and *j*, respectively; *s* is phase saturation; and a_i symbolizes the capillary exponent of phase *i* [81].

The three-phase relative permeability values also depend on the saturation distribution and saturation history [83]. The saturation history is related to the relative permeability hysteresis. Relative permeability hysteresis has been reported with both two-phase [84-86] and three-phase [87-88] laboratory data. Most of the three-phase relative permeability models proposed in the literature use the two-phase relative permeability data. In addition, common correlations such as Stone and Baker models have been commonly used in the literature to evaluate the three-phase relative permeability [83]. These models are not satisfactory in the case of three-phase flow in porous media. Thus, the three-phase flow parameters should be obtained as a function of saturations of two phases to apply for different wettability conditions [89-92]. In the current study, we use the three-phase relative permeability model proposed by Shahverdi and Sohrabi in 2012 [52], which also considers the hysteresis effects. Shahverdi and Sohrabi [52] assumed that the two-phase relative permeabilities and saturations affect the three-phase relative permeability values (k_{ri}^{3ph}) of phase *i* (where, *i*=gas, water or oil) as defined below:

$$k_{ro}^{3ph}(s_w, s_g) = \frac{\overline{s_o}}{(1-\overline{s_g})(1-\overline{s_w})} [k_{row} k_{rwg} + k_{rog} k_{rgw}] \tag{3-8}$$

$$k_{rw}^{3ph}(s_o, s_g) = \frac{\overline{s_w}}{(1-\overline{s_g})(1-\overline{s_o})}[k_{rwo}k_{rog} + k_{rwg}k_{rgo}] \quad (3\text{-}9)$$

$$k_{rg}^{3ph}(s_w, s_o) = \frac{\overline{s_g}}{(1-\overline{s_o})(1-\overline{s_w})}[k_{rgo}k_{row} + k_{rgw}k_{rwo}] \quad (3\text{-}10)$$

where *i* and *j* subscriptions can be oil, water or gas phases and k_{rij} is the two-phase relative permeability of phase *i* in the presence of phase *j*; and $\overline{s_i}$ is the normalized saturation of phase *i*, which depends on the flow direction (imbibition/drainage) as well as the initial state of the grid block, as given below[52]:

$$\overline{s_g} = \frac{s_g - s_g^*}{1 - s_w^* - s_o^* - s_g^*} \quad (3\text{-}11)$$

$$\overline{s_o} = \frac{s_o - s_o^*}{1 - s_w^* - s_o^* - s_g^*} \quad (3\text{-}12)$$

$$\overline{s_w} = \frac{s_w - s_w^*}{1 - s_w^* - s_o^* - s_g^*} \quad (3\text{-}13)$$

In Eqs. (3-11)−(3-13), the s_i^* values are defined based on different injection fluids, as listed in Table 3-1.

Table 3-1: The parameters used in the three-phase relative permeability model.

Three-phase relative permeability	Model parameters	WAG injection cycle		
		Gas	Oil	Water
k_{rg}^{3ph}	s_g^*	s_g^{start}	s_{gt}	s_{gt}
	s_w^*	s_{wc}	s_{wc}	s_w^{start}
	s_o^*	0	s_o^{start}	s_{ot}
k_{ro}^{3ph}	s_g^*	0	s_{gt}	s_{gt}
	s_w^*	s_{wc}	s_{wc}	s_w^{start}
	s_o^*	s_{org}	s_o^{start}	s_{ot}
k_{rw}^{3ph}	s_g^*	0	0	0
	s_w^*	s_{wc}	s_{wc}	s_{wc}
	s_o^*	0	0	0

In Table 3-1, s_i^{start} is the saturation of phase *i* at the beginning of the phase *i* injection process; and s_{gt} and s_{ot} denote the trapped/residual saturation of gas and oil, respectively. The two-phase relative permeability correlations are mentioned in Eqs. (A-11)-(A-16) Appendix A.

3.3.3. Boundary and Initial Conditions

Similar to the case study, we consider constant injection flowrate (25 cm^3/h) at the inlet section of the core and a constant back pressure (12.686 MPa) at the outlet of the core sample. The critical gas saturation is assumed to be 0.03, implying that for saturations higher than this value, the gas can travel within the porous medium. At the initial condition, only oil and connate water exist in the system, and no gas is present in the core, as shown below:

$$at\ t = 0,\ \begin{cases} s_{oi} = 0.82 \\ s_{wi} = s_{wc} = 0.18 \\ s_{gi} = 0.00 \end{cases} \tag{3-14}$$

3.3.4. Model Discretization and Numerical Solution Method

To solve the partial differential-algebraic system of three-phase flow equations, the IMPES (implicit pressure-explicit saturation) approach is employed. This method was originally developed by Sheldon et al. (1959) [93] and Stone and Garder (1961) [94]. It disconnects the relation between pressure and saturation in a system of governing equations. In this technique, the coupled system of equations is divided into two sets of separated pressure and saturation equations that can be solved by implicit and explicit time approximation, respectively. This approximation is accurate and simple to be applied, which requires less computational time and memory, compared to other techniques such as simultaneous solution (SS) [95]. IMPES is widely utilized in many process simulations in petroleum industry[96]. Figure 3-2 describes a simple procedure of mathematical modeling to simulate the WAG injection process in this study.

3.3.5. Advantages and Limitations of Model

One of the advantages of our study is that we tested used new three-phase relative permeability and capillary pressure models (which also include the hysteresis effects) to model a near miscible WAG injection process. The hysteresis effects have a remarkable impact on accurately simulate the cyclic imbibition and drainage displacement paths occurring in WAG injection process. Our mathematical model results show the reliable of these new auxiliary models for capturing the physics of a cyclic three-phase flow in porous media, such as near miscible WAG.

In our mathematical model, the following assumptions are made:

- Gravity effects are ignored
- 1D horizontal flow direction is considered in the core.
- Fluids and core compressibilities are neglected.
- Core is homogeneous and strongly water-wet.
- Capillary equilibrium holds in the system.
- Thermal equilibrium holds and temperature is constant at 38 ˚C.
- The capillary end-effects are not considered.

We simulate a case study where a 5 cm diameter core (2 inches) was used. The gravity effects are not significant for such small diameter and the 1D flow assumption is satisfactory. The parameters of the two-phase relative permeability correlations may need to be tuned, and optimized during each cycle. In the three-phase relative permeability model used, the constant parameters of the two-phase relative permeability are obtained using the experimental two-phase data, and they are then tuned to be used in our model. For more detail on tunning the two-phase relative permeability models please refer to Appendix A. During cyclic WF and GI of the WAG process, these parameters are optimized again, to account for the saturation and cyclic process hysteresis.

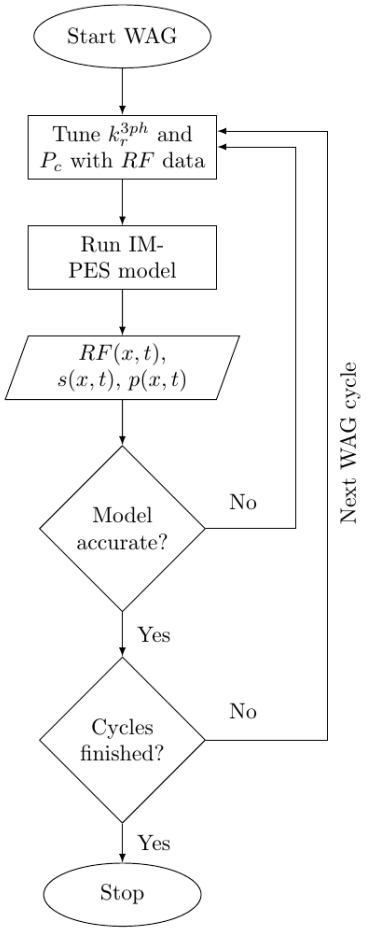

Figure 3-2: WAG injection modeling flowchart.

3.4 CASE STUDY

To verify our mathematical model capabilities, we use an experimental case study by Fatemi et al. [76]. They conducted a series of WAG injection tests in water-wet and mixed-wet core samples. Here, we use the experiments conducted in the sandstone water-wet cores. Their core-flood experiments were performed at a high-pressure (1840 Psi)and a temperature of 38 ˚C. Fatemi et al. [76] used cores with a length of 60.5 cm and a diameter of 5.08 cm (2 inches) with a permeability of 65 mD and porosity of 18%. They used synthetic brine composed of 16 g sodium chloride (NaCl) and 4 g calcium chloride ($CaCl_2$) in 2000 cm^3 deaerated distilled water. The brine salinity, density, and viscosity at 38˚C are 1000 mg/L, 992.96 kg/m^3, and 0.68 cP. The hydrocarbon phase in their study was a binary mixture of methane (C_1) and *n*-butane (nC_4). A sight-glass separator with the volume of 90 cm^3 was used to collect and measure the effluent (water, oil, gas) from the core. The cumulative produced volumes of the fluids were recorded in each time step using a camera to read the level of phases' interface with the accuracy of ±0.05 cm^3 for each recording point. The Quartzdyne gauges monitored the pressure across the core with

an accuracy of ±0.001 psi. Their experiments started with an initial oil saturation of 82% and an initial water saturation of 18 % as the initial process conditions. The WAG operation in the water-wet core was conducted in 3 cycles, including (in order) primary waterflooding (WF_1), primary gas injection (GI_1), secondary waterflooding (WF_2), secondary gas injection (GI_2), tertiary waterflooding (WF_3) and tertiary gas injection (GI_3). Both brine and gas phases were injected at an injection rate of 25 cm^3/hr. The average saturations of the oil and water (brine) phases trapped in the core after the final cycle (third GI) were reported to be 6% and 54%, respectively. A summary of the fluid properties, core characteristics, and core-flooding operating conditions appear in Table 3-2.

Table 3-2**:** A summary of the fluid, core, and process conditions in the case study.

WAG Attributes	Variable (unit)	Acting phase(s)	Value
Fluid	ρ (kg/m^3)	g	211.4
		o	317.4
		w	993.0
	μ (mPa.s)	g	0.0249
		o	0.0405
		w	0.68
	γ (mN/m)	og	0.04
		ow	55
Core	Lithology		Sandstone
	Wettability		Water-wet
	K (mD)		65
	ϕ		0.18
	L (cm)		60.5
	D (cm)		5.08
Operating condition	s_i (fraction PV)	g	0
		o	0.82
		w	0.18
	q (cm^3/h)		25
	P (psia)		1840
	T (˚C)		38

3.5 RESULTS AND DISCUSSIONS

The accuracy and robustness of the IMPES algorithm are examined in this part of the chapter. In our model, we consider a 1D core sample saturated with oil in the presence of initial water saturation. The core is then flooded with cyclic injections of water and gas for three cycles at 1840 psia. The modeling of WAG injection is conducted where a set of near-miscible gas data for the experimental WAG flooding runs are used.

3.5.1 Model Validation

Figure 3-3 compares the modeling results with the experimental data reported by Fatemi et al. [67]. The proposed WAG injection model is implemented in a water-wet core sample with the same fluid and rock properties of the experimental data. Our model accurately forecasts the experimental results of the WAG flooding tests. In Figure 3-3, we have identified cycles 1, 2, and 3 and the successive waterflooding (imbibition) and gas injection (drainage) recovery results from model and experiment.

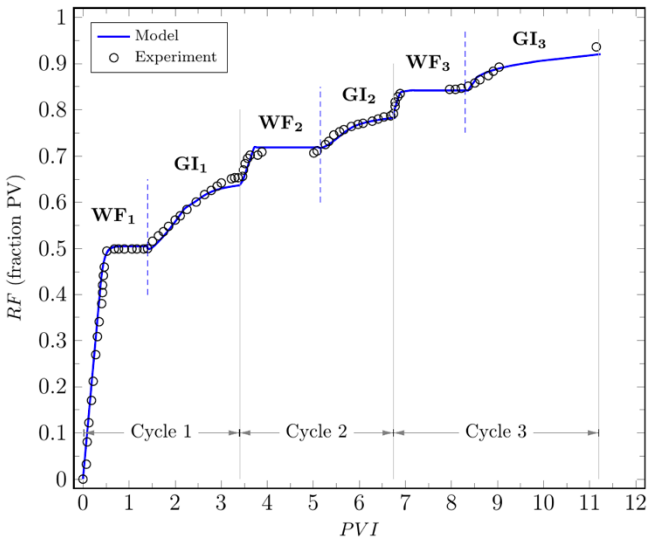

Figure 3-3: Comparison between the RF from near-miscible WAG injection from experimental and numerical modeling (q=25 cm^3/h, slug size=1 PV, and WAG ratio=1). Solid line shows simulation results and scatter points are experimental data from Fatemi et al. [67]

Based on Figure 3-3, after primary water flooding (WF_1), only 50% PV of the oil in the core is produced and a significant portion of the oil is trapped in the porous system. Because the core is strongly water-wet, no further oil production is expected upon waterflooding at this rate. More details on the waterflooding behavior in water-wet core and the effects from capillarity and viscous forces is available in Rezaei and Firoozabadi [97]. Because in the WF_1 stage, water and oil are the only phases, flowing in the

porous medium (there is no gas in the system during this step), we employ two-phase relative permeability and capillary pressure correlations to achieve the best match with the experimental results. After the primary WF, primary gas injection (GI_1) begins with 42 % oil and 58% water in the porous medium. In the GI_1, three-phase relative permeability and capillary pressure correlations are applied. The simulation results for the first GI process shows that by the end of the first cycle, 65 % of the oil is recovered. The WAG injection process is continued for two additional cycles, resulting in the ultimate recovery of 93%. According to Figure 3-3, an excellent match is observed between our mathematical model and experimental results. The recovery factor during each stage and also at the end of each stage is perfectly estimated by the model. The ultimate *RF* at the end of the last cycle is only slightly underestimated from the model. Our model is able to simulate the experimental data, accurately. The evolution of saturation in the core at different injection times (in PVI) for each step is plotted in Figure 3-4.

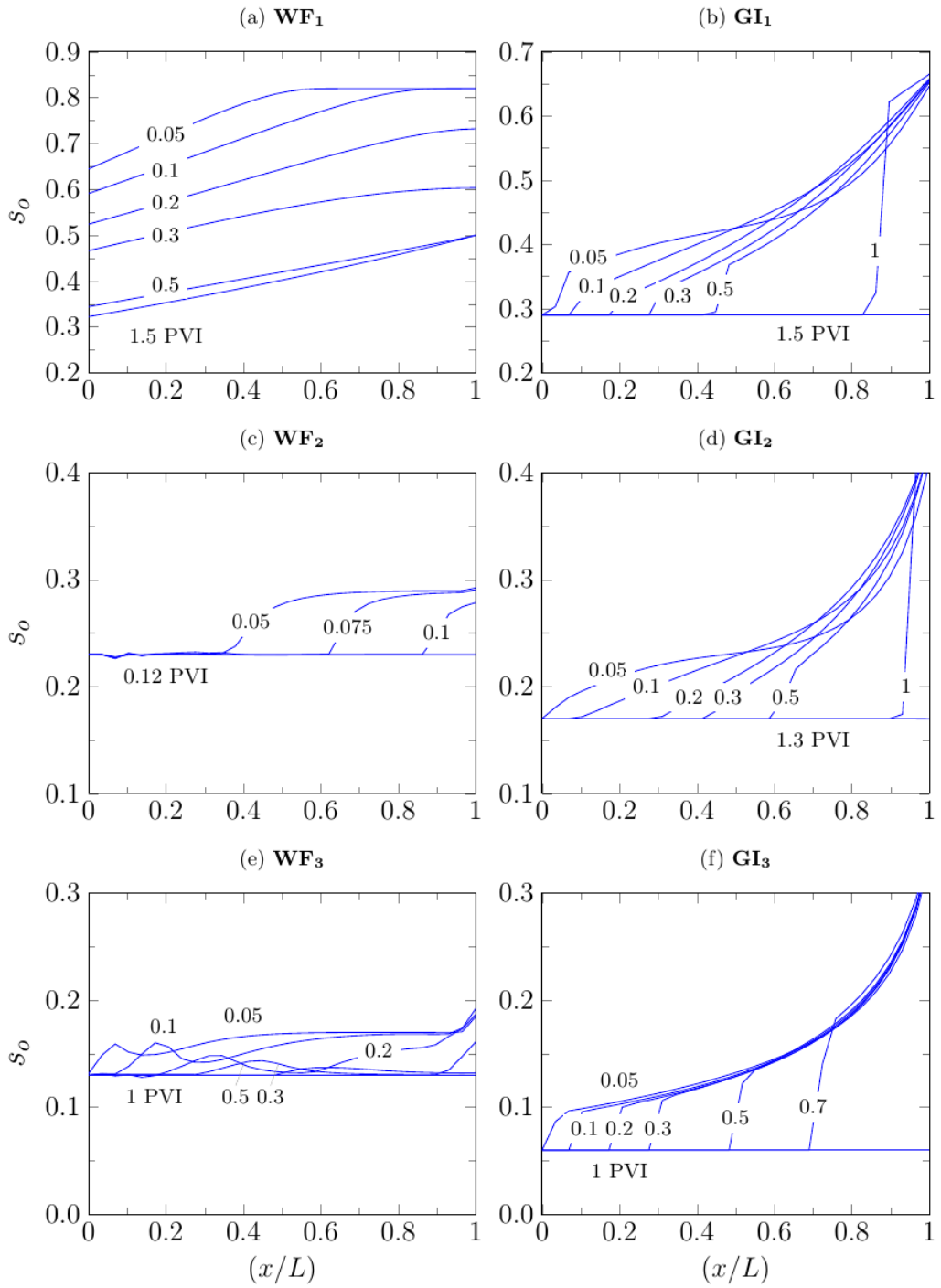

Figure 3-4: Oil saturation evolution profile in near-miscible WAG injection for different injection stages: (a) WF_1, (b) GI_1, (c) WF_2, (d) GF_2, (e) WF_3 and (f) GI_3 (q=25 cm^3/h, slug size=1 PV, and WAG ratio=1).

As it is shown in Figure 3-4., a more piston-like displacement is observed in the WF cycles compared to the GI cycles. This behavior is expected because of the higher mobility of the gas phase compared to

that of the water phase. After the primary WF, the ultimate oil saturation in the core is stabilized with less PVI in the WF cycles compared to the GI cycles.

The three-phase relative permeability and three-phase capillary pressure variables dependent on the saturation distribution and chronological cycle history. Hence, the selection of reliable models that include the hysteresis strongly affects the simulation results and consequently the recovery factor values. Comparing the results of the introduced model and the laboratory WAG injection tests confirms the reliability of the three-phase relative permeability models (see Table 3-3) where the hysteresis model used in this work is the model proposed by Shahverdi et al. [83] and the three-phase capillary model by Neshat et al. [81] is used in this study. Table 3-3 summarizes the recovery factor obtained by the model, the recovery factor is taken from the literature, and error percentages. In Table 3-3, we show a relative percent error in estimating the RF at the end of each cycle and also the maximum relative error attained during each cycle. The error calculation formula is expressed as:

$$Error\ (\%) = 100 \left| \frac{RF_{final}^{exp} - RF_{final}^{sim}}{RF_{final}^{exp}} \right| \tag{3-15}$$

Table 3-3**:** Comparison of RF of near-miscible WAG injection (1:1) obtained by the model and experimental work.

WAG Attributes		*RF* (HCPV)**		Relative	Max Error
Cycle	Process*	Sim	Exp	Error (%)	(%)
1	WF	0.5008	0.4997	0.220	15.750
	GI	0.6464	0.6559	-1.448	5.090
2	WF	0.7194	0.7201	-0.097	-1.718
	GI	0.7937	0.7912	0.316	13.690
3	WF	0.8430	0.8509	-0.928	10.190
	GI	0.9200	0.9358	-1.688	1.160

* WF=Water flooding cycle; GI=Gas injection cycle

** *RF* = Recovery factor; HCPV=Hydrocarbon pore volume; Sim=Simulation; Exp=Experimental

As it is observed from Table 3-3, our model could predict the ultimate recovery factor during each stage and cycle of WAG injection is estimated with excellent accuracy. The highest deviation between the model and simulation is at the end of first and last gas injection (GI_1 and GI_3) stages where in both cases, the model underestimates the experimental results with an error of -1.448% and -1.688%, respectively;

among the WF cycles, the WF_3 stage has the highest error in estimating the ultimate recovery with a relative error of -0.928%. The maximum error attained during all cycles is about 16%, which arises during the first WF cycle.

In Figure 3-5, we show a ternary plot for the saturation of the existing phases at the end of each WAG injection phase in the middle of core. The white filled circle shows the initial point of the WAG injection, after an initial oil saturation of 82% and water saturation of 18% are established (no gas is initially present). The blue arrows indicates the direction of change in the saturation of three phases, and the color of each circle shows the *RF* value at the end of that specific cycle. According to Figure 3-5, the successive WF and GI cycles change the ultimate *RF* to 94% at the end of GI_3. The oil saturation is initially 82%. In the first WAG cycle, the oil saturations decrease to 42% and 29% at the end of WF_1 and GI_1, respectively; in this cycle, the water saturation increases from 18% at an initial state to 58% at the end of WF_1 and then lowers to 47% after GI_1; the gas saturation is still 0% at the end of WF1 which increases to 24% by the end of GI_1. The oil saturation continues to decline during the second and third WAG injection cycles; the oil saturation at the end of WF_2, GI_2, WF_3, and GI_3 are 25%, 17%, 13%, and 6%, respectively. Unlike the oil phase, the core center saturation for water and gas alternatively increases and decreases due to the cyclic injection of water and gas phases. The water saturations at the end of WF_2, GI_2, WF_3, and GI_3 are 57%, 40%, 58%, and 38%, respectively. Therefore, the imbibition cycles increase the water saturation consistently to about 57–58%. The drainage cycles, however, tend to lower the ultimate water saturation for the core mid-point from 48–38%, but the majority of changes is in the first cycle. In the second and third WAG injection stages, the water saturation of core mid-point during the drainage cycles decreases to 40–38%. The gas saturation at the end of WF_2, GI_2, WF_3, and GI_3 are 18%, 43%, 29%, and 56%, respectively. The results show that the gas phase is persistently affected by the hysteresis imposed by the successive imbibition and drainage processes. It is concluded that between the strongly wetting phase (water) and strongly non-wetting phase (gas), the gas phase is affected by the cyclic hysteresis the most, while water is not significantly affected by the hysteresis.

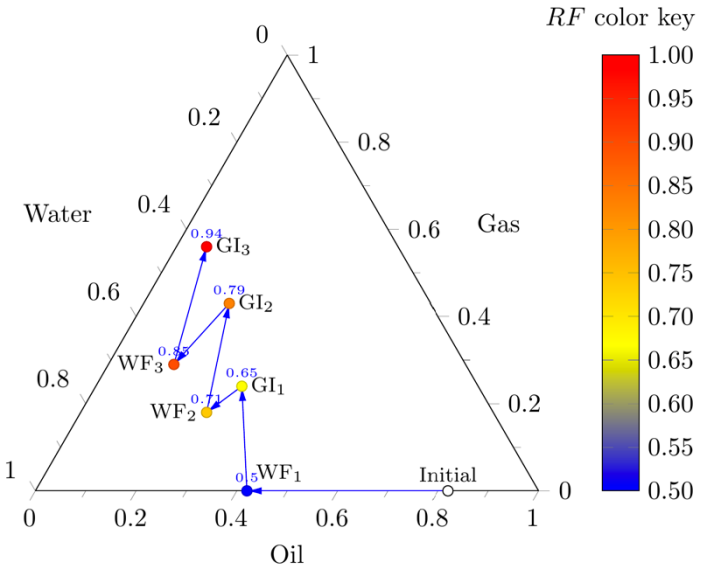

Figure 3-5: A ternary saturation profile (core center) for water-oil-gas system in WAG injection. The colored markers show saturation at the end of each stage along with the RF value (q=25 cm^3/h, slug size=1 PV, and WAG ratio=1).

3.5.2 Sensitivity Analysis

A parametric sensitivity analysis is conducted to investigate the impacts of the operational conditions (WAG ratio, WAG injection rate, and WAG slug size (PVI)) on the performance of a WAG injection process.

Effect of process: Referring to Figure 3-6, we investigate the behaviors of oil recovery upon WF, GI and near-miscible WAG (at WAG ratio=1) for a water-wet core. In Figure 3-6, the values of the recovery factor obtained by the near-miscible WAG injection are compared with those from primary GI and primary WF. The near-miscible WAG injection exhibits a higher performance than the stand-alone injection of water or gas. However, the breakthrough recovery upon primary WF is much lower than that in the primary GI, which is due to the wettability of the core that is strongly water-wet. The gas phase is the most non-wetting phase that tends to invade the percolating pathway of larger pores from the injection side to the production side. Interestingly, the breakthrough recovery for the stand-along GI process is even slightly higher than the *RF* at gas breakthrough after injecting the first gas cycle in WAG (i.e., after GI_1). The breakthrough *RF* upon primary WF, primary GI and WAG are about 50%, 75% and 93%, respectively. The near-miscible WAG process can, therefore, enhance the oil recovery factory considerably.

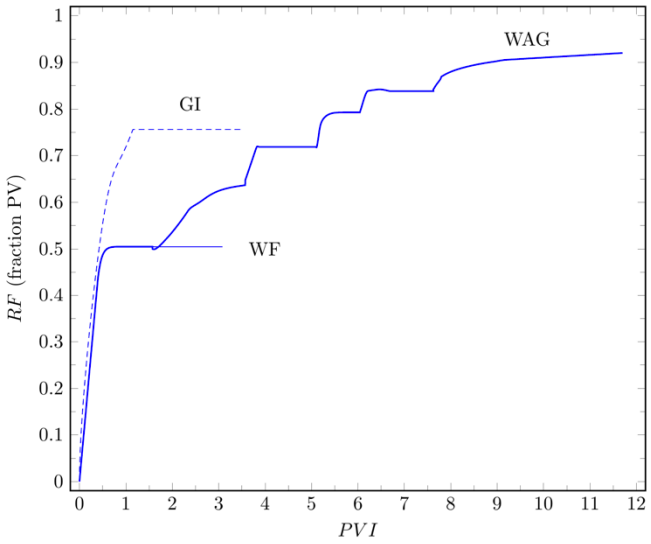

Figure 3-6: A comparison between the oil recovery behavior upon waterflooding (WF), gas injection (GI) and water-alternating-gas (WAG, 1) in a strongly water-wet core (q=25 cm^3/h).

Effect of WAG ratio*:* Finding the optimum WAG ratio is of significant parameters in designing a WAG injection process. Wettability is a parameter that also correlates with the effects from WAG ratio; the recovery performance of a WAG process is especially affected by the wettability at high WAG ratios [62]. At a high WAG ratio, lower oil recovery was reported upon WAG injection, which is even more pronounced in water-wet systems [98]. Optimal WAG ratio is also affected by the shape of water-blocking curve, which is the residual oil saturation versus the water saturation curve. The majority of published works report optimal WAG ratio of 1[98]. There are a few cases that report higher recovery at high WAG ratios (such as 3) for which a great portion of the recovered oil is obtained through an uneconomically high water-cut production [28].

To study the influence of the WAG ratio, we perform near-miscible WAG simulation for three different WAG ratios: 1, 0.5, and 2, as seen in Figure 3-7. According to Figure 3-7, the highest recovery factor is attained at the WAG ratio of 1 (*RF*=92.0%), while the WAG ratio of 0.5 gives the lowest recovery (*RF*=74.3%). At a WAG ratio of 2, at the beginning of the process (corresponding to high oil saturation in the system), oil trapping happens as a result of water blockage. Due to the water-wet nature of the rock, water tends to occupy the smaller pores and blocks the oil flow from larger pores. At high WAG ratios (of 2), the larger pores (with lower capillary pressure and higher oil content) have less chance to be invaded by the gas phase since the system is strongly water-wet and also due to the lower flowrate of the gas phase. However, water occupies smaller pores at early stages and invades a sequence of smaller pores towards the production zones, resulting in higher residual oil and early breakthrough of the water

phase (when WAG starts with the WF cycle). Hence, during this early period, the WAG process performs similar to a WF process. At later stages of WAG injection, as the amount of trapped oil decreases in the system, the lower oil recovery in the early WF and GI cycles is compensated by enhanced gas-oil contact in the system. However, the ultimate recovery (e.g., 87.0%) is still lower than the optimal WAG ratio of 1 (*RF*=92.0%).

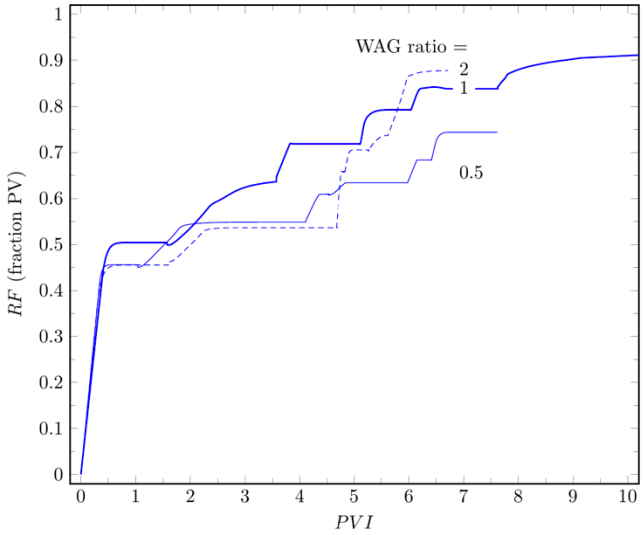

Figure 3-7: Effect of WAG ratio on the recovery performance of near-miscible WAG injection (q=25 cm^3/h, slug size=1 PV).

For the case of WAG ratio of 0.5, gas channeling happens due to high gas saturation, resulting in early gas breakthrough (BT) with a rapid decline in pressure, and consequently, a lower ultimate oil recovery factor. Thus, at a WAG ratio of 0.5, the gas phase travels at a higher velocity than the water phase. The higher velocity of the gas phase and its higher mobility results in viscous fingering, causing fluid instability and early breakthrough, which can be seen in lower ultimate recovery of 74.0%. Hence, our results confirm that the best WAG ratio for our system is 1, where both phases (gas and water) travel at the same velocity, resulting in more stable fluid's front, a delayed breakthrough of injected fluids, and consequently, lower residual oil saturation (S_{or}=0.066).

Effect of injection rate*:* We also examine the performance of near-miscible WAG injection at three injection rates of 10, 25 (corresponding to $N_{ca,ow}$= 2.76×10^{-6}), and 40 cm^3/h, using a constant WAG ratio of 1. As can be seen in Figure 3-8, there is no significant difference in the oil recovery performance as well as ultimate *RF* for the case of 10 and 25 cm^3/h. A slightly lower *RF* is achieved at primary WF at the highest injection rate of 40 cm^3/h; the lower recovery propagates through the next WAG cycles, and the ultimate *RF* is lowest for this case. This ultimate *RF* is, however, comparable to that for the case of

10 cm^3/h as it is observed in Figure 3-8. Because the core is strongly water-wet, no significant difference is seen in the primary WF at different injection rates. The recovery of all three cases after the primary WF are approximately 50% with the residual saturation of S_{or}=0.41. After that, the first GI process remarkably changes the recovery performance for different injection rates. As Figure 3-8 shows, all major differences of three case occurs during the GI cycles. Higher injection rates are more favorable, especially, in field applications, to contact (and therefore recover) more oil [99]. However, at very high injection rates, phase segregation may happen, resulting in early segregations of the water and gas phases in the reservoir. Early segregation of the phases is caused by the contrast in the density of reservoir fluid. It results in bypassing the oil zone when the injected phases find direct paths (gas phase at the top of the reservoir and water phase at the bottom) towards the production well to cause early breakthrough. It also leads to viscous fingering due to the dominancy of viscous forces, causing interface front instability. WAG studies show that [6] there is an optimum injection rate where the overall process performances are maximized at an intermediate injection rate. In our study, the flowrate of 25 cm^3/h gives the highest recovery factor of 92%, which can be compared to the ultimate recovery of 86% and 83% at 10 cm^3/h and 40 cm^3/h, respectively as it is summarized in Table 3-4. In the case of WAG injection at 10 cm^3/h, the process is continued for 2.5 cycles and ceased after the third WF injection. At the end of the third WF cycle, no more oil is produced after the breakthrough.

Table 3-4**:** WAG injection results at three different injection rates of 10, 25 and 40 cm^3/h.

Injection rate (cm^3/h)	RF	S_{or}	No. cycles	Total PVI
10	0.86	0.115	2.5	7.43
25	0.92	0.066	3	11.7
40	0.83	0.140	3	4.55

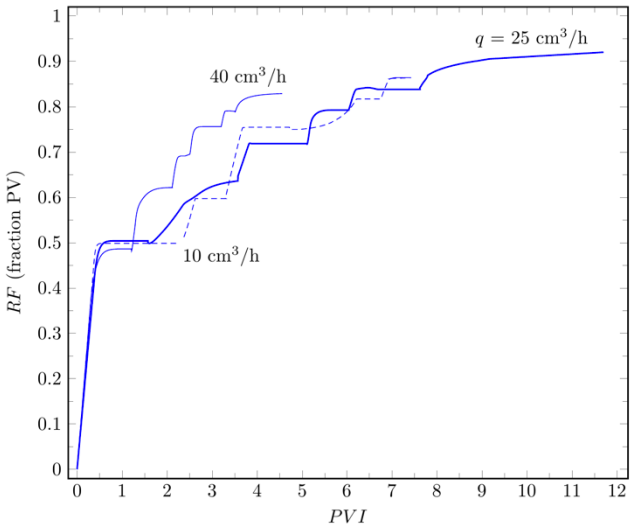

Figure 3-8: Effect of injection rate on oil recovery factor upon near-miscible WAG injection (slug size=1 PV, and WAG ratio=1).

Effect of oil viscosity*:* The oil viscosity affects mobility ratio of displacing and displaced fluids, residual oil saturation, and the ultimate recovery in the three-phase flow of oil, water, and gas in the WAG injection process. To evaluate the impacts of oil viscosity, the near-miscible WAG simulations are conducted, using different oil samples whose viscosities are 0.04, 0.4, and 4 cP (see Table 3-5 and Figure 3-9). All cases are simulated in three cycles, starting with primary WF, where the same injection rate of 25 cm^3/h and WAG ratio of 1 are used in all cases.

Table 3-5**:** Viscosity sensitivity analysis after WAG flooding process.

Oil viscosity (cP)	Total PVI	Ultimate *RF* (%)
0.04	11.7	92.0
0.4	14.2	79.0
4	18.5	69.4

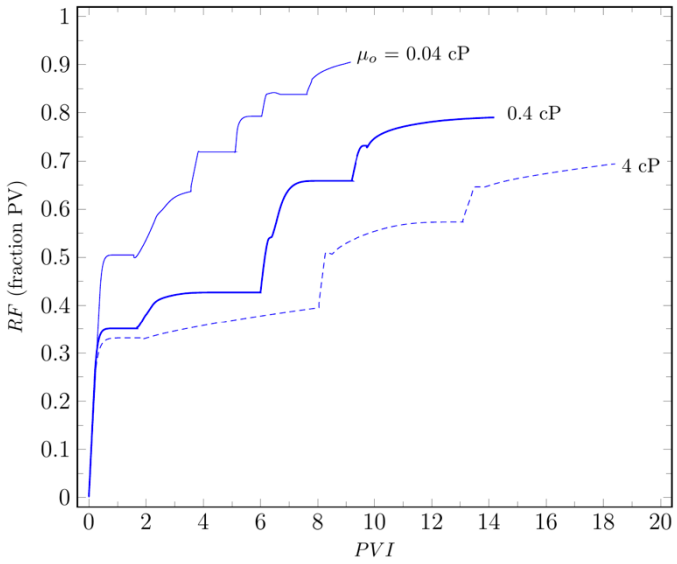

Figure 3-9: Influence of oil viscosity on oil recovery performance upon near-miscible WAG injection (q=25 cm^3/h, slug size=1 PV, and WAG ratio=1).

As it is observed in Figure 3-9, increasing the oil viscosity decreases the oil recovery factor. Unlike the effect of injection rate, the primary WF injection is also affected by changing the viscosity in the range 0.04 cP to 4 cP. This means that the viscous forces overcome the capillarity; otherwise, it was expected to obtain a similar *RF* at the breakthrough condition of WF_1. When the oil viscosity increases 0.04 cP to 0.4 cP, the ultimate recovery is decreased by 11%. Compared to the case of 0.04 cP, the ultimate *RF* with 4 cP oil is decreased by 21%. The oil viscosity strongly affects the behavior of WAG gas and water slug injections as well. As the viscosity of the oil increases, larger slug sizes of the injected fluid are needed to push the same amount of oil bank to the producing end of the core. As depicted in Figure 3-9, when the oil viscosity changes from 0.04 to 0.4 cP, the duration of each cycle (or injection period) becomes longer. This prolonged injection is especially pronounced in the GI stages due to a higher viscosity difference between the oil and gas phases. This condition leads to a greater mobility ratio (10 times). Thus, a higher *PVI* is required to push the oil bank. This finding is also in agreement with the Sohrabi et al. [18] observations in micromodel WAG injection experiments. They reported that the gas channels mainly through the oil-filled pores and reduces the recovery factor due to lower interfacial tension between the gas and oil in near-miscible flow [18].

Effect of WAG slug size*:* The influence of slug size (in PV) on the WAG injection performance is analyzed for which the results are shown in Figure 3-10. In this section, an injection rate of 25 cm^3/hr and a WAG ratio of 1 are considered. Figure 3-10 compares the oil recovery factor versus *PVI* for WAG injection with slug sizes of 0.2 PV, 0.5 PV and 1 PV. According to the results, an increase in the injection

slug size from 0.2 PV to 1 PV is favored as it improves the ultimate oil recovery. The increase in slug size causes more contact between the injected phases and the hydrocarbon phase and also the relative permeability to the injected phase, which allows overcoming the capillary forces that trap the oil. For instance, during the GI following a WF, there is a high entry capillary pressure for gas invasion into those pores that are occupied by the brine (from the previous injection process). Hence, the gas phase invades a new path in the porous media, which will subsequently push the oil toward the outlet of the core. It implies that the fluids obtain a greater chance to redistribute in the porous medium and to improve the sweep efficiency (and thereby, the ultimate oil recovery of the cycle) with increasing the slug size.

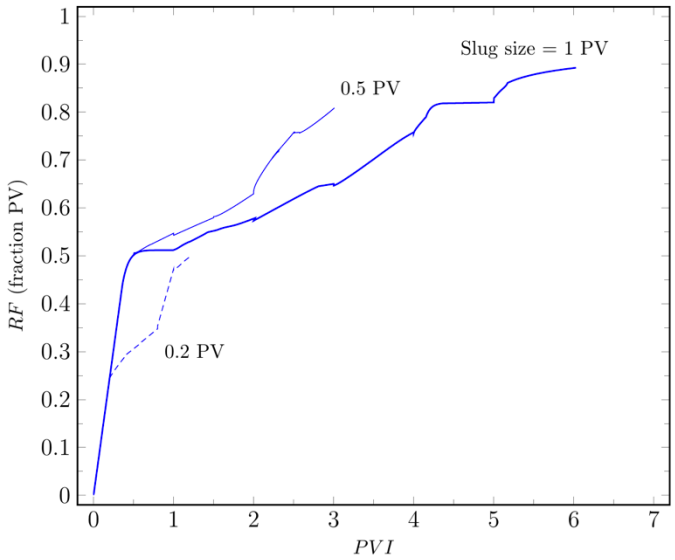

Figure 3-10: Effect of slug size on oil recovery performance upon near-miscible WAG injection (q=25 cm^3/h, and WAG ratio=1).

Effect of absolute permeability*:* We compare the WAG recovery profile for the cases of a core with permeability 65 mD, 200 mD and 500 mD to assess the impacts of the absolute permeability on the WAG injection performance in a water-wet core. The base case is attributed to the experimental work that used a 65 mD core sample (see Figure 3-11). The injection rate of 25 cm^3/h and WAG ratio of 1 are used in the simulation runs. According to Figure 3-11, changing the permeability from 65 mD to 500 mD slightly increases the breakthrough *RF* for the primary WF. A porous medium with a higher permeability leads to a greater recovery factor in the primary WF stage. This difference seems to propagate during next cycles of WAG injection; however, there is not a significant difference between the ultimate *RF* by varying the absolute permeability of the core from 65 mD to 500 mD in near-miscible WAG injection as it is observed in Figure 3-11. For the case of the high-permeability core, a lower number of cycles is required to attain the ultimate recovery compared the case of WAG injection in a

low-permeability core. For instance, in the case of WAG injection in the 200 mD permeability sample, which is approximately three times more permeable than the baseline (65 mD case), the process is completed in 2.5 cycles. At the 3rd WF process (WF_3), ultimate recovery of 92.5 % is obtained after 10 PVI, while the ultimate recovery of the 65 mD core is 92 % after 12 PVI. Figure 3-11 also illustrates that the ultimate recovery values of all three cases are similar (at about 92 %). This again highlights the effectiveness of the WAG process in minimizing the residual oil saturation in a water-wet system even at a wide range of core permeability.

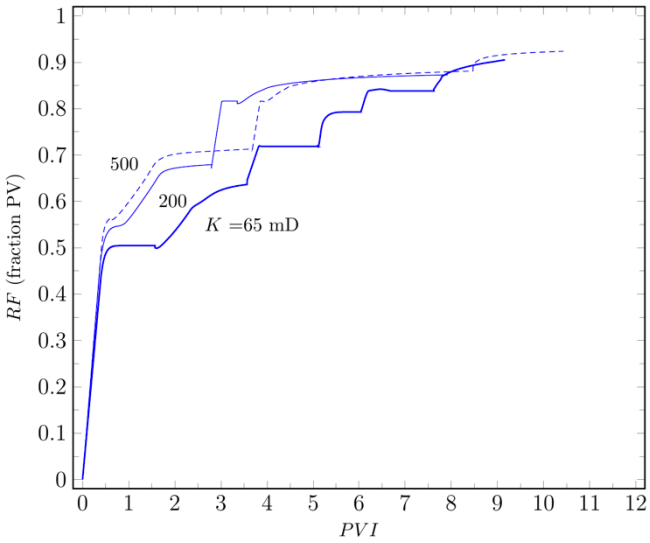

Figure 3-11: The effect of absolute permeability oil recovery performance upon near-miscible WAG injection (q=25 cm^3/h, slug size=1 PV, and WAG ratio=1).

Despite the extensive research and engineering studies on the WAG injection as an EOR technique, mathematical modeling of near-miscible WAG injection process has not been studied in the literature. Our model with three-phase capillary pressure and relative permeability considers the hysteresis effects and successfully captures the process physics. The proposed model can be used by other research and/or industrial sectors to suggest the optimal operation of near-miscible process, which can be not only used for oil recovery but also for the remediation operation. In other words, the introduced mathematical model can be utilized to estimate the optimal WAG ratio, WAG size, injection rate, and the cumulative fluids to obtain the optimal recovery in terms of technical, economic, and environmental prospects.

3.6 SUMMARY AND CONCLUSIONS

In the present study, we develop a dynamic three-phase flow mathematical model (IMPES) of near-miscible water-alternating-gas (WAG) injection process with enhanced oil recovery application. The accuracy of the mathematical model is verified using the experimental results taken from the literature

where the porous medium of the case study is a water-wet Berea sandstone core at 38˚C and 12.7 MPa. The effects of various variables such as WAG ratio and injection rate on the WAG performance are then studied. The following conclusions and recommendations for future works can be drawn based on the study outputs:

- By incorporating the three-phase relative permeability, capillary pressure, and hysteresis effects, an excellent match is attained between the experimental and simulation results. It is found that the three-phase relative permeability and capillary pressure models (including the three-phase hysteresis) proposed by Shahverdi and Sohrabi are suitable for the near-miscible WAG process studied in this research work.
- The absolute relative error in estimating the oil recovery factor at the end of each WF and GI cycle is less than 1.7%. The breakthrough times for individual injected fluids (gas and water) in three different cycles are also estimated with a high accuracy using the mathematical model. Hence, very good agreement is obtained between the predicted and real recovery values (and breakthrough times) over the three cycles of water-and-gas injection.
- By changing the WAG ratio in the model from 0.5 to 1 and to 2, it is noticed that the optimal operating condition is achieved at the WAG ratio of 1. Although the ultimate *RF* values of the 1 and 1 WAG ratios are not appreciably different, the WAG ratio of 0.5 leads to a substantially lower ultimate RF.
- The total amount of injected fluids to achieve an ultimate *RF* of 90% decreases from 11.7 PVI to less than a total PVI of 5 with increasing the injection rate from 25 ml/h to 40 ml/h. A comparison between the cases with the injection flow rates of 10 ml/h and 25 ml/h shows that after one WAG injection cycle, the recovery behaviors follow similar trends at these two injection rates.
- According to the simulation results, a *RF* of 50.1% is obtained upon primary WF, while the cumulative *RF* increases to 64.6% after the first GI. Implementing the secondary WF and GI cycle, the *RF* increases further to 71.9% and 79.4%, respectively. In the tertiary WF and GI cycle, the *RF* reaches 84.3% and 92.0%, respectively.
- By increasing the oil viscosity up to three orders of magnitude, the recovery factor decreases by 21 %. An increase in the oil viscosity not only reduces the ultimate recovery, it increases the duration (higher PVI) of each WF or GI process.
- It is revealed that a higher absolute permeability increases the production rate, while the ultimate recovery of the system does not alter remarkably.

- A lower fixed injection slug size results in less oil recovery in each cycle as there would be less contact and interactions between the phases to direct the hydrocarbon phase to the outlet of the porous sample.
- The hysteresis in decreasing and increasing the fluid's saturation affects the saturation of the non-wetting phase (gas) the most, while it does not appreciably affect the saturation of the most wetting phase (water).
- For future works, the effect of the gravity can be studied to discover the impact of gravity forces on the recovery of the system.
- One of the recommended case for next studies is to investigate other wettability states (e.g. oil-wet or water-wet) on recovery of near-miscible WAG injection process.

ACKNOWLEDGEMENTS

The authors would like to acknowledge the financial support provided by Memorial University (NL, Canada), Natural Sciences and Engineering Research Council of Canada (NSERC), InnovateNL (formerly RDC), and Equinor (formerly Statoil) Canada.

NOMENCLATURES

Acronyms

EOR	Enhanced oil recovery
GI	Gas injection
IFT	Interfacial tension
IOR	Improved oil recovery
IWAG	Immiscible WAG
IMPES	Implicit-pressure-explicit-saturation
MMP	Minimum miscible pressure
MWAG	Miscible WAG
PVI	Pore volume injection
RF	Recovery factor
WF	Waterflooding
WAG	Water-alternating-gas injection

Variables and Parameters

a	Capillary exponent
c	Capillary entry pressure
K	Absolute permeability
k_{ri}	Relative permeability of phase i
p	Pressure
s_i	Saturation of phase i
t	Time
x	Length

Greek Letters

μ	Viscosity
ρ	Density
σ	Interfacial tension
ϕ	Porosity
θ	Contact angle

Subscripts and Superscripts

C	Capillary pressure
D	Drainage
g	Gas phase
I	Imbibition
o	Oil phase
og	Oil-gas system
ow	Oil-water system
w	Water phase
wg	Water-gas system
r	Residual phase

References

1. Hustad, O. S.; Holt, T. In *Gravity stable displacement of oil by hydrocarbon gas after waterflooding*, SPE/DOE Enhanced Oil Recovery Symposium, Society of Petroleum Engineers: 1992.

2. Shpak, R. Modeling of Miscible WAG Injection Using Real Geological Field Data. Institutt for petroleumsteknologi og anvendt geofysikk, 2013.
3. Touray, S., Effect of water alternating gas injection on ultimate oil recovery. *Master of Engineering. Dalhousie University* **2013**, 25.
4. Rogers, J. D.; Grigg, R. B., A literature analysis of the WAG injectivity abnormalities in the CO2 process. *SPE Reservoir Evaluation & Engineering* **2001,** *4* (05), 375-386.
5. Kulkarni, M. M.; Rao, D. N., Experimental investigation of miscible and immiscible Water-Alternating-Gas (WAG) process performance. *Journal of Petroleum Science and Engineering* **2005,** *48* (1-2), 1-20.
6. Afzali, S.; Rezaei, N.; Zendehboudi, S., A comprehensive review on Enhanced Oil Recovery by Water Alternating Gas (WAG) injection. *Fuel* **2018,** *227*, 218-246.
7. Shahverdi, H. Characterization of three-phase flow and WAG injection in oil reservoirs. Heriot-Watt University, 2012.
8. Al Shamsi, H. A.; Al-Katheeri, A. B.; Al Ameri, A. F.; Abdulrahman, A. S.; Sajeel, K.; Al Yaaqoobi, A. In *Immiscible WAG Injection Pilots Performance and Lessons Learnt in Carbonate Reservoir. Onshore Abu Dhabi Oil Field, United Arab Emirates*, Abu Dhabi international petroleum conference and exhibition, Society of Petroleum Engineers: 2012.
9. Awan, A. R.; Teigland, R.; Kleppe, J., A survey of North Sea enhanced-oil-recovery projects initiated during the years 1975 to 2005. *SPE Reservoir Evaluation & Engineering* **2008,** *11* (03), 497-512.
10. Christensen, J. R.; Stenby, E. H.; Skauge, A. In *Review of WAG field experience*, International petroleum conference and exhibition of Mexico, Society of Petroleum Engineers: 1998.
11. Choudhary, M. K.; Parekh, B.; Dezabala, E.; Solis, H. A.; Pujiyono, P.; De Narvaez, Z.; Zambrano, J. In *Design, implementation and performance of a down-dip WAG pilot*, international petroleum technology conference, International Petroleum Technology Conference: 2011.
12. Kong, X.; Delshad, M.; Wheeler, M. F. In *A numerical study of benefits of adding polymer to WAG processes for a pilot case*, SPE Reservoir Simulation Symposium, Society of Petroleum Engineers: 2015.
13. Nadeson, G.; Anua, N. A. B.; Singhal, A.; Ibrahim, R. B. In *Water-alternating-gas (WAG) pilot implementation, a first EOR development project in Dulang field, offshore Peninsular Malaysia*, SPE Asia Pacific Oil and Gas Conference and Exhibition, Society of Petroleum Engineers: 2004.
14. Novosel, D. In *Initial results of WAG CO2 IOR pilot project implementation in Croatia*, SPE International Improved Oil Recovery Conference in Asia Pacific, Society of Petroleum Engineers: 2005.
15. Novosel, D. In *Thermodynamic Criteria and Final Results of WAG CO2 Injection in a Pilot Project in Croatia*, SPE Middle East Oil and Gas Show and Conference, Society of Petroleum Engineers: 2009.
16. Al-dhahli, A.; Geiger, S.; van Dijke, M. I. In *Three-phase pore-network modelling for mixed-wet carbonate reservoirs*, SPE Reservoir Characterisation and Simulation Conference and Exhibition, Society of Petroleum Engineers: 2011.

17. Dong, M.; Foraie, J.; Huang, S.; Chatzis, I. In *Analysis of immiscible water-alternating-gas (WAG) injection using micromodel*, Canadian International Petroleum Conference, Petroleum Society of Canada: 2002.
18. Sohrabi, M.; Henderson, G.; Tehrani, D.; Danesh, A. In *Visualisation of oil recovery by water alternating gas (WAG) injection using high pressure micromodels-water-wet system*, SPE Annual Technical Conference and Exhibition, Society of Petroleum Engineers: 2000.
19. Sohrabi, M.; Jamiolahmady, M., Mechanism of injectivity loss during water-alternating-gas (WAG) injection. *Gas (C1+ nC10)* **2005,** *5* (7), 0.0209.
20. Khan, M. Y.; Kohata, A.; Patel, H.; Syed, F. I.; Al Sowaidi, A. K. In *Water alternating gas WAG optimization using tapered WAG technique for a giant offshore Middle East Oil Field*, Abu Dhabi International Petroleum Exhibition & Conference, Society of Petroleum Engineers: 2016.
21. Kim, G.; Jang, H.; Cho, M.; Lee, J. In *Optimizing the Design Parameters for Performance Evaluation of the CO 2-WAG Process in a Heterogeneous Reservoir*, The Twenty-fifth International Ocean and Polar Engineering Conference, International Society of Offshore and Polar Engineers: 2015.
22. Namani, M.; Kleppe, J. In *Investigation of the effect of some parameters in miscible WAG process using black-oil and compositional simulators*, SPE Enhanced Oil Recovery Conference, Society of Petroleum Engineers: 2011.
23. Shandrygin, A.; Shelepov, V.; Ramazanov, R.; Andrianov, N.; Klemin, D.; Nadeev, A.; Yakimchuk, I. In *Mechanism of oil displacement during WAG in porous media with micro-inhomogeneities*, SPE Russian Petroleum Technology Conference, Society of Petroleum Engineers: 2015.
24. Van Dijke, M. I. J.; Sorbie, K. S.; Sohrabi, M.; Tehrani, D.; Danesh, A. In *Three-phase flow in WAG processes in mixed-wet porous media: pore-scale network simulations and comparison with micromodel experiments*, SPE/DOE Improved Oil Recovery Symposium, Society of Petroleum Engineers: 2002.
25. Al-Netaifi, A. S., Experimental investigation of CO2-miscible oil recovery at different conditions. *King Saud University, Saudi Arabia* **2008**.
26. Bou-Mikael, S. In *A new analytical method to evaluate, predict, and improve CO2 flood performance in sandstone reservoirs*, SPE/DOE Improved Oil Recovery Symposium, Society of Petroleum Engineers: 1996.
27. Christian, L.; Shirer, J.; Kimbel, E.; Blackwell, R., Planning a tertiary oil-recovery project for Jay/LEC fields unit. *SPE-994-PA* **1981,** *33* (08), 1,535-1,544.
28. Jackson, D.; Andrews, G.; Claridge, E. In *Optimum WAG ratio vs. Rock wettability in CO2 flooding*, SPE Annual Technical Conference and Exhibition, Society of Petroleum Engineers: 1985.
29. Jiang, H.; Nuryaningsih, L.; Adidharma, H. In *The effect of salinity of injection brine on water alternating gas performance in tertiary miscible carbon dioxide flooding: experimental study*, SPE Western Regional Meeting, Society of Petroleum Engineers: 2010.
30. Masoner, L.; Abidi, H.; Hild, G. In *Diagnosing CO2 flood performance using actual performance data*, SPE/DOE Improved Oil Recovery Symposium, Society of Petroleum Engineers: 1996.

31. Sharma, M.; Filoco, P., Effect of brine salinity and crude-oil properties on oil recovery and residual saturations. *SPE Journal* **2000,** *5* (03), 293-300.
32. Stalkup, F., Miscible flooding fundamentals. *Society of Petroleum Engineers Monograph Series* **1983,** *8*.
33. Suicmez, V. S.; Piri, M.; Blunt, M. J. In *Pore-scale modeling of three-phase WAG injection: Prediction of relative permeabilities and trapping for different displacement cycles*, SPE/DOE Symposium on Improved Oil Recovery, Society of Petroleum Engineers: 2006.
34. Rostami, P.; Mehraban, M. F.; Sharifi, M.; Dejam, M.; Ayatollahi, S., Effect of water salinity on oil/brine interfacial behaviour during low salinity waterflooding: A mechanistic study. *Petroleum* **2019**.
35. Amirian, E.; Dejam, M.; Chen, Z., Performance forecasting for polymer flooding in heavy oil reservoirs. *Fuel* **2018,** *216*, 83-100.
36. Khezrnejad, A.; James, L.; Johansen, T. In *Water enhancement using nanoparticles in water alternating gas (WAG) micromodel experiments*, SPE Annual Technical Conference and Exhibition, Society of Petroleum Engineers: 2014.
37. Al-Mamari, F.; Al-Shuraiqi, H.; Al-Wahaibi, Y. M. In *Numerical simulation and experimental studies of oil recovery via first-contact miscible water alternating gas injection within shaley porous media*, SPE/EAGE Reservoir Characterization and Simulation Conference, Society of Petroleum Engineers: 2007.
38. Bequette, B. W., Nonlinear control of chemical processes: A review. *Industrial & Engineering Chemistry Research* **1991,** *30* (7), 1391-1413.
39. Duchenne, S.; de Loubens, R.; Petitfrere, M.; Joubert, T. In *Modeling and Simultaneous History-Matching of Multiple WAG Coreflood Experiments at Reservoir Conditions*, Abu Dhabi International Petroleum Exhibition and Conference, Society of Petroleum Engineers: 2015.
40. Haajizadeh, M.; Narayanan, R.; Waldren, D. In *Modeling Miscible WAG Injection EOR in the Magnus Field*, SPE Reservoir Simulation Symposium, Society of Petroleum Engineers: 2001.
41. Heeremans, J. C.; Esmaiel, T. E.; Van Kruijsdijk, C. P. In *Feasibility study of WAG injection in naturally fractured reservoirs*, SPE/DOE Symposium on Improved Oil Recovery, Society of Petroleum Engineers: 2006.
42. Larsen, J. A.; Skauge, A. In *Simulation of the immiscible WAG process using cycle-dependent three-phase relative permeabilities*, SPE Annual Technical Conference and Exhibition, Society of Petroleum Engineers: 1999.
43. Rahmawati, S. D.; Whitson, C. H.; Foss, B., A mixed-integer non-linear problem formulation for miscible WAG injection. *Journal of Petroleum Science and Engineering* **2013,** *109*, 164-176.
44. Zuo, L.; Chen, Y.; Dengen, Z.; Kamath, J., Three-phase relative permeability modeling in the simulation of WAG injection. *SPE Reservoir Evaluation & Engineering* **2014,** *17* (03), 326-339.
45. Agada, S.; Geiger, S. In *Wettability, trapping and fracture-matrix interaction during WAG injection in fractured carbonate reservoirs*, SPE Improved Oil Recovery Symposium, Society of Petroleum Engineers: 2014.

46. Agada, S.; Geiger, S.; Elsheikh, A.; Oladyshkin, S., Data-driven surrogates for rapid simulation and optimization of WAG injection in fractured carbonate reservoirs. *Petroleum Geoscience* **2017,** *23* (2), 270-283.
47. Kløv, T.; Øren, P.; Stensen, J.; Lerdahl, T.; Berge, L.; Bakke, S.; Boassen, T.; Virnovsky, G. In *Pore-to-field scale modeling of WAG*, SPE Annual Technical Conference and Exhibition, Society of Petroleum Engineers: 2003.
48. Egermann, P.; Vizika, O.; Dallet, L.; Requin, C.; Sonier, F. In *Hysteresis in three-phase flow: experiments, modeling and reservoir simulations*, SPE European Petroleum Conference, Society of Petroleum Engineers: 2000.
49. Hustad, O. S.; Browning, D. J. In *A fully coupled three-phase model for capillary pressure and relative permeability for implicit compositional reservoir simulation*, SPE/EAGE Reservoir Characterization & Simulation Conference, 2009.
50. Jerauld, G., General three-phase relative permeability model for Prudhoe Bay. *SPE reservoir Engineering* **1997,** *12* (04), 255-263.
51. Larsen, J.; Skauge, A., Methodology for numerical simulation with cycle-dependent relative permeabilities. *SPE Journal* **1998,** *3* (02), 163-173.
52. Shahverdi, H.; Sohrabi, M., An improved three-phase relative permeability and hysteresis model for the simulation of a water-alternating-gas injection. *Spe Journal* **2013,** *18* (05), 841-850.
53. Sherafati, M.; Jessen, K. In *Modeling and simulation of WAG injection processes-the role of counter-current flow*, SPE Western Regional Meeting, Society of Petroleum Engineers: 2015.
54. Skauge, A.; Dale, E. I. In *Progress in immiscible WAG modelling*, SPE/EAGE Reservoir Characterization and Simulation Conference, Society of Petroleum Engineers: 2007.
55. Skauge, A.; Dale, E. In *Fluid Flow Properties of WAG Injection Processes*, IOR 2005-13th European Symposium on Improved Oil Recovery, 2005.
56. Juanes, R.; Patzek, T. W., Analytical solution to the Riemann problem of three-phase flow in porous media. *Transport in Porous Media* **2004,** *55* (1), 47-70.
57. Stone, H., Probability model for estimating three-phase relative permeability. *Journal of Petroleum Technology* **1970,** *22* (02), 214-218.
58. Beygi, M. R.; Delshad, M.; Pudugramam, V. S.; Pope, G. A.; Wheeler, M. F., Novel three-phase compositional relative permeability and three-phase hysteresis models. *SPE Journal* **2015,** *20* (01), 21-34.
59. Fayers, F.; Foakes, A.; Lin, C.; Puckett, D. In *An improved three phase flow model incorporating compositional variance*, SPE/DOE Improved Oil Recovery Symposium, Society of Petroleum Engineers: 2000.
60. Baker, L. In *Three-phase relative permeability correlations*, SPE Enhanced Oil Recovery Symposium, Society of Petroleum Engineers: 1988.
61. Todd, M.; Longstaff, W., The development, testing, and application of a numerical simulator for predicting miscible flood performance. *Journal of Petroleum Technology* **1972,** *24* (07), 874-882.
62. Stern, D. In *Mechanisms of miscible oil recovery: effects of pore-level fluid distribution*, SPE Annual Technical Conference and Exhibition, Society of Petroleum Engineers: 1991.
63. Shahrokhi, O.; Fatemi, M.; Sohrabi, M.; Ireland, S.; Ahmed, K. In *Assessment of three phase relative permeability and hysteresis models for simulation of water-alternating-gas*

(WAG) injection in water-wet and mixed-wet systems, SPE Improved Oil Recovery Symposium, Society of Petroleum Engineers: 2014.
64. Sohrabi, M.; Danesh, A.; Jamiolahmady, M., Visualisation of residual oil recovery by near-miscible gas and SWAG injection using high-pressure micromodels. *Transport in Porous Media* **2008,** *74* (2), 239-257.
65. Sohrabi, M.; Danesh, A.; Tehrani, D. H.; Jamiolahmady, M., Microscopic mechanisms of oil recovery by near-miscible gas injection. *Transport in Porous Media* **2008,** *72* (3), 351-367.
66. Sohrabi, M. Water Alternating Gas Injection (WAG) Studies. PhD thesis, Institute of Petroleum Engineering, Heriot-Watt University …, 2001.
67. Fatemi, S. M. Multiphase flow and hysteresis phenomena in oil recovery by water alternating gas (WAG) injection. Heriot-Watt University, 2015.
68. https://www.bp.com/en/global/corporate/energy-economics/statistical-review-of-world-energy/oil/oil-reserves.html.
69. Pudugramam, V. S., A numerical study of CO_2-EOR with emphasis on mobility control processes: Water Alternating Gas (WAG) and foam. **2013**.
70. Mashayekhizadeh, V.; Kord, S.; Dejam, M., EOR potential within Iran. *Special Topics & Reviews in Porous Media: An International Journal* **2014,** *5* (4).
71. Ahmed, T., *Reservoir engineering handbook*. Elsevier: 2006.
72. Holm, L., Propane-gas-water miscible floods in watered-out areas of the adena field, Colorado. *Journal of Petroleum Technology* **1972,** *24* (10), 1,264-1,270.
73. Moffitt, P.; Zornes, D. In *Postmortem analysis: lick creek meakin sand unit immiscible CO2 waterflood project*, SPE Annual Technical Conference and Exhibition, Society of Petroleum Engineers: 1992.
74. Watts, R. J.; Conner, W. D.; Wasson, J. A.; Yost, A. B. In *CO2 injection for tertiary oil recovery, Granny's Creek Field, Clay County, West Virginia*, SPE Enhanced Oil Recovery Symposium, Society of Petroleum Engineers: 1982.
75. Gharbi, R.; Peters, E.; Elkamel, A., Scaling miscible fluid displacements in porous media. *Energy & fuels* **1998,** *12* (4), 801-811.
76. Fatemi, S. M.; Sohrabi, M.; Jamiolahmady, M.; Ireland, S.; Robertson, G. In *Experimental investigation of near-miscible water-alternating-gas (WAG) injection performance in water-wet and mixed-wet systems*, Offshore Europe, Society of Petroleum Engineers: 2011.
77. Surguchev, L.; Korbol, R.; Haugen, S.; Krakstad, O. In *Screening of WAG injection strategies for heterogeneous reservoirs*, European petroleum conference, Society of Petroleum Engineers: 1992.
78. Tabatabaei Nezhad, S. A. R.; Rahimzadeh Mojarad, M.; Oskouei, P.; Javad, S.; Moghadas, J. S.; Farahmand, D. R. In *Experimental Study on Applicability of Water Alternating CO2 Injection in the Secondary and Tertiary Recovery*, International Oil Conference and Exhibition in Mexico, Society of Petroleum Engineers: 2006.
79. Virnovsky, G.; Vatne, K.; Iversen, J.; Signy, C. In *Three-phase capillary pressure measurements in centrifuge at reservoir conditions*, SCA2004-19, paper for the International Symposium of the Society of Core Analysts, Abu Dhabi, 2004; pp 5-9.

80. Zhou, Y.; Helland, J. O.; Hatzignatiou, D. G., Computation of three-phase capillary pressure curves and fluid configurations at mixed-wet conditions in 2D rock images. *SPE Journal* **2016,** *21* (01), 152-169.
81. Neshat, S. S.; Pope, G. A. In *Compositional Three-Phase Relative Permeability and Capillary Pressure Models Using Gibbs Free Energy*, SPE Reservoir Simulation Conference, Society of Petroleum Engineers: 2017.
82. Skjaeveland, S.; Siqveland, L.; Kjosavik, A.; Hammervold, W.; Virnovsky, G. In *Capillary pressure correlation for mixed-wet reservoirs*, SPE India Oil and Gas Conference and Exhibition, Society of Petroleum Engineers: 1998.
83. Shahverdi, H.; Sohrabi, M. In *Three-phase relative permeability and hystresis model for simulation of water alternating gas (WAG) injection*, SPE Improved Oil Recovery Symposium, Society of Petroleum Engineers: 2012.
84. Braun, E.; Holland, R., Relative permeability hysteresis: Laboratory measurements and a conceptual model. *SPE Reservoir Engineering* **1995,** *10* (03), 222-228.
85. Land, C. S., Calculation of imbibition relative permeability for two-and three-phase flow from rock properties. *Society of Petroleum Engineers Journal* **1968,** *8* (02), 149-156.
86. Osoba, J.; Richardson, J.; Kerver, J.; Hafford, J.; Blair, P., Laboratory measurements of relative permeability. *Journal of Petroleum Technology* **1951,** *3* (02), 47-56.
87. Eleri, O.; Graue, A.; Skauge, A.; Larsen, J. In *Calculation of three-phase relative permeabilities from displacement experiments with measurements of in-situ saturation*, Soc. Core Anal. Int. Symp., San Francisco, 1995.
88. Skauge, A.; Aarra, M. In *Effect of Wettability on the Oil Recovery by WAG*, Proceedings 7th European Symposium on Improved Oil Recovery, Moscow, 1993; pp 452-59.
89. Bradford, S. A.; Leij, F. J., Predicting two-and three-fluid capillary pressure-saturation relationships of porous media with fractional wettability. *Water Resources Research* **1996,** *32* (2), 251-259.
90. Egermann, P.; Mejdoub, K.; Lombard, J.-M.; Vizika, O.; Kalam, Z., Drainage three-phase flow relative permeability on oil-wet carbonate reservoir rock types: Experiments, interpretation and comparison with standard correlations. *Petrophysics* **2014,** *55* (04), 287-293.
91. Oak, M. In *Three-phase relative permeability of intermediate-wet Berea sandstone*, SPE Annual Technical Conference and Exhibition, Society of Petroleum Engineers: 1991.
92. Van Dijke, M.; Sorbie, K.; McDougall, S., Saturation-dependencies of three-phase relative permeabilities in mixed-wet and fractionally wet systems. *Advances in Water Resources* **2001,** *24* (3-4), 365-384.
93. Sheldon, J.; Cardwell Jr, W., One-dimensional, incompressible, noncapillary, two-phase fluid flow in a porous medium. **1959**.
94. Stone, H.; Garder Jr, A., Analysis of gas-cap or dissolved-gas drive reservoirs. *Society of Petroleum Engineers Journal* **1961,** *1* (02), 92-104.
95. Douglas Jr, J.; Peaceman, D.; Rachford Jr, H., A method for calculating multi-dimensional immiscible displacement. **1959**.
96. Chen, Z.; Huan, G.; Li, B., An improved IMPES method for two-phase flow in porous media. *Transport in porous media* **2004,** *54* (3), 361-376.
97. Rezaei, N.; Firoozabadi, A., Pressure evolution and production performance of waterflooding in n-heptane-saturated fired berea cores. *SPE Journal* **2014,** *19* (04), 674-686.

98. Bunge, A.; Radke, C., CO2 flooding strategy in a communicating layered reservoir. *SPE-994-PA* **1982,** *34* (12), 2,746-2,756.
99. Karim, F.; Berzins, T.; Schenewerk, P.; Bassiouni, Z.; Wolcott, J. In *Light oil recovery from cyclic CO2 injection: influence of drive gas, CO2 injection rate, and reservoir dip*, SPE Rocky Mountain Regional Meeting, Society of Petroleum Engineers: 1992.

100. Avraam, D.; Payatakes, A., Flow mechanisms, relative permeabilities, and coupling effects in steady-state two-phase flow through porous media. The case of strong wettability. *Industrial & engineering chemistry research* **1999,** *38* (3), 778-786.
101. Guzman, R.; Domenico, G.; Fayers, F.; Aziz, K.; Godi, A. In Three-phase flow in field-scale simulations of gas and wag injections, *European Petroleum Conference, Society of Petroleum Engineers* **1994**.
102. Ghomian, Y.; Pope, G. A.; Sepehrnoori, K. In Hysteresis and field-scale optimization of WAG injection for coupled CO_2-EOR and sequestration, *SPE Symposium on Improved Oil Recovery, Society of Petroleum Engineers* **2008**.

CHAPTER FOUR

The application of CFD simulation for multi-phase flow in fractured porous media in water-alternating-gas (WAG) injection process (under review)

Preface

A version of this manuscript has been submitted (under review) in the Journal of Hydrology. I am the primary author of this paper. Sohrab Zendehboudi and Nima Rezaei provided me with valuable tips/guidelines to conduct the literature review, and the CFD simulations. I prepared the first draft of the manuscript and then revised the manuscript based on the co-authors' feedback as well as the comments of the peer review process. The co-author Sohrab Zendehboudi also helped in model development, creating a proper manuscript structure, and revising all parts of the manuscript. The last co-author, Ioannis Chatzis provided comments on various section of the manuscript. He also edited the entire text.

Abstract

Naturally fractured reservoirs (NFR) are among major producers of oil and gas reservoirs that are commonly targeted for various enhanced oil recovery (EOR) techniques specially water-alternating-gas (WAG) injection. Production from NFRs is complicated due to the flow communication between the matrix and fractures in fractured porous media. The implementation of WAG injection in NFRs features inherent complexities not only related to the three-phase flow, saturation history, and cycle-dependent hysteresis of the individual phases, but also the fracture-matrix communication, fingering and early breakthrough of injecting phases in system and fracture medium specially during gas injection processes. Moreover, the experimental evaluation of WAG injection in a fractured system is expensive and time-consuming, if not impractical. This paper provides details on the computational fluid dynamic (CFD) simulation of WAG injection in a fractured system. We evaluate the impacts of hysteresis, fracture characteristics (aperture, orientation, and fracture density in the network), and the three-phase relative permeability of phases during the WAG injection using a CFD modeling approach. The model simulates an immiscible WAG injection and the modeling results are compared to the experimental data in a strong water-wet sand-pack. Similar to the experiments, we simulate Maroon crude as the oil phase, and synthetic brine, and pure CO_2 at 100^{o}C and atmospheric pressure. The results from our model are in excellent agreement with the experimental data. The absolute relative error is less than 12 % for predicting the ultimate oil recovery factors (*RF*) in water flooding (WF) and gas injection (GI) cycles. Including three-phase hysteresis, it significantly increases the accuracy of the WAG process simulation. Excluding the hysteresis effects, it remarkably decreases the instantaneous *RFs* at each cycle (especially GI cycles) as well as the ultimate *RF* by 4%. We also analyze the fracture pattern and configuration; adding fractures to the system increases the system effective permeability, leading to more contact between the injecting fluid and trapped oil, and consequently higher oil recovery. Connecting a vertical fracture to the horizontal fracture enhances the recovery through strong connections between vertical and horizontal blocks. An increase in the fracture aperture from 0.5 to 3 mm results in improving the *RF* (from 50 % to 59%). Fracture inclination angle does not considerably change the ultimate RF so that, the RF increases only by 2 %, if the inclination angle varies from 30^o to 90^o. Including the gravity forces in vertical systems results in overall improvement in *RF* through engaging both matrix and fracture media in all cycles. As the permeability contrast between matrix and fracture media decreases, the flow communication between the two regions increases and improves the recovery performance of the WAG process. Our simulation results can help to obtain a comprehensive view towards the effect of various parameters and operational conditions on WAG injection performance in fractured reservoirs.

Keywords: WAG injection; CFD modeling; Fractured reservoirs; Hysteresis effects; Three-phase capillary pressure; Three-phase relative permeability

4.1 Introduction

Natural fractured reservoirs contain a substantial portion of the world's remaining oil reserves. They feature complicated production, unforeseeable coupling of wells, instant fracture charges, early breakthrough, and low ultimate recovery [1-2]. The recovery performances and production mechanisms in fractured and un-fractured (conventional) reservoirs are completely different. One of the major factors that impacts the oil recovery from a fractured reservoir is the capillary pressure difference between the fracture and matrix blocks [3]. The experimental data on fracture characteristics, water breakthrough, and/or relative permeability values are rare and difficult to be implemented or unable to describe the same process in the field scale. Instead, the application of computer modelling and simulations eases these issues and provides an economical tool to study various factors such as viscous, capillary and gravitational forces at various scales of investigation.

Fractured reservoirs are associated with complex pore structure heterogeneities that include high flow conductivity in fractures and low contributions to flow in the pore matrix [4]. This complexity makes the design of EOR techniques difficult due to poor control of fluid injection into the system, resulting in low sweep efficiency and early breakthrough toward the producing wells [4]. Early breakthrough among all possible problems has been shown in several case studies, indicating very low overall hydrocarbon recovery in fractured reservoirs [5-7]. In addition, the lack of interconnected fracture networks in NFR systems makes the application of any conventional EOR technique less feasible [8].

One of the well understood and effective secondary oil recovery method in petroleum reservoirs is waterflooding (WF) with the purpose of maintaining the reservoirs pressure and displacing the oil toward the production wells. In NFRs, the oil displacement from the matrix blocks is a capillary dominated process, which is dependent on the wettability of the rock [3, 9-10]. In wettability conditions that are not favorable for the WF process (e.g., mixed-wet to oil-wet), the recovery method can be switched to gas injection, for achieving a higher oil RF. However, the high risk of by-passing oil due to gas high mobility can lead to early breakthrough of the gas phase [7]. The gas breakthrough is delayed upon gas injection to some extent when gravity becomes important. For such systems, the gas-oil gravity drainage mechanism increases the oil recovery rate by providing a driving mechanism as a result of flow communication between the matrix and fracture [11-13]. The availability limitation of the gas phase in some cases is another

limiting factor in the sole application of gas injection (as an EOR scenario) into a given naturally fractured reservoir.

Numerous EOR field scale projects in fractured carbonate reservoirs have been reported since early 1970. Among the reported processes, gas injection (GI) is the most common applied technique with a low oil recovery and production rate [14]. These reports also showed that WF is not a successful and common technique in such reservoirs due to very low recovery as a result of by-passing the oil saturated matrix blocks in the case of an oil-wet reservoir [15], The three-phase immiscible WAG injection in non-fractured reservoirs has previously been comprehensively studied [16-19], while the heterogeneous reservoirs including the interaction between the matrix and fractures on the performance of WAG injection has been overlooked.

WAG as a mature oil recovery technique, both in miscible and immiscible conditions, incorporates the advantages and merits of both gas injection (GI) and waterflooding (WF) techniques. WAG injection works through enhancing the microscopic (in GI) and macroscopic (in WF) sweep efficiencies, stabilizing the injection fluid's front, postponing the breakthroughs, and thereby, increasing the oil recovery, compared to two basic techniques [17]. WAG injection has been recognized as the main employed EOR technique (48%) in the North Sea fields, which is typically applied in clastic formations [4]. The application of WAG injection as an EOR technique is underway in carbonate reservoirs including offshore pre-salt Brazil carbonate reservoir [20] or carbonates in the Middle East.

Immiscible WAG injection over-performs the continuous WF or GI processes through various compiled mechanisms that are described below [21], namely:

- Enhancing the volumetric sweep efficiency through WF followed GI: The presence of free gas (through GI cycle) decreases the water three-phase relative permeability values, leading to the invasion of water phase into the by-passed zones.
- Reduction in oil viscosity caused by gas dissolution into the oil: Through this mechanism, the mobility ratio of the water-oil displacement becomes more favorable in an under-saturated reservoir.
- Oil swelling through dissolved (injected) gas: This mechanism results in less stock tank oil of residual oil, which leads to a higher recovery even in the case of no additional driving force for S_{or} reduction.
- Interfacial tension (IFT) reduction: In the case of lower $IFT_{o\text{-}g}$ than $IFT_{o\text{-}w}$, this mechanism passes the gas into the small pore throats that are not attainable for the water phase under the dominant pressure gradient.

- Lowering S_{or} is caused by three-phase hysteresis: In a water-wet reservoir, gas trapping during WF (imbibition displacement) cycles, which is also known as hysteresis, results in oil displacement even at low saturations and reduces the three-phase S_{or} value [21].

For a time, it was assumed that WAG injection is not beneficial to be implemented in NFRs [22]. However, there are many successful examples of the application of the WAG injection in fractured reservoirs [17, 23-25]. Reservoir heterogeneity is among significant parameters that directly affects the WAG process efficiency. Many failed EOR projects (in general) have been attributed to the reservoir heterogeneity or to the lack of understanding of the reservoirs' general structure [26]. In high fractured or stratified reservoirs, the operation of GI is not economical due to high recycle rate and early breakthrough of the injected gas [27]. Due to higher storage capacity of the matrix to trap the crude oil, capillary and gravity forces depending on the wettability of the system, have profound impacts on the recovery from fractured reservoirs, compared to the conventional reservoirs [28-29]. In some NFRs, during a WAG process, water and gas displace each other and by-pass the trapped oil in the pore matrix part of the system. Thus, the use of appropriate relative permeability and capillary pressure correlations significantly affects the predictions of flow between matrix and facture in a porous medium [4]. At the field scale, dual porosity or dual permeability models are applied to calculate the fluid transfer between matrix and fracture media. Although both models use transfer functions to simplify and simulate the exchange rate between two media, namely, matrix and fractures, this simplification results in neglecting the heterogeneity existing in the matrix properties, especially, in carbonate reservoirs [30-31]. Although the WAG injection in fractured reservoirs is difficult to be implemented and not economic, there are a few studies on WAG mathematical modeling or simulation in the literature.

Elfeel et al. (2016) analyzed three-phase flow during WAG injection at two scales (e.g., pore scale and intermediate scale). The latter scale is comparable to a scale of a single reservoir; fracture and matrix media are represented using a fine grid model. Their model applies empirical and pore-network modeling systems based on three-phase flow functions to study the effect of gravity and capillary forces in the matrix-fracture transfer system [4]. Their simulation results highlighted the impact of the hysteresis effects in fractured medium, which cause up to 10 % difference in predicted oil recovery. However, this difference is smaller in oil-wet systems due to the limited three-phase region and less impact of hysteresis [4]. A sensitivity analysis showed that wettability, block geometry, and matrix permeability highly affect the matrix-fracture transfer rates. They also suggested a new multiple interacting continua (MIC) model or a double block model [4]. The proposed model computed more accurate results for fracture-matrix transfer rates at a reduced computational cost [4].

In another study conducted by Aleidan *et al.*, three different injection modes including simultaneous water and gas injection (SWAG), WAG, and continuous gas injection (CGI) were applied on fractured and un-fractured carbonate cores [32]. They also considered different fracture patterns; at various fracture intensities, they studied the effect of shape factor including elongated slab and sugar cube models. Their simulation results showed that the improvement in recoveries of SWAG and WAG injection processes over the CGI is related to the higher conformance provided in water cycles, which controls the CO_2 mobility and decreases its flow through the fracture. It was also reported that the sugar cube model is better than the elongated slab model due to the presence of a vertical fracture in the middle of the core, which helps the gas phase to diffuse in matrix and to be in contact with more oil [32].

Heeremans et al. (2006) performed several fine scale single porosity simulations to correctly upscale the flow model to a dual porosity system. The recovery outputs were presented based on two dimensionless numbers i.e. capillary over viscous and gravity over viscous forces. Their generated proxy model optimized the WAG process; it was found that WAG injection increases the final recovery by 10 % higher than WF or CGI [33]. Their model also showed that the shape factor characterizing the nature of the fracture network does not significantly affect the recovery of the system, which was in consistent with field experiences [33].

Dehghan et al. (2012) performed an experimental study of WAG injection in a micromodel system with fracture elements. Their micromodel consisted of four matrix blocks surrounded by fractures to examine different scenarios such as continuous WF, CGI (nitrogen as the gas phase), and WAG injection with various slug injection arrangements. Their results showed higher recovery factor achieved by WAG injection than continuous WF and CGI in a fractured system. The optimum slug size injection was reported as 0.08 PV of waterflooding followed by 0.35 PV GI slugs, where the sweep efficiency from matrix blocks was maximized and gas/water production rate was reduced at the outlet. Han (2015) experimentally measured the PVT properties of Bakken crude oil-CO_2. Experiments were performed at six CO_2 concentrations with three flooding schemes including WF, GI, and miscible CO_2-WAG injection in tight and fractured Bakken formation. They also evaluated the CO_2 soaking effect in the fractured formation. Their results confirmed that breakthrough (BT) occurs much earlier in the fractured formation than the tight system [34]. Chakravati et al. (2004) conducted a series of core-flood experiments using both homogeneous and fractured cores. They found that in the fractured medium WAG injection remarkably delays the BT time (compared to the continuous GI) and accordingly results in higher oil recovery in such systems.

Agada[35] used a high-resolution simulation model to investigate the effects of non-wetting phase trapping and the miscible and immiscible WAG injection in a heterogeneous (carbonate) reservoir. They showed that the nature of the fracture system has a significant impact on the WAG recovery simulation results, especially in a low-intensity fracture system. While, in a high-intensity fracture reservoir, the fracture system's characteristics become less significant in the recovery process. To obtain the maximum recovery of a WAG process, analyzing and fine-tuning the critical parameters as well as providing an optimal design of the project are required. Inappropriate designs of WAG parameters in terms of the number of cycles, slug size volume, and injection rates of each WF and GI cycles result in weak process performance, low oil recovery and/or even damaging the formation [17]. Hence, optimization of all affecting factors as well as obtaining a comprehensive knowledge of reservoir characteristics (e.g., wettability and heterogeneity) provide a proper scheme to predict and control the gas and water mobility for recovery improvement [36-37].

Most of the WAG injection studies in the literature are experimental and/or modeling where the porous systems are homogeneous. WAG flooding in heterogeneous/fractured reservoirs is a common process, which is overlooked in available research works. Most of the research investigations conducted on this topic are experimental studies at environment pressure and temperature and no mathematical model including reservoir conditions in such cases has been provided so far.

In current study, a robust and reliable CFD model using COMSOL Multiphysics® is applied to investigate WAG injection in a fractured system with different fracture configurations, considering three-phase relative permeability and hysteresis. The results of this work provides a comprehensive understanding of fluid flow during WAG injection in a fractured reservoir through a systematic sensitivity analysis on fracture configurations and characteristics, which is useful for designing an optimum WAG injection process in fractured reservoirs.

The paper is structured as follows. After the introduction, the mathematical framework including a description on CFD model, governing and auxiliary equations, initial and boundary conditions, discretization, and numerical model are provided. We also discuss the limitations associated with this model. The model is applied to a case study with experimental results to verify our model. After assessing the model with case study data, in results and discussion section, the effects of various parameters on the recovery of WAG injection in the fractured system are investigated. Finally, the main conclusions and recommendations for future studies are listed.

4.2 CFD Modelling of WAG Injection in a Fractured Medium

In this work, we study the three-phase flow during a WAG injection process in porous media with fractures, using COMSOL Multiphysics® software.

4.2.1 Governing Equations

In this subsection, first, the mathematical framework of the introduced model is described followed by the numerical formulation, boundary and initial conditions, and numerical simulation in the COMSOL Multiphysics® environment. The governing equations for the three-phase flow system (containing gas, oil, and water) include mass balances for all phases, and Darcy's equation for the momentum balance. The gravity effects and dispersion phenomenon are neglected. We study the effect of gravity by changing the alignment of porous medium. The following equations apply for both the matrix and fracture domains:

$$\frac{\partial}{\partial x}\left[\frac{Kk_{r\alpha}}{\mu_\alpha}\left(\frac{\partial p_\alpha}{\partial x}\right)\right]+\frac{\partial}{\partial y}\left[\frac{Kk_{r\alpha}}{\mu_\alpha}\left(\frac{\partial p_\alpha}{\partial y}+\rho_\alpha.g\right)\right]+q_\alpha=\phi\frac{\partial s_\alpha}{\partial t}\qquad \alpha\in\{o,w,g\} \tag{4-1}$$

where the subscript α denotes the fluid phase which can be oil (o), water (w), and gas (g); p is the pressure; s represents the saturation; g is the gravitational constant, ρ and μ refer to the density and viscosity, respectively; q resembles the source/sink term, which can be the production or injection rate; ϕ and K are the rock porosity and absolute permeability (matrix or fracture), respectively; t is the time; and x introduces the spatial location.

We use the mathematical model to simulate the WAG process in which a fracture is simulated with a matrix having a significantly higher permeability but with a porosity lower than 1 (porosity of the fracture=0.85) (meaning the fracture is also a porous medium -not a hallow space between two slabs of matrix blocks-). Therefore, the Darcy's equation is assumed to apply to the fracture, as well.

4.2.2 Auxiliary Equations.

The physical constraint relates the phase saturations for all phases, as given below:

$$\sum_\alpha s_\alpha = s_o + s_w + s_g = 1 \tag{4-2}$$

where s_o, s_w, and s_g denote the saturations of the oil, water, and gas phases, respectively.

Measurements of the three-phase relative permeability and three-phase capillary pressure in laboratory are highly time-consuming, expensive, and challenging [38-39]. Hence, it would be of practical implications to use accurate and reliable three-phase relative permeability and three-phase capillary pressure models in the mathematical modeling framework of three phase flow behavior (such as in WAG), to compensate

for challenging experimental methodology that was mentioned. At equilibrium conditions, capillary pressure between two phases (p_c) is defined below as the pressure difference between the non-wetting and wetting phases (see Eq. (4-3)); the capillary pressure is a function of rock properties (ϕ, K, and wettability), fluids saturations, saturation distribution, and the interfacial tension between the phases.

$$p_c = p_{nw} - p_{wet} \tag{4-3}$$

in which, p_{nw} and p_{wet} denote the pressure of the non-wetting and wetting phases, respectively. To avoid confusion with the pressure of water phase (p_w), we use the notation p_{wet} for the pressure of the wetting phase (oil or water). We use the three-phase capillary pressure model by [40], which is a modified version of Skajaveland et al.'s two-phase capillary pressure model [41]. The proposed capillary pressure model is applicable to every rock wettability condition. The Eq. (A-1) in the appendix A used for the three-phase capillary pressure which is the generalized form of this model obtained using Gibbs free energy minimization framework. [40]. The entry capillary pressure and capillary exponent values should be estimated from experimental data.

In the two-phase systems (e.g., oil/water, oil/gas and/or water/gas), there are only two major displacement paths in which the saturation of one phase may decrease or increase. However, in a three-phase flow systems, there are infinite numbers of various displacement paths [42]. In other words, any three-phase flow system involves variations of the two independent saturations. Hence, measurement of the three-phase relative permeability for all possible displacement variations is not practical for the immiscible WAG injection displacement. The WAG process involves an inherent complexity from hysteresis that occurs due to the alternating saturation increase-and-decrease (for wetting and non-wetting phases), corresponding to the imbibition and drainage cycles. Hysteresis is a vital phenomenon that strongly affects the performance of a WAG process [42]. Thus, utilizing a reliable three-phase relative permeability and hysteresis model is an important step in simulation and modeling of processes involving the three-phase flow such as the WAG injection process. Larsen and Skauge developed a relative permeability model based on cyclic hysteresis effects during a WAG injection process [43]. The proposed model is developed to capture the reduced mobility and hysteresis loops during three-phase flow. The experimental wetting and non-wetting relative permeability data as well as the knowledge of the interaction of maximum non-wetting saturation and trapped non-wetting saturation are used in the model. Another model developed by Ranaee et al. to predict three-phase oil relative permeability based on a sigmoid-based model [44]. Their proposed model involves key effects of the pore-scale phase distributions within the suggested effective empirical model for oil relative permeability. The sigmoid-based model is capable to generate: (i) the amount of induced remobilization oil by gas injection in a water-wet

system. (ii) the transition in layer-drainage regime for low oil saturation ranges, and (iii) the consequent residual oil saturation reduction in a three-phase flow system. Lomeland and Ebeltoft proposed an analytical correlation for three-phase relative permeability and an LET function with an extended version LETx [45].

In current work, for the matrix domain, we apply the three-phase relative permeability (including hysteresis effects) proposed by Shahverdi and Sohrabi [42]. Their three-phase relative permeability model coupled with a hysteresis model are involved during an immiscible WAG injection process in water-wet systems. The model was excellently verified with experimental WAG injection data. The proposed model also incorporated all three sets of two-phase relative permeabilies (i.e. oil-water, oil-gas, and water-gas systems), while most of the proposed models only are accountant for two sets of relative permeability systems i.e. oil-water, and oil-gas systems. This model assumes that the three-phase relative permeability ($k_{r\alpha}^{3ph}$) of a given phase α is a function of the two-phase saturations and relative permeabilities for all three phases. The correlations are described in Eqs(A-2) –(A-5), appendix A.

For the three-phase relative permeability model in the fracture domain, we use a proposed model by [46], Eqs.(A-6)-(A-8), appendix A. To calculate the capillary pressure in the fracture domain, we use the [47] model, which is commonly used in modelling multiphase flow in porous media. The correlation is described in Eq. (A-9)-(A-10), appendix A.

4.2.3 Initial and Boundary Conditions

COMSOL Multiphysics® 5.4 uses a graphical user interface (GUI) that enables to model the problem. The analysis of the WAG injection process is performed, using a 2D domain, having two subdomains and eight boundaries for the fractured medium studied in this research as shown in Figure 4-1. The boundary condition for each boundary is listed in Table 4-1.

For each phase, the initial conditions $s_\alpha(x, z, t=0)$ are known from the initial phase saturations established in the experiments.

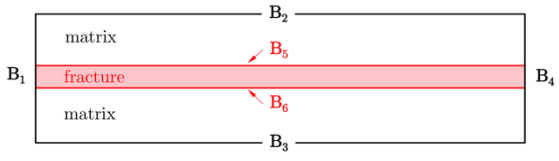

Figure 4-1: Boundaries of fractured porous medium during WAG injection for numerical modeling; the fracture domain is shown with red and matrix is shown with white. The matrix boundaries are B_1-B_4 and fracture boundaries are B_5 and B_6. The length and width are not scaled for better visibility.

Table 4-1: Boundary conditions for fractured medium in COMSOL Multiphysics®.

Boundary	BC
B_1	q_{inj} = cte
B_2	no flux
B_3	no flux
B_4	$p_o = 0$
B_5	flow continuity
B_6	flow continuity

4.2.4 Model Discretization and Numerical Method in COMSOL Multiphysics®

The COMSOL Multiphysics® uses a general form of the Darcy's law under the phase transport in porous media module, which is integrated into the continuity equation. The formula is presented for the phase α that can be either the wetting phase (wet) or the non-wetting phases (non-wet), as given below:

$$\delta_{st}.C_p\frac{\partial p_\alpha}{\partial t}+\nabla.\left[\delta_k\frac{k_\alpha}{\mu_\alpha}(\nabla p_\alpha+\rho_\alpha\,\vec{g}\,\nabla h)\right]=\delta_Q Q_\alpha \qquad \alpha\in\{wet,non-wet\} \tag{4-4}$$

where k_α is the effective permeability of phase α. The input parameters are the time scaling factor (δ_{st}), flux scaling factor (δ_k), source scaling factor (δ_Q), storage term (C_p), and source term (Q). The storage term (C_p) is a function of porosity, residual wetting saturation and the effective wetting saturation and pressure ($Cp=d\theta_w/dh_c$), where the θ_w is the saturation of the wetting phase, and the h_c is the capillary pressure function.

Values of δ_{st} = 0 and 1 are used for steady state system and dynamic systems, respectively. δ_k is the flux scaling factor, which is unity in our system; and Q refers to the source term.

For the geometry of the meshes, triangular mesh elements are applied as shown in Figure 4-2. Later on, we compare two different mesh sizes, *coarse* case and *extra-fine* case, to assess the effect of mesh size on the reliability and computational burden of our developed CFD model.

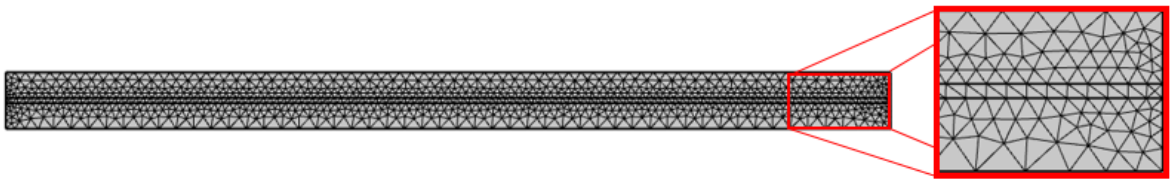

Figure 4-2: Schematic of model discretization in different regions.

4.2.5 Limitations and Assumptions

In our CFD model, the following assumptions are made:

- 2D fluid flow is considered.
- Except for one case (vertical injection), the effect of the gravity force is neglected.
- The porous medium is incompressible and non-deformable, having a constant porosity.
- The three phases are immiscible, and no reaction occurs between the phases in the model.
- The fluid and rock properties remain constant; no asphaltene precipitation and wettability alteration are considered upon CO_2 injection.
- Hysteresis is neglected in the fracture domain due to its low capillary pressure.
- All WAG injection cycles (both WF and GI) are conducted at a fixed slug size of 0.5 PVI.
- The fracture is modeled as a porous medium with much higher permeability and porosity than those in the surrounding matrix. In the experiments, the fracture pore space is created by steel wool [48].
- We study an idealized fracture system, containing 3 horizontal and 1 vertical fracture configurations, while in an actual system a variety of random fracture patterns and configurations are possible.

4.3 Case Study

To verify the simulation results, we use the WAG experimental results reported by Dorostkar et al. (2009). They conducted a series of CO_2-WAG flooding and hot CO_2-WAG flooding in fractured sand packs. In this study, we only use those data related to the CO_2-WAG experiments conducted in water-wet and fractured sand packs where the fracture (2 mm aperture) is simulated with a matrix of larger permeability and porosity. Their experiments were performed at the atmospheric pressure (to keep the immiscibility condition) and 100^{o}C. Dorostkar et al. (2009) used sand packs with the characteristics summarized in Table 4-2. The oil sample used in their experiments was provided from the Maroon

reservoir's crude oil in south of Iran. The brine used in their study was synthetic, with a similar composition to the formation brine of the Maroon reservoir. The injected gas was CO_2 with a viscosity and density of 0.0182 cP and 1.6×10^{-3} g/cm^3, respectively [48]. CO_2 and water were injected into the fractured sand pack at the same rate of 0.5 cm^3/min. The WAG injection tests were continued until no change in oil production was observed. The fluid, porous media, and operating conditions used in the experimental study by Dorostkar et al. [48] are provided in Table 4-2. A schematic of the model is also depicted in Figure 4-1.

Table 4-2 : Rock and fluid properties used in this study (provided from [48]).

Attribute	Variable (unit)	Acting phase(s)	Value
Fluid	ρ (g/cm^3)	g	0.0016
		o	0.8700
		w	0.9970
	μ (cP)	g	0.0182
		o	2.1680
		w	0.2822
	σ (mN/m)	og	50
		ow	75
Porous Medium	K_m (D)		1.1
	K_f (D)		5.0
	ϕ_m		0.28
	ϕ_f		0.85
	L (cm)		35.0
	D (cm)		4.2
	W_f (cm)		0.2
Operating Conditions	s_i (PV)	g	0.000
		o	0.849
		w	0.151
	q (cm^3/min)		0.5
	p (atm)		1
	T (°C)		100

4.4 Results and Discussions

In this section, we present the results of the CFD model that is developed for the WAG injection process, based on the case study experimental data. We use a relative tolerance of 1×10^{-4} for the absolute error. The value in the Relative tolerance field is a relative tolerance that controls the accuracy of the geometric representation of the swept object. The geometric representation is an approximation, which is necessary because it is not possible to exactly represent a swept object using NURBS (nonuniform rational basis splines). The default value is 10−4 (0.01%), for more details about the relative tolerance, you can refer to [49]. A 2D heterogeneous medium with matrix and fracture domains is used, consisting of 2416 domain mesh elements and 1026 boundary mesh elements. Similar to the case study, the fractured sample is initially saturated with oil and connate water saturation prior to starting the WAG injection cycles. Then, it is flooded with alternating injections of water-and-gas cycles. One pore volume injection (at the flow rate used in the case study) corresponds to 16300 seconds.

4.4.1 Mesh Sensitivity and Analysis

In the COMSOL Multiphysics®, the time-dependent set of equations for fluids flow in porous media are computed using finite element method (FEM). The accuracy of the calculated variables is significantly affected by the mesh properties used in the model. To obtain an optimum mesh configuration and size, we simulate the model using extra fine and coarse triangular meshes for the first waterflooding (WF_1) and first gas injection (GI_1) cycles, and compare the results, as reported in section 4. To compare the performance of the model using two different mesh sizes, we use measures such as absolute average relative deviation (AARD, in Eq. (4-5)) and the relative error (see Eq. (4-6)) in terms of the final recovery factor (RF_{final}) from experimental data and the CFD model for all of instantaneous *RFs* (N), as expressed below:

$$AARD\ (\%) = \frac{100}{N}\sum_{i=1}^{N}\left(\frac{\left|RF_i^{exp} - RF_i^{sim}\right|}{RF_i^{exp}}\right) \tag{4-5}$$

$$Error\ (\%) = 100\left|\frac{RF_{final}^{exp} - RF_{final}^{sim}}{RF_{final}^{exp}}\right| \tag{4-6}$$

The percent error results are given for the *RF* achieved by the end of the first water injection (WF_1) and first gas injection (GI_1) cycles. CPU time is also reported in Table 4-3, as a measure of computational burden due to mesh size. It also should be mentioned that the timestep for both cases are fixed and constant.

Table 4-3 : Effect of mesh size on processing time and error percentage for WF_1 and GI_1 injection cycles.

Mesh	#Nodes	CPU time (s)		% AARD		% Error	
		WF_1	GI_1	WF_1	GI_1	WF_1	GI_1
Extra fine	2416	17	1389	33.6	3.032	0.436	0.96
Coarse	1242	3	1005	34.1	6.241	1.854	9.14

The percent error results are given for the *RF* achieved by the end of the first water injection (WF_1) and first gas injection (GI_1) cycles. CPU time is also reported in Table 4-3, as a measure of computational burden due to mesh size. It also should be mentioned that the timestep for both cases are fixed and constant.

Table 4-4 reveals that by applying the extra fine mesh (which includes twice as much number of nodes) the CPU time is increased as expected, and the error is decreased (both AARD and relative error). The percentage of relative error in the RF_{final} is more affected by the mesh size for the gas injection cycle where the error in the ultimate recovery factor is changed by one order of magnitude. For the waterflooding cycle, both extra fine and coarse meshing result in accurate results where the error in the RF_{final} is < 2%. Overall, the GI cycle brings more computational burden, compared to WF. The CPU time for the GI is two orders of magnitude slower than the WF injection which most probably is occurred due to the three-phase flow system during GI that involves three-phase relative permeability, hysteresis, and capillary pressure in system. While in WF1 only two phases (oil and water) exist in the system.

4.4.2 Model Validation with Experimental Data

The schematic of the WAG injection cycles for the CFD model is illustrated in Figure 4-3. Each injection mode (WF or GI) volume is 0.5 PV; in the first WAG cycle, WF_1 and GI_1 are conducted; in the second cycle, WF_2 and GI_2 are employed; and finally, in the third cycle, WF_3 is implemented. Because the oil production is insignificant at this stage, the GI_3 stage is abandoned.

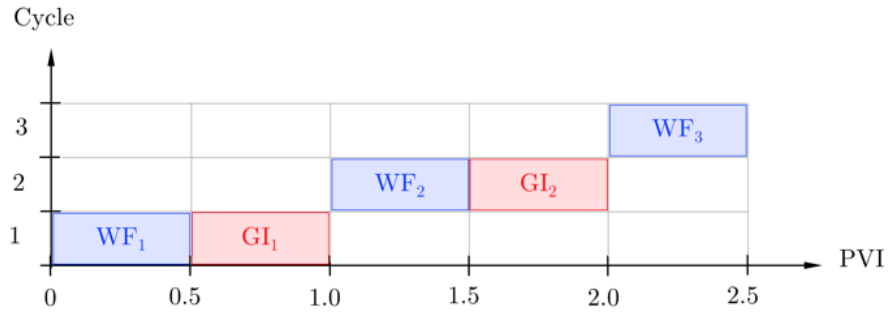

Figure 4-3: Schematic of WAG cycle injections scheduled in mathematical model.

After developing the CFD model, we compare its performance (outputs) with the experimental data for these 2.5 WAG injection cycles; the comparison is presented in Figure 4-4. For this simulation, the injection rate is 0.5 cm^3/min, using a WAG ratio of 1.0 and a slug size of 0.5 PV. The WAG ratio is defined as the volume of water slug size in WF cycles to that of the gas slug in the GI cycles. Here, we use constant slug sizes of water and gas in different cycles of water injection (WF_1, WF_2 and WF_3) and gas injection (GI_1, GI_2), as it is shown in Figure 4-3.

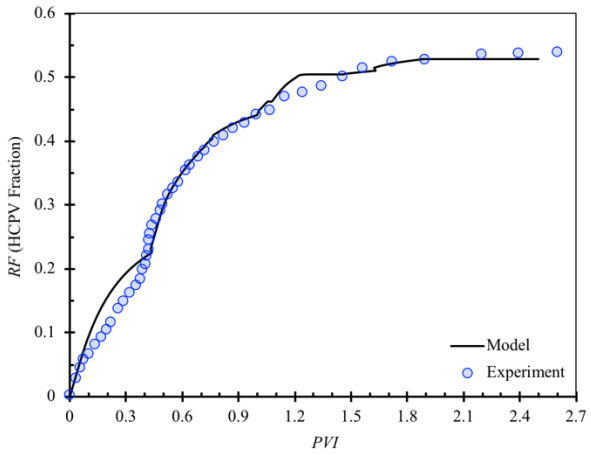

Figure 4-4: Comparison between the *RF* of WAG injection in a fractured system from experimental and numerical modeling works (q = 0.5 cm^3/min, slug size = 0.5 PV, and WAG ratio = 1). Solid line shows simulation results and scatter points are the experimental data from [48].

The first WAG cycle starts with the injection of water (WF_1) in a two-phase system, consisting of initial oil saturation of s_{oi} =0.849 pore volume (PV), and initial water saturation of s_{wi} =0.151 PV. In this stage, no gas is present (s_{gi} =0); therefore, two-phase relative permeability and two-phase capillary pressure models are applied in the WF_1 cycle. As it is clear from Figure 4-4, after 0.5 PV in WF_1, an oil recovery factor RF_{final}= 0.23 hydrocarbon pore volume (HCPV) fraction is achieved. Therefore, a high portion of

the oil in place is still trapped in the system (s_{or} =0.65 HCPV fraction). The first GI process starts at the initial oil saturation of 0.65 PV and initial water saturation of 0.35 PV, using injection rate q = 0.5 cm^3/min, which is constant during the 0.5 PVI. At this point, due to the presence of gas in the system (in addition to oil and water), three-phase capillary pressure and three-phase relative permeability correlations are utilized. By the end of GI_1 (after 0.5 PVI), a final recovery of 0.45 HCPV fraction is obtained. After the first GI, the second WF, second GI, and finally the third WF are performed in the fractured porous system, after which the RF_{final} =0.53 HCPV fraction and residual final oil saturation of 0.55 are obtained.

Based on Figure 4-4, the CFD model is capable of capturing the recovery performance behavior as an excellent match is attained between the model results and experimental data of WAG injection in heterogeneous porous medium. A summary of error values when estimating the RF in different WAG cycles is presented in Table 4-5, where the relative error is calculated based on RF at the end of each process; the maximum error is achieved during the 0.5 PVI in each process. The proposed CFD model is a suitable tool in estimating the oil recovery factor with a maximum relative error of 12%.

Table 4-5: Comparison of RF from model and experiments for WAG injection in a fractured porous medium; Experimental data are from [48].

WAG Attributes		s_{or}	*RF* (HCPV fraction)		Error* (%)	
Cycle	Process	(HCPV fraction)	Exp	Sim	Relative	Max
1	WF_1	0.65	0.220	0.230	-4.50	12.30
	GI_1	0.50	0.448	0.446	0.446	5.60
2	WF_2	0.42	0.502	0.503	-0.126	11.20
	GI_2	0.39	0.528	0.529	-0.189	0.571
3	WF_3	0.38	0.539	0.540	-0.237	0.230

* Relative error is defined based on RF at the end of each process while the maximum error is achieved.

For the simulation results in WF1, we tune two-phase relative permeability and capillary pressure data *a priori*. To do so, we used the experimental data from the literature and tuned the two-phase relative permeability and capillary pressure models using the pattern search optimization method. This is the reason for the overestimation in WF_1 cycle. We are able to obtain a perfect fit for this stage, but, preferred not to force the model to match the WAG production data as the recovery at the end of WF_1 is very close to that in the experiments. For the GI_2 to WF_3 cycles, the model parameters are tuned by using the production data of WAG due to unavailability of the three-phase capillary pressure and relative permeability behaviors for a system similar to the case study. There is also some overestimation in the

RF from our model corresponding to WF_2; however, the ultimate recovery is similar to the experimental data. This difference might be caused due to the slight change in the wettability of the rock from strongly water-wet to slightly oil-wet during the process.

4.4.3 Mobility Changes

In this section, we show the mobility of different phases, using fitted mathematical model. The mobility of each phase and the total mobility of system are calculated using Eqs. (4-7) and (4-8):

$$\lambda_\alpha = \frac{K k_{r\alpha}}{\mu_\alpha} \quad \alpha \in \{ o, w, g \} \tag{4-7}$$

$$\lambda_{Tot} = \sum_\alpha \lambda_\alpha \tag{4-8}$$

where λ_α is the phase mobility; α denotes different phases of oil, water, and gas; $k_{r\alpha}$ and μ_α are the three-phase relative permeability and viscosity of phase α, respectively; and K stands for the absolute permeability.

The interplay between the capillary and viscous forces can be described by the capillary number $N_{Ca}=v\mu/\sigma$ [50]; based on the operating conditions corresponding to the WAG experiments, $N_{Ca} \approx 2\times10^{-7}$ which reveals the dominancy of capillary force compared to viscous force during the WAG flooding process.

Plots of the phase mobility for oil, water, and gas are depicted in Figure 4-5 for both the matrix and fracture domains, at the middle of the core according to the model that is verified with the experimental data. The results for gas, water, and oil are consistently shown with red, blue, and black, respectively. Furthermore, the curves of phase mobility in the matrix and fracture are consistently shown with solid, and dashed lines respectively. The symbols of mobility of gas, water, and oil, in the fracture are $G|_f$, $W|_f$, and $O|_f$. Similarly, those for the matrix are distinguished with $G|_m$, $W|_m$, and $O|_m$.

During the primary waterflooding (WF_1), only water (wetting phase) and oil (non-wetting phase) exist in the system. By injecting the water in WF_1 (see Figure 4-5 (a)), the mobility of the water increases, while that of the oil phase decreases. The mobility values of the gas phase in the matrix and fracture are zero because at this stage, there is no gas phase in the system. Water advances into the network of smaller pore spaces in the matrix blocks with higher imbibition capillary pressure, knowing that water is the wetting phase. For this reason, the mobility of the water in the matrix is much higher than that in the fracture. The oil (non-wetting phase) can flow from matrix into fracture that has a lower resistance to flow. After WF_1, a high percentage of the oil (s_{or} = 0.65 HCPV fraction) is still trapped in the pores; when gas is injected into the system in GF_1 cycle (in Figure 4-5 (b)), it flows through the fracture, which

has a relatively lower entrance capillary pressure, compared to the matrix. Therefore, the mobility of the gas phase in the fracture becomes high. Since the saturation of the oil phase in fracture is higher than that in the matrix medium, oil recovery (due to increase in the oil mobility in the fracture) increases significantly. Because of the high mobility of the gas phase, total mobility increases in porous medium in GF_1 cycle. Most of the injected water from WF_1 is trapped in the matrix where the gas phase does not access in GF_1; hence, the mobility of the water in both matrix and fracture media remains constant during GF_1 cycle.

(a)

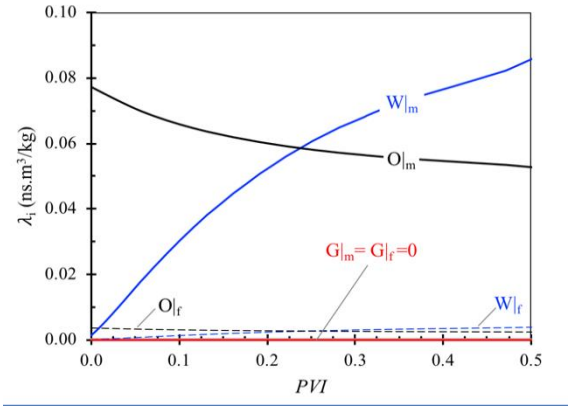

(b)

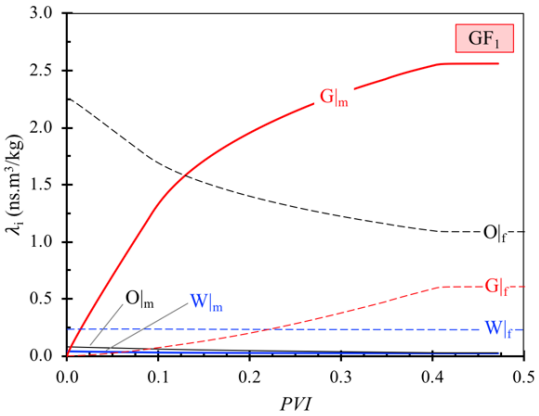

(c)

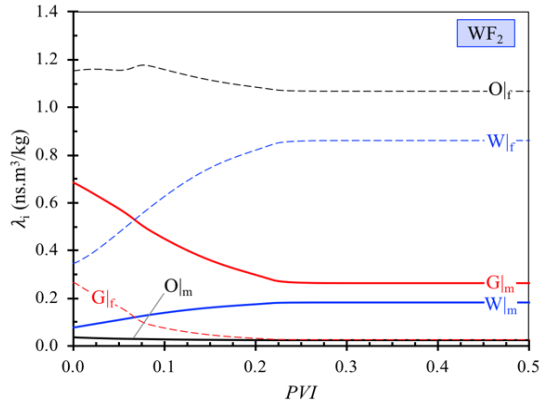

(d)

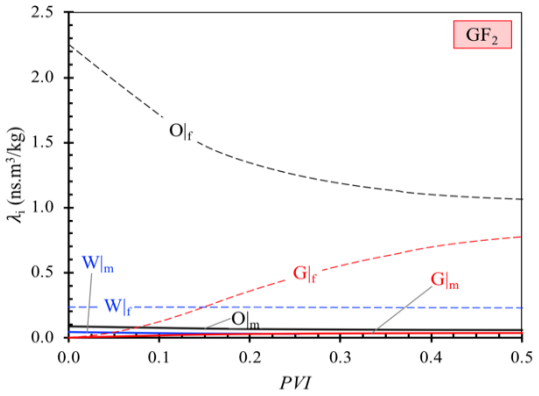

(e)

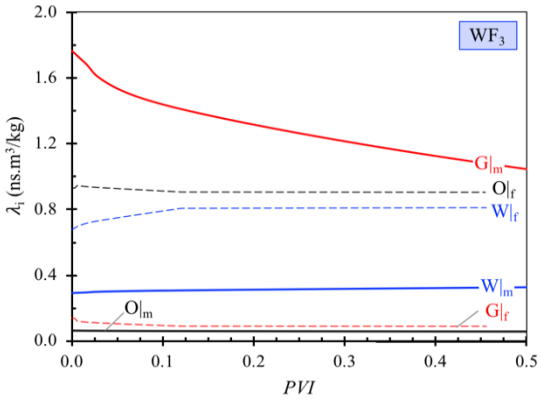

Figure 4-5: The phase mobility and total mobility changes of each process in the middle of the core, based on PVI in the matrix zone where (a): primary WF, (b):1st GI, (c): 2nd WF, (d): 2nd GI, and (e):3rd WF.

The mobility profiles for the secondary water injection (WF_2) are illustrated in Figure 4-5 (c). As it is expected, the mobility of the water phase increases sharply and that of the gas phase decreases. During the second WF (WF2), the dynamic of water mobility in both matrix and fracture is faster than those in the previous water injection cycle (i.e., WF_1). The mobility of the water phase stabilizes sooner (after about 0.2 PVI in Figure 4-5 (c)) in the WF_2 compared to WF_1. Because water is the most wetting phase, it does not advance through the larger pores (previously invaded by the gas phase). This is especially valid for the water phase in the fracture; consequently, the matrix domain contributes the most to oil production in WF cycles. For this reason, the mobility of gas phase in the fracture is low, which stabilizes quickly (<0.1 PVI in Figure 4-5 (c)). Because of insignificant production from the matrix zone by the water phase and gas entrapment in the fracture, the mobility of the oil phase does not change significantly during WF_2. The mobility of different phases during the secondary gas injection (GI_2) cycle is depicted in Figure 4-5 (d). The mobility of the gas phase increases in both matrix and fracture, while the oil mobility is low, which slightly decreases. This is due to the oil depletion in the fracture medium upon previous gas injection cycles. Therefore, there is a percolating pathway of gas phase (through the fracture) from the injection to the production points which will remain as the preferential pathway for the gas phase. In tertiary waterflooding (WF_3) process, the flow communication between the matrix and fracture is ceased due to the hysteresis effect and high mobility of gas in the fracture as a result of high gas saturation. Therefore, no significant oil production is observed in *RF* data during WF_3. The mobility of the gas phase in the matrix also decreases and the mobility of the oil and water phases do not significantly change.

4.4.4 Hysteresis Effect

In this section, we present the effect of hysteresis on the performance of WAG, using the tuned model. To model the results without the hysteresis effects, we use a different relative permeavility model that overlooks the hysteresis. Measurements of the three-phase relative permeability are difficult and are time-demanding; especially, when the steady-state method is used [51]. Numerous empirical models such as Stone-I, Stone-II, and Baker are introduced to estimate the three-phase relative permeability values from two-phase data [52-54]. Various theoretical and experimental studies confirm the dependency of the relative permeability to parameters such as rock and fluid properties including fluid viscosity, interfacial tension, injection rate, wettability, immobile water saturation, pore size distribution, and especially the saturation history [55]. The dependency of relative permeability to fluid saturation history is described as relative permeability hysteresis, which becomes significant in three-phase flow systems [51]. Cyclic dependency of the three-phase hysteresis permeability becomes important in tertiary oil recovery processes such as WAG injection and cyclic steam stimulation (CSS) processes [51]. Simulation studies showed remarkable uncertainties associated with applying three-phase relative permeability models in gas and WAG injections at field scales [56]. The simulation results of oil recovery with and without including hysteresis revealed that a higher oil recovery is obtained by incorporating hysteresis effect in relative permeability correlations, compared to the no-hysteresis case [57]. In the case of involving hysteresis effects, a higher oil recovery is obtained over a longer period which is attributed to the effect of trapped gas, blocking the oil flow from high-permeability pore spaces.

To study the impact of relative permeability hysteresis on the behavior of three-phase flow in WAG, we use the Stone model (see Eqs. (4-9) – (4-13)) [53] which excludes any hysteresis effects (Stone, 1970). In this phase of the study, we model three cycles of WAG injection with 0.5 PV slug size at WAG injection ratio of 1 and operating conditions similar to the previous case with hysteresis.

$$s_o^* = \frac{(s_o - s_{or})}{1 - s_{wc} - s_{or}}, \; s_o \geq s_{or} \tag{4-9}$$

$$s_w^* = \frac{(s_w - s_{wc})}{1 - s_{wc} - s_{or}} \tag{4-10}$$

$$s_g^* = \frac{s_g}{1 - s_{wc} - s_{or}} \tag{4-11}$$

$$B_\alpha = \frac{k_{ro\alpha}}{1 - s_\alpha^*} \tag{4-12}$$

$$k_{ro}^{3ph} = s_o^* . B_w . B_g \tag{4-13}$$

where α stands for phases (oil, water, and gas); B_α is defined factor; s_{or} and s_{wc} are the residual oil saturation and connate water saturation, respectively; k_{row} is the two-phase oil relative permeability for

oil-water system; and k_{ro}^{3ph} represents the three-phase oil relative permeability. Similar formulations are applied for the three-phase gas and three-phase water relative permeabilities.

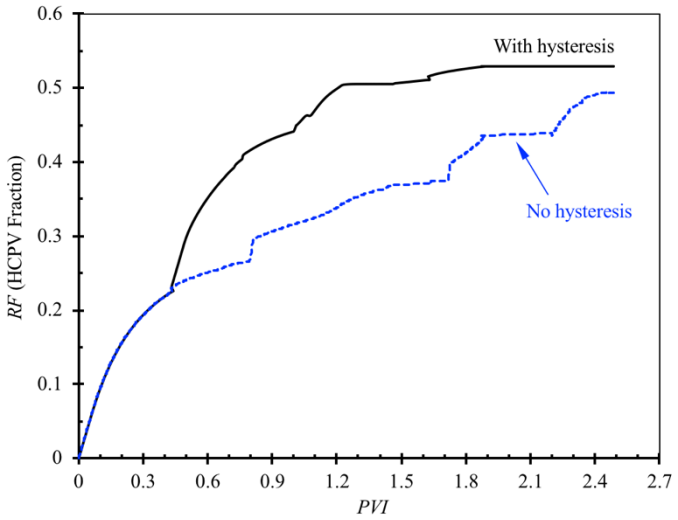

Figure 4-6: WAG injection recovery factor in two cases of with and without involving the hysteresis three-phase relative permeability effects.

The recovery factor results, using the Stone model are compared with those of WAG injection, considering the hysteresis relative permeability by [42] as seen in Eqs. (4-5) – (4-8)). Figure 4-6 display the results of oil recovery with and without the hysteresis effects. As observed in Figure 4-6, there is no significant difference between the models with and without hysteresis during WF_1 because no gas is present and water is the most wetting phase. A higher amount of oil is recovered when the three-phase relative permeability hysteresis is considered. This is especially true about the oil recovery in the gas injection cycles (GI_1 and GI_2). This observation is in agreement with our previous findings that the three-phase relative permeability and capillary pressure affect the non-wetting phase (gas) the most, while they do not considerably affect the behavior of the most wetting phase (water) [16]. More details on the importance/influence of capillarity and viscous forces during WF_1 are available in the literature [58]. The magnitudes of ultimate oil recovery factor upon injecting 2.5 PV successive cycles of water-and-gas (0.5 PV each) are estimated to be *RF*=0.53 and 0.44 HCPV fraction for the models with and without the three-phase hysteresis, respectively. The higher *RF* in cyclic injection of water and gas— when the hysteresis effects are taken into account—may be explained by the gas trapping in the system due to hysteresis that reduces the mobility of the gas phase (see Figure 4-5(c)). Consequently, this effect will prevent water to flow into the fracture, resulting in a lower water-cut and a lower gas-to-oil ratio. Because the majority of the oil resides in the matrix with smaller pores, the gas trapping in the larger pores

(especially in the fracture domain) leads to a higher sweep efficiency, and therefore, a higher oil recovery compared to the case without the three-phase relative permeability hysteresis. This finding is in agreement with micro-scale advancement of phases into small and large pores [59].

4.4.5 Core Alignment

In the naturally fractured reservoirs (NFRs), pressure-driven mechanisms of producing hydrocarbon may not be an effective strategy for oil production. In such reservoirs, the presence of the fracture, as a highly permeable path, provides a direct channel for the injected fluid (especially the gas phase) towards the production zone, reducing the oil recovery efficiency [60-61]. Gravity drainage is reported as an efficient process producing from NFRs [62-64]. Low residual oil saturation was reported after conducting gravity drainage tests in highly permeable media and in sandstones [65].

To examine the effect of gravity forces on the WAG injection performance, a set of immiscible WAG simulation runs are conducted in the porous media with and without the gravity effects. We change the orientation of the porous medium to account for the gravity by aligning it vertically; due to the small size of the porous medium, the gravity effect is minimal in the model that is held horizontally. Figure 4-7 shows a schematic of horizontal and vertical alignments of the porous system.

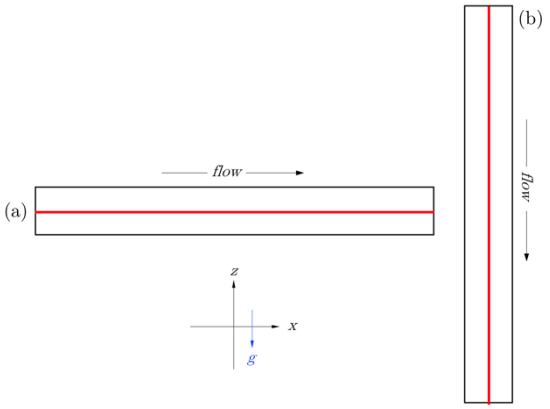

Figure 4-7: Two different core alignments to study the effect of gravity in immiscible WAG injection performance (a): horizontal (along *x*-axis) and (b): vertical (along *z*-axis). The gravity vector *g* is applied in -*z* direction.

For the analysis of gravity, all fluid and rock properties, and the operational conditions are the same for both the horizontal and vertical model alignments. The effect of gravity is demonstrated in Figure 4-8 using simulation results. The WAG injection scenario is the same as that shown in Figure 4-3 where the WAG ratio is 1, and each WAG cycle is 0.5 PV. According to Figure 4-8, including the gravity force improves the oil recovery. Due to significant contribution of gravity force in overall driving forces and the flow communication between the matrix and fracture [2], the ultimate *RF* after 2.5 PVI is higher in the

vertical mode; the ultimate RF_{final}=0.62 and 0.53 HCPV fraction are achieved in the vertical and horizontal models, respectively, which is about 17% (relative) increase in the *RF* due to the gravity.

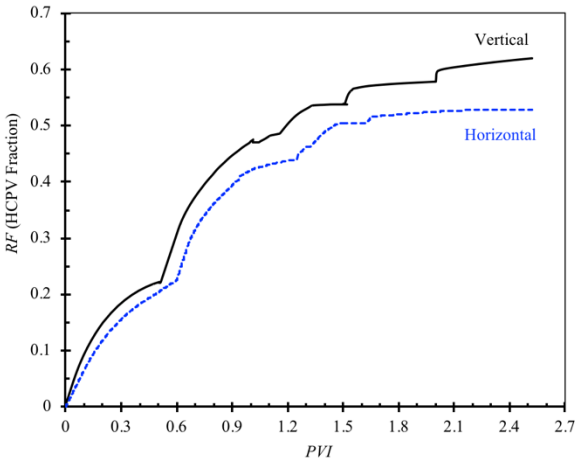

Figure 4-8: Effect of gravity on *RF* of immiscible WAG injection. WAG ratio = 1 and WAG slug size = 0.5 PV.

In both cases, similar RF values are obtained by the end of WF_1 cycle. However, due to the existence of gravity forces in the vertical case, the instantaneous *RF*s in the vertical mode are higher. During later cycles, especially during the WF_2 and WF_3 cycles, more oil is recovered in the vertical model, compared to the horizontal case. The presence of gravity also improves the drainage of continuous oil and water films from pore corners, which is more significant during the later stages of injection cycles when the oil production rate decreases. During the GI cycles, the flow communication can also drive the fluids from matrix to fracture. This flow communication will postpone the gas breakthrough; as a result, the RF_{final} is higher in GI cycles when gravity is considered. By sweeping the oil from matrix to the high permeable fracture medium, the fracture will become the main source of oil production and improve the overall recovery rate from the system. The flow of oil from matrix to fracture is considerably less in horizontal case where no gravity is considered. The oil flow from matrix to fracture postpones the channeling and early breakthrough of the injected fluids especially the gas phase. In WF_3 cycle, the recovery plot reveals that the oil recovery is not ceased in the vertical model even after 0.5 PV. Thus, unlike the recovery behavior in the horizontal model, both matrix and fracture contribute to the oil production when gravity is considered. Further WAG cycles can be injected to increase the ultimate oil recovery in the vertical model.

4.4.6 Fracture Aperture

The effect of fracture aperture on the oil recovery of the fractured system during the WAG injection process is investigated in a set of designed simulation runs (see Table 4-6). In this section, four different aperture sizes are simulated to study the oil recovery of WAG injection. All simulated models use the same fluid, fracture, and matrix properties (except for the aperture size). In all cases, a WAG injection scenario similar to that shown in Figure 4-3 is followed.

Figure 4-9 illustrates the impact of the fracture aperture on the *RF* performance during the immiscible WAG injection process. In all cases, a WAG ratio of one, and WAG slug size of 0.5 PV are used. The temperature and pressure are 100˚C and 1 atm, respectively.

Table 4-6: Effect of fracture aperture on WAG injection.

Fracture aperture (mm)	s_{or} (HCPV fraction)	*RF* (HCPV fraction)
0.5	0.424	0.500
1	0.415	0.511
2	0.399	0.530
3	0.348	0.590

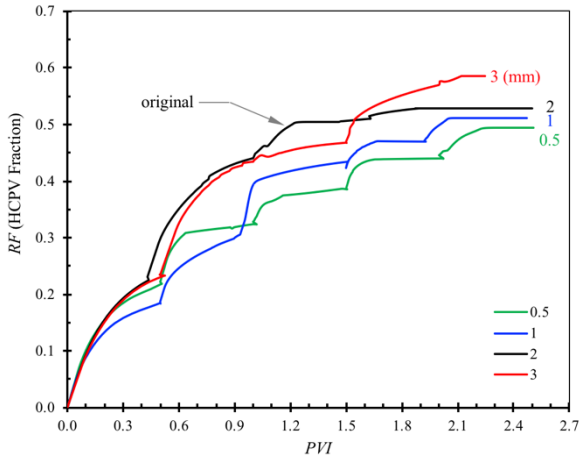

Figure 4-9: Influence of fracture aperture size on oil recovery performance upon immiscible WAG injection in a fractured medium (q = 0.5 cm^3/min, slug size = 0.5 PV, and WAG ratio = 1).

According to Figure 4-9 and Table 4-6, by enlarging the aperture size of the fracture in the model, the oil recovery of the porous system increases. The model with the 3 mm aperture size results in the highest oil recovery (in each cycle) and reaches the RF_{final} = 0.59 HCPV fraction, at fixed PVI for all cases.

Moreover, the production is ceased at 2.24 PVI, compared to other cases in which the production is continued for 2.5 PVI. The shorter time of process in the cases with higher fracture aperture size may occurs due to the faster drainage of oil from fracture (that contains more oil) and faster imbibition in matrix blocks as the water tends to sweep into the matrix blocks rather than fracture medium with a high capillary entrance. Note that the fracture is simulated both in model and experiments with a porous domain with a significantly higher porosity and permeability. The fracture has a porosity of near 85%. Because the overall recovery from the fracture is higher than that from the matrix, the overall recovery factor from the fractured model increases with increasing fracture aperture, because the pore volume of oil residing in fracture increases accordingly. Upon an increase in the fracture aperture, the overall permeability of the model also increases, resulting in a greater recovery rate from the model. At very low aperture values, the fracture block acts similar to the matrix. Looking closely at the instantaneous *RFs* for the case with the largest fracture aperture size (b=3 mm), most of the jumps in the instantaneous *RFs* occur during the GI cycles rather than the WF cycles. The ultimate *RF* obtained during WAG injection in a case with 0.5 mm fracture aperture is 0.5 HCPV fraction.

The discussion on the loss of capillarity in the fracture when the aperture increases above a critical value is not valid in our case study because the fracture medium is a porous medium with higher permeability and porosity for which capillary continuity holds. By increasing the fracture aperture, only the width of this higher permeability region increases, and the critical aperture size will not be materialized. More details about the critical aperture size and its effects on recovery performance is available in the literature [2, 50, 66-68].

4.4.7 Permeability contrast between matrix and fracture

The flow properties of the NFRs is governed by the flow through fracture and matrix as well as the flow communication between these two regions. One of the important parameters affecting the flow distribution along the porous medium is the permeability of matrix and its contrast with the fracture permeability. To investigate this effective parameter, a set of WAG injection with three different K_m/K_f ratios (by changing the matrix permeability) is conducted. All three cases are conducted with a WAG ratio of 1, and constant injection rate of 0.5 cm^3/min, with 2.5 cycles and at the constant PVI of 0.5 for each injection mode (WF or GI). The ratio of $K_m/K_f = 0.22$ is considered as the base case and two other ratio of $K_m/K_f = 0.1$ and $K_m/K_f = 0.3$ are compared with the base case to examine the effect of increasing and decreasing of this ratio.

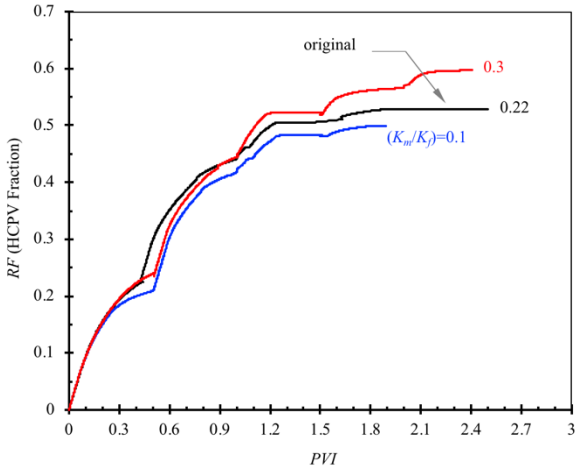

Figure 4-10: Influence of permeability contrast (K_m/K_f ratio) between matrix and fracture on oil recovery performance upon immiscible WAG injection (q = 0.5 cm^3/min, slug size = 0.5 PV, and WAG ratio = 1).

As the ratio of K_m/K_f increases and approaches unity, the permeability contrast between matrix block and fracture vanishes. Figure 4-10 presents the results of permeability contrast comparison according to the *RF* data versus the PVI. Comparing the simulated results for the case of K_m/K_f = 0.1 and the base case where K_m/K_f = 0.22, shows that by lowering the matrix permeability the oil recovery significantly decreases—especially during WF injection modes. At K_m/K_f =0.1, and during WF_1 cycle, the water (as the wetting phase) prefers to invade into the matrix blocks due to high capillary entrance, bypassing the fracture. Because the majority of HCPV resides in the matrix, decreasing the matrix-to-fracture permeability ratio increases the effect of hysteresis and more oil will be trapped in the matrix. Also because the fracture permeability is held constant, by decreasing the matrix-to-fracture permeability, the overall permeability of the porous medium decreases which also decreases the rate of oil production as well. The overall *RF* increases upon gas injection as the gas phase invades into the fracture medium due to its lower capillary entrance and drains the trapped oil of that zone. In the second WF, water flows through the low permeable matrix blocks and has a less chance to sweep the oil towards the producing zone, so low *RF* is resulted. However in second GI, the gas faces a high resistance for entering into the matrix medium and flows through its direct path in the fracture which is previously drained, quickly breakthroughs and no significant oil is recovered. The RF_{final} = 0.5 HCPV fraction is obtained this case; K_m/K_f = 0.1. At a higher matrix-to-fracture permeability ratio of K_m/K_f = 0.3, the WAG injection performance generally improves in all cycles as shown in Figure 4-10. Significant increases in the oil recovery are resulted in the WF_1 and WF_2 cycles for the highest permeability contrast ratio, compared to the base case (K_m/K_f = 0.22). At a higher matrix permeability, both the recovery and recovery rate

from the matrix blocks increases upon water injection. Also, due to less permeability contrast between matrix and fracture, flow communication between these two regions enhances and improves the oil recovery from the system. Increasing the matrix permeability also raises the chance of the gas phase to invade into the larger pore continuum in the matrix to recover the oil from both the matrix and fracture zones. Therefore, the chance for undesired viscous fingering phenomena decreases, which causes delayed the breakthrough time (consequently, higher *RF* at the breakthrough). The ultimate RF_{final} = 0.6 HCPV fraction is resulted after 2.5 cycles of WF and GI in the case of K_m/K_f = 0.3 which is (relatively) 20% higher than the low matrix permeability case of K_m/K_f = 0.1.

4.4.8 Fracture Inclination

A series of simulations are conducted to study the influence of fracture orientation on the *RF* during the immiscible WAG injection. The simulations are performed, using a fracture aperture size of 2 mm. We compare the horizontal fracture with three other cases where the fracture is inclined by 30^o, 60^o and 90^o with respect to the horizontal axis. Figure 4-11 shows the results of the simulations based on the oil *RF* for 3 cycles of WAG injection with the slug size of 0.5 PVI. According to these results, the ultimate *RF* of all cases are so close, between 0.47–0.49 HCPV fraction (see Table 4-7). The ultimate recovery is however, lower than the case of horizontal fracture.

Table 4-7: Simulated results of WAG injection in different fractured models.

Inclination (˚)	s_{or} (HCPV fraction)	*RF* (HCPV fraction)
30	0.440	0.471
60	0.442	0.481
90	0.432	0.491

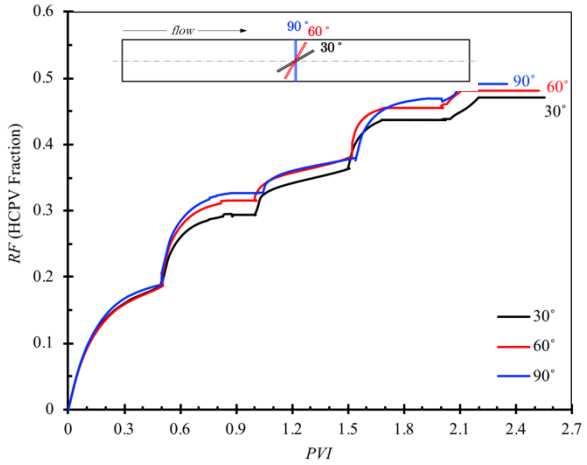

Figure 4-11: The effect of fracture inclination angle on oil recovery performance upon immiscible WAG injection (q = 0.5 cm^3/min, slug size = 0.5 PV, and WAG ratio = 1).

During the WF_1 cycle, all three cases have a similar *RF* performance which is attributed to the strongly water-wet condition of the system. Since the rock is strongly water-wet the wetting phase which is water tends to stick to the rock surface as an adhering thin film and displaces the oil towards the production zones. During the primary WF, since the system only contains two phases (water and oil), water which is the wetting phase prefers to invade into matrix blocks rather than the fracture. When water reaches to the fracture (with any inclination angle) due to low capillary entrance, it bypasses the fracture, so the fracture inclination angle does not mainly affect on the oil recovery during primary WF. When injecting gas into the system, increasing the inclination angle postpones the gas breakthrough and results in a higher recovery factor at the breakthrough condition at higher inclination angles. This reveals that the oil drainage from inclined fractures is more facilitated as the gas phase enters to the fracture and also the flow communication between fracture and matrix blocks is improved. Furthermore, in waterflooding cycles, this difference between recoveries of different inclination angles become less pronounced. This is due to the less access of water to the fracture medium at any inclination angle. However, during all cycles the differences in *RF* values of all three cases is not more than 4%.

4.4.9 Fracture Pattern

Fracture configuration and pattern highly affect the fluid flow in the porous systems. To evaluate the effect of fracture pattern during the WAG injection on oil recovery, three different fractured porous media are considered. In Figure 4-12(a), there is only one fracture in the middle of the horizontal model; the case shown in Figure 4-12(b) contains two horizontal fractures with similar properties as those in the

case of (a); the model shown in Figure 4-12(c) contains one horizontal and one vertical fracture in the middle of the core with the same properties at the first two cases. We also compare the performance with a homogeneous model (without fracture) as shown in Figure 4-12(d).

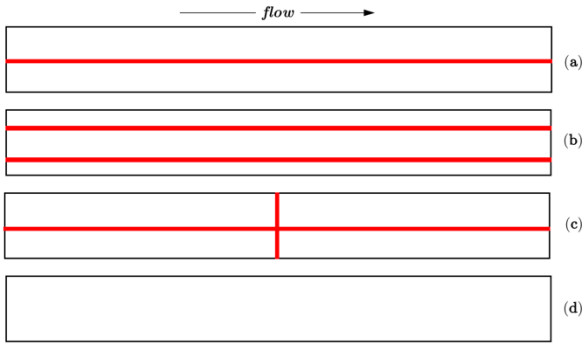

Figure 4-12: Fracture patterns in different porous media models. Pattern (a) is the original model used in the experiments and pattern (d) is the homogeneous model.

For the WAG injection process in all of the fracture configurations shown in Figure 4-12, three cycles of 0.5 PV slugs are injected at a WAG ratio = 1; the injection flow rate is fixed at 0.5 cm^3/min). Table 4-8 and Figure 4-13 show the results of *RF* for these three cases. According to Figure 4-13, adding fracture to the system substantially increases the both the instantaneous and ultimate *RFs*.

Table 4-8: Residual saturation and recovery factors of WAG injection in different models.

Model	s_{or} (HCPV fraction)	*RF* (HCPV fraction)
a	0.380	0.540
b	0.263	0.690
c	0.290	0.658
d	0.250	0.703

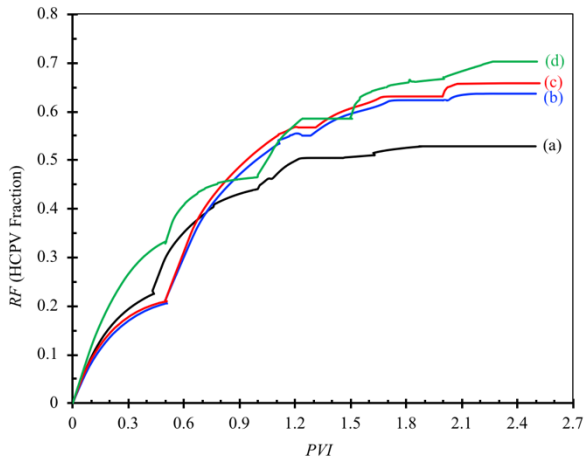

Figure 4-13: Effect of fracture pattern on the recovery performance of immiscible WAG injection (q = 5 cm^3/min, slug size = 0.5 PV).

As Figure 4-13 shows, model (d) results in the highest RF with ultimate recovery of 0.71 HCPV fraction after three cycles of WAG injection. The model (c) shows a close *RF* dynamics compared to the case (b) with ultimate *RF*=0.69 HCPV fraction; furthermore, model (a) with only one horizontal fracture is the original case that simulates the experimental condition and has the lowest ultimate *RF*=0.54 HCPV fraction among all fractured models. The higher RF in model (b) and (c) compared to the model (a) occurs mainly for the reason that by adding fracture to the medium the effective permeability will increase, leading to increase more contact between the injecting fluid and more oil production of oil. This effect is more highlighted during first GI cycle, where the gas (non-wetting phase) has more chance to occupy the fracture medium which highest oil saturation remained from the previous WF cycle. The injected water (wetting phase) does not advance into the fracture, and it enters into the matrix medium and sweeps the trapped oil in the matrix medium due to the low capillary entrance of the added fracture. Another reason for a slight small increase in the ultimate *RF* in model (c) over model (b) is related to the inter-connection of the horizontal and vertical fractures though which a larger extent of oil communication between matrix and fracture network is possible. This latter phenomena occurs if the capillary continuity holds for the vertical fracture in the model (c). The capillary continuity will be lost in the vertical fracture if the aperture increases above a threshold value, making the capillary pressure insignificant. The importance of the fracture aperture is analyzed in the section 4.6.

Model (b) adds a second horizontal fracture with the same characteristics of the first one (length, and petrophysical properties) while in model (c) the vertical fracture occupies less pore volume. This difference is more important when the matrix blocks become the main source for the oil production

(especially, during the WF cycles), resulting in more production, and consequently a higher *RF* from case (c) compare to that in case (b). The highest difference in the *RF*s of the model (b) and model (c) occurs at the GI_1 process when the gas invades into the fractures, sweeping the oil from the fracture medium; in the GI_2 both models do not contribute much to the oil recovery and the *RF*s become comparable between the two models. This is due to the movement of the gas phase into the drained fractures, where gas already founds its direct path to the producing zone through the fracture (due to less capillary entrance of the fracture and high capillary entrance of matrix blocks); so gas instantly flows through its path and the condition for breakthrough occurs. So, after GI_1 process, most of the recovery from the system is achieved during the WF cycles rather than those during the GIs, since water phase has more chance to flow into the matrix blocks as the main source of oil production and sweep the trapped oil from that zones. Although the fracture pattern in the case (c) shows some instantaneous higher RF values comparing to the case (b), the difference in the ultimate *RF* between the two models is less than 2% HCPV.

4.4.10 Interfacial Tension

One of the main active mechanisms in WAG injection is the interfacial tension reduction. The value of the interfacial tension significantly affects relative permeability curves. For instance, in a completely miscible system, the interfacial tension value is zero and the relative permeability of phases is a linear function of saturation with a slope of 1. To study the effect of interfacial tension for oil-water and oil-gas systems on the performance of the WAG injection, the low interfacial tension values ($\sigma_{\text{oil-water}}$=15 mN/m and $\sigma_{\text{oil-gas}}$ =10 mN/m) are considered in the simulations (see Figure 4-14) and the outputs are compared with the results of the original case study.

For both cases, the WAG injection processes are performed at the WAG ratio of 1, with 2.5 cycles at 0.5 slug size for each injection mode. According to Figure 4-14, lowering the interfacial tension values for both systems (water-oil and oil-gas) significantly increases the instantaneous and ultimate recovery factor of the WAG process (by 21.76%). The lower interfacial tension facilitates the oil displacement in the matrix zone, where it might be untouched by water, especially during the GI cycles. On the other hand, the amount of trapped gas is a strongly affected by the interfacial tension; a lower interfacial tension value results in more gas-oil contact and higher gas entrapment (hysteresis) in the system. Lower interfacial tension values also increase the recovery factor of the WF cycles and delays the breakthrough time of the water phase (see Figure 4-14).

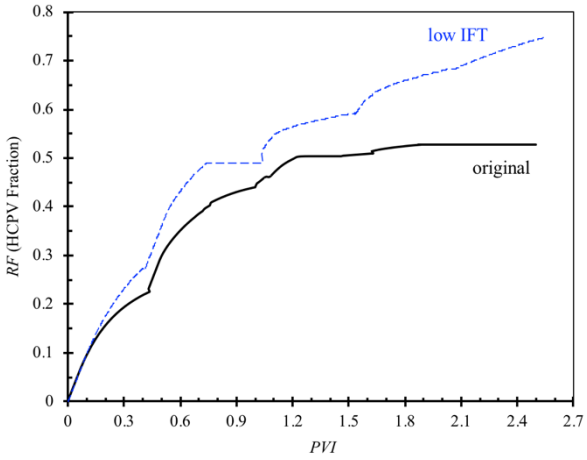

Figure 4-14: Effect of interfacial tension (IFT) reduction on oil recovery factor during WAG process (q=0.5 cm^3/min, slug size=0.5 PV).

In the last WF cycle (3rd WF), the recovery factor trend shows that the production is not ceased if the system is continued for further injection cycles of water and gas injection for the case of low interfacial tension (IFT), while at a higher interfacial tension condition, the recovery factor reaches to a plateau in which no more oil is expected to be recovered from the system even by injecting more water and gas.

4.4.11 WAG Ratio

WAG ratio is one of the important operating variables in designing a WAG flooding process. Unlike the oil-wet and mixed-wet systems, WAG ratio profoundly affects the fluid flow of phases during a WAG injection process [69]. To examine the impact of WAG ratio on WAG process in the fractured porous medium, three different WAG ratios of 1, 0.5, and 0.25 are taken into account. For the WAG ratios 0.25 and 0.50, the injection rate of the gas is fixed as the original case, and the injection rate of the water is multiplied by 0.25 and 0.5, respectively. Figure 4-15 describes the simulation results of this sensitivity analysis. According to Figure 4-14, the highest ultimate recovery factor is obtained at the WAG ratio of 1 (*RF* = 52.86%); by decreasing the WAG ratio to 0.5 (*RF* = 47.20 %) and 0.25 (*RF* = 38.74 %) the recovery factor is significantly reduced. WAG injection at low WAG ratios (e.g., 0.25) results in very low *RF* in the first WF cycle (~6.5 %), compared to two others (11.5% and 22.5% for the WAG ratios of 0.5 and 1, respectively), due to the low injection rate of the water to sweep the entire matrix zone. Since the porous system is strongly water-wet, more RF reduction occurs and the water breakthrough is delayed during the WF cycles, compared to the GI cycles. It should be noted that the rate of oil recovery during the GI cycles almost shows the same behaviour as the gas (due to the wettability of the system and its preference) mostly flows through the fracture medium.

At higher WAG ratios (e.g., 1), the water has more chance to be in contact with higher portion of trapped oil bank in small pores and displace more oil. Furthermore, at the WAG ratio of 1, two displacing phases of water and gas are traveling at the same velocity in the porous medium that provides a continuous and stable front in which the fluid mobility (especially the gas phase) is controlled, and thereby, a higher recovery is achieved.

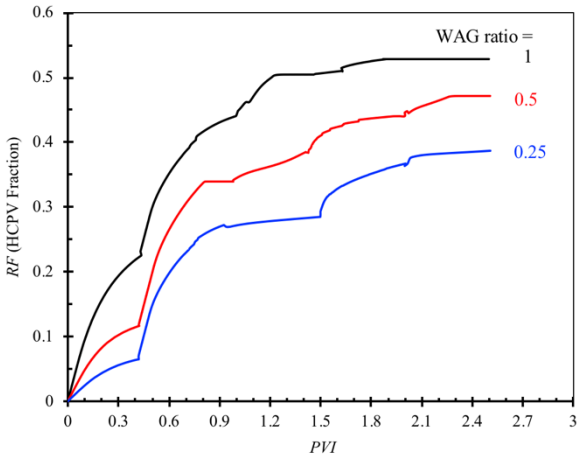

Figure 4-15: Influence of WAG ratio on recovery factor (2.5 cycles, slug size = 0.5 PV).

The performance of enhanced oil recovery techniques is mostly influenced by the heterogeneity of the applied reservoirs. WAG injection as a mature EOR technique has been widely used in naturally fractured reservoirs. Despite many research and engineering studies conducted on this topic, no comprehensive, robust, and reliable model is provided to simulate immiscible WAG injection in fractured systems. The CFD model proposed in this study uses three-phase relative permeability and hysteresis and three-phase capillary pressure in a fractured porous medium during immiscible WAG injection. The verified model can be used to study the effect of different parameters including the fracture configuration and pattern, fracture aperture, fracture inclination angle, mobility, and velocities of phases on the recovery performance of WAG injection This introduced CFD model can be used by industrial and environmental sectors to avoid additional time and financial costs; it can also help to obtain a comprehensive knowledge of immiscible WAG injection in heterogeneous/fractured reservoirs.

4.5 Summary and Conclusions

In this study, we simulate immiscible water-alternating-gas (WAG) injection into porous media with fractures, using CO_2 as the gas phase; the model is implemented in COMSOL Multiphysics® for enhanced oil recovery application. The simulations are conducted at atmospheric pressure and 100 ^oC temperature. Water and gas are sequentially injected with WAG ratio of 1, using slug size of 0.5 PV in

a strong water-wet sand pack where Maroon crude is used as the oil phase. The following conclusions are obtained from this study:

- The three-phase flow model with three-phase relative permeability and capillary pressure models is reliable in simulating the WAG process in fractured porous media. The maximum error in estimating the recovery factor is 12%.
- During the water flooding cycles, the mobility of water and oil in the matrix dominates the overall fluid mobility while in the gas injection cycles, the mobility of the gas and oil in the fracture dominates overall fluid mobility.
- The hysteresis effects results in higher ultimate oil recovery after 2.5 PVI. With and without hysteresis, the ultimate oil recovery factor values are 0.53 and 0.49 HCPV fraction, respectively.
- The hysteresis effects are mostly due to the gas trapping in the larger pores (such as those in fracture).
- Having a vertical fracture connected to a horizontal fracture in the system enhances the oil recovery through improving the matrix-fracture flow communication.
- Increasing the fracture aperture in the case in which the fracture is a high permeable porous medium leads to an increase in oil recovery at a fixed slug size and PVI.
- Increasing the fracture aperture increases the recovery and recovery rate of the oil phase. However, at later cycles, the early gas breakthrough reduces the incremental recovery.
- Fracture inclination angle does not remarkably change the ultimate *RF*; by changing the inclination angle from 30^o to 90^o, the *RF* is increased only by 2%.
- Including the gravity forces in vertical systems causes an overall improvement in *RF* through engaging both matrix and fracture media in all cycles. It increases the *RF* by 9%, compared to the horizontal model where no gravity force is applied to the system.
- As the permeability contrast between matrix and fracture media decreases, the flow communication between the two regions increases and improves the recovery performance of the WAG process.
- Lowering the IFT between phases significantly increases the oil recovery by providing more contact between phases.
- At a WAG ratio of 1, the highest oil recovery is obtained, while by lowering the WAG ratio, the fluid front is not stable and less oil is recovered from the system.
- In the current study, we focused on immiscible WAG injection. It is recommended that the miscible WAG injection in heterogeneous reservoirs is also examined in future work.

ACKNOWLEDGEMENTS
The authors would like to acknowledge the financial support provided by Memorial University (NL, Canada), Natural Sciences and Engineering Research Council of Canada (NSERC), InnovateNL (formerly RDC), and Equinor (formerly Statoil) Canada.

NOMENCLATURES

Acronyms

AARD	Average absolute relative deviation
CFD	Computational fluid dynamics
EOR	Enhanced oil recovery
FAWAG	Foam assistant water alternating gas injection
FEM	Finite element method
GI	Gas injection
HCPV	Hydrocarbon pore volume
IOR	Improved oil recovery
IWAG	Immiscible WAG
M	Mobility ratio
NFR	Natural fractured reservoir
PVI	Pore volume injection
PVT	Pressure volume temperature
RF	Recovery factor
SWAG	Simultaneous water and gas injection
WF	Waterflooding
WAG	Water-alternating-gas injection

Variables and Parameters

a	Capillary exponent
B	Three-phase relative permeability factor (Stone model)
c	Capillary entry pressure
C_p	Storage term
D	Diameter
g	Gravity acceleration constant
h	Height

L	Length
K	Absolute permeability
k_α	Effective permeability of the phase α
k_{rij}	Relative permeability of phase i in the ij two-phase system
k_{ri}^{3ph}	Three-phase relative permeability of phase i
N_{ca}	Capillary number
p	Pressure
p_{di}	Fracture entry pressure of phase i
Q	Source term
s	Phase saturation
t	Time
T	Temperature
v	Velocity
W	Width
x	x-axis coordinate (horizontal)
z	z-axis coordinate (vertical)

Greek Letters

α	Phase (gas, oil, and water)
δ	Scaling factor
ϕ	Porosity
λ	Mobility; Pore size distribution index
μ	Viscosity
ρ	Density
θ	Contact angle
σ	Interfacial tension

Subscripts and Superscripts

c	Capillary pressure
f	Fracture
$final$	Final state
g	Gas phase
k	Flux (in scaling factor)

m	Matrix
o	Oil phase
og	Oil-gas system
Q	Storage (in scaling factor)
ow	Oil-water system
w	Water phase
wg	Water-gas system
r	Residual phase
st	Time (in scaling factor)
Tot	Total

References

1. Beydoun, Z. R., Arabian plate oil and gas: why so rich and so prolific? *Episodes-Newsmagazine of the International Union of Geological Sciences* **1998,** *21* (2), 74-81.
2. Zendehboudi, S.; Rezaei, N.; Chatzis, I., Effects of fracture properties on the behavior of free-fall and controlled gravity drainage processes. *Journal of Porous Media* **2012,** *15* (4).
3. Firoozabadi, A., Recovery mechanisms in fractured reservoirs and field performance. *Journal of Canadian Petroleum Technology* **2000,** *39* (11).
4. Elfeel, M. A.; Al-Dhahli, A.; Geiger, S.; van Dijke, M. I., Fracture-matrix interactions during immiscible three-phase flow. *Journal of Petroleum Science and Engineering* **2016,** *143*, 171-186.
5. Davidson, D.; Snowdon, D., Beaver River Middle Devonian Carbonate: Performance review of a high-relief, fractured gas reservoir with water influx. *Journal of Petroleum Technology* **1978,** *30* (12), 1,672-1,678.
6. Denoyelle, L.; Bardon, C.; Couve de Murville, E., Interpretation of a CO_2/N_2 injection field test in a moderately fractured carbonate reservoir. *SPE Reservoir Engineering* **1988,** *3* (01), 220-226.
7. Panda, M.; Ambrose, J. G.; Beuhler, G.; McGguire, P. L., Optimized eor design for the Eileen west end area, Greater Prudhoe bay. *SPE Reservoir Evaluation & Engineering* **2009,** *12* (01), 25-32.
8. Dehghan, A.; Ghorbanizadeh, S.; Ayatollahi, S., Investigating the fracture network effects on sweep efficiency during WAG injection process. *Transport in porous media* **2012,** *93* (3), 577-595.
9. Behbahani, H.; Blunt, M. J., Analysis of imbibition in mixed-wet rocks using pore-scale modeling. *Spe Journal* **2005,** *10* (04), 466-474.
10. Schmid, K.; Geiger, S., Universal scaling of spontaneous imbibition for arbitrary petrophysical properties: Water-wet and mixed-wet states and Handy's conjecture. *Journal of Petroleum Science and Engineering* **2013,** *101*, 44-61.

11. Hagoort, J., Oil recovery by gravity drainage. *Society of Petroleum Engineers Journal* **1980,** *20* (03), 139-150.
12. O'Neill, N., Fahud field review: a switch from water to gas injection. *Journal of petroleum technology* **1988,** *40* (05), 609-618.
13. Van Dijkum, C.; Walker, T. In Fractured reservoir simulation and field development, Natih field, Oman, *SPE Annual Technical Conference and Exhibition, Society of Petroleum Engineers* **1991,** SPE-22917-MS.
14. Manrique, E. J.; Muci, V. E.; Gurfinkel, M. E., EOR field experiences in carbonate reservoirs in the United States. *SPE Reservoir Evaluation & Engineering* **2007,** *10* (06), 667-686.
15. Shedid, S. A., Influences of fracture orientation on oil recovery by water and polymer flooding processes: An experimental approach. *Journal of Petroleum Science and engineering* **2006,** *50* (3-4), 285-292.
16. Afzali, S.; Ghamartale, A.; Rezaei, N.; Zendehboudi, S., Mathematical modeling and simulation of water-alternating-gas (WAG) process by incorporating capillary pressure and hysteresis effects. *Fuel* **2019**, 116362.
17. Afzali, S.; Rezaei, N.; Zendehboudi, S., A comprehensive review on enhanced oil recovery by water alternating gas (WAG) injection. *Fuel* **2018,** 227, 218-246.
18. Dong, M.; Foraie, J.; Huang, S.; Chatzis, I., Analysis of immiscible water-alternating-gas (WAG) injection using micromodel tests. *Journal of Canadian Petroleum Technology* **2005,** *44* (02).
19. Van Dijke, M. I. J.; Sorbie, K. S., Pore-scale modelling of three-phase flow in mixed-wet porous media: multiple displacement chains. *Journal of Petroleum Science and Engineering* **2003,** *39* (3-4), 201-216.
20. Pizarro, J. O. D. S.; Branco, C. C. M. In Challenges in implementing an EOR project in the pre-salt province in Deep Offshore Brasil, *SPE EOR conference at oil and gas West Asia, Society of Petroleum Engineers* **2012,** SPE-155665-MS.
21. Righi, E. F.; Royo, J.; Gentil, P.; Castelo, R.; Del Monte, A.; Bosco, S. In Experimental study of tertiary immiscible WAG injection, *SPE/DOE Symposium on Improved Oil Recovery, Society of Petroleum Engineers* **2004,** SPE-89360-MS.
22. Haghighat, S. WAG Modeling in Fractured Reservoirs. *Thesis Report MTA/PW/04-15 TU Delft*, **2004**.
23. Awan, A. R.; Teigland, R.; Kleppe, J., A survey of North Sea enhanced-oil-recovery projects initiated during the years 1975 to 2005. *SPE Reservoir Evaluation & Engineering* **2008,** *11* (03), 497-512.
24. Brodie, J. A.; Jhaveri, B. S.; Moulds, T. P.; Mellemstrand Hetland, S. In Review of gas injection projects in BP, *SPE Improved Oil Recovery Symposium, Society of Petroleum Engineers* **2012** SPE-154008-MS.
25. Christensen, J. R.; Stenby, E. H.; Skauge, A. In Review of WAG field experience, *International petroleum conference and exhibition of Mexico, Society of Petroleum Engineers* **1998**.
26. Donaldson, E. C.; Chilingarian, G. V.; Yen, T. F., Enhanced oil recovery, II: Processes and operations. *Elsevier*, **1989**.

27. Pariani, G.; McColloch, K.; Warden, S.; Edens, D., An approach to optimize economics in a West Texas CO_2 flood. *Journal of Petroleum Technology* **1992,** *44* (09), 984-1,025.
28. Gang, T.; Kelkar, M. G. In History matching for determination of fracture permeability and capillary pressure, *SPE Annual Technical Conference and Exhibition, Society of Petroleum Engineers* **2006**.
29. Gilman, J. R.; Kazemi, H., Improved calculations for viscous and gravity displacement in matrix blocks in dual-porosity simulators (includes associated papers 17851, 17921, 18017, 18018, 18939, 19038, 19361 and 20174). *Journal of petroleum technology* **1988,** *40* (01), 60-70.
30. Al-Kobaisi, M.; Kazemi, H.; Ramirez, B.; Ozkan, E.; Atan, S., A critical review for proper use of water/oil/gas transfer functions in dual-porosity naturally fractured reservoirs: part II. *SPE Reservoir Evaluation & Engineering* **2009,** *12* (02), 211-217.
31. Ramirez, B. A.; Kazemi, H.; Al-Kobaisi, M.; Ozkan, E.; Atan, S. In A Critical Review for Proper Use of Water-Oil-Gas Transfer Functions in Dual-Porosity Naturally Fractured Reservoirs-Part I, *SPE Annual Technical Conference and Exhibition, Society of Petroleum Engineers* **2007**.
32. Al Eidan, A. A.; Mamora, D. D.; Schechter, D. S. In Experimental and Numerical Simulation Studies of Different Modes of CO_2 Injection in Fractured Carbonate Cores, *SPE Enhanced Oil Recovery Conference, Society of Petroleum Engineers* **2011**.
33. Heeremans, J. C.; Esmaiel, T. E.; Van Kruijsdijk, C. P. In *Feasibility study of WAG injection in naturally fractured reservoirs, SPE/DOE symposium on improved oil recovery, Society of Petroleum Engineers* **2006**.
34. Han, L. Optimum Water-Alternating-Gas (CO_2-WAG) Injection in the Bakken Formation. *Faculty of Graduate Studies and Research, University of Regina,* **2015**.
35. Agada, S.; Geiger, S. In Wettability, trapping and fracture-matrix interaction during WAG injection in fractured carbonate reservoirs, S*PE Improved Oil Recovery Symposium, Society of Petroleum Engineers* **2014**.
36. Bahagio, D., Ensemble Optimization of CO_2 WAG EOR. *Faculty of Civil Engineering and Geoscience, TU Delft, Master Thesis* **2013**.
37. Chen, S.; Li, H.; Yang, D.; Tontiwachwuthikul, P., Optimal parametric design for water-alternating-gas (WAG) process in a CO_2-miscible flooding reservoir. *Journal of Canadian Petroleum Technology* **2010,** *49* (10), 75-82.
38. Virnovsky, G.; Vatne, K.; Iversen, J.; Signy, C. In Three-phase capillary pressure measurements in centrifuge at reservoir conditions, *Proceedings SCA2004-19, paper for the International Symposium of the Society of Core Analysts, Abu Dhabi,* **2004**.
39. Zhou, Y.; Helland, J. O.; Hatzignatiou, D. G., Computation of three-phase capillary pressure curves and fluid configurations at mixed-wet conditions in 2D rock images. *SPE Journal* **2016,** *21* (01), 152-169.
40. Neshat, S. S.; Pope, G. A. In Compositional Three-Phase Relative Permeability and Capillary Pressure Models Using Gibbs Free Energy, *SPE Reservoir Simulation Conference, Society of Petroleum Engineers* **2017**.
41. Skjaeveland, S.; Siqveland, L.; Kjosavik, A.; Hammervold, W.; Virnovsky, G. In Capillary pressure correlation for mixed-wet reservoirs, *SPE India Oil and Gas Conference and Exhibition, Society of Petroleum Engineers* **1998**.

42. Shahverdi, H.; Sohrabi, M. In Three-phase relative permeability and hystresis model for simulation of water alternating gas (WAG) injection, *SPE Improved Oil Recovery Symposium, Society of Petroleum Engineers* **2012**.
43. Larsen, J.; Skauge, A., Methodology for numerical simulation with cycle-dependent relative permeabilities. *SPE Journal* **1998,** *3* (02), 163-173.
44. Ranaee, E.; Porta, G. M.; Riva, M.; Blunt, M. J.; Guadagnini, A., Prediction of three-phase oil relative permeability through a sigmoid-based model. *Journal of Petroleum Science and Engineering* **2015,** *126*, 190-200.
45. Ebeltoft, F. L. E. In Versatile Three-Phase Correlations for Relative Permeability and Capillary Pressure, *International Symposium of the Society of Core Analysis, Napa Valley, California, USA. SCA*, **2013**; pp 1-14.
46. Lei, G.; Wang, C.; Yuan, T.; Yang, L., An Analytical Equation to Predict Oil-Gas-Water Three-Phase Relative Permeability Curves in Fractures. *Improved Oil and Gas Recovery* **2017,** *1*.
47. Brooks, R. H.; Corey, A. T., Properties of porous media affecting fluid flow. *Journal of the irrigation and drainage division* **1966,** *92* (2), 61-90.
48. Dorostkar, M.; Mohebbi, A.; Sarrafi, A.; Soltani, A., A laboratory study of hot WAG injection into fractured and conventional sand packs. *Petroleum Science* **2009,** *6* (4), 400-404.
49. Multiphysics, C., Comsol multiphysics reference manual. *COMSOL: Grenoble, France* **2013**, 1084.
50. Chatzis, I.; Morrow, N. R., Correlation of capillary number relationships for sandstone. *Society of Petroleum Engineers Journal* **1984,** *24* (05), 555-562.
51. Fatemi, S. M. Multiphase flow and hysteresis phenomena in oil recovery by water alternating gas (WAG) injection. *Heriot-Watt University, PhD Thesis* **2015**.
52. Baker, L. In Three-phase relative permeability correlations, *SPE Enhanced Oil Recovery Symposium, Society of Petroleum Engineers* **1988**.
53. Stone, H., Probability model for estimating three-phase relative permeability. *Journal of Petroleum Technology* **1970,** *22* (02), 214-218.
54. Stone, H., Estimation of three-phase relative permeability and residual oil data. *Journal of Canadian Petroleum Technology* **1973,** *12* (04).
55. Avraam, D.; Payatakes, A., Flow mechanisms, relative permeabilities, and coupling effects in steady-state two-phase flow through porous media. The case of strong wettability. *Industrial & engineering chemistry research* **1999,** *38* (3), 778-786.
56. Guzman, R.; Domenico, G.; Fayers, F.; Aziz, K.; Godi, A. In Three-phase flow in field-scale simulations of gas and wag injections, *European Petroleum Conference, Society of Petroleum Engineers* **1994**.
57. Ghomian, Y.; Pope, G. A.; Sepehrnoori, K. In Hysteresis and field-scale optimization of WAG injection for coupled CO_2-EOR and sequestration, *SPE Symposium on Improved Oil Recovery, Society of Petroleum Engineers* **2008**.
58. Rezaei, N.; Firoozabadi, A., Pressure evolution and production performance of waterflooding in n-heptane-saturated fired berea cores. *SPE Journal* **2014,** *19* (04), 674-686.
59. Sabti, M.; Alizadeh, A.; Piri, M. In Three-phase flow in fractured porous media: experimental investigation of matrix-fracture interactions, *SPE Annual Technical Conference and Exhibition, Society of Petroleum Engineers* **2016**.

60. Firoozabadi, A. Research program on fractured petroleum reservoirs. Quarterly report, January 1--March 31, 1994. *Reservoir Engineering Research Inst., Palo Alto, CA (United States)* **1994**.
61. Pinder, G. F.; Gray, W. G., Essentials of multiphase flow and transport in porous media. *John Wiley & Sons* **2008**.
62. Kazemi, H. In Naturally fractured reservoirs, *Third International Forum on Reservoir Simulation, Baden, Austria* **1990**.
63. Kazemi, H.; Gilman, J., Multiphase flow in fractured petroleum reservoirs. In *Flow and Contaminant Transport in Fractured Rock*, Elsevier **1993**; pp 267-323.
64. Sahimi, M., Flow and transport in porous media and fractured rock: from classical methods to modern approaches. *John Wiley & Sons* **2011**.
65. Dumore, J.; Schols, R., Drainage capillary-pressure functions and the influence of connate water. *Society of Petroleum Engineers Journal* **1974,** *14* (05), 437-444.
66. Chatzis, I.; Kantzas, A.; Dullien, F. In On the investigation of gravity-assisted inert gas injection using micromodels, long Berea sandstone cores, and computer-assisted tomography, *SPE Annual Technical Conference and Exhibition, Society of Petroleum Engineers* **1988**.
67. Dejam, M.; Hassanzadeh, H., Formation of liquid bridges between porous matrix blocks. *AIChE journal* **2011,** *57* (2), 286-298.
68. Parsaei, R.; Chatzis, I., Experimental investigation of production characteristics of the gravity-assisted inert gas injection (GAIGI) process for recovery of waterflood residual oil: effects of wettability heterogeneity. *Energy & fuels* **2011,** *25* (5), 2089-2099.
69. Bunge, A.; Radke, C., CO2 flooding strategy in a communicating layered reservoir. *Journal of Petroleum Technology* **1982,** *34* (12), 2,746-2,756.
70. Shahverdi, H.; Sohrabi, M., An improved three-phase relative permeability and hysteresis model for the simulation of a water-alternating-gas injection. *Society of Petroleum Engineers Journal* **2013,** *18* (05), 841-850.
71. Hirasaki, G. J., Sensitivity coefficients for history matching oil displacement processes. *Society of Petroleum Engineers Journal* **1975,** *15* (01), 39-49.

CHAPTER FIVE

Hybrid Mathematical Modelling of Three-Phase Flow in Porous Media: Application to Water-Alternating-Gas Injection

Preface

A version of this manuscript has been submitted to the Journal of Natural Gas Science and Engineering, and also presented in the 70th Canadian Society of Chemical Engineering Conference (CSChE). I am the primary author of this paper. All authors were involved in the objectives definition, development of methodology steps, and design of paper structure. I carried out a majority of the literature review, and the modeling with the aid of technical comments from co-authors, Sohrab Zendehboudi and Nima Rezaei and Omid Mohammadzadeh. I prepared the first draft of the manuscript and then revised the manuscript based on the co-authors' feedback and reviewers' comments received from the journal. The co-authors, Sohrab Zendehboudi and Nima Rezaei, had considerable contribution in revising the manuscript in terms of editorial and technical aspects. Omid Mohammadzadeh helped in results interpretation, and statistical analysis, and also had a final look to edit the manuscript if some corrections were still needed.

Abstract

Machine learning algorithms are extensively used to reduce the complexity of applied problems in various fields, including energy. Water-alternating-gas (WAG) is an enhanced oil recovery (EOR) process that is widely implemented to increase the hydrocarbon recovery. Accurate prediction of the WAG performance is of great importance in the optimal management of the hydrocarbon resources. In the current work, a hybrid mathematical model is proposed for the near-immiscible WAG process. We use data-driven sub-models, including least square support vector machine (LSSVM) and adaptive neuro-fuzzy inference system (ANFIS) in series with an empirical model (EM) and a first principle model (FPM) to study three-phase flow in porous media. The LSSVM and ANFIS sub-models predict the two-phase water-oil, gas-oil, and gas-water relative permeabilities. The outputs from these models are supplied to the empirical models (EMs) to estimate the three-phase relative permeabilities for oil, gas, and water phases. We examine the accuracy of oil recovery estimates from each model and compare it with experimental data for one WAG injection process involving three water- and gas-injection cycles. For a strongly water-wet sandstone system, we use a total number of 1,457 training data points to develop three sets of two-phase relative permeability data that is applied in the WAG injection process. Statistical analysis is conducted on model results, in which we use coefficient of determination, standard deviation, and error analysis. The model developed using LSSVM shows a better prediction performance in estimating the relative permeabilities, compared to that using ANFIS. The relative importance parameter analysis shows that for the LSSVM sub-model, water saturation is the most influencing input parameter for the gas-water and oil-water systems while for the gas-oil system, gas saturation is the most important input parameter. The results from the WAG process also shows a better performance for the LSSVM, compared to the ANFIS. Using the models proposed in this work, some hybrid models are developed to forecast the ultimate recovery factor (RF) in the testing phase. The predicted ultimate RF values are 92.0%, 91.6%, and 82.9% for the correlation-based EM-FPM, LSSVM-EM-FPM, and ANFIS-EM-FPM hybrid models, respectively, in comparison to the measured ultimate RF value of 93.6% after three cycles of water- and gas-injection. Among the proposed hybrid models, the LSSVM-EM-FPM model significantly removes the non-linearity of the two-phase relative permeabilities. The absolute maximum error in estimating the ultimate oil RF is 1.7%, 2.5%, and 11.4% for the EM-FPM, LSSVM-EM-FPM, and ANFIS-EM-FPM hybrid models in the testing phase, respectively. In general, the LSSVM-EM-FPM hybrid model possess the same level of accuracy as that of the EM-FPM hybrid model, but with significantly less model complexity and non-linearity. Thus, the LSSVM-EM-FPM hybrid model can be

used in demanding applications such as optimization and control of this oil recovery process, leading to a better resource management.

Keywords: WAG injection; Three-phase relative permeability; LSSVM; ANFIS; Machine learning; Recovery factor.

5.1 Introduction

The WAG injection has been successfully field tested as a promising EOR technique. Through controlling the frontal mobility, the WAG injection process features a lower residual oil saturation compared to traditional waterflooding or gas injection especially in miscible condition [1]. Generally, four mechanisms are responsible for enhanced productivity of the WAG injection process, including: 1) changing the oil density as well as reducing its viscosity as a result of the interactions between the oil phase and the light components of the injecting gas phase, depending on the temperature, pressure, and composition of the oil and gas phases, 2) changing the three-phase relative permeability of the phases that result more stable fluid fronts, 3) trapping of the non-wetting phase(i.e. gas), and 4) reducing the interfacial tension (IFT) between the phases upon compositional changes, leading to lower residual oil saturations [1].

During a WAG injection process, some complex displacement patterns occur due to highly non-monotonic saturation variations of all three phases [2]. Since the WAG process involves subsequent injections of different fluids, simulation of the process performance is more complicated than that of a typical three-phase flow system [3]. The WAG injection process is challenging in terms of fluid-fluid interactions, surface and interfacial tension effects, capillary and phase trapping, wettability, and pore size distributions [4]. It is thus important to further explore the vital characteristics of the WAG process such as relationships between relative permeabilities of the phases while studying the flow behavior in such complex systems.

In a WAG flooding process, directional hysteresis occurs in the magnitudes of the relative permeability during the changes in saturation history between the subsequent imbibition and drainage displacements in the system [5-6]. Three-phase relative permeability data are necessary to model the distribution and transport of oil, water, and, gas in porous media; and to evaluate the pressure and velocity distribution of the available phases [7]. Relative permeability functions integrate the effects fluid and rock properties, and fluid saturations in porous media [8]. Skauge and Larsen [9] used dynamic WAG injection experiments and measured unsteady three-phase relative permeability values using consecutive cycles of water-and-gas injections for different porous media wetting conditions. In each cycle, the relative permeability of all the phases showed irreversible hysteresis effects. The gas phase saturation profiles (as the most non-

wetting phase) caused more hysteresis effects in all porous media compared to the wetting phase. Relative permeability of the most non-wetting phase (gas) was affected by the hysteresis the most, compared to hysteresis effects on the relative permeability of most wetting (water) and intermediate wetting (oil) phases; at a constant saturation, the gas relative permeability was lower during the imbibition cycles when compared to that in drainage cycles [9]. In another study, Larsen and Skauge proposed a three-phase relative permeability model that accounted for local hysteresis effects for wetting, non-wetting, and intermediate wetting phases. The proposed model assumed reversible hysteresis loops which was applied for WAG flooding process. The model inputs were the initial phase saturations and relative permeability of wet, non-wet, and intermediate-wet phases [10]. Egermann et al. proposed a three-phase relative permeability model for a WAG injection process; it was found that the hysteresis effects depend on both the saturation and displacement histories [11].

Obtaining two-phase relative permeability data is more straightforward than those of the three-phase, as the lower number of phases decreases the available saturation paths. However, a three-phase flow system has infinite number of saturation paths that makes it difficult to estimate the three-phase relative permeability values. Hence, the evaluation of the three-phase relative permeability data has been the subject of numerous studies [12]. In the literature, two main approaches are followed to estimate the three-phase relative permeability data: 1) direct measurements using coreflooding experiments, and 2) predictions made from two-phase relative permeability data. In the first approach, the three-phase relative permeability values are obtained using steady-state or unsteady-state experiments. In addition, there are various empirical correlations to estimate the three-phase relative permeability values using the two-phase data [13]. One of the primitive correlations that estimate the three-phase relative permeability was introduced by Stone, that is widely known as "Stone I" model [14]. In this model, the three-phase relative permeability data are predicted based on measured two-phase data points. The Stone I model assumes that water and gas are separated in the system, and the oil bank displacements by water and gas are two independent processes [14]. However, the error associated with the Stone I model (and similar models) is high, making these relative permeability correlations unreliable for modelling the three-phase flow in porous media. Therefore, several investigations are performed to enhance the accuracy of the existing three-phase relative permeability models against experimental data [15-16]. These studies also revealed that there is no single model that can fit to the experimental data from different sources which is not surprising, considering variation in the rock and fluid properties involved in different experimental studies. Two-phase relative permeabilities are non-linear functions of the phase saturations, which are influenced by various parameters such as phase saturation history, pore size distribution, pore structure,

wettability, permeability and porosity, overburden pressure, the IFT between fluids, fluid properties (e.g., viscosity and density), initial wetting phase saturation, and the flow rate [17-30]. The two-phase relative permeabilities do not only control the fluid flow and saturation distribution in two-phase systems, but their values and behavior also significantly affect the fluid flow in three-phase systems. However, the relative influence of the two-phase relative permeabilities and the impact of rock and fluid properties in three-phase systems have not been clearly understood and quantified in the literature [31].

Smart tools such as artificial neural network (ANN) models enable us with robust toolboxes to conduct non-linear and multidimensional interpolations. These models are being extensively applied in various sectors from biology to engineering. However, the application of ANN (and connectionist) models in the petroleum industry and specifically in EOR processes is still in its infancy. In this work, we utilize two of the most known smart tools, namely LSSVM and ANFIS, for prediction of the three-phase relative permeabilities based on the two-phase data.

Vapnik [32] proposed the idea of support vector machine (SVM) to address typical problems and limitations that are encountered in the ANN modeling, such as overfitting, convergence to local minima, and inconsistence or unrepeatable results [33]. Additionally, although the structure of the SVM is simpler than ANN (less model parameters and no hidden nodes), it converges to a global minima. The SVM network topology and is only obtained through the training stage and does not demand a priori knowledge about its structure [34-35]. In general, the SVM model develops a robust machine learning approach that uses statistical learning theory, leading to reliable generalization of the performance [36]. The SVM algorithm results in an optimum hyperplane that features a minimum threshold distance from all experimental data points. The SVM model is extensively applied in classification application to divide the experimental data points to various classes with distinct boundaries [37-38]. Due to the extensive uncertainty, complexity, and non-linear behaviors associated with various data and properties reported in the petroleum industry, the SVM model is considered as a reliable tool in dealing with these challenges [39]. There are modified versions of the SVM model that are applied for data analysis in the oil and gas industry. For instance, Fayazi et al. predicted natural gas viscosity using least square support vector machine (LSSVM) model [40]. In another work, Esmaeili et al. used supervised (learning) LSSVM model to predict the effect of temperature on two-phase oil-water relative permeability data [31]. The LSSVM model has also been used for other oil and gas related applications such as predicting the phase equilibrium conditions of clathrate hydrate, modelling freezing point depression of electrolyte solutions, calculating minimum miscibility pressure for CO_2-oil systems, and estimating dew point pressure for a gas condensate system [35, 41-42].

The fuzzy neural network models benefit from the learning capability in the ANNs and knowledge demonstration capability of the fuzzy logic [43]. Adaptive neuro-fuzzy inference system (ANFIS) eliminates the drawbacks of the neural networks, such as the lack of transparency in explaining the main decision, and the weaknesses involved in the learning stage of fuzzy logic. ANFIS is able to predict systems with acceptable accuracy in various subjects/disciplines such as engineering, medicine, transportation, business, and economics [44]. This success led to extensive developments in various modifications[45], applications[45], and reviews and surveys[44] of the fuzzy neural network systems. Among proposed neuro fuzzy models, ANFIS introduced by Jang in 1993[46] has attracted many interests. However, ANFIS also faces major limitations such as high dimensionality and training complexity, which impose restrictions on problems with large datasets. ANFIS algorithm has been extensively used in petroleum engineering research studies to predict, for instance, permeability and porosity, injection profile and well placement, oil viscosity, minimum miscibility pressure (MMP), asphaltene precipitation, reservoir oil solution gas-oil ratio, and oil recovery factor [47-56]. Shamshirband et al. used the multilayer perceptron artificial neural network (MLP-ANN), ANFIS, and LSSVM models to estimate the oil relative permeability in a sandstone reservoir at various temperatures [57]. Their proposed models linked the oil relative permeability to the corresponding input parameters such as water saturation, temperature, and water and oil viscosities. Their results showed that the LSSVM model leads to the best performance based on the graphical and statistical error analysis. In another study, Roghanian et al. used ANFIS and identified the complex relation between rock and fluid properties and water-oil relative permeability key points including: maximum water and oil relative permeability values, cross point saturation, and cross point relative permeability [58].

In this work, the LSSVM, ANFIS, and a correlation-based empirical model (EM) are used to determine the two-phase relative permeability values in three systems of oil-water, oil-gas, and gas-water. The predicted values are then embedded in a first principle model (FPM) of WAG flooding process to estimate the ultimate recovery factor for comparison with some experimental data. We structure this chapter as follows: after the introduction, we provide the mathematical framework, including the mathematical model and numerical solution. The theoretical framework of data acquisition and analysis, and the training procedure of the ANFIS and LSSVM models are then given. We also discuss the limitations associated with the applied models. After evaluating the two-phase relative permeability predictions by the ANFIS and LSSVM models, we discuss the oil recovery factor, three-phase relative permeability of all the phases, and the relative importance of all the input parameters. The models are

then applied to a case study and the predictions are compared with the experimental results. Finally, the main conclusions drawn from the results are listed.

5.2 Theoretical Frameworks of LSSVM and ANFIS Models

5.2.1 LSSVM Model

For a specific set of the experimental data $\{(x_1, y_1), (x_2, y_2), \dots, (x_N, y_N)\}$ in which $x_i \in R^n$ and $y_i \in R$ are the input and output variables, respectively, the following relationship is applied by the SVM algorithm to evaluate the separation plane [59-62]:

$$y = w^T.\varphi(x) + b \tag{5-1}$$

where w is weight factor; $\varphi(x)$ is a non-linear function; T is matrix transpose operation; and b is bias term. Through this non-linear function, the data (x_i) are mapped into the n-dimensional feature space. When the given dataset is divided into two linearly separable classes (1 and 2), the constraints in Eq. (5-2) applies [35,59-63]. For $y_i = +1$, the input data x_i belong to class 1 and for $y_i = -1$ the input data belong to class 2.

$$\begin{cases} w^T.\varphi(x) + b \geq +1 & y_i = +1 \\ w^T.\varphi(x) + b \leq -1 & y_i = -1 \end{cases} \tag{5-2}$$

The margin is set as a distance between the plane passing through the data points of class 1 or 2 with values of $y_i = +1$ and $y_i = -1$, respectively. The constraints presented in Eq. (5-2) can be generalized as seen in Eq. (5-3) for a separable case. Using a slack variable ($\zeta_i \geq 0$), Cortes and Vapnik extended the inequality constraints for a non-separable case (see Eqs. (5-3) – (5-5)) [64].

$$y_i[w^T.\varphi(x_i) + b] \geq +1, \quad i = 1,2,3, \dots, N \tag{5-3}$$

$$y_i[w^T.\varphi(x_i) + b] \geq 1 - \zeta_i, \quad i = 1,2,3, \dots, N \tag{5-4}$$

$$\zeta_i \geq 0, \quad i = 1,2,3, \dots, N \tag{5-5}$$

Similar to other conventional optimization algorithms, the LSSVM algorithm uses constraints to introduce objective or cost function(s). An objective function (also called, cost function) can be developed (see Eq. (5-6)), using the constraints and a constant value C (which is a positive and real number); the cost function provides a trade-off between the classification error and margin [40]:

$$Cost(w, \zeta) = \frac{1}{2} w^T.w + \frac{C}{2} \sum_{i-1}^{N} \zeta_i^p \tag{5-6}$$

Using the Lagrangian multipliers α and β, and by imposing its derivate equal to zero, the constraints minimization (in Eq. (5-4) and Eq.(5-6)) changes to an unconstraint minimization as seen in Eq. (5-7) [40]:

$$U(w,b,\alpha,\beta,\zeta) = \frac{1}{2}w^T.w + \frac{C}{2}\sum_{i-1}^{N}\zeta_i^p - \sum_{i=1}^{N}\alpha_i(\,y_i[w^T.\varphi(x_i)+b] - 1 + \zeta_i) - \sum_{i=1}^{N}\beta_i\zeta_i \qquad (5\text{-}7)$$

The LSSVM algorithm is a modified version of the SVM model in which a linear set of equations are solved instead of the quadratic equations of the SVM. Hence, a new cost function (Eq. (5-8)) is obtained in which the parameter ζ is the regression error and γ is the model tuning parameter [31]:

$$R(w,\zeta) = \frac{1}{2}w^T.w + \frac{\gamma}{2}\sum_{i-1}^{N}\zeta_i^2 \qquad (5\text{-}8)$$

In the LSSVM algorithm, similar constraints to those of the SVM algorithm (Eq. (5-4)) are applied which include the equality constraints instead of the inequality constraint (Eq. (5-3)), as given below [31]:

$$y_i[w^T.\varphi(x)+b] = 1-\zeta_i, \quad i = 1,2,3,\dots,N \qquad (5\text{-}9)$$

The following Lagrangian function is developed that uses the Lagrangian multiplier α[38, 65]:

$$U(w,b,\alpha,\beta,\zeta) = \frac{1}{2}w^T.w + \frac{\gamma}{2}\sum_{i-1}^{N}\zeta_i^2 - \sum_{i=1}^{N}\alpha_i(\,y_i[w^T.\varphi(x)+b] - 1 + \zeta_i) \qquad (5\text{-}10)$$

where α can be either a positive or a negative value depending on the formulation of the LSSVM algorithm. The optimum point is met where the derivatives of Eq. (5-10) with respect to $b, \alpha,$ and ζ become zero. The following equations are resulted from the derivation of Eq. (5-10) [38, 65]:

$$\begin{cases} \frac{\partial U}{\partial w} = 0 \quad => w = \sum_{i=1}^{N}\alpha_i\, y_i\varphi(x_i) \\ \frac{\partial U}{\partial b} = 0 \quad => \sum_{i=1}^{N}\alpha_i\, y_i = 0 \\ \frac{\partial U}{\partial \zeta_i} = 0 \quad => \alpha_i = \gamma\zeta_i, i = 1,2,\dots,N \\ \frac{\partial U}{\partial \alpha_i} = 0 \quad => y_i[w^T.\varphi(x_i)+b] = 1-\zeta_i,, i = 1,2,\dots,N \end{cases} \qquad (5\text{-}11)$$

$$\begin{bmatrix} o & 1_N^T \\ 1_N & \Omega + \gamma^{-1}I_N \end{bmatrix}\begin{bmatrix} b \\ \alpha \end{bmatrix} = \begin{bmatrix} 0 \\ Y \end{bmatrix} \qquad (5\text{-}12)$$

Eq. (5-12) is Karush-Kuhn-Trucker equation in which $\alpha = [\alpha_1, \alpha_2, \dots, \alpha_N]^T$, $y = [y_1, y_2, \dots, y_N]^T$, and $1 = [1,1,\dots,1]^T$; furthermore, $\Omega \in R^{N\times N}$ represents the kernel matrix with a size of $N \times N$, and I_N refers

to the identity matrix. In Eq. (5-12), w and ζ parameters are removed. The transformation (ψ) of the input variables to feature space is simplified by using kernel function $K(x_i, x_j)$:

$$\Omega_{ij} = \psi^T(x_i)\psi(x_j) = K(x_i, x_j) \tag{5-13}$$

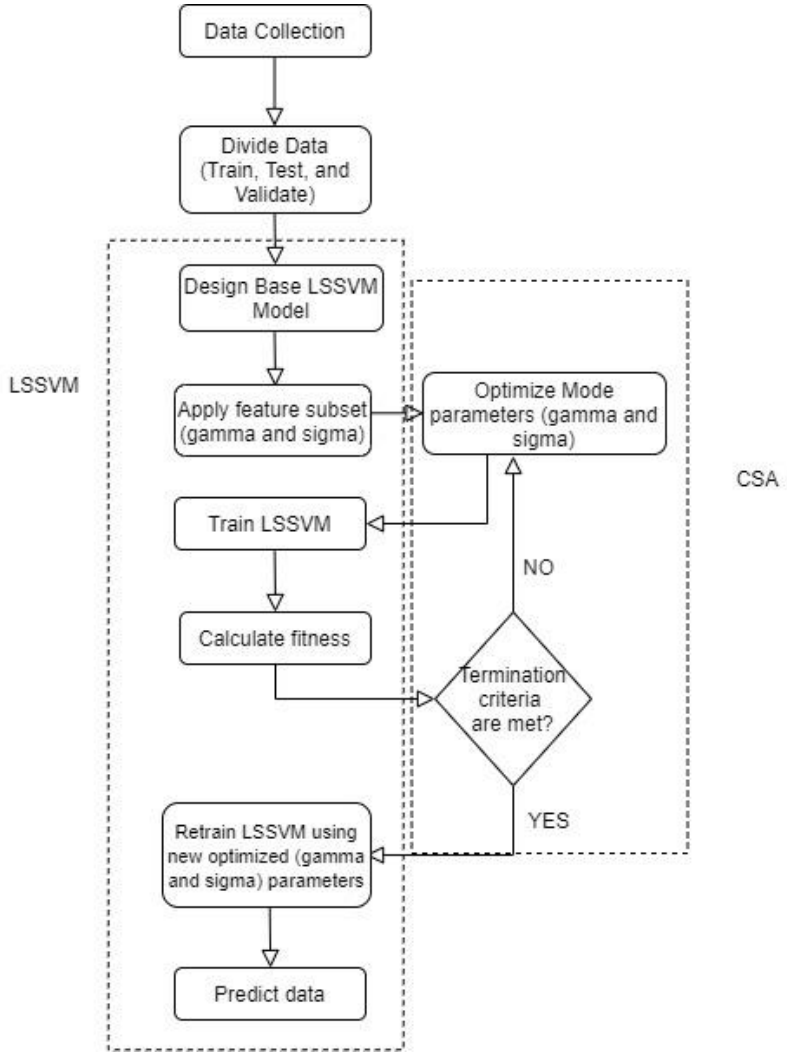

Figure 5-1:A schematic of LSSVM-CSA model used in current work [66].

Numerous kernel function are proposed in the literature, such as polynomial, linear, spline, and radial basis function (RBF) [67-70]. In the current study, we use the RBF kernel function (Eq. (5-14)) in which $\sigma^2$is the squared variance of the Gaussian distribution function that is be minimized in the SVM algorithm [31].

$$K(x, x_i) = \exp\left(\frac{-\|x_i - x\|^2}{\sigma^2}\right) \tag{5-14}$$

Figure 5-1 shows a schematic of the general algorithm of a LSSVM-CSA applied in this study.

5.3 ANFIS model

The ANFIS model hybridizes the fuzzy inference system (FIS) and ANN to minimize the drawbacks associated with each of these stand-alone models [46]. ANFIS is an adaptive multi-layer feed forward network which is originally applied for forecasting target parameters in nonlinear systems [71-72]. The ANFIS model structure, consisting of nodes in five different layers, is based on fuzzy values being determined during the training stage [71-72]. The flowchart for the ANFIS model, including its hybrid optimization algorithm, is illustrated in Figure 5-2.

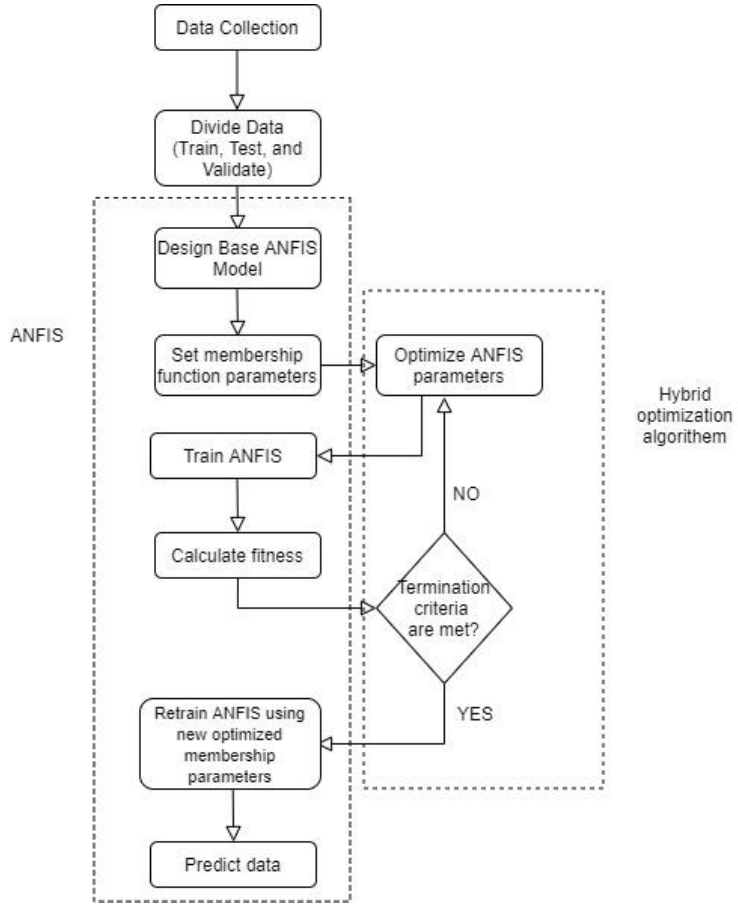

Figure 5-2: Simplified flowchart of the ANFIS model optimized by a hybrid algorithm [66].

In this approach, each node is designed using its membership function. The O_i^j represents the output of the i^{th} node in the layer j. For example, in the first layer where j=1, the i^{th} node refers to an adaptive node with the input of x (or y). The linguistic label attributed for this node is referred as A_i (or B_{i-2}). The membership function for a given node is formed as follows [73]:

$$O_i^1 = \mu_{Ai}(x); \quad i = 1,2$$

or,

$$O_i^1 = \mu_{Bi-2}(y); \quad i = 3,4 \tag{5-15}$$

The O_i^1 symbolizes the membership function of a given fuzzy set A (A_1, A_2, B_1 or B_2) that calculates the step where the input (x or y) correlates to the quantifier A. The membership functions (MFs) can also be obtained (for A and B) by a generalized bell function as follows [73]:

$$\mu_{Ai}(x) = \frac{1}{1+\left\|\frac{x-r_i}{p_i}\right\|^{2q_i}} \tag{5-16}$$

where p_i, q_i, and r_i represent the set parameters. The shape of functions depends on these set parameters. For the next layer (j=2), the inputs are multiplied using the nodes, and their product is represented as [73]:

$$O_i^2 = w_i \mu_{Ai}(x)\mu_{Bi}(y); \quad i = 1,2 \tag{5-17}$$

Each product node resembles the rules of firing strength. In the third layer, also known as the normalization layer, the ratio of firing strength of node i^{th} to the summation of all rules firing strengths is determined as follows [73]:

$$O_i^3 = \bar{w}_i = \frac{w_i}{w_1+w_2}, \quad i = 1,2 \tag{5-18}$$

In the fourth layer, the i^{th} node computes the portion of the i^{th} rule to the total output, defined by the following equation [73]:

$$O_i^4 = \bar{w}_i z_i = \bar{w}_i(a_i x + b_i y + c_i), \quad i = 1,2 \tag{5-19}$$

where $\bar{w}_i$ refers to the normalized firing strength (the output from the 3rd layer); a_i, b_i, and c_i denote the set parameters which are known as the consequent parameters.

In the fifth layer, the final output is calculated by the summation of all entering signals to a node as given below [73]:

$$O_i^5 = \sum_i \bar{w}_i z_i = \frac{\sum_i w_i z_i}{\sum_i wi} \tag{5-20}$$

5.4 WAG Injection Model Characteristics

The WAG injection process is a three-phase flow application in porous medium, in which both the wetting (water) and non-wetting (gas) phases are injected sequentially [74-75]. The numerical modelling of

WAG injection process is challenged by the complexities related to the three-phase flow and its cyclic injection nature.

5.4.1 Mathematical Model Development

In this research, we use a 1D core and apply implicit-pressure explicit-saturation (IMPES) method as the first principal model (FPM) for the WAG injection process. Details of the mathematical foundation for the three phase flow in porous medium are described in our previous work [76].

The three-phase relative permeability values are related to the saturation history as well as the saturation distribution. The saturation history of each phase causes relative permeability hysteresis; there are reported laboratory hysteresis results for from saturation history in two-phase and (to a less extent) in the three-phase tests [6, 77-78]. The majority of the reported three-phase relative permeability models that are available in the literature infer the three-phase results from the two-phase relative permeability data. Stone and Baker models are among the most commonly used relative permeability correlations that do not perform well in calculating the three phase relative permeability data [16]. The three-phase flow parameters (e.g., relative permeability and capillary pressure) should be obtained as a function of saturations of the various phases in the system [79-82]. In the current mathematical modeling study, three-phase relative permeability model by Shahverdi and Sohrabi is used [83]. This model accounts for the three-phase hysteresis effects in which the three-phase relative permeability values of phase *i* (k_{ri}^{3ph}) is defined as [83]:

$$k_{ro}^{3ph}(s_w, s_g) = \frac{\overline{s_o}}{(1-\overline{s_g})(1-\overline{s_w})}[k_{row}k_{rwg} + k_{rog}k_{rgw}] \tag{5-21}$$

$$k_{rw}^{3ph}(s_o, s_g) = \frac{\overline{s_w}}{(1-\overline{s_g})(1-\overline{s_o})}[k_{rwo}k_{rog} + k_{rwg}k_{rgo}] \tag{5-22}$$

$$k_{rg}^{3ph}(s_w, s_o) = \frac{\overline{s_g}}{(1-\overline{s_o})(1-\overline{s_w})}[k_{rgo}k_{row} + k_{rgw}k_{rwo}] \tag{5-23}$$

where *i* and *j* subscriptions are the three available phases (e.g., oil, water, or gas), and k_{rij} refers to the two-phase relative permeability of phase *i* in the presence of phase *j*. The s_i stands for the saturation of phase *i*. In the current study, the two-phase relative permeability values are calculated using correlation-based, LSSVM, and ANFIS models as described in the next sections.

The $\overline{s_i}$ is the normalized saturation for the phase *i*, that is affected by the initial saturation values and the injection cycle (i.e., gas injection, or water injection), as given below [83]:

$$\overline{s_g} = \frac{s_g - s_g^*}{1 - s_w^* - s_o^* - s_g^*} \tag{5-24}$$

$$\overline{s_o} = \frac{s_o - s_o^*}{1 - s_w^* - s_o^* - s_g^*} \tag{5-25}$$

$$\overline{s_w} = \frac{s_w - s_w^*}{1 - s_w^* - s_o^* - s_g^*} \tag{5-26}$$

In Eq. (5-24) to Eq.(5-26), the s_i^* values are defined for different phases.

Table 5-1 summarizes the three-phase relative permeability model parameters (see Eq. (5-21) to Eq. (5-26)) that are used in our simulation. In Table 5-1, s_α^{start} is the starting point saturation of phase α when injection cycle is started; and s_{gt} and s_{ot} denote the trapped/residual saturations of gas and oil, respectively.

Table 5-1: The parameters used in the three-phase relative permeability model in the porous medium [83].

Three-phase relative permeability	Model parameters	WAG injection cycle		
		Gas	Oil	Water
k_{rg}^{3ph}	s_g^*	s_g^{start}	s_{gt}	s_{gt}
	s_w^*	s_{wc}	s_{wc}	s_w^{start}
	s_o^*	0	s_o^{start}	s_{ot}
k_{ro}^{3ph}	s_g^*	0	s_{gt}	s_{gt}
	s_w^*	s_{wc}	s_{wc}	s_w^{start}
	s_o^*	s_{org}	s_o^{start}	s_{ot}
k_{rw}^{3ph}	s_g^*	0	0	0
	s_w^*	s_{wc}	s_{wc}	s_{wc}
	s_o^*	0	0	0

In this work, the three-phase flow in a 5 cm diameter core plug in the context of the WAG injection process is simulated. In the modeling phase, the assumption of 1D flow is rationale because the effect of gravity is not expected to be significant due to the small diameter of the core sample. The two-phase permeability values are obtained through smart tools (ANFIS and LSSVM) or EMs. During each injection cycle, the parameters of the two-phase relative permeability model should be tuned, when using EMs. The two-phase relative permeability data calculated using the optimized EMs will then be embedded in the three-phase relative permeability model to calculate the three-phase relative permeability of each phase.

Figure 5-3 depicts a schematic of the flowchart applied in this study.

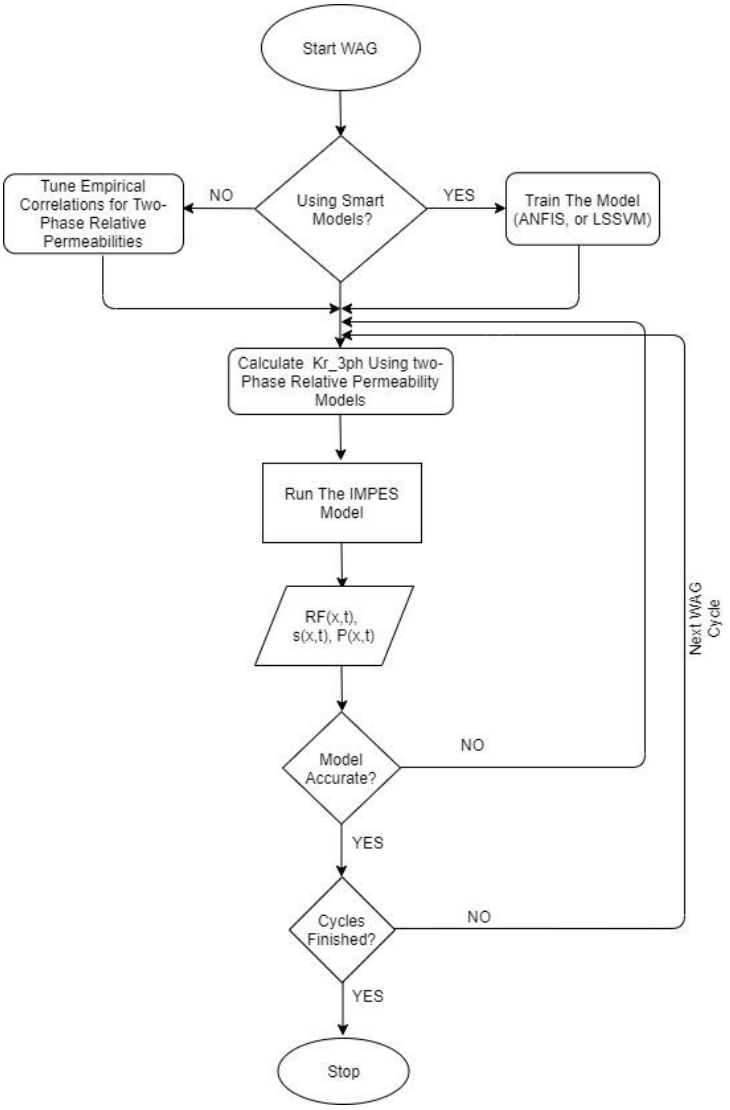

Figure 5-3: WAG injection modeling flowchart applied in current study.

5.4.2 Empirical Models (EMs)

EMs are important tools to calculate relative permeability values for a given wetting condition. The EMs are only applicable within the range of experimental conditions based on which they have been developed; therefore, generalization beyond the experimental conditions is risky. This lack of generalization capability can be a major source of error in predicting the relative permeability data for the desire processes. However, availability of these correlations, in addition to their capability of being easily tuned for various processes and conditions, have made them practical tools to predict relative permeability values. In this research, two EMs are employed to calculate the two-phase relative permeabilities in order to be embedded later in the three-phase relative permeability model proposed by Shahverdi et al. [16]. The three-phase relative permeability data calculated from Shahverdi et al. [16] model

are then used in a FPM for a three-cycle WAG injection process. Among the numerous suggested EMs in the literature, two of the most known models are Mualem's model (Eqs. (5-27)-(5-29)), which is a modified version of Van Genuchten model, and Hirasaki's model (Eqs. (30)-(32)) [84-85].

$$k_{rw}(s_w) = \overline{s_w}^{0.5}\left(1-\left(1-\overline{s_w}^{\frac{1}{m}}\right)^{m}\right)^{2} \tag{5-27}$$

$$k_{rn}(s_n) = \overline{s_n}^{\frac{1}{3}}\left(1-\left(1-\overline{s_n}^{\frac{1}{m}}\right)\right)^{2m} \tag{5-28}$$

$$\overline{s_\alpha} = \frac{s_\alpha - s_{\alpha r}}{1-\sum_\alpha s_{\alpha r}} \tag{5-29}$$

where the subscription *w* denotes the wetting phase; *n* refers to the non-wetting phase; $s_{\alpha r}$ symbolizes the residual saturation of the phase α; k_{rn} and k_{rw} denotes the two-phase relative permeability of the non-wet and wetting phase, respectively; and *m* is the model parameter which is obtained through optimization.

$$k_{rw} = k_{rw}^0 {S_D}^{n_w} \tag{5-30}$$

$$k_{rn} = k_{rnw}^0 (1-S_D)^{n_n} \tag{5-31}$$

$$S_D = \frac{S_w - S_{wi}}{1-S_{wi}-S_{nr}} \tag{5-32}$$

Where k_{rw} and k_{rn} denote the two-phase relative permeability values for the wetting phase and non-wetting phase, respectively; k_{rw}^0 and k_{rn}^0 are the end-point relative permeability values for the wetting phase and non-wetting phase, respectively; s_w is the saturation of the wetting phase; s_{wi} and s_{nr} refer to the initial wetting saturation and residual saturation of the non-wetting phases, respectively; and n_w and n_n refer to the model parameters for the wetting and non-wetting phases, respectively, which are obtained by fitting the model to the experimental data.

5.5 Modelling of WAG Injection Process Using LSSVM and ANFIS Algorithms

5.5.1 Data Acquisition, Quality check, and Analysis

In machine learning applications, the capability of the model in terms of robustness, accuracy, and universality highly depends on the quality of the input data [86-88]. A review of the previous studies shows that relative permeabilities are related to rock properties (permeability and porosity), fluid properties (saturation, or viscosity), and operating conditions (pressure and temperature) [89-92]. In the current study, we use different datasets for three systems of oil-water, oil-gas, and gas-water in order to predict the two-phase relative permeability values for each phase. A total number of 2,116 raw datapoints are borrowed from the literature. After performing an initial raw data quality check and analysis, several datasets (10 datasets from the oil-gas system, 3 datasets from the oil-water system, and 8 datasets from

the gas-water system) are discarded due to inconsistencies. Indeed, the modeling is conducted with a total number of 1,457 data points. The details of the database utilized in each system are described in Table 5-2. All the collected data belong to strongly water-wet sandstone rocks to match the wettability conditions of the proposed case study.

Table 5-2: The details of database utilized in each system.

Input	Gas-Oil (510 data points)		Oil-Water (626 data points)		Gas-Water (321 data points)	
	Variable	Range	Variable	Range	Variable	Range
1	S_{wc}	0.03–0.50	S_w	0.052–1	P(kPa)	0.3–24233
2	S_{org}	0.05–0.48	T(˚C)	21.1–200	K (mD)	0.004–3515
3	S_{gc}	0.006–0.25	μ_o (cP)	0.419–1190	ϕ	0.0416–0.37
4	k (mD)	1.48–3650	μ_w (cP)	0.136–1.1	T (˚C)	25–120
5	ϕ	0.063–0.39	K (mD)	152–95000	S_w	0.1–1
6	S_g	0–0.95				

ANFIS Training phase. In the ANFIS algorithm, the input and output data are first normalized in the range of -1 to +1 to make the predictions computationally efficient and enhance their accuracy. In this study, we use Takagi-Sugeno fuzzy model for the ANFIS algorithm. The optimization parameters for the relative permeability prediction by ANFIS model are listed in Table 5-3 for all three systems.

Table 5-3: Optimization parameters used in the ANFIS model for oil-water, oil-gas, and water-gas systems.

ANFIS parameter	System		
	Oil-Water	Oil-Gas	Gas-Water
Fuzzy structure	Takagi-Sugeno	Takagi-Sugeno	Takagi-Sugeno
Initial FIS for training	genfis2	genfis2	genfis2
Membership function type	Gaussian	Gaussian	Gaussian
Output membership function	Linear	Linear	Linear
Cluster center's influence range	0.7	0.5	0.4
Number of inputs	5	6	5
Number of outputs	1	1	1
Training maximum epoch number	200	200	200
Initial step size	0.1	0.1	0.1
Step size decrease rate	0.9	0.9	0.9
Step size increase rate	1.1	1.1	1.1

LSSVM Training phase. The LSSVM model contains two adjustable parameters (σ^2, and γ) which are optimized during the prediction process. In the current study, we use coupled simulated annealing (CSA) optimization method. The optimization search algorithm is repeated to converge to the global-optima. By having the optimum values of σ and γ, the unknown vector (α) and the bias term (b) are computed for relative permeabilities in all three-systems (two-phase relative permeability).

5.5.2 Advantages and Limitations of the Models

Overall, the AI modelling tools are classified into three main categories: the black-box (data-driven) models which include all the connectionist tools; the white-box (first principal) models; and the grey-box (hybrid) models combined with either white-box or black-box models [93]. The black-box models provide a higher computational speed and efficiency compared to other models while requiring minimum knowledge of the targeted phenomena. The black-box models (such as LSSVM and ANFIS), however, are heavily dependent on the data. One of the main limitations of the black-box models is their low capability in extrapolating data [94]. On the other hand, the white-box models are highly dependent on the physics and the type of the phenomena being modeled; they are able to provide a deep understanding of the processes/phenomena since they can be developed before starting the modelling procedure. The accuracy of a model is limited by its assumptions. The major advantages and limitations of the applied models, in the current study, are listed in Table 5-4.

Table 5-4**:** Limitations and advantages of the smart tools used in this study.

Model	Advantages	Disadvantages
LSSVM	• High accuracy and generalization capabilities • No over-fitting or under-fitting problem [95] • Applicability in systems with limited data points [96]. • No local minima; leads to a global optimum. • Less complexity in the model structure compared to ANN [97] • No need for prior knowledge of the network topology. • Contains only two adjustable parameters (σ^2 and γ). • High computational speed and high efficiency [98].	• Lack of the sparsity limits the method for large scale processes [99]. • Employing the sum square error without regularization results in less accuracy in data prediction.
ANFIS	• Capturing the non-linear structure of a process • High adaption capability • Rapid learning capacity • Handling both numerical and linguistic knowledge. • Employing the ANN ability to classify data and identifying parameters. • Applicable in data involving crisp input and crisp output [43].	• High computational cost due to the complex structure and gradient learning which is more significant while dealing with large inputs. • Implies a trade-off between interpretability and accuracy. • Limited number and type of membership function [43].

5.6 Results and Discussions

In three-phase flow systems of oil-water, oil-gas, and gas-water, we first predict the two-phase relative permeability values and use them in the three-phase relative permeability model. In this section, we first present the criteria applied to evaluate the prediction performance of different proposed methods. Second, the models are optimized, and the trained models are hybridized with the FPM to estimate the ultimate recovery factor as an important measure of the WAG recovery performance. The reliability and precision of the predictions are then assessed through comparison with the experimental data, for both the ultimate recovery factor and the three-phase relative permeability values.

The reliability and robustness of the predictions derived from the developed models are examined using various statistical quality and error analysis measures such as coefficient of determination (R^2), mean error (ME), standard deviation (std), and root mean square error (RMSE). These statistical parameters are defined for a dataset of *N* samples, each expressed as (x_1, x_2,… , x_k, y) where k is the number of input features; x_j is the independent input j variable; and y denotes the target value according to the following equations:

$$R^2 = 1 - \frac{\sum_{i=1}^{N}(y_i-(y_p)_i)^2}{\sum_{i=1}^{N}((y_p)_i-\bar{y_i})^2} \quad (5\text{-}33)$$

$$Error = y_i - (y_p)_i \quad (5\text{-}34)$$

$$ME = \frac{\sum_{i=1}^{N}(Error_i)}{N} \quad (5\text{-}35)$$

$$std=\sqrt{\frac{\sum_{i=1}^{N}(Error-ME)^2}{N-1}} \quad (5\text{-}36)$$

$$RMSE = \sqrt{\frac{\sum_{i=1}^{N}(y_i-(y_p)_i)^2}{N}} \quad (5\text{-}37)$$

where y_i is the output variable for the i^{th} sample data, and $(y_p)_i$ represents the corresponding output value predicted by the model. The R^2 parameter measures how much of the variations in the data is explained by the correlation; a good fit is represented by an R^2 value close to 1. The *std* is a measure of the amount of variation or dispersion of the data. The *RMSE* and *ME* measure the prediction accuracy, and the error values close to zero are desired.

5.6.1 Evaluation of the Two-Phase Relative Permeability Prediction Models

To predict the two-phase relative permeability values for a system, the independent input variables (described in Table 5-2) are embedded into the developed models (hybrid LSSVM-CSA and ANFIS). We use the CSA optimization technique to optimize the LSSVM model parameters (σ and γ) as listed

in Table 5-5. The RBF is also applied in the LSSVM algorithm as the kernel function with the optimized σ and γ values. The statistical quality measures for the two-phase relative permeability predictions are presented in Table 5-6.

Table 5-5**:** Values of the optimized γ and σ parameters for the two-phase relative permeability predictions made using the LSSVM-CSA algorithm.

Relative permeability	Parameter	
	σ	γ
k_{row}	1.37990	35885.0
k_{rwo}	0.48102	703.0
k_{rog}	4.81019	2.05
k_{rgo}	0.09347	1.6987
k_{rwg}	0.65554	30.7757812
k_{rgw}	2.3409	64.79675

Table 5-6**:** The statistical quality measurements for the ANFIS and LSSVM-CSA models.

System	Statistical parameter	ANFIS						LSSVM-CSA					
		$(k_r)_{non\text{-}wet}$			$(k_r)_{wet}$			$(k_r)_{non\text{-}wet}$			$(k_r)_{wet}$		
		Training	Test	Validate	Training	Test	Validate	Training	Test	Validate	Training	Test	Validate
Oil-Water	Standard error	0.0735	0.06726	0.03270	0.01867	0.24867	0.14028	0.01846	0.04732	0.03709	0.00507	0.01826	0.01679
	Mean error	1.19e-08	4.81e-04	5.96e-03	-2.31e-07	4.81e-03	1.72e-02	-1.01e-13	-6.20e-3	-1.04e-2	2.12e-16	-4.71e-4	-5.68e-3
	RMSE	0.0150	0.0415	0.0177	0.0391	0.0943	0.0873	0.0184	0.0475	0.0382	0.0051	0.0188	0.0176
	R^2	0.9838	0.9820	0.9954	0.9827	0.9684	0.9763	0.9997	0.9987	0.9987	0.9995	0.9968	0.9939
Gas-Water	Standard error	0.09883	0.07584	0.05963	0.03112	0.07612	0.27639	0.01284	0.02660	0.02710	0.01888	0.04880	0.07047
	Mean error	-1.16e-06	1.43e-03	-6.62e-02	-2.23e-08	-1.33e-03	-1.62e-03	-9.60e-09	7.36e-4	-2.48e-4	2.47e-08	1.42e-4	1.56e-3
	RMSE	0.02457	0.02580	0.01542	0.04002	0.01849	0.21482	0.01279	0.02729	0.02646	0.01880	0.04770	0.0706063
	R^2	0.9151	0.9541	0.9946	0.9874	0.9940	0.9758	0.9898	0.9727	0.9917	0.9898	0.9892	0.9936
Gas-Oil	Standard error	0.02560	0.06592	0.01131	0.01717	0.08530	0.08269	0.006267	0.01891	0.00625	0.01650	0.08250	0.07958
	Mean error	-5.75e-08	7.70e-3	3.10e-2	7.04e-08	2.00e-03	-9.21e-02	-9.42e-14	8.35e-3	-1.92e-3	9.23e-18	2.89e-3	-8.83e-3
	RMSE	0.04220	0.03176	0.02574	0.07311	0.06051	0.08999	0.06258	0.04935	0.06182	0.01650	0.08210	0.07910
	R^2	0.9650	0.9781	0.9963	0.9606	0.9841	0.9928	0.9966	0.9953	0.9939	0.9847	0.9893	0.9958

The values of R^2 for both the developed models are close to 1 for all the two-phase fluid flow systems, demonstrating an excellent fit of the predicted values to the experimental data. The higher R^2 values associated with the LSSVM-CSA model predictions for all the fluid flow systems suggest the superiority of this model over the ANFIS model. The regression plots for the two-phase flow systems are presented in Figure 5-4 to Figure 5-6. According to these plots and the statistical analysis measures presented in Table 5-6, both models are well trained; the LSSVM-CSA model is more accurate in predicting the target values of the experimental data in the training phase, which results in smaller mean error values.

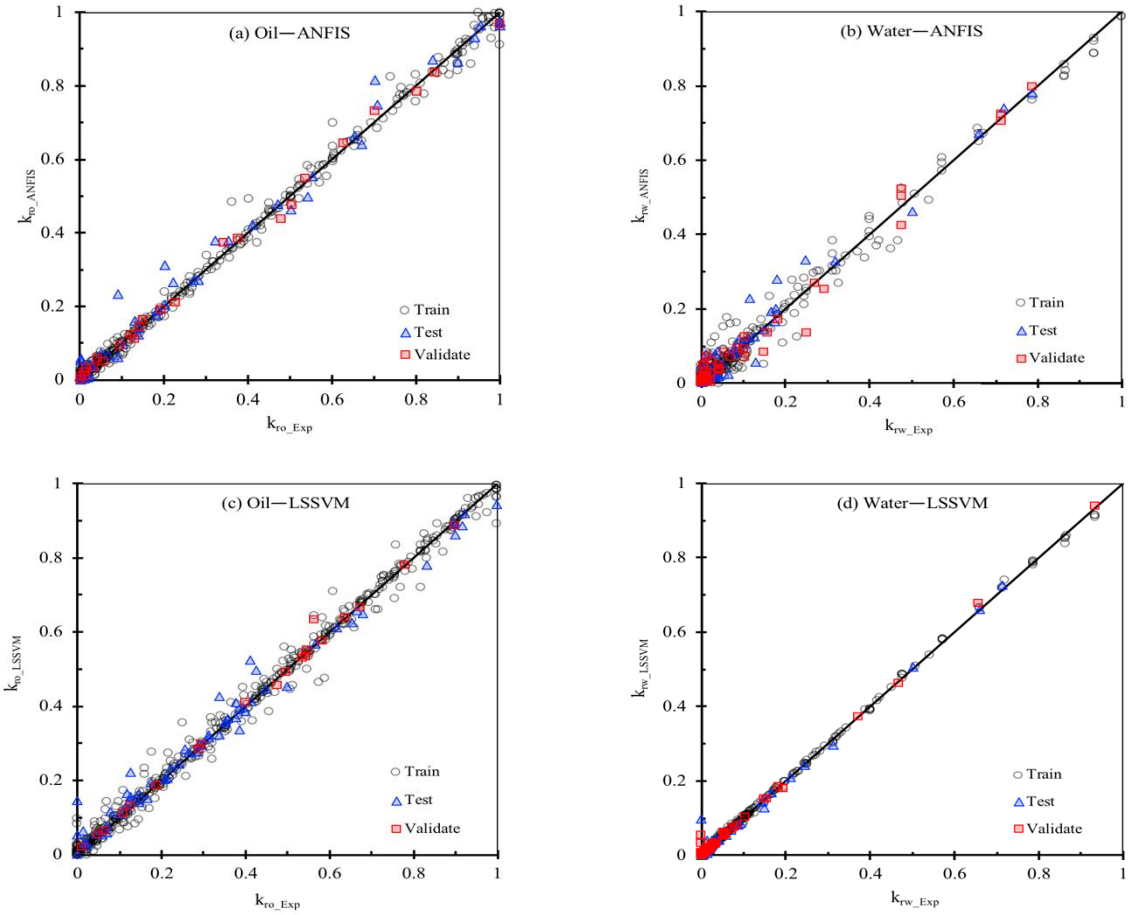

Figure 5-4: Regression plots for the oil-water flow system, displaying predicted versus measured (a) oil relative permeability using ANFIS model, (b) water relative permeability using ANFIS model, (c) oil relative permeability using LSSVM-CSA model, and (d) water relative permeability using LSSVM-CSA model.

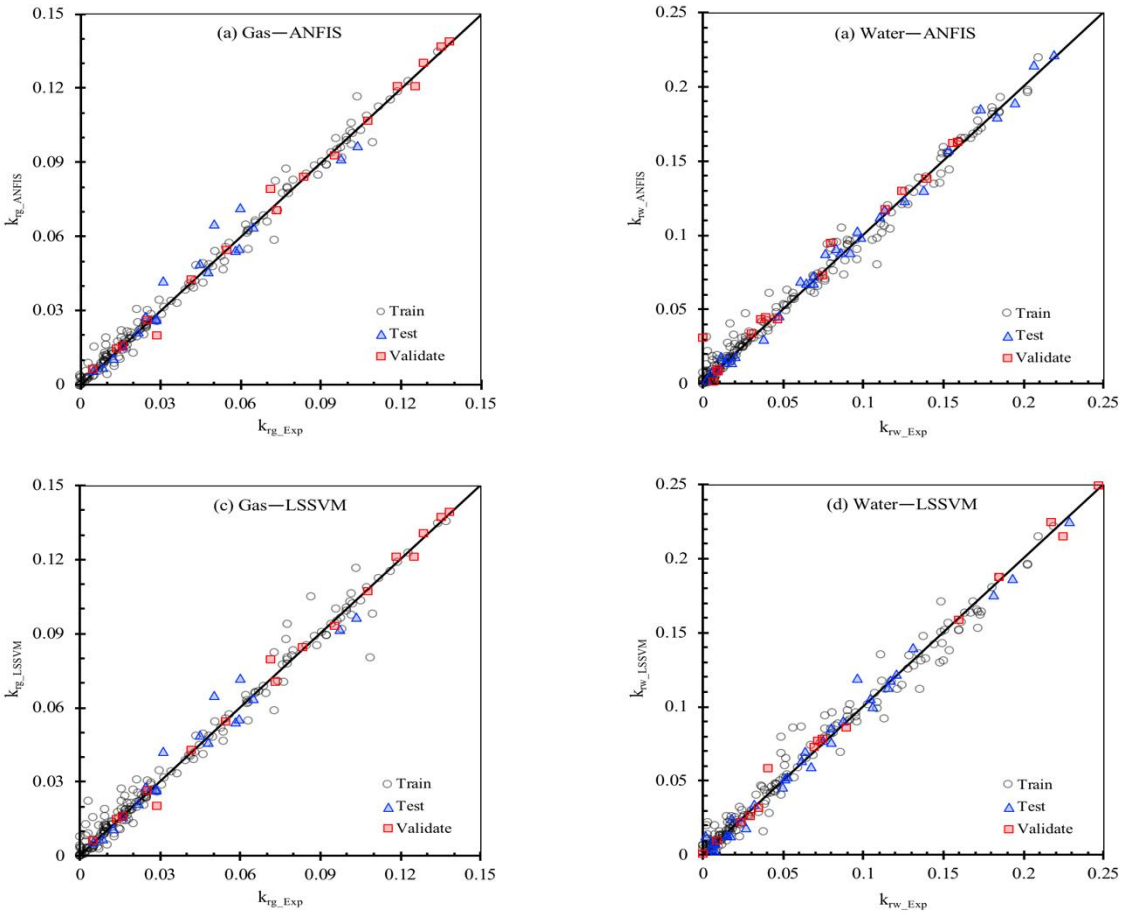

Figure 5-5: Regression plots for the gas-water flow system, displaying predicted versus measured (a) gas relative permeability using ANFIS model, (b) water relative permeability using ANFIS model, (c) gas relative permeability using LSSVM-CSA model, and (d) water relative permeability using LSSVM-CSA model.

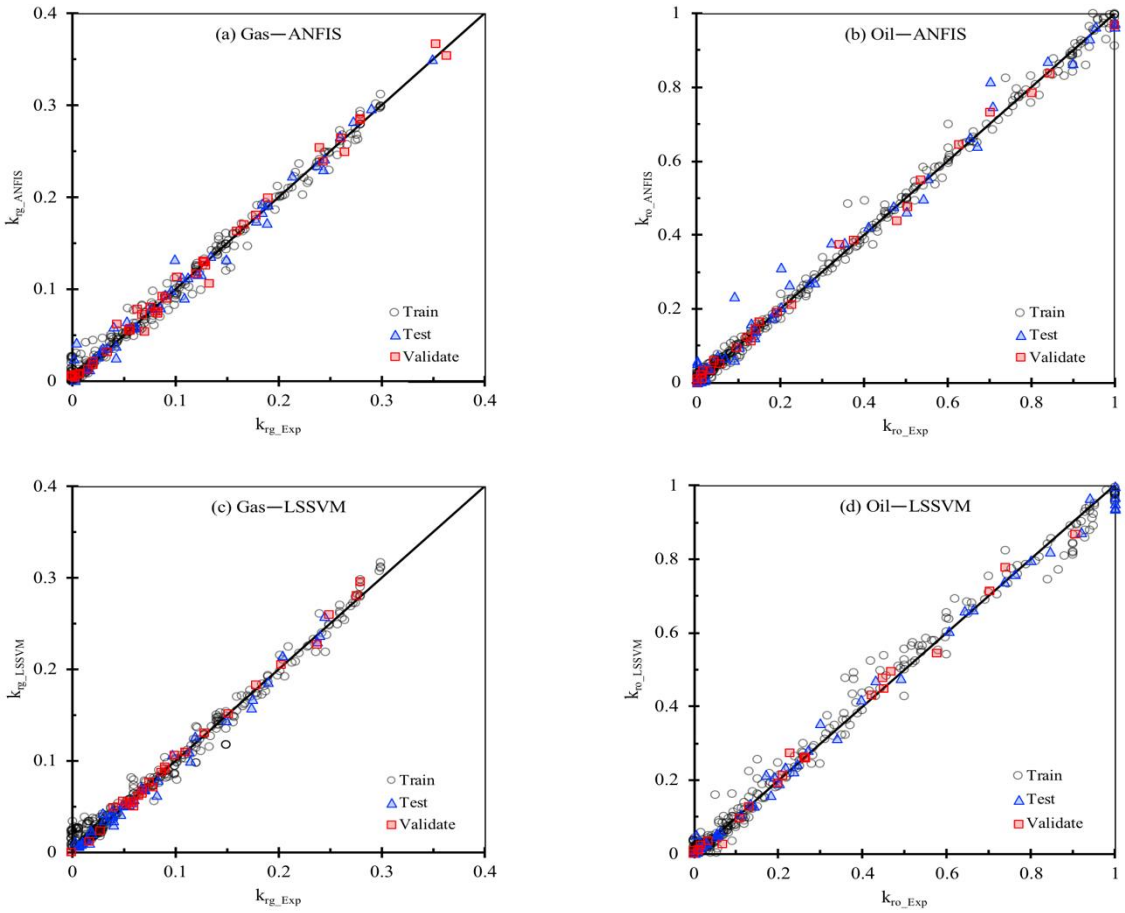

Figure 5-6: Regression plots for the gas-oil flow system, displaying predicted versus measured (a): gas relative permeability using ANFIS model, (b) oil relative permeability using ANFIS model, (c) gas relative permeability using LSSVM-CSA model, and (d) oil relative permeability using LSSVM-CSA model.

5.6.2 Evaluation of the Models in Predicting WAG Injection Ultimate Recovery Factor

To evaluate the performance of the developed black-box models (i.e. LSSVM-CSA and ANFIS) as well as that of the correlation-based EM (EM-FPM) model, the calculated values of the two-phase relative permeability are compared with the experimental data of a WAG injection process, containing three consecutive cycles in which water and gas are injected. In the selected experiment, the WAG injection process was conducted in a strongly water-wet porous medium, starting with a primary waterflooding stage (WI1) where no initial gas was present (i.e. s_{gi}=0). The process was then continued with the first gas injection stage (GI1). The consecutive water and gas injection processes were continued three times. The process was terminated after the third gas injection stage (GI3) during which no significant oil production occurred. The WAG injection process was

performed at a WAG ratio of 1:1, i.e. the water and gas injection flow rates were equal and set at q=25 cm^3/hr.

The plot of recovery factor versus the dimensionless time based on the predictions and experimental data is presented in Figure 5-7. The data associated with this plot are provided in Table 5-7.

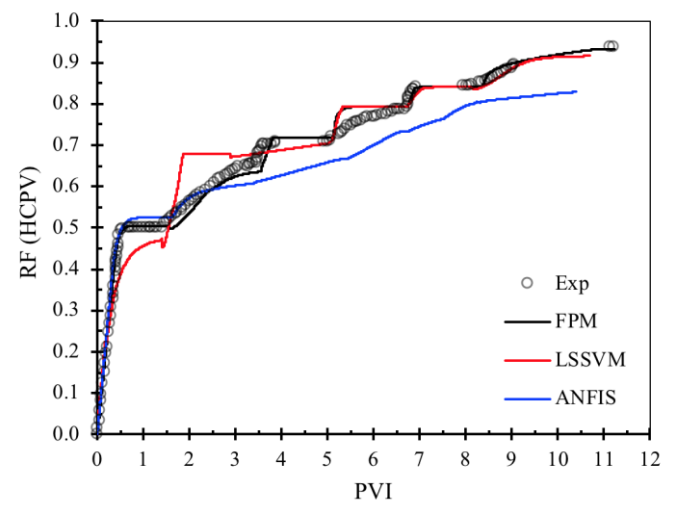

Figure 5-7: Comparison between the predicted versus measured *RF* values (q=25 cm^3/hr, WAG ratio=1).

Table 5-7**:** The predicted and experimentally measured RF values for the WAG injection process in a water-wet medium. Experimental data are from Fatemi et al. [100].

Cycle	Process	RF_{End} (HCPV)				Relative error in RF_{End}			Max relative error			Processing Time (s)	
		Exp	Model	LSSVM	ANFIS	Model	LSSVM	ANFIS	Model	LSSVM	ANFIS	LSSVM	ANFIS
1	WF1	0.4997	0.5008	0.4750	0.5294	-0.0022	0.04943	-0.0594	0.01575	0.12625	-0.05203	60	300
	GI1	0.6559	0.6464	0.6783	0.6098	0.01448	-0.0342	0.0703	0.0509	-0.2082	0.07121		
2	WF2	0.7201	0.7194	0.7017	0.6588	0.00097	0.02555	0.0851	-0.0172	-0.0302	0.11533	75	480
	GI2	0.7912	0.7937	0.7927	0.7318	-0.0032	-0.0019	0.0751	0.01369	-0.0635	0.10658		
3	WF3	0.8509	0.8430	0.8414	0.8047	0.00929	0.01117	0.0543	0.01019	2.46E-05	0.1151	75	480
	GI3	0.9358	0.9200	0.9157	0.8288	0.01688	0.02148	0.11434	0.01160	0.01457	0.0894		

By the end of the primary waterflooding stage (WI1), 50% of the initial oil in place is recovered based on the experimental data. The numerical simulation model, developed based on two-phase relative permeability correlation, is able to predict a RF of 50.08% at the end of the WI1 stage, implying the excellent accuracy of the numerical simulation model. The ANFIS model, however, has a less accuracy compared to the numerical simulation model, and results in a RF value of 53.94% at the end of the WI1 stage with a breakthrough time of PVI=0.566. The LSSVM-CSA model, on the other hand, underestimates the RF at the end of WI1 stage (i.e. 47.50%) as well as the breakthrough time (i.e. PVI=0.406).

When the first gas injection stage starts, the models need to account for the presence of three phases that are simultaneously flowing in the porous medium, using the three-phase capillary pressure and relative permeability models. At the end of the first cycle (i.e. end of the GI1 stage), the correlation-based numerical simulation model predicts a RF of 64.64%, which is in an excellent agreement with the experimental RF value of 65.59%. The LSSVM-CSA and ANFIS models predict the RF values at the end of the first injection cycle at 67.83% and 60.98%, respectively. Two additional injection cycles are then implemented, and the measured as well as predicted RF values at the end of each cycle, along with the statistical quality measures of relative error and maximum relative error, with respect to the experimental data, are all listed in Table 5-7. The maximum relative error specifies the highest relative error of all the instantaneous *RF* values during each cycle. The relative error, however, shows the relative error involved in estimating the ultimate recovery factor values (RF_{End}) using each model during each injection process (GI or WI). The WAG injection process is continued for a total dimensionless time of 11.24 *PVI*. Considering the accuracy measures and predicted values of the RF at each cycle of the WAG injection (Table 5-7 and Figure 5-7), the ANFIS model is found to be the less successful method in predicting the correct trend and values of the experimental data; this results in significant error values. The greatest relative error in predicted ultimate RF, i.e. 11.43%, is associated with this model. Also, the greatest maximum error of 11.53% occurs for instantaneous *RF* at the end of all cycles. The LSSVM-CSA model shows a better performance in terms of predicting the instantaneous *RF*s at the end of each cycle, as well as the ultimate *RF* at the end of the third cycle. This results in a predicted ultimate RF of 91.57%, compared to the corresponding experimental ultimate *RF* value of 93.58%. The LSSVM-CSA model also outperforms the ANFIS model in terms of computational cost and simulation speed (Table 5-7).

The saturation distribution of available phases and the chronological history of phase displacement control the values of three-phase relative permeability and capillary pressure. Therefore, the model performance is greatly influenced by reliability of the capillary pressure and relative permeability models. In the next section, we provide a comparison between the performance of the proposed models to predict the values of the three-phase relative permeability in WAG injection process; we also provide the relative importance analysis for different input parameters.

5.6.3 Relative Importance (RI) of Input Parameters

To evaluate the impact of each input parameter on the output of a predictive model, the Pearson's correlation (PC) coefficient is used as a measure of the strength of the association between two continuous variables. This coefficient measures the linear correlation between the two variables; it gives information about the magnitude of the association, or correlation, as well as the direction of the relationship between two continuous variables. The PC coefficient is based on the ratio of the covariance of two desired variables to the product of their respective standard deviations [101-102].

The second coefficient to evaluate the RI of the input parameters is Spearman's correlation (SC) coefficient, which is regarded as the ranked-based version of the PC coefficient. The SC coefficient is a non-parametric measure of the rank correlation, which assesses how well the relationship between the two continuous variables can be defined using a monotonic function [101, 103]. Similar to the PC coefficient, the SC coefficient varies between -1 and +1 and the absolute value of the SC coefficient indicates the strength of the monotonic relationship between the two variables [101]. The closer the absolute value of the SC coefficient to 0, the weaker the monotonic relationship between the two variables. Similar to the PC coefficient, the SC coefficient can be 0 for variables with non-monotonic manner, but unlike the PC coefficient, the SC coefficient can be 1 for both linearly related variables and non-linear variables.

The last rank-order parameter is Kendal's Correlation (KC) coefficient that captures the association between two ordinal (not necessarily interval) variables. The KC coefficient describes the discrepancy between the number of concordant and discordant pairs [101, 103]. The KC coefficient is a measure of the rank correlation; in other words, the similarity of the orderings of the data when ranked by each of the quantities. The Kendall correlation between two variables is high when observations have a similar rank between the two variables. An example could be the KC

coefficient of 1 for an identical rank between the two variables. However, when the observations have a dissimilar rank between the two variables, the KC coefficient has a low magnitude. For instance, it holds the value of -1 when the observations have a fully different rank between the variables. This coefficient can be 1 for a wider range of scenarios, compared to the PC coefficient. In general, the Relative Importance (RI) can be obtained considering the magnitude of the mentioned coefficients in the [-1, +1] interval. A positive RI value (RI > 0) indicates a positive monotonic association whereas a negative RI value (RI < 0) denotes a negative monotonic association between the variables. In the case of no association between the variables, the RI becomes zero.

Figure 5-8 shows the impact of each input parameter on the values of the two-phase k_{rw}, k_{ro}, and k_{rg} in gas-water, oil-water, and oil-gas systems, respectively. Since the trend of coefficients for both LSSVM-CSA and ANFIS models are the same, only the data generated by LSSVM-CSA are used in this section. In a two-phase system, the RI values for k_{rwg} and k_{rgw} are the same except for the saturation as the input variable. The trio of all three coefficients i.e. Pearson, Spearman, and Kendal show the same behaviors for all input variables in the three systems. Input parameters with a larger RI values have a greater impact on the output value. In all systems, the saturation imposes the largest impact on the output two-phase relative permeability prediction which is logically sensible. In the gas-water system shown in Figure 5-8(a), the pressure and temperature have the largest and lowest impacts on the output prediction, respectively. Therefore, changes in pressure results in a comparatively greater change in the relative permeability values. All coefficients are positive for this system, indicating that by increasing each input parameter, the output variable increases. Figure 5-8(b) depicts the RI value for individual input parameters in the oil-water system to predict oil relative permeability. According to panel (b) of Figure 5-8, the water saturation has the largest effect on the output variable. Also, all coefficients are negative, meaning that by increasing the water saturation, the oil relative permeability decreases. The water viscosity exhibits the lowest effect on the oil relative permeability, and increasing oil viscosity and rock permeability negatively affect the oil relative permeability (an increase in these parameters leads to a reduction in the oil relative permeability). In Figure 5-8 (c), the gas saturation is the most influential input parameter in the oil-gas system, while the gas critical saturation is the second important parameter negatively affecting the predicted gas relative permeabilities. In all three cases, the coefficients showed the same trend with a slight difference for each input parameter. However, in different

system the sensitivity of coefficients might be different for different input variables. For instance, in the panel "c", for all input parameters, the Spearman coefficient shows more *RI* variations compared to the Kendal and Pearson coefficients. However, the Pearson coefficient in the same panel exhibits less sensitivity of *RI* to the variables, and results in almost the same values for critical gas saturation, permeability, and porosity of the system.

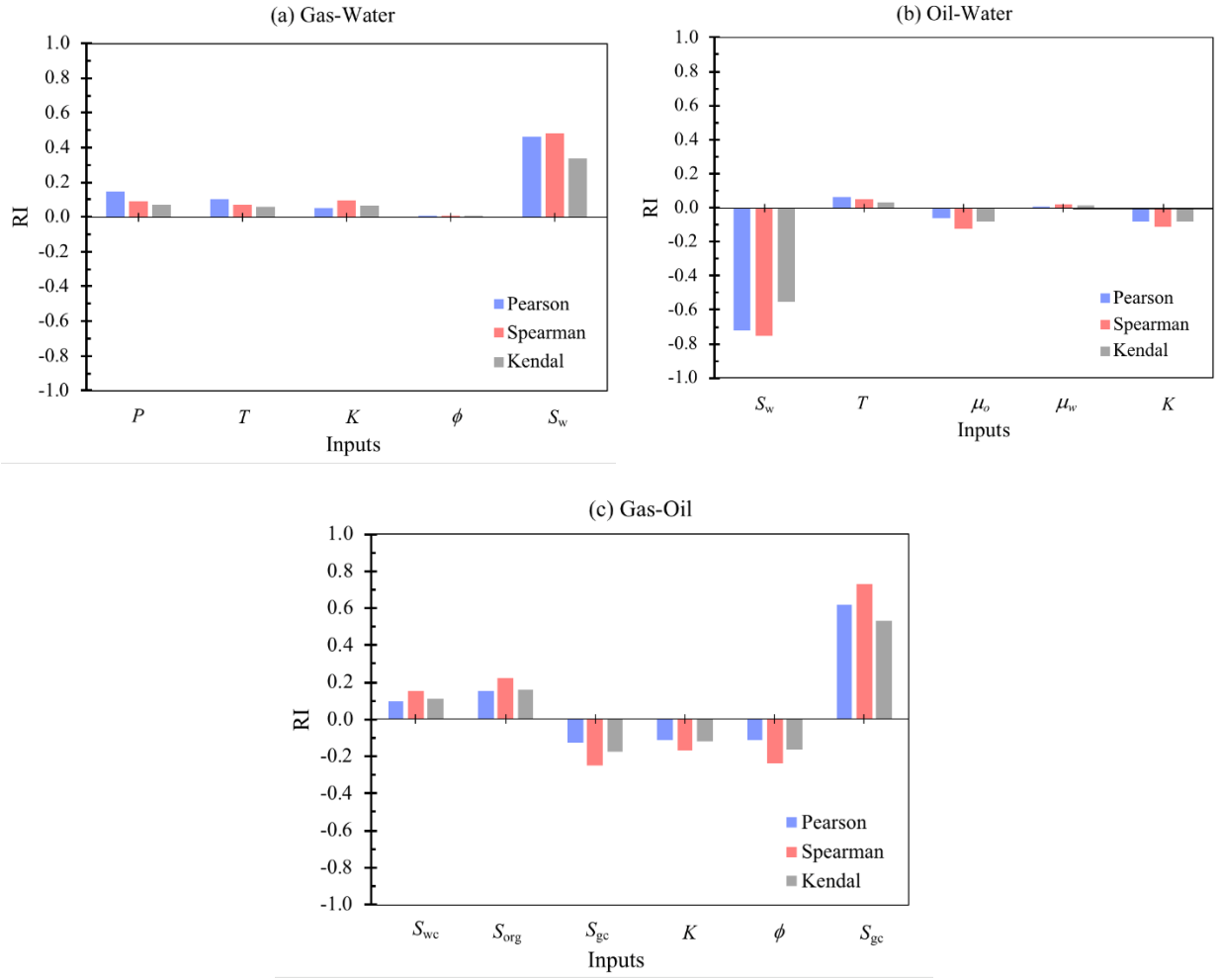

Figure 5-8: Calculated relative importance of each input parameter in the (a) gas-water, (b) oil-water, and (c) gas-oil flow system to predict water relative permeability using LSSVM-CSA model.

5.6.4 Three-Phase Relative Permeability Comparison

The accurate estimation of the three-phase relative permeability values, which is one of the main objectives of this study, is crucial for reliably evaluating the performance of the WAG injection process. In this section, the oil, water, and gas relative permeabilities, obtained using all the proposed smart models as well as the numerical simulation model, for all the gas and water injection cycles associated with the WAG injection case study are presented. For this purpose,

first, the two-phase relative permeability values are calculated using EM's as well as ANFIS and LSSVM-CSA algorithms over the same range of saturations experienced in the experimental work. Then, the three-phase relative permeability values are determined using the model developed by Shahverdi et al. [16] (Eq. (5-1) – (5-3)) by incorporating the two-phase relative permeability data. In all the plots, the experimental three-phase relative permeability values are also presented for comparison purposes.

Three-phase relative permeability data in GI cycles. In Figure 5-9, the three-phase gas relative permeability (K_{rg}^{3ph}) values obtained using the proposed models for the first, second, and third gas injection cycles of the WAG injection case study are plotted, along with the experimental data. It is clear that as the injection process proceeds, the K_{rg}^{3ph} value significantly decreases at corresponding gas saturation values. This can be attributed to the dependency of the K_{rg}^{3ph} on the saturation history in a water-wet medium. Even though the same drainage displacement process takes place during GI1, GI2 and GI3 stages, the successively decreasing K_{rg}^{3ph} values at similar gas saturation levels reveals the importance of periodic displacement transition from imbibition to drainage on magnitude of the non-wetting phase relative permeability. Of particular importance, among all other reasons, could be the blockage of the free gas phase by invading water phase during the prior imbibition stage(s). This apparently irreversible gas trapping restricts the flow of free gas in the next gas injection cycle, which results in K_{rg}^{3ph} reduction.

As for the reliability of the K_{rg}^{3ph} predictions, the ANFIS model is clearly the least reliable predictive tool, whereas the correlation-based EM results in the best fit to the experimental data. The discrepancy between the predicted and measured K_{rg}^{3ph} data is more pronounced at lower gas saturation values. As the initial gas saturation in the porous medium increases from GI1 to GI3 stage, the accuracy of the models predictions with respect to the measured values increases.

A comparison between the predicted versus measured three-phase water relative permeability (K_{rw}^{3ph}) values during the gas injection cycles is presented in Figure 5-9. The changes in the K_{rw}^{3ph} values between the GI1 and GI2 stages over the same range of water saturations are minimal, showing that the saturation history does not play an important role. However, the K_{rw}^{3ph} values in GI3 decrease by about 30% compared to the corresponding values in the previous two gas injection stages. At smaller water saturation values, all the predictive models overestimate the K_{rw}^{3ph} values

when compared to the experimental data. However, at greater water saturation values, the deviation of the predictions from the measured values becomes negligible. The best K_{rw}^{3ph} predictions are obtained using the correlation-based EM over the entire range of water saturations while the estimations with the lowest accuracy belong to the ANFIS model, especially at lower ranges of water saturation.

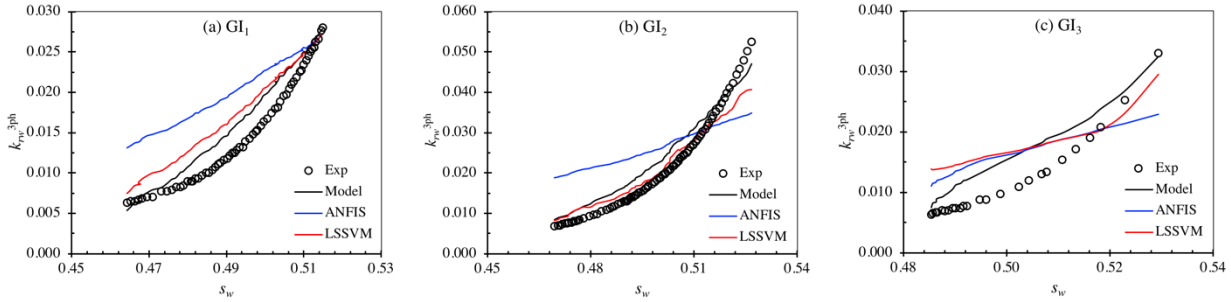

Figure 5-9: Comparison of the K_{rw}^{3ph} values in the (a) first, (b) second, and (c) third GI cycles using correlation-based EM as well as ANFIS, and LSSVM-CSA algorithms.

In the GI cycles, the three-phase oil relative permeability (K_{ro}^{3ph}) values predicted by the proposed models are also compared with the experimental data (see Figure 5-10). The oil phase is mobilized at less oil saturation levels through consecutive GI cycles, which is due to the decrease in oil saturation in porous medium while conducting further WAG injection cycles. The effect of saturation history on K_{ro}^{3ph} values is also evident in Figure 5-10, and the transition between the imbibition and drainage processes in each cycle remarkably improves the K_{ro}^{3ph} values and successively decreases the residual oil saturation through consecutive injection cycles. Similar to the case of K_{rw}^{3ph} and K_{rg}^{3ph}, the K_{ro}^{3ph} experimental data are best fitted with the correlation-based EM. However, the ANFIS and LSSVM-CSA models have similar predictive performance while obtaining K_{ro}^{3ph} data. All the proposed ANN models underestimate the K_{ro}^{3ph} values at lower oil saturations, especially when approaching the residual oil saturation conditions. This might be due to the wettability alteration of the rock towards the less water-wet state during the gas injection cycles at the experimental temperature and pressure. The used models do not account for the changes in the rock and fluid properties, which results in smaller K_{ro}^{3ph} values during the gas injection stages.

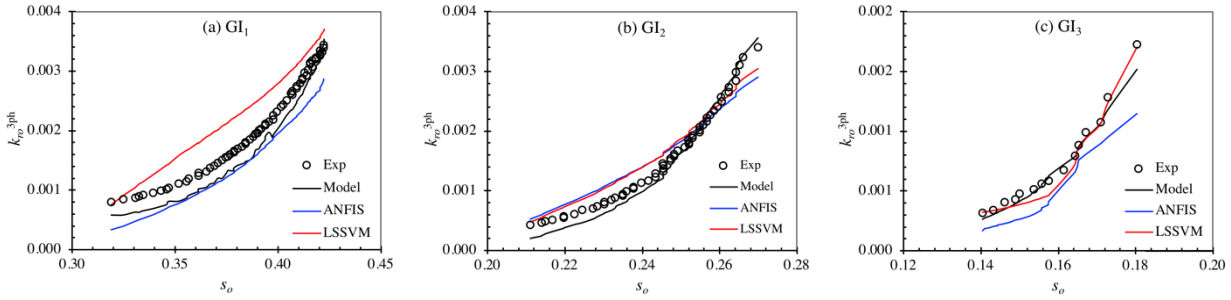

Figure 5-10: Comparison of the K_{ro}^{3ph} values in the (a) first, (b) second, and (c) third GI cycles using correlation-based model as well as ANFIS and LSSVM-CSA algorithms.

Three-phase relative permeability data during WI stages. The relative permeability predictions during the WI stages are depicted in Figure 5-11 to Figure 5-13. During the WI1 stage, only water and oil are present in the porous medium; therefore, the two-phase oil-water relative permeability data are presented in Figure 5-11 (a), 12(a) and 13(a).

Unfortunately, the experimental data are not available for the WI stages. Therefore, for the comparison purposes, we select the correlation-based EM predictions as the baseline relative permeability data owing to its excellent performance (it accurately predicts the experimental results obtained in the GI stages). We compare the relative permeability values predicted by the ANFIS and LSSVM-CSA models during WI stages with the results obtained from the EM model as our baseline. Both the ANFIS and LSSVM-CSA models are in good agreement with the baseline relative permeability curve during the first WI stages for oil, water, and gas (Figure 5-11 (a), 12(a) and 13(a)). However, in the second and third WI stages, the ANFIS and LSSVM-CSA models lead to less accurate three-phase relative permeability values compared to the baseline correlation-based EM. During the WI stages, the same common trends in relative permeability data are observed as those in the GI stages. For instance, the importance of cyclic displacement process transition from imbibition to drainage is evident in mobilizing the lower oil saturations as the WAG injection process proceeds (see panels (b) and (c) of Figure 5-11). This also depicts itself in successively decreasing residual oil saturation values through the cyclic injection stages. Figure 5-12 demonstrates that the end-point water relative permeability value during WI2 and WI3 stages does not significantly vary. The LSSVM-CSA model performs well in following the trend and values of the baseline data as depicted in all two- and three-phase relative permeability plots. The effect of saturation history on K_{rg}^{3ph} during the WI stages (Figure 5-13 (a) and 13(b)) is significant, resulting in reduced gas relative permeability at similar saturation levels. The residual gas

saturation subsequently decreases over the WI stages. The results given in Figure 5-11 and Figure 5-13 also reveal that the oil and gas relative permeabilities during the WI2 and WI3 cycles considerably decrease as the water breakthrough occurs. This is more significant in the case of gas relative permeability (Figure 5-13) during the WI2 and WI3 cycles, when the gas saturation change is negligible after the water breakthrough.

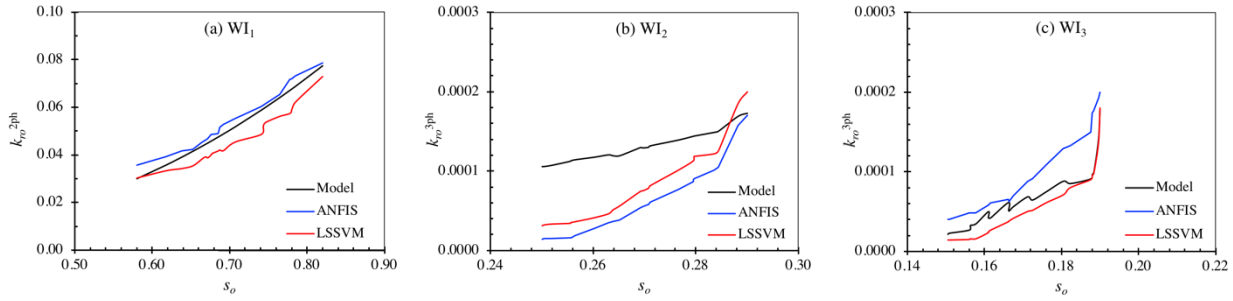

Figure 5-11: Comparison of the K_{ro}^{3ph} values in the (a) first, (b) second, and (c) third WI cycles using correlation-based EM as well as ANFIS and LSSVM-CSA algorithms (Note: due to zero gas saturation during WI1 stage, the (a) plot expresses the two-phase oil relative permeability data).

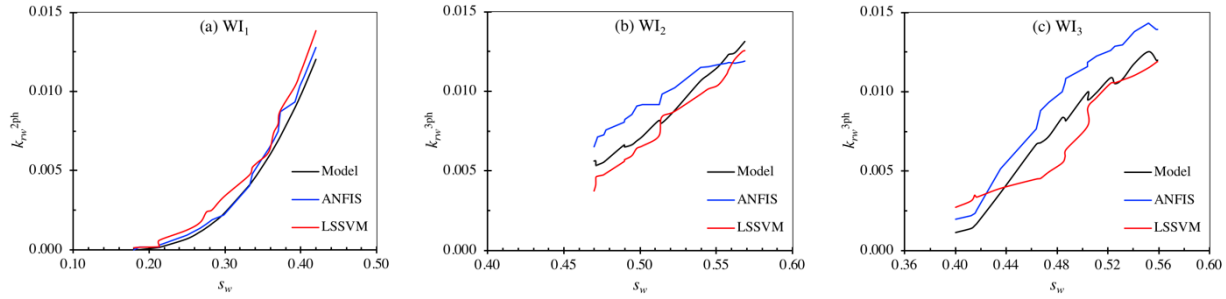

Figure 5-12: Comparison of the K_{rw}^{3ph} values in the (a) first, (b) second, and (c) third WI stages using correlation-based EM as well as ANFIS and LSSVM-CSA algorithms (Note: due to zero gas saturation during WI1 stage, the (a) plot expresses the two-phase water relative permeability data).

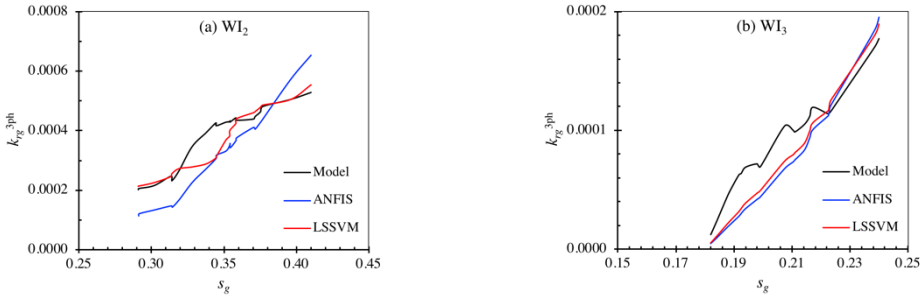

Figure 5-13: Comparison of the K_{rg}^{3ph} data in (a) first, (b) second, and (c) third WI stages using correlation-based EM as well as ANFIS and LSSVM-CSA algorithms.

5.7 Summary and Conclusions

In the current study, we use various hybrid models to predict the three-phase relative permeability data for a high-pressure WAG injection experiment. The LSSVM-CSA and ANFIS models are employed to predict the two-phase relative permeability curves, and then a three-phase relative permeability correlation is used with input values from the two-phase data. In another effort, the we used the two-phase relative permeability empirical models by Mualem [88] and Hirasaki [89] to obtain the two-phase data, which are then implemented in the three-phase relative permeability correlation model. To assess the reliability of the predictions, the instantaneous and ultimate RF values, along with the relative permeability data are selected as the objective functions to be compared against the experimental data. The experimental data are taken from the literature, for a water-wet Berea sandstone core at temperature and pressure equal to 38 ^{o}C 12.7 MPa, respectively. The following conclusions are drawn based on this study:

- The statistical quality measures reveal that the LSSVM-CSA and ANFIS models can be successfully trained for relative permeability predictions with relatively small errors.
- The LSSVM-CSA model exhibits a better predictive performance by generating less errors (RMSE, Mean Error, and Error_std) associated with the training, testing, and validating stages for the two-phase flow systems.
- The correlation-based EM as well as the LSSVM-CSA and ANFIS algorithms used in this study predict the ultimate RF values of 92%, 91.57%, and 82.88%, respectively, in comparison with the experimental measured value of 93.58% at the end of the WAG injection process.
- According to the PC, SC, and KC coefficients in the gas-water system, the pressure and temperature have the largest and lowest impacts on the output predictions, respectively. All coefficients are positive for this system, indicating that by increasing each input parameter, the output variable increases.
- The RI analysis of oil-water system shows that the water viscosity has the lowest impact on two-phase relative permeability values and water saturation, oil viscosity, and rock permeability negatively influence oil relative permeability meaning that by increasing these parameters, the oil relative permeability decreases and vice versa.
- The gas saturation is the most influential input parameter in the oil-gas system, while the gas critical saturation is the second influential parameter; it negatively affects on the predicted gas relative permeabilities (similar to the rock permeability and porosity).

- The best fit to the experimental three-phase relative permeability data is attained by correlation-based EM, while the ANFIS model leads to the less-accurate predictions.
- The three-phase water relative permeability values in three GI and WI cycles show less hysteresis compared to the gas relative permeabilities.
- The amount of residual oil saturations at the end of each WI or GI stage has a decreasing trend due to the cyclic nature of the saturation history transition between the imbibition and drainage processes during the WAG injection process.

Acknowledgements
The authors would like to acknowledge the financial support provided by Memorial University (NL, Canada), Natural Sciences and Engineering Research Council of Canada (NSERC), InnovateNL, and Equinor Canada.

Nomenclatures

Acronyms

ANN	Artificial neural network
ANFIS	Adaptive neuro-fuzzy inference system
Cost	Cost function
CSA	Coupled simulated annealing
EOR	Enhanced oil recovery
EM	Empirical model
FIS	Fuzzy inference system
FPM	First principal model
GI	Gas injection
IFT	Interfacial tension
IOR	Improved oil recovery
IWAG	Immiscible WAG
IMPES	Implicit-pressure-explicit-saturation
LSSVM	Least square support vector machine
ME	Mean error
MF	Membership function
MMP	Minimum miscibility pressure

PVI	Pore volume injection
PC	Pearson's coefficient
RBF	Radial basis kernel function
RF	Recovery factor
RI	Relative importance
RMSE	Root mean square error
SC	Spearman's coefficient
Std	Standard deviation
SVM	Support vector machine
WI	Water injection
WAG	Water-alternating-gas injection

Variables and Parameters

a	Capillary exponent
b	Bias term
c	Capillary entry pressure
K	Absolute permeability
k_{ri}	Relative permeability of phase i
k_{ri}^{o}	Endpoint elative permeability of phase i
p	Pressure
Q	Membership function
s_i	Saturation of phase i
s_{ic}	Critical saturation of phase i
t	Time
T	Temperature
w	Weight factor
x	Length

Greek Letters

μ	Viscosity
μ_{Ai}	Generalized bell function
ρ	Density

σ	Variance of the Gaussian function
ϕ	Porosity
θ	Contact angle
ζ	Regression error
ψ	Non-linear function

Subscripts and Superscripts

C	Capillary pressure
D	Drainage
g	Gas phase
I	Imbibition
o	Oil phase
og	Oil-gas system
org	Residual oil after GI
ow	Oil-water system
w	Water phase
wg	Water-gas system
r	Residual phase

References

1. Talabi, O. A.; Moreno, J. E.; Malhotra, R. K.; Liu, Y. In *Practical Upscaling of WAG Hysteresis Parameters from Core to Full-Field Scale Part II*, SPE/IATMI Asia Pacific Oil & Gas Conference and Exhibition, Society of Petroleum Engineers: 2019.
2. Sherafati, M.; Jessen, K., Dynamic relative permeability and Simulation of WAG injection processes. *Transport in Porous Media* **2017,** *117* (1), 125-147.
3. Aghabozorgi, S.; Sohrabi, M.; Facanha, J. In *Estimation of Three-phase Oil Relative Permeability in WAG Experiments*, Offshore Technology Conference Brasil, Offshore Technology Conference: 2019.
4. Moghadasi, L.; Ranaee, E.; Renna, D.; Bartosek, M.; Maddinelli, G.; Masserano, F.; Cominelli, A.; Inzoli, F.; Guadagnini, A. In *Combining Two-and Three-Phase Coreflooding Experiments for Reservoir Simulation Under WAG Practices*, International Petroleum Technology Conference, International Petroleum Technology Conference: 2020.

5. Carlson, F. M. In *Simulation of relative permeability hysteresis to the nonwetting phase*, SPE annual technical conference and exhibition, Society of Petroleum Engineers: 1981.
6. Land, C. S., Calculation of imbibition relative permeability for two-and three-phase flow from rock properties. *Society of Petroleum Engineers Journal* **1968,** *8* (02), 149-156.
7. Aziz, K.; Settari, A., Petroleum reservoir simulation: Applied science publ. *Ltd., London* **1979**.
8. Rogers, J. D.; Grigg, R. B., A literature analysis of the WAG injectivity abnormalities in the CO2 process. *SPE Reservoir Evaluation & Engineering* **2001,** *4* (05), 375-386.
9. Skauge, A.; Larsen, J. A. In *Three-phase relative permeabilities and trapped gas measurements related to WAG processes*, SCA 9421, proceedings of the International Symposium of the Society of Core Analysts, Stavanger, Norway, 1994.
10. Larsen, J.; Skauge, A., Methodology for numerical simulation with cycle-dependent relative permeabilities. *SPE Journal* **1998,** *3* (02), 163-173.
11. Egermann, P.; Vizika, O.; Dallet, L.; Requin, C.; Sonier, F. In *Hysteresis in three-phase flow: experiments, modeling and reservoir simulations*, SPE European petroleum conference, Society of Petroleum Engineers: 2000.
12. Corey, A. T.; Rathjens, C.; Henderson, J.; Wyllie, M., Three-phase relative permeability. *Journal of Petroleum Technology* **1956,** *8* (11), 63-65.
13. Land, C. S., Comparison of calculated with experimental imbibition relative permeability. *Society of Petroleum Engineers Journal* **1971,** *11* (04), 419-425.
14. Stone, H., Estimation of three-phase relative permeability and residual oil data. *Journal of Canadian Petroleum Technology* **1973,** *12* (04).
15. Delshad, M.; Delshad, M.; Pope, G.; Lake, L., Two-and three-phase relative permeabilities of micellar fluids. *SPE Formation Evaluation* **1987,** *2* (03), 327-337.
16. Shahverdi, H.; Sohrabi, M. In *Three-phase relative permeability and hystresis model for simulation of water alternating gas (WAG) injection*, SPE Improved Oil Recovery Symposium, Society of Petroleum Engineers: 2012.
17. Akin, S.; Castanier, L. M.; Brigham, W. E. In *Effect of temperature on heavy-oil/water relative permeabilities*, SPE Annual Technical Conference and Exhibition, Society of Petroleum Engineers: 1998.
18. Amott, E., Observations relating to the wettability of porous rock. *Transactions of the AIME* **1959,** *216* (01), 156-162.
19. Anderson, W. G., Wettability literature survey-part 1: rock/oil/brine interactions and the effects of core handling on wettability. *Journal of petroleum technology* **1986,** *38* (10), 1,125-1,144.

20. Ashrafi, M.; Souraki, Y.; Torsaeter, O., Effect of temperature on athabasca type heavy oil–water relative permeability curves in glass bead packs. *Energy and Environment Research* **2012,** *2* (2), 113-126.
21. Ashrafi, M.; Souraki, Y.; Torsaeter, O., Investigating the temperature dependency of oil and water relative permeabilities for heavy oil systems. *Transport in porous media* **2014,** *105* (3), 517-537.
22. Bennion, D.; Moore, R.; Thomas, F., Effect of relative permeability on the numerical simulation of the steam stimulation process. *Journal of Canadian Petroleum Technology* **1985,** *24* (02).
23. Bennion, D.; Thomas, F.; Schulmeister, B.; Ma, T. In *A Correlation of the low and high temperature water-oil relative permeability characteristics of typical western Canadian unconsolidated bitumen producing formations*, Canadian International Petroleum Conference, Petroleum Society of Canada: 2006.
24. Closmann, P.; Waxman, M.; Deeds, C., Steady-state tar/water relative permeabilities in Peace River cores at elevated temperature. *SPE Reservoir Engineering* **1988,** *3* (01), 76-80.
25. Esfahani, M. R.; Haghighi, M., Wettability evaluation of Iranian carbonate formations. *Journal of Petroleum Science and Engineering* **2004,** *42* (2-4), 257-265.
26. Hamouda, A. A.; Karoussi, O., Effect of temperature, wettability and relative permeability on oil recovery from oil-wet chalk. *Energies* **2008,** *1* (1), 19-34.
27. Maini, B. B.; Okazawa, T., Effects of temperature on heavy oil-water relative permeability of sand. *Journal of Canadian Petroleum Technology* **1987,** *26* (03).
28. Polikar, M.; Ali, S.; Puttagunta, V., High-temperature relative permeabilities for Athabasca oil sands. *SPE reservoir engineering* **1990,** *5* (01), 25-32.
29. Polikar, M.; Ferracuti, F.; Decastro, V.; Puttagunta, R.; Ali, S., Effect of temperature on bitumen-water end point relative permeabilities and saturations. *Journal of Canadian Petroleum Technology* **1986,** *25* (05).
30. Weinbrandt, R.; Ramey Jr, H.; Casse, F., The effect of temperature on relative and absolute permeability of sandstones. *Society of Petroleum Engineers Journal* **1975,** *15* (05), 376-384.
31. Esmaeili, S.; Sarma, H.; Harding, T.; Maini, B., A data-driven model for predicting the effect of temperature on oil-water relative permeability. *Fuel* **2019,** *236*, 264-277.
32. Vapnik, V., *The nature of statistical learning theory*. Springer science & business media: 2013.
33. Hann, T. H.; Steurer, E., Much ado about nothing? Exchange rate forecasting: Neural networks vs. linear models using monthly and weekly data. *Neurocomputing* **1996,** *10* (4), 323-339.

34. Rafiee-Taghanaki, S.; Arabloo, M.; Chamkalani, A.; Amani, M.; Zargari, M. H.; Adelzadeh, M. R., Implementation of SVM framework to estimate PVT properties of reservoir oil. *Fluid Phase Equilibria* **2013,** *346*, 25-32.
35. Shokrollahi, A.; Arabloo, M.; Gharagheizi, F.; Mohammadi, A. H., Intelligent model for prediction of CO2–reservoir oil minimum miscibility pressure. *Fuel* **2013,** *112*, 375-384.
36. Übeyli, E. D., Least squares support vector machine employing model-based methods coefficients for analysis of EEG signals. *Expert Systems with Applications* **2010,** *37* (1), 233-239.
37. Suykens, J., Support Vector Machines and Kernel Based Learning. *Tutorial: IJCNN, Montreal,[Online], Available from:< http://www. esat. kuleuven. ac. be/sista/lssvmlab/ijcnn2005_4. pdf* **2003**.
38. Suykens, J. A.; Vandewalle, J., Least squares support vector machine classifiers. *Neural processing letters* **1999,** *9* (3), 293-300.
39. Nowroozi, S.; Ranjbar, M.; Hashemipour, H.; Schaffie, M., Development of a neural fuzzy system for advanced prediction of dew point pressure in gas condensate reservoirs. *Fuel Processing Technology* **2009,** *90* (3), 452-457.
40. Fayazi, A.; Arabloo, M.; Shokrollahi, A.; Zargari, M. H.; Ghazanfari, M. H., State-of-the-art least square support vector machine application for accurate determination of natural gas viscosity. *Industrial & Engineering Chemistry Research* **2014,** *53* (2), 945-958.
41. Sinehbaghizadeh, S.; Roosta, A.; Rezaei, N.; Ghiasi, M. M.; Javanmardi, J.; Zendehboudi, S., Evaluation of phase equilibrium conditions of clathrate hydrates using connectionist modeling strategies. *Fuel* **2019,** *255*, 115649.
42. Yarveicy, H.; Moghaddam, A. K.; Ghiasi, M. M., Practical use of statistical learning theory for modeling freezing point depression of electrolyte solutions: LSSVM model. *Journal of Natural Gas Science and Engineering* **2014,** *20*, 414-421.
43. Salleh, M. N. M.; Talpur, N.; Hussain, K. In *Adaptive Neuro-Fuzzy Inference System: Overview, Strengths, Limitations, and Solutions*, International Conference on Data Mining and Big Data, Springer: 2017; pp 527-535.
44. Kar, S.; Das, S.; Ghosh, P. K., Applications of neuro fuzzy systems: A brief review and future outline. *Applied Soft Computing* **2014,** *15*, 243-259.
45. Hussain, K.; Salleh, M.; Najib, M., Analysis of techniques for anfis rule-base minimization and accuracy maximization. **2015**.
46. Jang, J.-S., ANFIS: adaptive-network-based fuzzy inference system. *IEEE transactions on systems, man, and cybernetics* **1993,** *23* (3), 665-685.

47. Rostami, A.; Baghban, A.; Mohammadi, A. H.; Hemmati-Sarapardeh, A.; Habibzadeh, S., Rigorous prognostication of permeability of heterogeneous carbonate oil reservoirs: Smart modeling and correlation development. *Fuel* **2019,** *236*, 110-123.
48. Zargari, H.; Poordad, S.; Kharrat, R., Porosity and permeability prediction based on computational intelligences as artificial neural networks (ANNs) and adaptive neuro-fuzzy inference systems (ANFIS) in southern carbonate reservoir of Iran. *Petroleum science and technology* **2013,** *31* (10), 1066-1077.
49. Karkevandi-Talkhooncheh, A.; Sharifi, M.; Ahmadi, M., Application of hybrid adaptive neuro-fuzzy inference system in well placement optimization. *Journal of Petroleum Science and Engineering* **2018,** *166*, 924-947.
50. Wei, M.; Bai, B.; Sung, A. H.; Liu, Q.; Wang, J.; Cather, M. E., Predicting injection profiles using ANFIS. *Information Sciences* **2007,** *177* (20), 4445-4461.
51. Barati-Harooni, A.; Najafi-Marghmaleki, A., Implementing a PSO-ANFIS model for prediction of viscosity of mixed oils. *Petroleum Science and Technology* **2017,** *35* (2), 155-162.
52. Karkevandi-Talkhooncheh, A.; Hajirezaie, S.; Hemmati-Sarapardeh, A.; Husein, M. M.; Karan, K.; Sharifi, M., Application of adaptive neuro fuzzy interface system optimized with evolutionary algorithms for modeling CO2-crude oil minimum miscibility pressure. *Fuel* **2017,** *205*, 34-45.
53. Rahimzadeh Kivi, I.; Ameri Shahrabi, M.; Akbari, M., The development of a robust ANFIS model for predicting minimum miscibility pressure. *Petroleum science and technology* **2013,** *31* (20), 2039-2046.
54. Keybondorian, E.; Taherpour, A.; Bemani, A.; Hamule, T., Application of novel ANFIS-PSO approach to predict asphaltene precipitation. *Petroleum Science and Technology* **2018,** *36* (2), 154-159.
55. Zamani, H. A.; Rafiee-Taghanaki, S.; Karimi, M.; Arabloo, M.; Dadashi, A., Implementing ANFIS for prediction of reservoir oil solution gas-oil ratio. *Journal of Natural Gas Science and Engineering* **2015,** *25*, 325-334.
56. Mahmoud, A. A.; Elkatatny, S.; Chen, W.; Abdulraheem, A., Estimation of oil recovery factor for water drive sandy reservoirs through applications of artificial intelligence. *Energies* **2019,** *12* (19), 3671.
57. Shamshirband, S.; Baghban, A.; Sasanipour, J.; Hadipoor, M., On the Investigation of Temperature Effects on Oil Relative Permeability: Robust Modeling and Data Assessments. **2019**.
58. Roghanian, R.; Asadolahpour, S.; Rasaei, M., The prediction of water-oil relative permeability key points using an adaptive neuro-fuzzy inference system. *Petroleum science and technology* **2014,** *32* (16), 2004-2019.

59. Amendolia, S. R.; Cossu, G.; Ganadu, M. L.; Golosio, B.; Masala, G. L.; Mura, G. M., A comparative study of K-Nearest Neighbour, Support Vector Machine and Multi-Layer Perceptron for Thalassemia screening. *Chemometrics and Intelligent Laboratory Systems* **2003,** *69* (1), 13-20.
60. Ghiasi, M. M.; Esmaeili-Jaghdan, Z.; Halali, M. A.; Lee, M.; Abbas, A.; Bahadori, A., Development of soft computing methods to predict moisture content of natural gases. *Journal of the Taiwan Institute of Chemical Engineers* **2015,** *55*, 36-41.
61. Ghiasi, M. M.; Mohammadi, A. H., Determination of methane-hydrate phase equilibrium in the presence of electrolytes or organic inhibitors by using a semi-theoretical framework. *Energy Technology* **2013,** *1* (9), 519-529.
62. Shokrollahi, A.; Arabloo, M.; Gharagheizi, F.; Mohammadi, A. H., Intelligent model for prediction of CO2 – Reservoir oil minimum miscibility pressure. *Fuel* **2013,** *112*, 375-384.
63. Ghiasi, M. M.; Arabloo, M.; Bahadori, A.; Zendehboudi, S., Prediction of methanol loss in liquid hydrocarbon phase during natural gas hydrate inhibition using rigorous models. *Journal of Loss Prevention in the Process Industries* **2015,** *33*, 1-9.
64. Cortes, C.; Vapnik, V., Support-vector networks. *Machine Learning* **1995,** *20* (3), 273-297.
65. De Brabanter, J.; De Moor, B.; Suykens, J. A.; Van Gestel, T.; Vandewalle, J. P., *Least squares support vector machines*. World scientific: 2002.
66. Seyyedattar, M.; Ghiasi, M. M.; Zendehboudi, S.; Butt, S., Determination of bubble point pressure and oil formation volume factor: Extra trees compared with LSSVM-CSA hybrid and ANFIS models. *Fuel* **2020**, 116834.
67. Ghiasi, M. M.; Bahadori, A., A NEW CORRELATION FOR ACCURATE ESTIMATION OF NATURAL GASES WATER CONTENT. *Petroleum & Coal* **2014,** *56* (5).
68. Ghiasi, M. M.; Hajinezhad, A.; Yousefi, H.; Mohammadi, A. H., CO2 loading capacity of DEA aqueous solutions: Modeling and assessment of experimental data. *International Journal of Greenhouse Gas Control* **2017,** *56*, 289-301.
69. Saghafi, H.; Ghiasi, M. M.; Mohammadi, A. H., CO2 capture with aqueous solution of sodium glycinate: Modeling using an ensemble method. *International Journal of Greenhouse Gas Control* **2017,** *62*, 23-30.
70. Ghiasi, M. M.; Mohammadi, A. H., Development of reliable models for determination of required monoethanolamine (MEA) circulation rate in amine plants. *Separation Science and Technology* **2015,** *50* (14), 2248-2256.

71. Ying, L.-C.; Pan, M.-C., Using adaptive network based fuzzy inference system to forecast regional electricity loads. *Energy Conversion and Management* **2008,** *49* (2), 205-211.
72. Ameli, F.; Hemmati-Sarapardeh, A.; Tatar, A.; Zanganeh, A.; Ayatollahi, S., Modeling interfacial tension of normal alkane-supercritical CO2 systems: Application to gas injection processes. *Fuel* **2019,** *253*, 1436-1445.
73. Dashti, A.; Raji, M.; Razmi, A.; Rezaei, N.; Zendehboudi, S.; Asghari, M., Efficient hybrid modeling of CO2 absorption in aqueous solution of piperazine: Applications to energy and environment. *Chemical Engineering Research and Design* **2019,** *144*, 405-417.
74. Surguchev, L.; Korbol, R.; Haugen, S.; Krakstad, O. In *Screening of WAG injection strategies for heterogeneous reservoirs*, European petroleum conference, Society of Petroleum Engineers: 1992.
75. Tabatabaei Nezhad, S. A. R.; Rahimzadeh Mojarad, M.; Oskouei, P.; Javad, S.; Moghadas, J. S.; Farahmand, D. R. In *Experimental Study on Applicability of Water Alternating CO2 Injection in the Secondary and Tertiary Recovery*, International Oil Conference and Exhibition in Mexico, Society of Petroleum Engineers: 2006.
76. Afzali, S.; Ghamartale, A.; Rezaei, N.; Zendehboudi, S., Mathematical modeling and simulation of water-alternating-gas (WAG) process by incorporating capillary pressure and hysteresis effects. *Fuel* **2019**, 116362.
77. Braun, E.; Holland, R., Relative permeability hysteresis: Laboratory measurements and a conceptual model. *SPE Reservoir Engineering* **1995,** *10* (03), 222-228.
78. Osoba, J.; Richardson, J.; Kerver, J.; Hafford, J.; Blair, P., Laboratory measurements of relative permeability. *Journal of Petroleum Technology* **1951,** *3* (02), 47-56.
79. Bradford, S. A.; Leij, F. J., Predicting two-and three-fluid capillary pressure-saturation relationships of porous media with fractional wettability. *Water Resources Research* **1996,** *32* (2), 251-259.
80. Egermann, P.; Mejdoub, K.; Lombard, J.-M.; Vizika, O.; Kalam, Z., Drainage three-phase flow relative permeability on oil-wet carbonate reservoir rock types: Experiments, interpretation and comparison with standard correlations. *Petrophysics* **2014,** *55* (04), 287-293.
81. Oak, M. In *Three-phase relative permeability of intermediate-wet Berea sandstone*, SPE Annual Technical Conference and Exhibition, Society of Petroleum Engineers: 1991.
82. Van Dijke, M.; Sorbie, K.; McDougall, S., Saturation-dependencies of three-phase relative permeabilities in mixed-wet and fractionally wet systems. *Advances in Water Resources* **2001,** *24* (3-4), 365-384.

83. Shahverdi, H.; Sohrabi, M., An improved three-phase relative permeability and hysteresis model for the simulation of a water-alternating-gas injection. *Spe Journal* **2013,** *18* (05), 841-850.
84. Mualem, Y., A new model for predicting the hydraulic conductivity of unsaturated porous media. *Water resources research* **1976,** *12* (3), 513-522.
85. Hirasaki, G. J., Sensitivity coefficients for history matching oil displacement processes. *Society of Petroleum Engineers Journal* **1975,** *15* (01), 39-49.
86. Ahmed, T. H., Comparative study of eight equations of state for predicting hydrocarbon volumetric phase behavior. *SPE Reservoir Engineering* **1988,** *3* (01), 337-348.
87. Ghiasi, M. M.; Zendehboudi, S., Decision tree-based methodology to select a proper approach for wart treatment. *Computers in biology and medicine* **2019,** *108*, 400-409.
88. Gharagheizi, F.; Eslamimanesh, A.; Mohammadi, A. H.; Richon, D., Artificial neural network modeling of solubilities of 21 commonly used industrial solid compounds in supercritical carbon dioxide. *Industrial & engineering chemistry research* **2011,** *50* (1), 221-226.
89. Botset, H. G., Flow of gas-liquid mixtures through consolidated sand. *Transactions of the AIME* **1940,** *136* (01), 91-105.
90. Fatt, I., The network model of porous media. *Transactions of the AIME* **1956,** *207* (01), 144-181.
91. Wyckoff, R.; Botset, H., The flow of gas-liquid mixtures through unconsolidated sands. *Physics* **1936,** *7* (9), 325-345.
92. Leverett, M.; Lewis, W., Steady flow of gas-oil-water mixtures through unconsolidated sands. *Transactions of the AIME* **1941,** *142* (01), 107-116.
93. Hamedi, H.; Ehteshami, M.; Mirbagheri, S. A.; Zendehboudi, S., New deterministic tools to systematically investigate fouling occurrence in membrane bioreactors. *Chemical Engineering Research and Design* **2019,** *144*, 334-353.
94. Zendehboudi, S.; Rezaei, N.; Lohi, A., Applications of hybrid models in chemical, petroleum, and energy systems: A systematic review. *Applied Energy* **2018,** *228*, 2539-2566.
95. Le-Clech, P.; Jefferson, B.; Judd, S. J., Impact of aeration, solids concentration and membrane characteristics on the hydraulic performance of a membrane bioreactor. *Journal of Membrane Science* **2003,** *218* (1), 117-129.
96. Samanta, B., Gear fault detection using artificial neural networks and support vector machines with genetic algorithms. *Mechanical Systems and Signal Processing* **2004,** *18* (3), 625-644.

97. Lesjean, B.; Rosenberger, S.; Laabs, C.; Jekel, M.; Gnirss, R.; Amy, G., Correlation between membrane fouling and soluble/colloidal organic substances in membrane bioreactors for municipal wastewater treatment. *Water science and technology* **2005,** *51* (6-7), 1-8.
98. Diez, V.; Ezquerra, D.; Cabezas, J. L.; García, A.; Ramos, C., A modified method for evaluation of critical flux, fouling rate and in situ determination of resistance and compressibility in MBR under different fouling conditions. *Journal of Membrane Science* **2014,** *453*, 1-11.
99. Deng, L. Development of specific membrane bioreactors for membrane fouling control during wastewater treatment for reuse. 2015.
100. Fatemi, S. M. Multiphase flow and hysteresis phenomena in oil recovery by water alternating gas (WAG) injection. Heriot-Watt University, 2015.
101. Chok, N. S. Pearson's versus Spearman's and Kendall's correlation coefficients for continuous data. University of Pittsburgh, 2010.
102. Tatar, A.; Moghtadaei, G. M.; Manafi, A.; Cachadiña, I.; Mulero, Á., Determination of pure alcohols surface tension using Artificial Intelligence methods. *Chemometrics and Intelligent Laboratory Systems* **2020,** *201*, 104008.
103. Tatar, A.; Moghtadaei, G. M.; Manafi, A.; Cachadiña, I.; Mulero, Á., Determination of pure alcohols surface tension using Artificial Intelligence methods. *Chemometrics and Intelligent Laboratory Systems* **2020**, 104008.

CHAPTER SIX

Application of Gene Expression Programming (GEP) in Modeling Hydrocarbon Recovery in WAG Injection Process

Preface

A version of this manuscript has been submitted to the Natural Resources Research Journal. I am the primary author of this manuscript. Sohrab Zendehboudi, Mohamadi-Baghmolaei, and I were involved in the definition of objectives, modeling approach, and design of the manuscript. I prepared the first draft of the manuscript and subsequently revised the manuscript based on the feedback/comments from the co-authors. The co-author, Sohrab Zendehboudi, significantly helped in reviewing and revising the manuscript. The co-author, Mohamadi-Baghmolaei, also contributed to the developing the method and creating the structure of the paper.

Abstract

Water alternating gas (WAG) injection has been successfully applied as a tertiary recovery technique. WAG injection is well-known and widely being acceptable due to providing stabilized front, and mobility control of fluids for better conformance, possible oil saturation reduction, and mobilizing the oil phase even at low saturations. Forecasting WAG flooding performance using fast and robust models is of great importance to attain a better understanding of the process, optimize the operational conditions, and avoid high-cost blind tests in laboratory and/or pilot scales. In this study, we introduce a novel correlation to determine the performance of near-miscible WAG injection in strongly water-wet sandstones.

The new model is developed using gene expression programming (GEP) technique. We conduct dimensional analysis with the Buckingham's π theorem technique to generate dimensionless numbers using eight key parameters. Seven dimensionless numbers are employed as the input variables of the desired correlation for predicting the recovery factor of a near-miscible WAG injection. A proper and reliable mathematical model is used to generate the required training and testing data for the development of the correlation using GEP algorithm. The provided data points are then separated into two subsets: training (67 %) to develop the model and testing (33 %) to assess the models' capability. Conducting error analysis, statistical measures and graphical illustrations are provided to evaluate the effectiveness of the proposed model. The statistical analysis shows that the developed GEP-based correlation is able to generate target data with high precision such that the training phase leads to R^2= 92.85 % and *MSE*=1.38e-3, and R^2= 91.93 % and *MSE*=4.30e-3 are attained for the testing phase. The relative importance of the input dimensionless groups is also determined. According to the sensitivity analysis, decreasing the oil-water capillary number results in a significant reduction in RF in all cycles. Increasing the magnitudes of oil to gas viscosity ratio and oil to water viscosity ratio lowers the RF of each cycle. It is found that oil to gas viscosity ratio has a higher impact on RF value, compared to oil to water viscosity ratio due to a greater viscosity difference between the oil and gas phases. It is expected that the GEP as a fast and reliable tool can be useful to find vital variables such as relative permeability in complex transport phenomena such as three-phase flow in porous media.

Keywords: WAG injection; Gene expression programing; Statistical analysis; Empirical correlation; Oil recovery

6.1 Introduction

Water alternating gas (WAG) injection is among the common enhanced oil recovery (EOR) techniques; this recovery method has been recognized as a cost effective and successful method for greater oil production [1-2]. In the past decades, there have been some field applications, numerical simulations, and laboratory experiments on WAG injection processes [1-2]. In a study conducted by Skauge et al. [3], it was reported that the WAG injection can increase the oil recovery factor by 5-10 % in the field scale.

Modeling and simulation of the WAG injection processes have been investigated in the literature to explore the effect of various key variables such as WAG ratio, number of cycles [4-11], wettability [9, 12-14], relative permeability and hysteresis [6, 9, 11-12, 14-21] on WAG performance. One of the main problems in modeling and optimizing a WAG injection process is development of appropriate and reliable correlations between rock/fluid properties and the amount of residual phases in the reservoir [22]. The cyclic nature of the WAG process and the three-phase flow in the porous medium add extra burden in terms of computational costs and modeling robustness. The main focus of most previous simulation and modeling studies related to WAG is on the analytical solution of the governing equations of three-phase flow, and three-phase relative permeabilities during the oil production [23-24].

Despite the availability of several correlations for determination of three-phase relative permeability and capillary pressure for a WAG flooding [18, 25], they fail in situations where the mass transfer between phases occurs, particularly when one phase disappears. Dynamic behaviors caused by evaporation of residual oil and dissolution of the injected gas in the residual oil also add extra complexities to the WAG process. Many past studies were not able to have a proper evaluation of WAG process performance due to incorporation of inappropriate three-phase relative permeability or capillary pressure expressions/data in their models [26-29].

In the oil and gas industry, laboratory coreflood experiments have been conventionally used as a representative of actual hydrocarbon reservoirs to evaluate the effectiveness of EOR processes such as WAG flooding prior to the field applications. Coreflood experiments can be also used to quantify flow properties such as capillary pressure and relative permeability curves. The acquired data from a small laboratory model can be utilized to predict the behavior of other similar systems [30]. In the last decades, several research investigations have focused on the WAG performance [31], WAG process simulation [32], WAG pilot tests [1-2], WAG process mechanisms [33], WAG hysteresis

[34], and WAG management [35]. However, the WAG process has not been well-developed and understood yet. One of the overlooked aspects in WAG process is the development of predictive tools prior to conducting pilot and field tests [36]. In some cases, complicated and timely simulations and modeling approaches are employed to examine the efficiency of the WAG process. For instance, the computational time for simulation and optimization of some reservoirs, particularly heterogeneous cases, might be thousands of hours [37]. Moreover, the optimization process conducted by simulation modeling is based on one parameter at a time process without involving the effect of interactions between uncertain parameters on the process output [38]. Therefore, fast and low-cost tools for assessment of WAG injection are required to overcome this issue.

As the first step in the prediction process, it is necessary to establish a set of relationships between the two systems, i.e., the given system (i.e. laboratory system) which is used to predict the behavior of the target similar system, and the one of actual interest, the prototype. These relationships are generally known as the scaling laws, similarity laws, or similarity requirements [30]. The scaling process eventually leads to developing dimensionless numbers, which are known as dimensionless scaling groups.

Smart computational tools have been extensively utilized for prediction of reservoir fluid and rock properties, optimization, and performance assessment of EOR techniques [39-42]. In recent years, various optimization techniques such as genetic algorithm (GA) and particle swarm optimization (PSO) have been widely used as reliable approaches to optimize different upstream and downstream processes in oil and gas industry [43]. The primary version of GA was then modified into a new algorithm called, genetic programming (GP) approach. The gene expression programming (GEP) is a new and updated version of GA that addresses most of drawbacks/concerns of previous versions [44]. Generally, GEP is able to obtain a solution for regression problems [45]. Unlike the GP program that the individuals' population are symbolically considered as expression trees (ETs), the individuals' populations are regarded as the linear chromosomes in the GEP algorithm [46-47]. GEP method has been employed in various research subjects in petroleum engineering, including estimating mixture viscosity in solvent-assisted oil recovery process [48], CO_2 solubility in crude oil [49], minimum miscibility pressure (MMP) of live oil systems [50], petroleum emulsions' viscosity [51], surfactant retention in porous media [52], residual gas saturation during spontaneous and forced imbibition processes [53], and oil price [54]. However, the application of this smart technique has not been reported for predicting the oil recovery of near

miscible-WAG injection process in the open sources. Near-miscible WAG injection studies are limited to few experimental investigations, which are highly time consuming, expensive, and more importantly not comprehensive in terms of sensitivity analysis. Today, with significant developments in computer and data science, it is feasible to introduce robust, fast, and reliable models to predict the performance of complex EOR processes such as WAG injection. The main objective of this work is to conduct the scaling analysis using the data provided by the validated and reliable implicit-pressure-explicit-saturation (IMPES) model for development of a robust empirical model, which is able to predict the recovery factor of near-miscible WAG injection.

This chapter is structured as follows. After the introduction, in the theory and background section, we provide a brief description of the WAG process and a background on dimensional analysis approaches, and the introduction/fundamentals of GEP algorithm. In the methodology section, the application of dimensionless model and its principles for generating the required data are discussed. Then, the design of experiment is provided, which is required to know the number of required runs, data, and dimensionless scaling groups. Afterwards, the analysis of variance (ANOVA), procedure of the GEP algorithm, and the model development are described. In the results and discussions, the results of the ANOVA test and the relative importance of the input parameters are elaborated. We also discuss the results of the testing and training phases, statistical error analysis, GEP correlation, and sensitivity analysis. In the last section of this chapter, the summary and main conclusions are given.

6.2 Theory and Background

6.2.1 WAG Mechanisms

Gas injection (GI) and water flooding (WF) are the two conventional and common methods in oil and gas production among the tertiary and secondary techniques [55]. The efficiency of these methods depends on efficiencies at both macroscopic volumetric sweep efficiency and microscopic displacement sweep efficiency scales [56].

The major drawbacks during GI processes are gas fingering phenomenon caused by unfavorable mobility ratio, low volumetric sweep efficiency [57]; and early gas breakthrough occurrence which has been reported in various pilot and field applications [58-60] caused by the gas fingering and channeling in layers with high permeability. The main issues with the GI effectivity are related to the mobility of the fluids and reservoir conformance [57]. On the other hand, the cyclic injection of

water and gas (in WAG injection) reduces the effective permeability of the gas phase, resulting in a stabilized fluids' fronts and thereby, enhancing the overall sweep efficiency of the system. Gravity segregation is another governing mechanism during a WAG flooding process which is caused by the density difference between the active phases in the medium [61]. Gravity segregation enhances the vertical sweep efficiency through sweeping the bypassed oil at the bottom of the reservoir (from the GI cycle) in the WF cycle [61]. Figure 6-1 depicts a schematic of a general WAG injection process and the phases' distributions for oil, gas, and water in a typical reservoir.

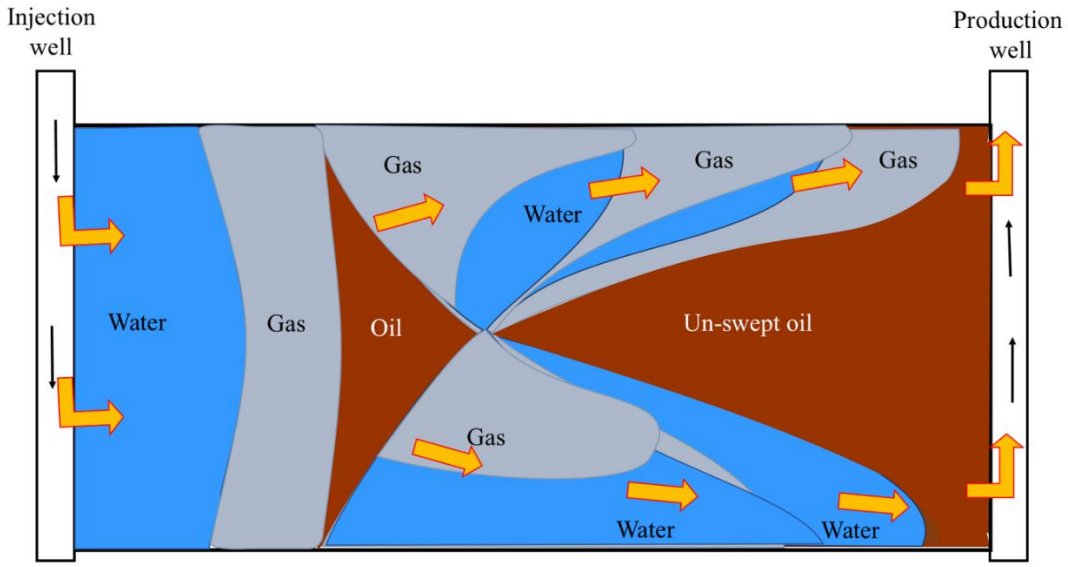

Figure 6-1: A schematic of WAG process in a hypothetical oil reservoir (Modified after Shahverdi et al.) [62].

6.2.2 Dimensional Analysis

Two conventional techniques are proposed to generate the dimensionless groups: inspectional analysis [63-64], and dimensional analysis [61, 65-69]. The inspectional analysis is on the basis of the differential equations that govern the flow displacement, while the dimensional analysis performs based on the pertinent variables that directly affect the system behavior. In the inspectional analysis, the differential governing equations of the process along with the initial and boundary conditions are transformed into dimensionless forms through normalizing variables into the equations [63-64]. This transformation leads to obtaining the dimensionless dependent variables, dimensionless independent variables, and dimensionless scaling groups. In contrary to the inspectional analysis, in dimensionless analysis, only the pertinent variables are required, and the governing equations are not transformed. In this technique, to obtain the dimensionless scaling

groups, the power products of the variables are rendered to dimensionless forms. This leads to generating a set of homogeneous linear algebraic equations [61, 65-69]. The solutions of these equations provide a set of complete independent, though not unique, dimensionless numbers. Using a set of variables and applying the Buckingham's π theorem result in generating the number and the forms of the dimensionless groups. Many studies have focused on applications of the theory of scaling and similarity laws for fluid flow in porous media [61, 65, 68, 70-79]. Initially, Leverett et al. [80] used the dimensionless groups in a research on immiscible displacement of oil by water, which was later extended by Klinkenberg [81]. Asghari et al. [82] used the data provided by the past performance of waterflooding in the Weyburn field to develop an empirical correlation for predicting CO_2 flooding performance. Two different correlations were introduced based on different injection schemes in the Weyburn field. The first correlation was developed according to the WAG injection through vertical wells and the second one was based on the horizontal injection using the Kinder Morgan CO_2 Scoping model and the field production data. However, in their proposed model, only the oil production rate and CO_2 and water injection rates were accounted to develop the model and other field or operational variables were not included. Shunhua et al. suggested a new model for generating dimensionless CO_2 flood forecast such as total injection (DTI), CO_2 injection (DCI), tertiary oil production (DEOR), CO_2 production (DCP) , for various WAG injection approaches [83]. A Microsoft Excel VBA program (for injecting CO_2 pulses) was utilized to generate the prototypes for forecasting the performance of the system. Their new methodology (Pulse method) was verified using mechanistic simulation results of finite element for different WAG injection processes and/or different CO_2 injection slug sizes [83]. Khalil et al. [38] introduced a simple data-driven model to assess the miscible CO_2-WAG injection in an Iraqi oilfield. They employed a central composite design (CCD) to introduce a proxy model. They applied ANOVA to examine the effectiveness of the variables and their combinations within the model. The proposed proxy model determined the incremental oil recovery (ΔFOE) as a function of reservoir properties and operational conditions including permeability, porosity, ratio of vertical to horizontal permeability, cyclic length, bottomhole pressure, ratio of CO_2 over water slug size, and CO_2 slug size.

6.2.3 Fundamentals of GEP

Current genetic algorithm (GA) and genetic programing (GP) techniques have been widely used in common regression engineering problems such as function fitting and time series predictions [84-

[86]. In the GA algorithm, individuals are represented as the linear strings with fixed lengths (chromosome) during all evolution levels. This prevents GA to be applied in some complex function fitting problems [87]. However, in GP algorithm, individuals are represented as the non-linear objects with different sizes and shapes. GP algorithm is normally capable of analyzing very complex functions; however, the variety in object sizes often hinders the evolutionary procedure to obtain an optimum solution [88]. In contrast, gene expression programming (GEP) is a new approach in developing computer programs with focus on learning models and discovering knowledge [44, 89]. GEP combines the features of GA and GP algorithms, while it differs from these two evolutionary approaches mainly in chromosome encoding. In GEP algorithm, the individuals are encoded as the chromosomes and are considered as the linear strings with fixed lengths [44, 90]. GEP has more flexibility and power for exploring the search space by separating the genotype and phenotype. The designed chromosomes in GEP are simple and linear. GEP demonstrates significant advantages over its peers; for instance, compared to the GA, GEP performs approximately 2-4 orders of magnitude faster in solving general problems due to its unique individual functioning [44, 87]. GEP is a full-fledged genotype/phenotype system in which the genotype is totally separated from the phenotype. However, in GP, the genotype and phenotype are one element; indeed, it is a simple replicator system. GEP works based on two elements (e.g., chromosomes and ETs). The chromosomes encode the candidate solution and transform the actual solution candidates into an ET. The transition process of the chromosomes into an ET is inspired by the biological process of genes encoded (in an DNA) into proteins [91].

6.3 Methodology

6.3.1 Data Collection

The applicability, reliability, and accuracy of any correlation/model are strongly linked to the identified input variables as well as validity and reliability of employed data points used in the development stage [47, 92-97]. The most important parameters affecting a WAG injection process include the fluid and rock properties and operational conditions. Due to the lack of adequate experimental data for near-miscible WAG flooding processes, a suitable and reliable mathematical model is used [33]. The mathematical simulator approach is a one-dimensional model, with implicit-pressure explicit-saturation (IMPES) solution scheme. In the following subsections, the governing and auxiliary equations required for developing the mathematical model are provided. For more

details about the model development, technical readers may visit the study conducted by Afzali et *al.* [33].

6.3.2 Governing Equations

For a three-phase, incompressible flow system, the governing equations to be solved are the mass/molar balances for all presented phases. The final form of the governing equations for an immiscible three-phase (e.g., oil, water, and gas) system, after neglecting the phase dispersion and gravity effects and applying the Darcy's Law (as the momentum balance equation) can be written as follows:

$$\nabla.\left(\frac{\rho_i K k_{ri}}{\mu_i}\frac{\partial p_i}{\partial x}\right) + q_i = \frac{\partial}{\partial t}(\phi \rho_i s_i) \quad i \in \{o, w, g\} \tag{6-1}$$

where the subscript *i* denotes the water, oil, and gas phases; *p* represents the pressure; *s* refers to the saturation; ρ and μ are the density and viscosity of the fluid, respectively; *q* symbolizes the source/sink term (i.e. production or injection rate); *K* and ϕ stand for the absolute permeability and porosity of the rock, respectively; *t* refers to the time; and *x* is the spatial location.

6.3.3 Auxiliary Equations

Eq. (6-2) indicates the relationship between the saturations of three phases existing in the system:

$$s_o + s_w + s_g = 1 \tag{6-2}$$

where s_w, s_o, and s_g refer to the water, oil, and gas saturations, respectively.

For an accurate simulation of the three-phase flow in WAG injection, selecting reliable three-phase relative permeability and three-phase capillary pressure models is essential. Using direct measurement method of three-phase capillary pressure data from coreflooding tests is time-consuming and practically challenging [98-99].

The capillary pressure (p_c) between two phases is defined as the pressure difference between the non-wetting phase and wetting phase (see Eq. (6-3)), which is a function of fluids' saturations and distribution, and rock properties such as porosity and permeability.

$$p_c = p_{nw} - p_w \tag{6-3}$$

in which, p_{nw} and p_w represent the non-wetting and wetting phases' pressures, respectively.

In this work, we use a three-phase capillary pressure model suggested by Neshat et al. [100], derived based on the Gibbs free energy. The proposed model is an extended/modified version of a two-

phase capillary pressure model introduced by Skjaveland et *al.* [101]. This capillary pressure model is appropriate to be used for all types of rock in terms of different wettability states. The general form of the applied capillary pressure model is presented by Eq. (6-4).

$$p_{c,ij} = \sigma_{ij}\, cos\,(\theta_{ij}) \sqrt{\frac{\varphi}{K}} \left(\frac{c_o}{(\frac{s_{nw}-s_{nwr}}{1-s_{nwr}})^{ao}} + \frac{c_w}{(\frac{s_w-s_{wr}}{1-s_{wr}})^{aw}} \right) \tag{6-4}$$

in which, $p_{c,ij}$ introduces the three-phase capillary pressure between phases *i* and *j*, where the subscripts *i* and *j* refer to each of the phases: oil, water, or oil.; σ_{ij} and θ_{ij} denote the interfacial tension and the contact angle between phases *i* and *j*, respectively; c_i and c_j symbolize the capillary entry pressure for the phases *i* and *j*, respectively; *s* shows the saturation of a phase; and a_i stands for the capillary exponent for the phase *i* [100]. The subscripts *nw* and *w* refer to the non-wetting and wetting phases, respectively.

The following assumptions are considered to develop the mathematical model:

- Gravity forces are neglected.
- The flow direction is considered in 1D horizontal in the system.
- The core and fluids are assumed to be incompressible.
- Core is strongly water-wet and homogeneous.
- The equilibrium of capillary forces is held in the system.
- The temperature of the system is 38 ˚C and the thermal equilibrium holds in the system.
- The capillary end-effects are neglected.

In the current work, we simulate a case study, in which a 5 cm (2 inches) core was utilized. Since the diameter of the core is small, the gravity effects are insignificant and 1D flow assumption is satisfactory for the simulation. The two-phase relative permeability parameters are needed to be tuned and optimized in each cycle. To do so, the experimental two-phase data are used for tuning the two-phase relative permeability models. Afterwards, the tuned two-phase relative permeability models are being used in the three-phase relative permeability model.

For each of WF and GI cycles in the WAG injection process, these parameters are optimized again, to incorporate the saturation and cyclic process hysteresis.

6.3.4 Design of Experiments (DOE)

Due to the three-phase flow in the porous medium and the cyclic nature of the WAG flooding, the number of influential variables is higher than other conventional oil recovery techniques. Using a

design of experiment (DOE) approach can reduce the computational costs required for mathematical modeling runs. The key aspect of a DOE is the selection of controlling factors. In this study, oil viscosity (μ_o), gas and water injection rates (q_g and q_w), system permeability (K), pore volume injection of fluids (PVI), and number of cycles (N) are chosen to determine the dimensionless numbers and their significance. Using a two-level full factorial DOE, each parameter is studied at two levels with the upper and lower bounds coded as +1 and -1. Table 6-1 shows the upper and lower levels of all variables.

Table 6-1: Design matrix of factors.

Factors	Level	
	Low (-1)	High (+1)
μ_o (Pa.h)	1.11e-8	1.11e-8
q_w (m^3/hr)	25e-6	40e-6
q_g (m^3/hr)	25e-6	40e-6
K (mD)	65	200
PVI	0.5	1
N	0.5	3

In the case of six factors (variables) at two levels, the model run design is called 2^6 full factorial design. Thus, the total of 96 runs are required with no replicates of each run to obtain each response.

6.3.5 Dimensionless Scaling Groups

As mentioned before, having an adequate knowledge of WAG process helps use the Buckingham's π Theorem and derive the dimensional groups in the dimensional analysis. We consider six variables, four fixed parameters, and the recovery factor (RF) as the response variable to obtain the dimensionless numbers (see Table 6-2).

Table 6-2: Variables needed to develop the dimensionless numbers.

Variables	Fixed Parameters	Response Variable
μ_o (cP)	σ_{ow}(N/m)	*RF*
q_w (m^3/h)	σ_{og} (N/m)	
q_g (m^3/h)	μ_w(cP)	
K (mD)	μ_g(cP)	
PVI		
N		

Hence, seven dimensionless numbers are introduced using the Buckingham's π Theorem, which are listed below:

$$\pi_1 = \frac{\sigma_{ow}.K}{\mu_w.q_w} \quad (6\text{-}5)$$

$$\pi_2 = \frac{\sigma_{og}.K}{\mu_g.q_g} \quad (6\text{-}6)$$

$$\pi_3 = \frac{\mu_o}{\mu_g} \quad (6\text{-}7)$$

$$\pi_4 = \frac{\mu_o}{\mu_w} \quad (6\text{-}8)$$

$$\pi_5 = \frac{q_w}{q_g} \quad (6\text{-}9)$$

$$\pi_6 = PVI \quad (6\text{-}10)$$

$$\pi_7 = N \quad (6\text{-}11)$$

where σ_{og} and σ_{ow} denote the interfacial tension between the oil-gas and oil-water phases, respectively; μ_i refers to the viscosity of the phase *i*; q_w and q_g represent the water and gas injection rates; *PVI* is the pore volume injection during each injection mode (WF or GI); and *N* introduces the number of injected cycles.

6.3.6 Analysis of Variance (ANOVA)

Lorenzen and Anderson [102] reported that ANOVA is the most accurate method to investigate the significant effects of factors. In the ANOVA table, the *F* test and *P* values represent the main and interaction effects, respectively [103]. The *P* value denotes the probability of error involved in the

obtained results [104-105]. Accordingly, the smaller values of *P*, the more significant the corresponding coefficient term is [106]. The *P* value corresponds to an α value of 0.05. For a factor with α lower than 0.05, the factor is considered as significant. In this study, we perform an ANOVA analysis for the simulation results and corresponding dimensionless numbers. Table 6-3 presents the results of the ANOVA to show the significance of each factor, statistically. Thus, the relevancy and importance of the input variables in a WAG flooding process can be determined through implementing the ANOVA.

Table 6-3: Analysis of variance (ANOVA) table to assess design parameters in porous and non-porous media.

Source	*Sum Sq*	*d.f*	*F*	*P*
π_1	0.0092	2	6.66	0.0018
π_2	0.01592	1	10.45	0.001
π_3	0.01	4	200.243	<0.0001
π_4	0.0153	1	40.34	0.00132
π_5	0.01888	1	12.39	0.0007
π_6	0.06351	1	4.67	0.0023
π_7	0.06137	4	348.21	<0.0001
Error	0.15638	8		
Total	0.19418	22		

6.3.7 GEP Procedure

As previously mentioned, the GEP algorithm uses two entities: the ETs and chromosomes. A chromosome consists of constant and variable terminals as well as pre-arranged functions in one or more genes with equal lengths [91]. The function and variables are the input data, while the constant values are generated by the algorithm within a range specified by the user. Each gene contains a head made of functions, variables, and constants, and a tail of terminals [91]. The size of the head (*h*) is specified by the user; however, the size of the tail (*t*) is computed as a function of "*h*" and a parameter "*n*", which defines as the number of elements in the function sets. The tail size of a chromosome can be obtained using the following equation:

$$t=h(n-1)+1 \quad (6\text{-}12)$$

where *t* and *h* are the tail and head of the gene; and *n* represents the number of elements of the function used in the head of the gene. Figure 6-2 demonstrates an example of a two-gene chromosome resulted by four functions of $\times, \div, +,$ and $\sqrt{}$, and three terminals including *a*,*b*, and *c*. In Figure 6-2, both the mathematical and the equivalent expression tree forms using Kara language are illustrated.

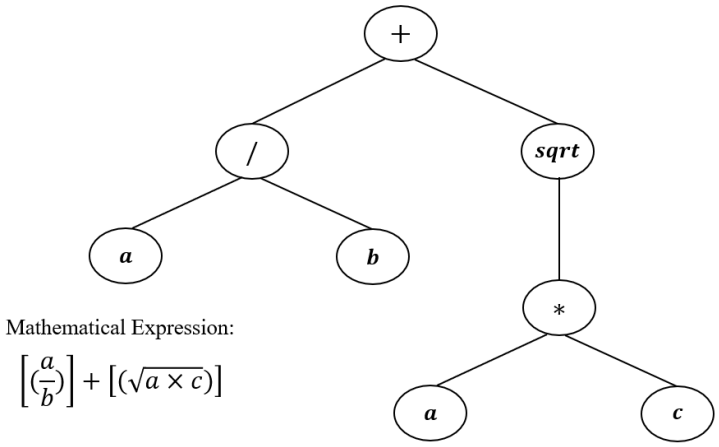

Figure 6-2: A typical two-gene chromosome with its corresponding mathematical expression (Modified after Gharagheizi et *al*. [47]).

Every character sets in one spot from zero to seven, which is shown by 01234567. In the case of multigenetic chromosomes, all ETs are connected by their root nodes through a linking function such as Boolean function [107]. The computational procedure of GEP algorithm is summarized in the following steps [46]:

1- Initializing the population through generating random chromosomes of a certain number of individuals.
2- Fitting the population individuals according to the fitness functions.
3- Selecting some individuals and copying them for the next generation based on their fitness, such as the simple elitism [88].
4- Applying the same procedure for the new population including the selection of the environment, expression of genomes, selection of the population individuals, and reproduction with modification.

5- Repeating the previous steps until the termination criteria are met.

6.3.8 Model Development Steps

Using the GEP algorithm, there is no need to assume pre-specified correlation formats for accurate prediction of target data. Hence, the GEP's computation process finds the most accurate forms of independent parameters by itself. As previously discussed, the main parameters affecting the *RF* of a WAG injection process are oil viscosity, water and gas injection flowrates, permeability of the system, *PVI*, and the number of injected cycles (*N*). Therefore, the variables are used to generate the dimensionless numbers; these groups are assumed as correlating parameters for predicting the *RF* of WAG flooding:

$$\pi_i = f(\mu_o, q_w, q_g, PVI, K, N, \text{Fixed parameters}) \quad (6\text{-}13)$$

where $RF_{WAG} = f(\pi_i)$

The following steps are taken to develop a newly WAG *RF* correlation:

1- Generating the population using random chromosome individuals and applying correlation formats as pars trees using the functions or operators (*, +, -), and terminals which are functions of input variables and output results (*RF* of WAG).

2- Computing the fitness value for each individual of the generated population using the following objective function (*OF*):

$$OF = \frac{100}{N}\sum_i^N \frac{|RF_{prd}(i) - RF_{exp}(i)|}{RF_{exp}(i)} \quad (6\text{-}14)$$

where *N* is the number of data points used for the GEP implementation, and subscriptions "*prd*" and "*exp*" denote the *RF* values predicted by the GEP algorithm and the *RF* values generated by the verified mathematical model to be used as the experimental (or target) data, respectively.

3- Selecting some individuals and copying them into the next generation based on their fitness (simple elitism). In this work, the tournament method is implemented to select adequate varieties of the population in each generation [45-46].

4- Applying the genetic operators on selected chromosomes, including:

- Replication operator: This operator copies the chromosome's structure selected in step 3.
- Mutation operator: As the most important step in the GEP algorithm, the mutation can occur anytime and at any position in a genome, as long as the mutated chromosome meets the validity criteria. The mutation operator changes the head and tail terminals, while the original structure of the chromosome is preserved.
- Inversion: The inversion operator is only applied to the heads of genes, where any sequence is randomly selected and employed. The inversion operator by random selects the chromosome, the gene to be modified, and the initiation and termination points of the sequence to be inverted.

5- Transposition and insertion sequence elements: A portion of the genomes, which can be activated and jumped to another place in the chromosome, are called the transposable elements of the GEP program. Ferreira divided these elements into three types [46]: "short fragments with either a terminal or function in the first position transpose to the head of genes, short fragments with a function in the first position that transpose to the rest of the head of genes (root IS elements or RIS elements), and entire genes that transpose to commencing of chromosomes."

6- Recombination: This step normally involves two parent chromosomes to produce two new chromosomes through combining various parts of the parents through three approaches: linking one-point recombination, two-point recombination, and gene recombination [46]. Accordingly, the new generation will be reproduced, and the procedure is continued until the termination criteria are met.

In this study, the data are distributed into two categories: training and testing/validation sub-data sets by a ratio of 67 % and 33 %, respectively. The training phase is carried out for the developing the model. After this stage, the validation data set is used to assess the validity of the model. Figure 6-3 illustrates a schematic flowchart of the procedure applied in this study to develop a correlation for recovery factor of WAG.

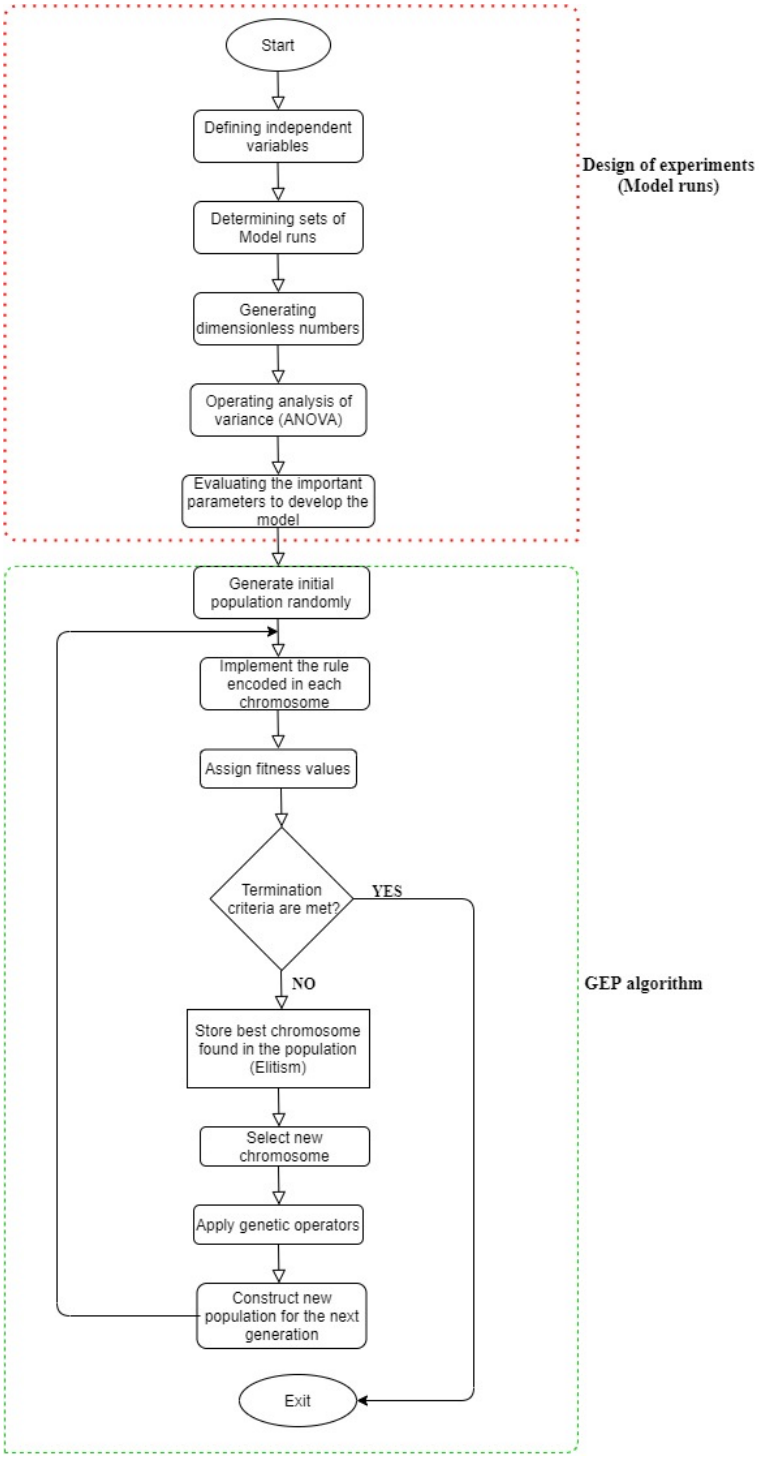

Figure 6-3: A schematic flowchart of workflow for developing the WAG recovery factor correlation in this research.

6.4 Results and Discussions

6.4.1 Model Development

In order to develop a new reliable correlation for estimating the WAG injection using the GEP approach, some important factors/parameters in the GEP strategy including population size, number of chromosomes, head size, number of genes, type of the fitness function, map operators, and number of constants per genes are required. The optimal/adjusted parameters for this work are listed in Table 6-4. For instance, the number of constants per gene determines the maximum number of constants that can be allocated for a gene. The higher numbers of constant, more complicated, and accurate the algorithm becomes. Therefore, a balance should be between the accuracy and degree of complexity while selecting the optimized GEP configuration. The optimal parameters are normally found randomly for development of any new correlation through GEP.

Table 6-4: The optimal GEP parameters.

Configuration	Value
Population size	96
No of chromosomes	33
Head size	8
No. of genes	4
Fitness function	*RMSE*
Map operators	$+, -, ^{\wedge}, \times, \div, \sqrt{}, Ln, Log, \ldots$
No. of constant per gene	10

In this modeling method, 67 % of data for the oil recovery factor are allocated to the training step. Then, 33 % of the entire database is considered as unseen data for the testing phase. It is found that the model is satisfactory and can predict the unseen data within almost the same accuracy obtained in the training phase. The model is developed based on the GEP algorithm using the GeneXproTools software [108]. To examine the accuracy of the newly developed model, a systematic error analysis should be conducted. The statistical parameters including mean square error (*MSE*), root mean square error (*RMSE*), mean absolute error (*MAE*), residual standard error (*RSE*), relative absolute error (*RAE*), and coefficient of determination (R^2) are used for statistical analysis of the developed model. Thus, the error analysis can effectively test the reliability and accuracy of the

proposed model. For instance, the R^2 parameter demonstrates the degree of match between the target data generated by the mathematical model and the calculated *RF* data using the new proposed correlation. Equations (6-15) to (6-19) express the mathematical formulas of the statistical measures used in this study.

Table 6-5 presents the results of statistical error analysis for both the training and testing phases. The low values of error as well as the high magnitudes of correlation of determination ($R^2_{Training}$ = 0.93 and $R^2_{Testing}$= 0.92) for both phases confirm the effectiveness and precision of the new GEP correlation.

$$MSE = \frac{1}{n}\sum_{i=1}^{n}(RF(i)_{exp} - RF(i)_{prd})^2 \quad (6\text{-}15)$$

$$RMSE = \sqrt{\frac{1}{n}\sum_{i=1}^{n}(RF(i)_{exp} - RF(i)_{prd})^2} \quad (6\text{-}16)$$

$$MAE = \frac{1}{n}\sum_{i=1}^{n}(RF(i)_{exp} - RF(i)_{prd}) \quad (6\text{-}17)$$

$$RSE = \sqrt{\frac{1}{n-2}\sum_{i=1}^{n}(RF(i)_{exp} - RF(i)_{prd})^2} \quad (6\text{-}18)$$

$$RAE = \frac{\sum_{i=1}^{n}|RF(i)_{exp} - RF(i)_{prd}|}{\sum_{i=1}^{n}|RF(i)_{exp} - ave(RF_{\exp})|} \quad (6\text{-}19)$$

Table 6-5: Statistical analysis of training and testing results.

Error statistics	Training	Testing
MSE	1.38E-03	4.30E-03
RMSE	3.72E-02	6.56E-02
MAE	3.06E-02	5.15E-02
RSE	7.15E-02	0.232917
RAE	0.268548	0.478682
Correlation Coefficient	0.963596	0.876774
R^2	0.928518	0.9193

Moreover, cross plots or parity diagrams and residual scattering error distribution plots are provided to graphically investigate the error analysis. After conducting the ANOVA test, the selected dimensionless numbers ($\pi_1$to π_7) are introduced as variables to the GEP simulator for

generating the correlation. The final form of the developed correlation using the GEP algorithm for predicting the recovery factor of a WAG process is expressed as follows:

$$A_1 = \frac{1-\left[(1-\pi_1\times 1e-2).\frac{c_{11}.\pi_4}{c_{10}^2}\right]}{c_{13}.c_{15}.c_{18}.(d_2-d_5)} \tag{6-20}$$

$$A_2 = \frac{(\left[(\pi_7-c_{22}).\pi_1^3.\pi_2.c_{28}\times 1e-10\right]^4+\pi_7^{c_{29}^4})}{2} \tag{6-21}$$

$$A_3 = \frac{[(c_{35}-c_{32})+(\pi_6.\pi_7^2)+\pi_5.c_{32}+\pi_6.\pi_7]}{4}.\frac{\pi_4^2}{\pi_3} \tag{6-22}$$

$$A_4 = \exp(1+\pi_5-\pi_3).c_{49}.\left[(\pi_2.\pi_7\times 1e-4)+\frac{\pi_3-\pi_5-\pi_2\times 1e-4-c_{42}}{2}\right] \tag{6-23}$$

$$RF = A_1 + A_2 + A_3 + A_4 \tag{6-24}$$

The constant values of Eqs. (6-20) to (6-24) are listed in Table 6-6.

Table 6-6: The constant values obtained for Eqs. (6-20) to (6-24).

Constant	Value
C13	-4.7530
C15	-5.4106
C18	-7.5887
C11	6.7068
C10	2.2652
C28	11.5608
C29	0.7480
C22	-59.7849
C35	-7.7281
C32	9.5931
C49	8.75E-02
C42	0.4019

Table 6-7 shows the statistical information of the input variables, i.e. dimensionless numbers ($\pi_1$to π_7) including the minimum, maximum, standard deviation, slope, intercept, correlation, and *R-square* versus the response variable which is the *RF*.

Figure 6-4 demonstrates the newly developed correlation in the form of an expression tree (ET) diagram. The generated ET consists of four sub-ETs (four genes) and each sub-ET is linked with the "addition" operator to the others. The input values to the model ($\pi_1$to π_7) are expressed as $d_0$to d_6 within the sub-ETs.

Table 6-7: The statistics of the input variables to develop the new correlation with regard to the response variable (*RF*).

Attribute	π_1	π_2	π_3	π_4	π_5	π_6	π_7
Importance	1.89E-02	1.70E-02	3.66E-01	1.88E-01	2.30E-02	1.53E-02	0.371409
Minimum	3.16E-02	4.71E-02	1.608696	6.17E-02	0.625	0.5	1
Maximum	1.56E-01	0.231884	16.08696	0.616667	1.6	1	3
Average	8.22E-02	0.124819	8.621603	0.330495	1.065625	0.757813	2.140625
Median	7.39E-02	1.10E-01	1.608696	6.17E-02	1	1	2
Standard Deviation	4.63E-02	7.19E-02	7.292794	0.279557	0.358444	2.52E-01	0.833185
R^2 (vs Response)	2.62E-03	2.30E-04	3.24E-01	0.324006	4.51E-03	4.12E-03	0.567451

Figure 6-4: The correlation introduced for prediction of WAG *RF* in the form of an expression tree.

6.4.2 Relative Importance (RI) of Input Variables

The importance of each input variable (e.g., dimensionless numbers) used for developing a correlation is associated with the weight and effect of the variable on the objective function; this is important for better design and optimization of the corresponding operation. The relative importance of the dimensionless numbers generated in this study is depicted in Figure 6-5. According to Figure 6-5, π_7 or the number of WAG cycles has the highest impact on the developed

correlation with a relative importance (RI) of 37.14 %. This is logical since through injecting consecutive WAG injection cycles (and thereby increasing the number of cycles (*N*)), higher recovery factor is expected from the porous system. After π_7, $\pi_3$and $\pi_4$are reported as the most important parameters. According to Figure 6-5, there is a noticeable difference between the ratio of oil to gas viscosities (π_3) and the viscosity ratio of oil to water (π_4) in terms of variable importance. This is due to a higher viscosity difference between the oil phase and the gas phase, compared to the oil and water system. Moreover, the injection rate ratio of the water to the gas (π_5), inverse of oil-water capillary number (π_1), inverse of oil - gas capillary number (π_2), and *PVI* injection (π_6) have the relative importance values of 2.30 %, 1.89 %, 1.69 %, and 1.52 %, respectively.

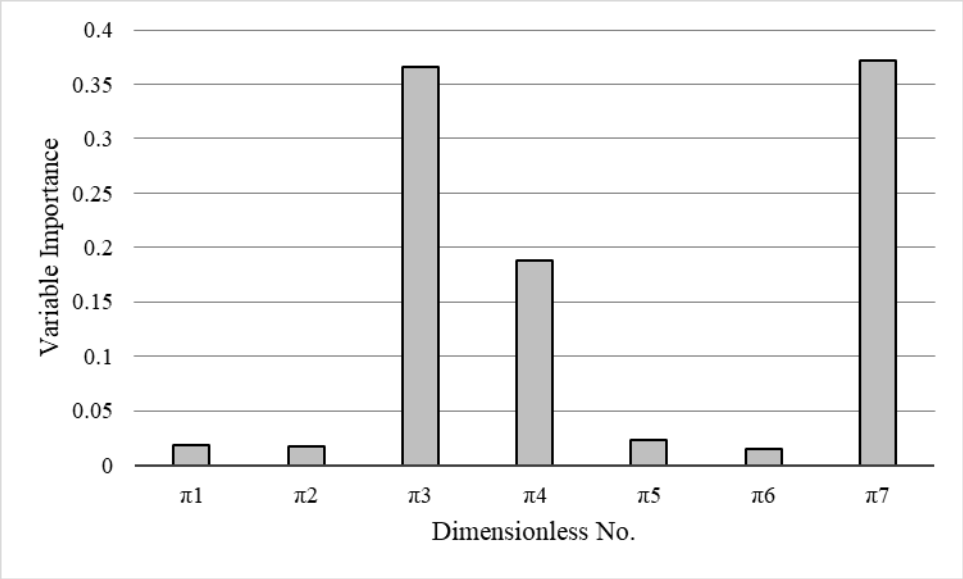

Figure 6-5: Relative importance of all input variables included in the new correlation for RF determination of WAG injection process.

In Figure 6-6, the cross plots show a part of error analysis for the training and testing phases of the employed connectionist tool. As clear from Figure 6-6a and Figure 6-6b, a good match is noticed between the target data and RF predictions based on the newly developed correlation. The magnitudes of the coefficient of determination R^2=0.9285 for the training phase, and the coefficient of determination R^2=0.9193 for the testing phase confirm that the proposed correlation is reliable and accurate for predicting oil recovery factor in a WAG injection process.

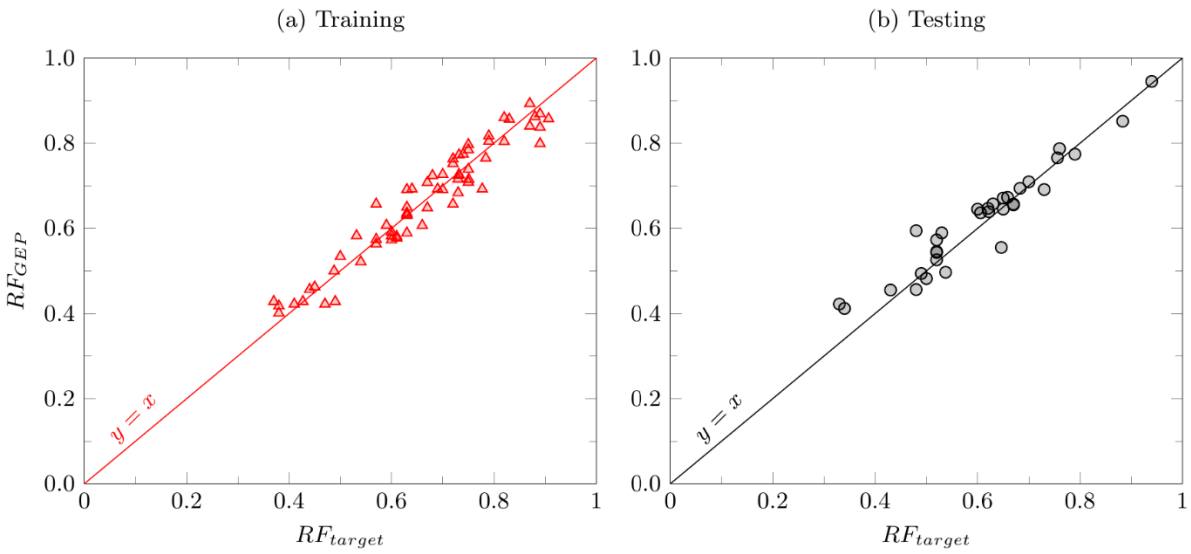

Figure 6-6: Cross plot of training data against the target values.

Figure 6-7 shows the residual plot with the residual error, e_i (Eq. (6-25)), on the *y*-axis and the predicted recovery factor values on the *x*-axis.

$$e_i = RF_{i,Target} - RF_{i,GEP} \tag{6-25}$$

According to Figure 6-7, for both testing and training phases, the absolute residual error values are less than 0.1. It is concluded that the obtained data are unbiased within an average approximately zero around the zero residual line; it also indicates a homoscedastic behavior (constant variance).

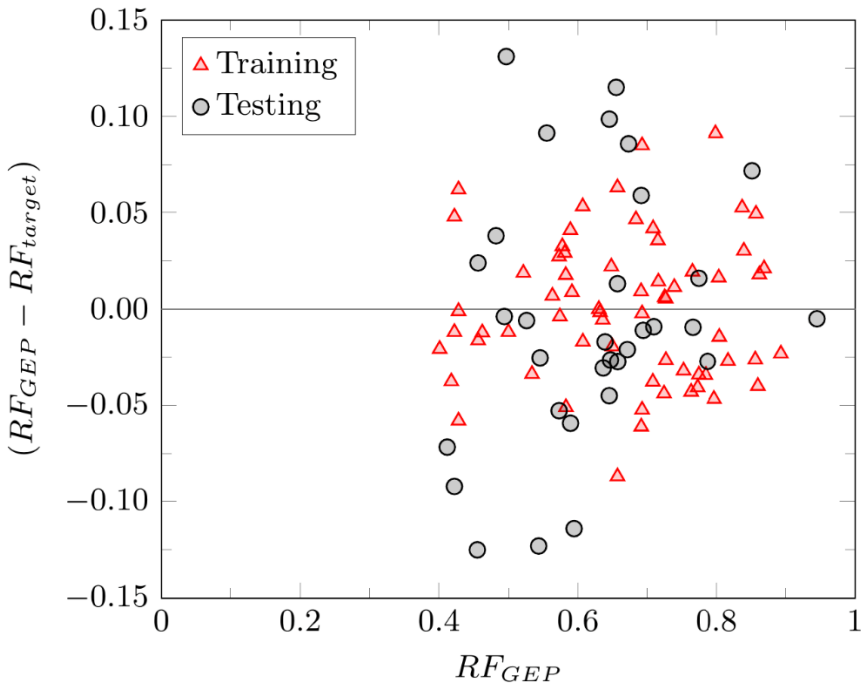

Figure 6-7: Scatter residual error plot of training and testing phases.

6.4.3 Evaluation of Developed Correlation

To assess the performance of the newly developed correlation (Eqs. (6-20) – (6-24)), the predicted recovery factors of a three-cycle WAG injection process are compared with the experimental data and the results obtained by the mathematical model. In the selected experiments, the WAG flooding process was conducted at the near-miscible condition (T=38 °C, and P=12.7 MPa), and in a strongly water-wet sandstone starting with a primary waterflooding (two-phase flow where s_{gi}=0). The process was then followed with the first gas injection in which the first cycle of the WAG injection was complete (N=1). The consecutive injections of water and gas continued for three cycles (N=3). The process was terminated after the third gas injection where no significant amount of oil was recovered from the porous system. In the experiments, the process was conducted at WAG ratio of 1:1 with a constant gas injection rate (e.g., q_{inj}=25 cm^3/hr). The recovery factor against the number of injected cycles (N) based on the experimental data, predicted values by the new correlation, and the estimated values by the mathematical model is presented in Figure 6-8.

Table 6-8: Comparison of RF of near-miscible WAG injection obtained by the developed correlation, mathematical model, and experimental work.

N	RF_{GEP} (%)	*Relative Error*$^{GEP\text{-}Exp}$ *(%)*	RF_{Target} (%)	*Relative Error*$^{GEP\text{-}Target}$ *(%)*	RF_{Exp} (%)
0.5	59.35	18.77126	50.08	18.51038	49.97
1	69.2	5.503888	64.64	7.054455	65.59
1.5	76.08	5.651993	71.94	5.754796	72.01
2	81.56	3.083923	79.37	2.759229	79.12
2.5	86.22	1.328006	84.3	2.27758	85.09
3	90.32	3.48365	92.00	1.826087	93.58

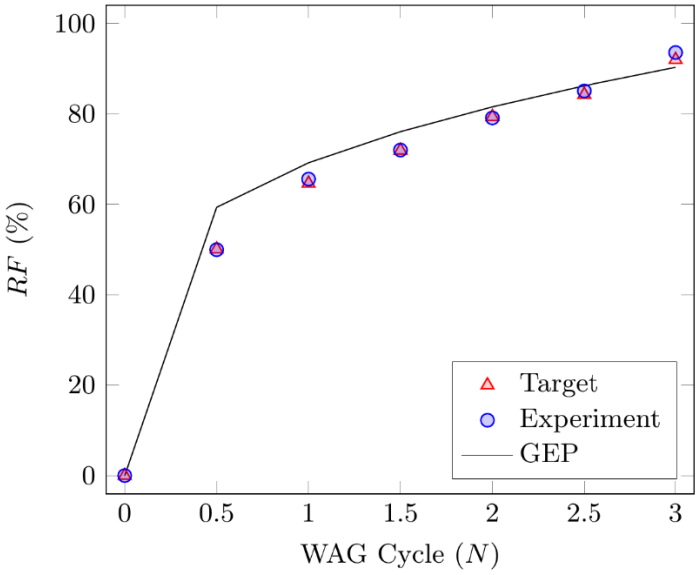

Figure 6-8: Comparison of RF of near-miscible WAG injection obtained by the developed correlation, mathematical model, and experimental work.

After the primary water flooding (*N=0.5*), the recovery factor of *RF*=50.00 % was obtained in the experimental run. The mathematical model is able to predict a recovery factor of *RF*=50.08 %, confirming the accuracy and reliability of the numerical model. The newly developed correlation forecasts a recovery factor of *RF*=59.35 % at the end of the primary waterflooding. Following the production operation by conducting the first gas injection (*N*=1), the experiment resulted in the recovery factor of *RF*= 65.59 %; this was predicted by the mathematical model with the recovery factor of *RF*=64.64 %, implying excellent agreement. The proposed correlation predicts the

recovery factor of *RF*= 69.20 % for this stage. After that, two more cycles were injected to the porous medium and the final recoveries of *RF*=93.58 %, 92.00 %, and 90.32 % were obtained through the experimental phase, numerical model, and newly developed correlation, respectively. The details of the recovery factor at each injection mode are given in Table 6-8. The relative errors in estimating the recovery factor at different cycles (*N*=1 to 3) are also listed in Table 6-8. According to Table 6-8 and Figure 6-8, it is found that the correlation developed by the GEP algorithm is able to successfully predict the RF of the intermediate cycles and more importantly the ultimate recovery factor with the relative error of 3.48 % at *N*=3.

Comparing the methodology used in this chapter (Chapter 6) with the ones in chapter 3, and 5, depending on the purpose of the study and the availability of the data each one of these techniques can be useful. For instance, to have a mechanistic overview on WAG injection process, fluid flow, including the saturation history and saturation distribution in the porous medium, the application of IMPES method (described in chapter 3, and 5) is recommended. However, if the data for recovery factors of a case are available and one aims to acquire an overview only over the performance (RF) of a system by changing the key parameters and their interactions (dimensionless numbers) the application of a specified correlation generated by the GEP algorithm is more beneficial.

6.4.4 Effect of Capillary Number

The efficiency of oil recovery techniques depends on interplay between various forces at pore scale and macroscopic scale [109]. The capillary and viscous forces are not in favor of each other during implementing an EOR/IOR process. The capillary forces are responsible for entrapment of fluids during immiscible/near-miscible processes. However, viscous forces of the displacing (injecting) phase act against the capillary forces. The capillary forces are affected by the interfacial tension (IFT) between phases, wettability state of the system, and the pore geometry in which the blobs entrapment of phases occurs. Viscous forces, on the other hand, are governed by the permeability of the rock, applied pressure drop, and the viscosity of the displacing phase [110]. In oil and gas industry, the capillary desaturation curves are well recognized for highlighting the properties and geometry of the porous systems as well as the fluids distribution within the pores [111]. Increasing the capillary number has always been set as a target for designing EOR/IOR processes in order to achieve a higher oil recovery from reservoirs. Capillary number (N_{ca}) is defined as the ratio of viscous forces to capillary forces [112]. There are numerous expressions for the capillary number.

Among the proposed versions, the capillary number introduced by Saffman and Taylor [113] is the most common form, as given below:

$$N_{ca} = \frac{v\mu}{\sigma} \tag{6-26}$$

where the v is the superficial velocity; μ stands for the viscosity of the displacing phase; and σ refers to the interfacial tension between fluids.

In this work, after applying the Buckingham's π Theorem, a variation (inverse) of the capillary number between the oil-water (N_{ca}^{ow}) and oil-gas (N_{ca}^{og}) systems are generated as follows:

$$\pi_1 = \frac{\sigma_{ow}.K}{\mu_w.q_w} = \frac{1}{N_{ca}^{ow}} \tag{6-27}$$

$$\pi_2 = \frac{\sigma_{og}.K}{\mu_g.q_g} = \frac{1}{N_{ca}^{og}} \tag{6-28}$$

where σ_{og} and σ_{ow} denote the interfacial tension between the oil-gas and oil-water phases, respectively. μ_i refers to the viscosity of phase *i;* q_w and q_g represent the water and gas injection rates; and *K* is the permeability of the medium. Since π_1 and π_2 show approximately the same relative importance within the developed correlation for predicting the RF of the WAG flooding process, a sensitivity analysis on the impact of π_1 on RF of WAG injection is conducted. To investigate the impact of capillary number (the inverse of π_1) on oil recovery factor, the results of WAG recovery factor for three cycles (*N*=1,2,3) at three orders of magnitude of π_1 are compared in Figure 6-9. According to the results presented in Figure 6-9, by increasing the π_1 from the initial value of 8.16e-5 (corresponding to the value at the experimental condition) to 8.16e-2, and 8.16e-1, the ultimate recovery factor of WAG injection decreases from 90.32 % to 85.79 %, and 75.03 %, respectively. This implies that the recovery factor of a WAG injection process decreases by 16.92 % upon a decrease in the capillary number by four orders of magnitude. The same trend of RF reduction at higher values of π_1 is noticed at the end of the first and middle injection cycles. Increasing $\pi_1$by four orders of magnitude (corresponds to decreasing the capillary number by four orders of magnitude) lowers the ultimate *RF*s of the first (*N=1*), and the second (*N=2*) cycles by 22 % and 23.1 %, respectively. This result highlights the dominancy of viscous forces at low capillary numbers, resulting in more oil trapping in the porous medium and decrease in oil *RF* during various cycles of a WAG flooding process.

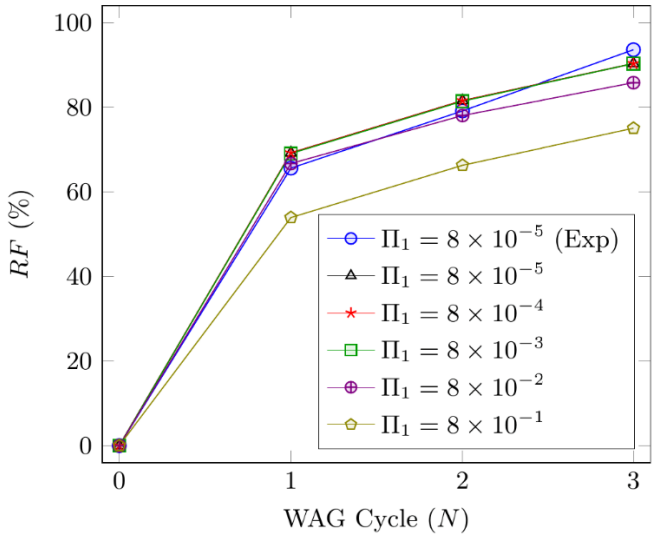

Figure 6-9: Effect of oil inverse capillary number (π_1) on the recovery factor of near-miscible WAG injection using the GEP correlation.

6.4.5 Effect of Viscosity Ratio (π_3, π_4)

The viscosity of fluids in three-phase flow of oil, water, and gas affects the mobility ratio (M) of the displaced (oil) and displacing phases, residual oil saturation, and finally the recovery factor of a WAG flooding process. The mobility ratio is defined as follows:

$$M = \frac{\frac{k_{r,ing}}{\mu_{ing}}}{\frac{k_{r,ed}}{\mu_{ed}}} \tag{6-29}$$

In Eq. (6-29), k_{ring} and k_{red} represent the relative permeability of the displacing (water or gas) and displaced (oil) phases, respectively. μ_{ing} and μ_{ed} denote the viscosities of the displacing and displaced phases.

In this research, two of the introduced dimensionless groups describe the ratio of oil to gas, and oil to water viscosities ($\pi_3 = \frac{\mu_o}{\mu_g}, \pi_4 = \frac{\mu_o}{\mu_w}$), which considerably affect the RF of WAG flooding. To evaluate the impact of the viscosity ratio, WAG simulations are conducted at different values of π_3 and π_4 (Figure **06-10** and Figure 6-11). All cases are simulated using the developed correlation in all three cycles (N=1,2,3), where the rest of dimensionless groups are fixed at the base condition corresponding to the experimental data. We examine the performance of the WAG injection at three values of π_3: 1.59 (the base value), 2, and 3. The simulation outputs are shown in Figure **06-10**. The *RF* results reveal that in all cycles by increasing the π_3 value, the RF decreases. When π_3 increases from 1.59 ($RF^{ultimate}$= 90.32 %) to 2 ($RF^{ultimate}$= 84.14 %), and 3

($RF^{ultimate}$= 76.66 %), the ultimate recovery factors of WAG injection after three cycles of injection decrease by 6.84 % and 15.12 %, for π_3=2, and π_3=3, respectively. Increasing π_3 also decreases the oil recovery at the first and second injection cycles, significantly. The *RF* results at each cycle are provided in Table 6-9. The results are consistent with the previous studies in which the higher viscosity difference between the oil and gas leads to unfavorable high mobility ratio, bypassing the oil bank (gas channeling), and early gas breakthrough [33].

The sensitivity analysis is also performed, considering different values of $\pi_4 = \frac{\mu_o}{\mu_w}$. The simulations are conducted using the experimental conditions and at three cycles of consecutive injections of water and gas for three values of π_4: 0.061 (reference value corresponding to the experimental condition), 0.10, and 0.12. The outputs of the simulations for three cycles of WAG injection are demonstrated in Figure 6-11 and Table 6-9. Based on the simulation results of the WAG process using the GEP correlation (Eqs. (6-19)-(6-23)), increasing the values of π_4 from 0.061 to 0.10, and 0.12, lowers the ultimate recovery factor by 6.72 % and 10.11 %, respectively. This appears to be logical as the π_4 (the ratio of oil to water viscosity) increases the mobility ratio of the oil (as the displaced phase) and water (as the displacing phase) which is unfavorable, resulting in front instability of fluids and considerable residual oil saturation. Comparing Figure **06-10** and Figure 6-11 also highlights the superior impact of π_3 on *RF* of WAG injection over the impact of π_4 ; this is also confirmed while assessing the relative importance of the variables (dimensionless groups). This is due to higher viscosity difference between oil and gas, compared to the difference of oil-water viscosities, leading to higher potential of oil trapping and early breakthrough, and thereby the *RF* is affected more (greater reduction) at higher values of π_3, compared to π_4.

Table 6-9: π_3 and π_4 sensitivity analysis to assess WAG flooding process.

$\pi_3 = \frac{\mu_o}{\mu_g}$	*N*	*RF (%)*	$\pi_4 = \frac{\mu_o}{\mu_w}$	*RF (%)*
1.59E+00	1	69.20	0.0611	69.20
	2	81.56		81.56
	3	90.32		90.32
2.00E+00	1	63.15	0.100	62.14
	2	75.46		74.89
	3	84.14		84.25
3.00E+00	1	57.00	0.120	59.40
	2	70.00		73.42
	3	76.66		81.19

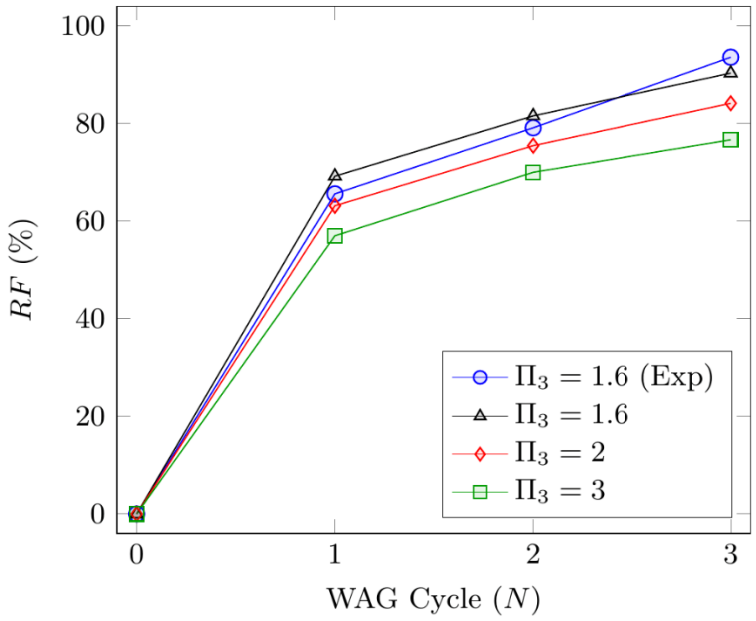

Figure 06-10: Effect of oil to water viscosity ratio (π_3) on the recovery performance of near-miscible WAG injection based on the developed correlation.

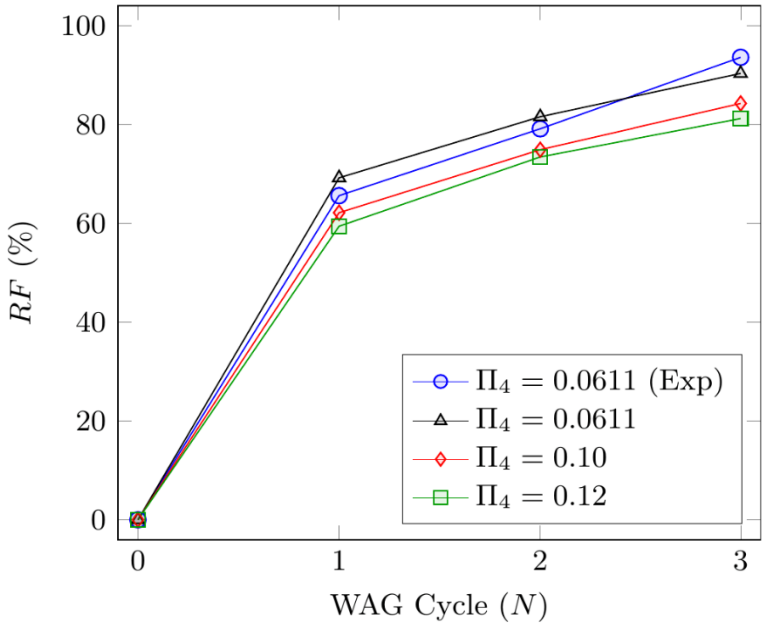

Figure 6-11: Impact of oil to gas viscosity ratio (π_4) on the recovery performance of near-miscible WAG injection based on the GEP correlation.

6.5 Summary and Conclusions

In this study, we develop a new correlation for predicting the recovery factor (RF) of a near-miscible water alternating gas (WAG) injection process. The model is developed using dimensionless groups made of the key fluid, rock, and process characteristics that impact the *RF* of a near-miscible WAG flooding process. Seven dimensionless groups are generated using the dimensional analysis approach through employing the Buckingham's π theorem. The dimensionless numbers are used as the input variables for the newly introduced evolutionary algorithm gene expression programming (GEP) model to develop a reliable predictive tool for *RF* of WAG processes. The accuracy of the proposed correlation is verified using an experimental case study taken from the literature in which a near-miscible WAG flooding was conducted in a strongly water-wet sandstone at 38 ^{o}C and 12.7 MPa. Based on the error analysis, the newly proposed GEP model shows a very good match with the target data. For example, R^2= 92.85 % and *MSE*=1.38e-3 are attained for the training phase. The results of the relative importance (*RI*) of input variables indicate that the number of injected cycles (N, π_7) has the highest impact on the

developed correlation with an RI of 37.14 %. After π_7, $\pi_3$and $\pi_4$are reported as the most essential parameters with an *RI* of 36.61 %, 18.84 %, and 2.30 %, respectively.

The predicted recovery factors of a three-cycle WAG injection process are compared with the experimental data; the results obtained by the mathematical model show that the correlation developed by the GEP algorithm is able to successfully predict the *RF* of the intermediate cycles and more importantly the ultimate recovery factor with the relative error of 3.48 % at *N*=3.

According to the sensitivity analysis, increasing oil-water capillary number leads to an increase in *RF* in all cycles. In addition, an increase in the magnitudes of oil to gas viscosity ratio and/or oil to water viscosity ratio causes a reduction in *RF* of each cycle in the WAG flooding process. It is found that the viscosity ratio of oil and gas has a greater influence on the *RF* value, compared to viscosity ratio of oil and water because of a greater viscosity difference between oil and gas phases.

For future work, due to the lack of predictive tools for WAG injection process, it is recommended to conduct similar procedures to develop empirical correlations for WAG injection in other porous systems such as fractured and/or heterogeneous porous media. The presented results in this work are based on experimental data of a near-miscible WAG injection in a strongly water-wet Berea sandstone core. This research work can be extended for other miscibility conditions such as miscible/immiscible, at other wettability states and rock lithologies.

ACKNOWLEDGEMENTS

We highly appreciate the support of Equinor Canada, InnovateNL, Natural Sciences and Engineering Research Council of Canada (NSERC), and Memorial University (Canada) over this research study.

NOMENCLATURES

Acronyms

ANOVA	Analysis of variance
CCD	Central composite design
DCI	Dimensionless CO_2 injection
DCP	Dimensionless CO_2 production
DEOR	Dimensionless tertiary oil recovery
DOE	Design of experiment
DTI	Dimensionless total injection

EOR	Enhanced oil recovery
ET	Expression tree
GA	Genetic algorithm
GEP	Gene expression programming
GI	Gas injection
GP	Genetic programming
IFT	Interfacial tension
IOR	Improved oil recovery
IMPES	Implicit-pressure-explicit-saturation
M	Mobility ratio
MMP	Minimum miscible pressure
MSE	Mean square error
N	Number of injected cycles
OF	Objective function
PSO	Particle swarm optimization
PVI	Pore volume injection
RAE	Relative absolute error
RF	Recovery factor
RI	Relative importance
RMSE	Root mean square error
RSE	Residual standard error
WF	Waterflooding
WAG	Water-alternating-gas

Variables and Parameters

a	Capillary exponent
C_{ij}	Correlation constant values
C_i	Capillary constant
F	The main effect of factors in ANOVA
K	Absolute permeability
k_{ri}	Relative permeability of phase i

p	Pressure
P_{value}	The interaction effect of factors in ANOVA
q	Flowrate
R^2	Coefficient of determination
s_i	Saturation of phase i
t	Time
v	velocity
x	Length

Greek Letters

μ	Viscosity
ρ	Density
σ	Interfacial tension
ϕ	Porosity
θ	Contact angle
π_i	Dimensionless number

Subscripts and Superscripts

ave	Average
ca	Capillary
D	Drainage
ed	Displaced phase (oil)
exp	Experiment
g	Gas phase
ing	Displacing phase
I	Imbibition
nw	Non-wetting phase
o	Oil phase
og	Oil-gas system
ow	Oil-water system
r	Residual phase
w	Wetting phase

References

1. Afzali, S.; Rezaei, N.; Zendehboudi, S., A comprehensive review on enhanced oil recovery by water alternating gas (WAG) injection. *Fuel* **2018,** *227*, 218-246.
2. Christensen, J. R.; Stenby, E. H.; Skauge, A. In Review of WAG field experience, *International petroleum conference and exhibition of Mexico, Society of Petroleum Engineers* **1998**.
3. Skauge, A.; Stensen, J. Å. In Review of WAG field experience, *1st International Conference and Exhibition, Modern Challenges in Oil Recovery,* **2003**; pp 19-23.
4. Al-Mamari, F.; Al-Shuraiqi, H.; Al-Wahaibi, Y. M. In Numerical simulation and experimental studies of oil recovery via first-contact miscible water alternating gas injection within shaley porous media, *SPE/EAGE Reservoir Characterization and Simulation Conference, Society of Petroleum Engineers* **2007**.
5. Bequette, B. W., Nonlinear control of chemical processes: A review. *Industrial & Engineering Chemistry Research* **1991,** *30* (7), 1391-1413.
6. Duchenne, S.; de Loubens, R.; Petitfrere, M.; Joubert, T. In Modeling and simultaneous history-matching of multiple WAG coreflood experiments at reservoir conditions, *Abu Dhabi international petroleum exhibition and conference, Society of Petroleum Engineers* **2015**.
7. Haajizadeh, M.; Narayanan, R.; Waldren, D. In Modeling miscible WAG injection EOR in the Magnus field, *SPE reservoir simulation symposium, Society of Petroleum Engineers* **2001**.
8. Heeremans, J. C.; Esmaiel, T. E.; Van Kruijsdijk, C. P. In Feasibility study of WAG injection in naturally fractured reservoirs, *SPE/DOE Symposium on Improved Oil Recovery, Society of Petroleum Engineers* **2006**.
9. Larsen, J. A.; Skauge, A. In Simulation of the immiscible WAG process using cycle-dependent three-phase relative permeabilities, *SPE Annual Technical Conference and Exhibition, Society of Petroleum Engineers* **1999**.
10. Rahmawati, S. D.; Whitson, C. H.; Foss, B., A mixed-integer non-linear problem formulation for miscible WAG injection. *Journal of Petroleum Science and Engineering* **2013,** *109*, 164-176.
11. Zuo, L.; Chen, Y.; Dengen, Z.; Kamath, J., Three-phase relative permeability modeling in the simulation of WAG injection. *SPE Reservoir Evaluation & Engineering* **2014,** *17* (03), 326-339.
12. Agada, S.; Geiger, S. In Wettability, trapping and fracture-matrix interaction during WAG injection in fractured carbonate reservoirs, *SPE Improved Oil Recovery Symposium, Society of Petroleum Engineers* **2014**.
13. Agada, S.; Geiger, S.; Elsheikh, A.; Oladyshkin, S., Data-driven surrogates for rapid simulation and optimization of WAG injection in fractured carbonate reservoirs. *Petroleum Geoscience* **2017,** *23* (2), 270-283.

14. Kløv, T.; Øren, P.; Stensen, J.; Lerdahl, T.; Berge, L.; Bakke, S.; Boassen, T.; Virnovsky, G. In Pore-to-field scale modeling of WAG, *SPE Annual Technical Conference and Exhibition, Society of Petroleum Engineers* **2003**.
15. Egermann, P.; Vizika, O.; Dallet, L.; Requin, C.; Sonier, F. In Hysteresis in three-phase flow: experiments, modeling and reservoir simulations, *SPE European petroleum conference, Society of Petroleum Engineers* **2000**.
16. Hustad, O. S.; Browning, D. J. In A fully coupled three-phase model for capillary pressure and relative permeability for implicit compositional reservoir simulation, *SPE/EAGE Reservoir Characterization & Simulation Conference*, **2009**.
17. Jerauld, G., General three-phase relative permeability model for Prudhoe Bay. *SPE reservoir Engineering* **1997,** *12* (04), 255-263.
18. Larsen, J.; Skauge, A., Methodology for numerical simulation with cycle-dependent relative permeabilities. *SPE Journal* **1998,** *3* (02), 163-173.
19. Shahverdi, H.; Sohrabi, M., An improved three-phase relative permeability and hysteresis model for the simulation of a water-alternating-gas injection. *Spe Journal* **2013,** *18* (05), 841-850.
20. Sherafati, M.; Jessen, K. In Modeling and simulation of WAG injection processes-the role of counter-current flow, *SPE Western Regional Meeting, Society of Petroleum Engineers* **2015**.
21. Skauge, A.; Dale, E. I. In Progress in immiscible WAG modelling, *SPE/EAGE Reservoir Characterization and Simulation Conference, Society of Petroleum Engineers* **2007**.
22. Dale, E. I.; Skauge, A., Fluid flow properties of WAG injection processes. *IOR 2005-13th European Symposium on Improved Oil Recovery* **2008,** 2214-4609.
23. Juanes, R.; Patzek, T. W., Analytical solution to the Riemann problem of three-phase flow in porous media. *Transport in Porous Media* **2004,** *55* (1), 47-70.
24. Stone, H., Probability model for estimating three-phase relative permeability. *Journal of Petroleum Technology* **1970,** *22* (02), 214-218.
25. Kulkarni, M. M.; Rao, D. N., Experimental investigation of miscible and immiscible Water-Alternating-Gas (WAG) process performance. *Journal of Petroleum Science and Engineering* **2005,** *48* (1), 1-20.
26. Delshad, M.; Pope, G. A., Comparison of the three-phase oil relative permeability models. *Transport in Porous Media* **1989,** *4* (1), 59-83.
27. Fenwick, D. H.; Blunt, M. J., Network modeling of three-phase flow in porous media. *SPE Journal* **1998,** *3* (01), 86-96.
28. Shahverdi, H.; Sohrabi, M., Relative Permeability Characterization for Water-Alternating-Gas Injection in Oil Reservoirs. *SPE Journal* **2015**.
29. Spiteri, E. J.; Juanes, R., Impact of relative permeability hysteresis on the numerical simulation of WAG injection. *Journal of Petroleum Science and Engineering* **2006,** *50* (2), 115-139.
30. Gharbi, R. B. In Neural Network Prediction Model of Miscible Displacements in Heterogeneous Reservoirs, *Middle East Oil Show, Society of Petroleum Engineers* **2003**.

31. Giordano, R.; Redman, R.; Bratvedt, F., A new approach to forecasting miscible WAG performance at the field scale. *SPE Reservoir Evaluation & Engineering* **1998,** *1* (03), 192-200.
32. Kohata, A.; Willingham, T.; Yunus Khan, M.; Al Sowaidi, A. In Extensive miscible water alternating gas WAG simulation study for a giant offshore oil field, *Abu Dhabi International Petroleum Exhibition & Conference, Society of Petroleum Engineers* **2017**.
33. Afzali, S.; Ghamartale, A.; Rezaei, N.; Zendehboudi, S., Mathematical modeling and simulation of water-alternating-gas (WAG) process by incorporating capillary pressure and hysteresis effects. *Fuel* **2020,** *263*, 116362.
34. Belazreg, L.; Raub, M. R. A.; Hanifah, M. A. B.; Ghadami, N. In WAG cycle dependent hysteresis modelling through an integrated approach from laboratory to field scale, Malaysia oil fields, *SPE/IATMI Asia Pacific oil & gas conference and exhibition, Society of Petroleum Engineers* **2017**.
35. Sanchez, N. L. In Management of water alternating gas (WAG) injection projects, *Latin American and Caribbean petroleum engineering conference, Society of Petroleum Engineers* **1999**.
36. Belazreg, L.; Mahmood, S. M., Water alternating gas incremental recovery factor prediction and WAG pilot lessons learned. *Journal of Petroleum Exploration and Production Technology* **2020,** *10* (2), 249-269.
37. Jaber, A. K.; Awang, M. B.; Lenn, C. P., Box-Behnken design for assessment proxy model of miscible CO_2-WAG in heterogeneous clastic reservoir. *Journal of Natural Gas Science and Engineering* **2017,** *40*, 236-248.
38. Jaber, A. K.; Alhuraishawy, A. K.; AL-Bazzaz, W. H. In A Data-Driven Model for Rapid Evaluation of Miscible CO_2-WAG Flooding in Heterogeneous Clastic Reservoirs, *SPE Kuwait Oil & Gas Show and Conference, Society of Petroleum Engineers* **2019**.
39. Ghiasi, M. M.; Shahdi, A.; Barati, P.; Arabloo, M., Robust modeling approach for estimation of compressibility factor in retrograde gas condensate systems. *Industrial & Engineering Chemistry Research* **2014,** *53* (32), 12872-12887.
40. Kamari, A.; Nikookar, M.; Sahranavard, L.; Mohammadi, A. H., Efficient screening of enhanced oil recovery methods and predictive economic analysis. *Neural Computing and Applications* **2014,** *25* (3-4), 815-824.
41. Nejatian, I.; Kanani, M.; Arabloo, M.; Bahadori, A.; Zendehboudi, S., Prediction of natural gas flow through chokes using support vector machine algorithm. *Journal of Natural Gas Science and Engineering* **2014,** *18*, 155-163.
42. Rashid, S.; Ghamartale, A.; Abbasi, J.; Darvish, H.; Tatar, A., Prediction of Critical Multiphase Flow Through Chokes by Using A Rigorous Artificial Neural Network Method. *Flow Measurement and Instrumentation* **2019,** *69*, 101579.
43. Holland, J. H., Adaptation in natural and artificial systems: an introductory analysis with applications to biology, control, and artificial intelligence. *MIT press* **1992**.
44. Ferreira, C., Gene expression programming: a new adaptive algorithm for solving problems. *arXiv preprint cs/0102027* **2001**.
45. Koza, J. R.; Koza, J. R., Genetic programming: on the programming of computers by means of natural selection. *MIT press* **1992**; Vol. 1.

46. Ferreira, C., Gene expression programming: mathematical modeling by an artificial intelligence. *Springer* **2006**; Vol. 21.
47. Gharagheizi, F.; Ilani-Kashkouli, P.; Farahani, N.; Mohammadi, A. H., Gene expression programming strategy for estimation of flash point temperature of non-electrolyte organic compounds. *Fluid Phase Equilibria* **2012,** *329*, 71-77.
48. Rostami, A.; Hemmati-Sarapardeh, A.; Mohammadi, A. H., Estimating n-tetradecane/bitumen mixture viscosity in solvent-assisted oil recovery process using gep and gmdh modeling approaches. *Petroleum Science and Technology* **2019,** *37* (14), 1640-1647.
49. Rostami, A.; Arabloo, M.; Kamari, A.; Mohammadi, A. H., Modeling of CO_2 solubility in crude oil during carbon dioxide enhanced oil recovery using gene expression programming. *Fuel* **2017,** *210*, 768-782.
50. Kamari, A.; Arabloo, M.; Shokrollahi, A.; Gharagheizi, F.; Mohammadi, A. H., Rapid method to estimate the minimum miscibility pressure (MMP) in live reservoir oil systems during CO_2 flooding. *Fuel* **2015,** *153*, 310-319.
51. Umar, A. A.; Saaid, I. M.; Sulaimon, A. A.; Pilus, R. M., Predicting the Viscosity of Petroleum Emulsions Using Gene Expression Programming (GEP) and Response Surface Methodology (RSM). *Journal of Applied Mathematics* **2020**.
52. Kamari, A.; Sattari, M.; Mohammadi, A. H.; Ramjugernath, D., Reliable method for the determination of surfactant retention in porous media during chemical flooding oil recovery. *Fuel* **2015,** *158*, 122-128.
53. Rostami, A.; Raef, A.; Kamari, A.; Totten, M. W.; Abdelwahhab, M.; Panacharoensawad, E., Rigorous framework determining residual gas saturations during spontaneous and forced imbibition using gene expression programming. *Journal of Natural Gas Science and Engineering* **2020,** *84*, 103644.
54. Mostafa, M. M.; El-Masry, A. A., Oil price forecasting using gene expression programming and artificial neural networks. *Economic Modelling* **2016,** *54*, 40-53.
55. Mashayekhizadeh, V.; Kord, S.; Dejam, M., EOR potential within Iran. *Special Topics & Reviews in Porous Media: An International Journal* **2014,** *5* (4).
56. Ahmed, T., Reservoir engineering handbook. *Elsevier* **2006**.
57. Pudugramam, V. S., A numerical study of CO_2-EOR with emphasis on mobility control processes: Water Alternating Gas (WAG) and foam. *Thesis Dissertation, The University of Texas at Austin* **2013**.
58. Holm, L., Propane-gas-water miscible floods in watered-out areas of the adena field, Colorado. *Journal of Petroleum Technology* **1972,** *24* (10), 1,264-1,270.
59. Moffitt, P.; Zornes, D. In Postmortem analysis: lick creek meakin sand unit immiscible CO_2 waterflood project, *SPE Annual Technical Conference and Exhibition, Society of Petroleum Engineers* **1992**.
60. Watts, R. J.; Conner, W. D.; Wasson, J. A.; Yost, A. B. In CO_2 injection for tertiary oil recovery, Granny's Creek Field, Clay County, West Virginia, *SPE Enhanced Oil Recovery Symposium, Society of Petroleum Engineers* **1982**.
61. Gharbi, R.; Peters, E.; Elkamel, A., Scaling miscible fluid displacements in porous media. *Energy & fuels* **1998,** *12* (4), 801-811.

62. Shahverdi, H. Characterization of three-phase flow and WAG injection in oil reservoirs. *Thesis Dissertation, Heriot-Watt University,* **2012**.
63. Birkhoff, G., Hydrodynamics, a study in logic, fact, and similitude. *Bull. Amer. Math. Soc* **1951,** *57*, 497-499.
64. Ruark, A. E., Inspectional analysis: A method which supplements dimensional analysis. *Journal of the Elisha Mitchell Scientific Society* **1935,** *51* (1), 127-133.
65. Bear, J., Dynamics of fluids in porous media. *Courier Corporation* **2013**.
66. Buckingham, E., On physically similar systems; illustrations of the use of dimensional equations. *Physical review* **1914,** *4* (4), 345.
67. Focken, C. M., Dimensional methods and their applications, *British Journal for the Philosophy of Science* **1955** 5 (20):344-346.
68. Peters, E. J.; Afzal, N.; Gharbi, R., On scaling immiscible displacements in permeable media. *Journal of Petroleum Science and Engineering* **1993,** *9* (3), 183-205.
69. Spies, O. R., Dimensional analysis and theory of models, R*obert E. Krieger publishing company* **1980.**
70. Collins, R. E., Flow of fluids through porous materials, *United States*, **1976**.
71. Greenkorn, R., Flow models and scaling laws for flow through porous media. *Industrial & Engineering Chemistry* **1964,** *56* (3), 32-37.
72. Li, D.; Lake, L. W., Scaling fluid flow through heterogeneous permeable media. *SPE Advanced Technology Series* **1995,** *3* (01), 188-197.
73. Loomis, A. G.; Crowell, D. C., *T*heory and application of dimensional and inspectional analysis to model study of fluid displacements in petroleum reservoirs. *US Department of the Interior, Bureau of Mines* **1964,** Vol. 6546.
74. Nielsen, R. L.; Tek, M., Evaluation of scale-up laws for two-phase flow through porous media. *Society of Petroleum Engineers Journal* **1963,** *3* (02), 164-176.
75. Rapoport, L.; Leas, W., Properties of linear waterfloods. *Journal of Petroleum Technology* **1953,** *5* (05), 139-148.
76. Shook, M.; Li, D.; Lake, L. W., Scaling immiscible flow through permeable media by inspectional analysis. *IN SITU-NEW YORK*- **1992,** *16*, 311-311.
77. Sorbie, K.; Feghi, F.; Pickup, G.; Ringrose, P.; Jensen, J., Flow regimes in miscible displacements in heterogeneous correlated random fields. *SPE Advanced Technology Series* **1994,** *2* (02), 78-87.
78. Waggoner, J.; Castillo, J.; Lake, L. W., Simulation of EOR processes in stochastically generated permeable media. *SPE formation evaluation* **1992,** *7* (02), 173-180.
79. Wygal, R., Construction of models that simulate oil reservoirs. *Society of Petroleum Engineers Journal* **1963,** *3* (04), 281-286.
80. Leverett, M.; Lewis, W.; True, M., Dimensional-model studies of oil-field behavior. *Transactions of the AIME* **1942,** *146* (01), 175-193.
81. Engleberts, W.; Klinkenberg, L. In Laboratory Experiments on the Displacement of Oil by Water From Packs of Granular Materials, *Proc*, **1951**.
82. Asghari, K.; Dong, M.; Shire, J.; Coleridge, T. J.; Nagrampa, J.; Grassick, J., Development of a correlation between performance of CO_2 flooding and the past

performance of waterflooding in Weyburn oil field. *SPE Production & Operations* **2007,** *22* (02), 260-264.
83. Liu, S.; Sahni, V.; Hsu, C.-F. In A novel method of forecasting CO_2 flood performance for various WAG injection schemes by analyzing injection pulses, *SPE Improved Oil Recovery Symposium, Society of Petroleum Engineers* **2014**.
84. Chung, S. H.; Chan, H. K., A two-level genetic algorithm to determine production frequencies for economic lot scheduling problem. *IEEE Transactions on Industrial Electronics* **2011,** *59* (1), 611-619.
85. Tsai, C.-C.; Huang, H.-C.; Chan, C.-K., Parallel elite genetic algorithm and its application to global path planning for autonomous robot navigation. *IEEE Transactions on Industrial Electronics* **2011,** *58* (10), 4813-4821.
86. Zhang, X.; Hu, S.; Chen, D.; Li, X., Fast covariance matching with fuzzy genetic algorithm. *IEEE Transactions on Industrial Informatics* **2011,** *8* (1), 148-157.
87. Varadan, V.; Leung, H., Reconstruction of polynomial systems from noisy time-series measurements using genetic programming. *IEEE Transactions on Industrial Electronics* **2001,** *48* (4), 742-748.
88. Ferreira, C., Function finding and the creation of numerical constants in gene expression programming. In *Advances in soft computing, Springer* **2003**; pp 257-265.
89. Li, X.; Zhou, C.; Xiao, W.; Nelson, P. C. In Prefix gene expression programming, *Proc. Genetic and Evolutionary Computation Conference, Washington, Citeseer* **2005**; pp 25-31.
90. Zuo, J.; Tang, C.; Zhang, T. In Mining predicate association rule by gene expression programming, *International Conference on Web-Age Information Management, Springer* **2002**; pp 92-103.
91. Teodorescu, L.; Sherwood, D., High energy physics event selection with gene expression programming. *Computer Physics Communications* **2008,** *178* (6), 409-419.
92. Gharagheizi, F.; Abbasi, R.; Tirandazi, B., Prediction of Henry's law constant of organic compounds in water from a new group-contribution-based model. *Industrial & engineering chemistry research* **2010,** *49* (20), 10149-10152.
93. Gharagheizi, F.; Eslamimanesh, A.; Mohammadi, A. H.; Richon, D., Determination of critical properties and acentric factors of pure compounds using the artificial neural network group contribution algorithm. *Journal of Chemical & Engineering Data* **2011,** *56* (5), 2460-2476.
94. Hemmati-Sarapardeh, A.; Mahmoudi, B.; Mohammadi, A. H., Experimental measurement and modeling of saturated reservoir oil viscosity. *Korean Journal of Chemical Engineering* **2014,** *31* (7), 1253-1264.
95. Mehrpooya, M.; Gharagheizi, F., A molecular approach for the prediction of sulfur compound solubility parameters. *Phosphorus, Sulfur, and Silicon* **2009,** *185* (1), 204-210.
96. Mohammadi, A. H.; Eslamimanesh, A.; Gharagheizi, F.; Richon, D., A novel method for evaluation of asphaltene precipitation titration data. *Chemical Engineering Science* **2012,** *78*, 181-185.

97. Rafiee-Taghanaki, S.; Arabloo, M.; Chamkalani, A.; Amani, M.; Zargari, M. H.; Adelzadeh, M. R., Implementation of SVM framework to estimate PVT properties of reservoir oil. *Fluid Phase Equilibria* **2013,** *346*, 25-32.
98. Virnovsky, G.; Vatne, K.; Iversen, J.; Signy, C. In Three-phase capillary pressure measurements in centrifuge at reservoir conditions, *International Symposium of the Society of Core Analysts, Abu Dhabi* **2004**, pp 5-9.
99. Zhou, Y.; Helland, J. O.; Hatzignatiou, D. G., Computation of three-phase capillary pressure curves and fluid configurations at mixed-wet conditions in 2D rock images. *SPE Journal* **2016,** *21* (01), 152-169.
100. Neshat, S. S.; Pope, G. A. In Compositional Three-Phase Relative Permeability and Capillary Pressure Models Using Gibbs Free Energy, *SPE Reservoir Simulation Conference, Society of Petroleum Engineers* **2017**.
101. Skjaeveland, S.; Siqveland, L.; Kjosavik, A.; Hammervold, W.; Virnovsky, G. In Capillary pressure correlation for mixed-wet reservoirs, *SPE India Oil and Gas Conference and Exhibition, Society of Petroleum Engineers* **1998**.
102. Lorenzen, T.; Anderson, V., Design of experiments: a no-name approach. *CRC Press* **1993**.
103. Safa, Y.; Bhatti, H. N., Biosorption of Direct Red-31 and Direct Orange-26 dyes by rice husk: Application of factorial design analysis. *Chemical Engineering Research and Design* **2011,** *89* (12), 2566-2574.
104. Antony, J., Training for design of experiments using a catapult. *Quality and reliability engineering international* **2002,** *18* (1), 29-35.
105. C Montgomery, D., Montgomery Design and Analysis of Experiments. *John Wiley* **1997**.
106. George, E.; Hunter, J. S.; Hunter, W. G.; Bins, R.; Kirlin IV, K.; Carroll, D., Statistics for experimenters: design, innovation, and discovery. *Wiley New York, NY*, USA:: **2005**.
107. Chen, Y.; Chen, D.; Khan, S. U.; Huang, J.; Xie, C., Solving symbolic regression problems with uniform design-aided gene expression programming. *The Journal of Supercomputing* **2013,** *66* (3), 1553-1575.
108. https://www.gepsoft.com/, Gepsoft Limited, *A predictive modeling software company located in Portugal* **2020**.
109. Agbalaka, C. C.; Dandekar, A. Y.; Patil, S. L.; Khataniar, S.; Hemsath, J. In The effect of wettability on oil recovery: A review, *SPE Asia Pacific Oil and Gas Conference and Exhibition, Society of Petroleum Engineers* **2008**.
110. Delshad, M.; Bhuyan, D.; Pope, G.; Lake, L. In Effect of capillary number on the residual saturation of a three-phase micellar solution, *SPE Enhanced Oil Recovery Symposium, Society of Petroleum Engineers* **1986**.
111. Bethel, F.; Calhoun, J. C., Capillary desaturation in unconsolidated beads. *Journal of Petroleum Technology* **1953,** *5* (08), 197-202.
112. Chatzis, I.; Morrow, N. R., Correlation of capillary number relationships for sandstone. *Society of Petroleum Engineers Journal* **1984,** *24* (05), 555-562.

113. Saffman, P. G.; Taylor, G. I., The penetration of a fluid into a porous medium or Hele-Shaw cell containing a more viscous liquid. *Proceedings of the Royal Society of London. Series A. Mathematical and Physical Sciences* **1958,** *245* (1242), 312-329.

CHAPTER SEVEN

Summary and Recommendations for Future Work

This study focuses on modeling and simulation of WAG injection process using various tools including mathematical modeling, CFD simulator-COMSOL Multiphysics, smart models such as ANFIS and LSSVM-CSA, and evolutionary algorithm such as GEP. In each phase of this study, a different WAG injection scenario is studied. Numerical modeling and simulation tools are used to investigate the effect of various process and system parameters affecting the efficiency of the WAG processes. This thesis includes seven chapters: Introduction and overview (chapter one), literature review (chapter two), mathematical modeling of near-miscible WAG injection in a homogeneous system (chapter three), CFD simulation of WAG injection in a fractured porous medium (chapter four), using data-driven sub-models such as least square support vector machines (LSSVM) and adaptive neuro-fuzzy inference system (ANFIS) in series with an empirical model (EM) and a first principle model (FPM) of three-phase flow in porous media (chapter five), and applying the dimensional analysis technique to generate dimensionless groups of key parameters to develop a new correlation based on gene expression programming (GEP) algorithm leading to predicting RF of a WAG process (chapter six). The current chapter (chapter 7) includes the summary and recommendations.

7.1 Literature Review (Chapter 2)

Implementation of a new EOR/IOR project requires a comprehensive knowledge of previous successful and failed experiences, and adequate understanding of the technical and non-technical aspects of this recovery process. This knowledge may be derived from reviewing similar projects that were reported in the literature. Despite great applications of WAG injection in hydrocarbon reservoirs and extensive studies, the last comprehensive review goes back to 1998, focusing on the field applications only. There are a few review papers that are more updated; however, they are either dedicated to a particular aspect of WAG (such as CO_2 abnormalities), or applications in a specific geographical region (such as North Sea). An updated comprehensive study, covering recent experiences and lessons that are learnt from previous studies seems to be imperative. This chapter reviews the WAG theory, applications, governing mechanisms of fluid displacement and oil production from pore to field scale, and the most common challenges and operational problems along with the remedies during WAG projects. The effects of important variables such as reservoir properties, fluid properties, and operating conditions on the performance of WAG are studied from experimental, simulation and modeling, and pore-scale investigations. The main findings/conclusions of the first phase are as follows:

- CO_2 is the most common gas used in the WAG operations and it has advantages over N_2 or O_2. The use of high-pressure air has been recently suggested due to its abundance.
- Brine composition and salinity are important parameters in WAG. Low salinity water injection has been recently proposed for the water cycles; although the performance of LSW in waterflooding is proven, its performance in WAG is controversial in the literature.
- Five-spot pattern is found the most common injection pattern employed in the WAG projects. However, it may result in poor volumetric sweep efficiency due to extensive upward gas migration. Horizontal wells may be alternatively used to overcome this problem.
- WAG injection at equal volumes of water and gas cycles (WAG ratio = 1:1) is preferred and results in optimal oil production. However, the WAG ratio does not influence the oil recovery performance in mixed-wet formations.
- The saturation history in individual drainage and imbibition processes, and the chronological cycle history of water and gas injection in the WAG will significantly affect the distribution of fluids in three-phase flow. Mathematical modeling of WAG demands the inclusion of these two types of three-phase hysteresis effects that if accounted, will increase the oil mobility and decrease the gas mobility, resulting in more realistic predictions.
- In both miscible and immiscible WAG recovery processes, an accurate relative permeability model is needed to determine reliable values of fluids distribution and production in the three phase flow in porous media. The relative permeability models become less accurate in near miscible conditions when mass transfer between the two phases occurs. Due to the complexity of the WAG flow pattern, the classical techniques to obtain relative permeability may not be efficient.
- Wettability significantly controls the performance of WAG process. Optimal values of injection rate, WAG ratio, number of cycles, brine salinity and polymer additive concentration will be significantly affected by the wettability.
- Tapering (WAG ratio variation) is a potential strategy to control excessive gas production. It also reduces the response time and accelerates the oil bank, reaching the production wells.

- The most common challenges in WAG operation are early gas breakthrough, injectivity loss, corrosion, and the potential for asphaltene and hydration formation. The potential solutions for those problems originated by the adverse mobility ratio include hybrid gel treatment, viscosity reduction WAG (VR-WAG), and polymer additives in water.

7.2 Numerical and Analytical Modeling of WAG Injections in Homogeneous System in Near-Miscible Condition (Chapter 3, 5, and 6)

The main objective of this phase of the thesis is to study the three-phase flow modeling of near-miscible WAG process for EOR implication, using implicit pressure explicit saturation (IMPES) method. The mathematical model simulates a WAG case study in a strongly water-wet Berea core, using synthetic oil and brine at 38 ˚C and 12.7 MPa. Three cycles of water and gas injections are used in the WAG operation. The recovery data from our mathematical model is in excellent agreement with the experimental data of near-miscible WAG process. The absolute relative error is less than 1.7% while estimating the ultimate recovery factor of the oil in WF and GI stages of all three cycles. We also study the effects of main variables such as injection rate, WAG ratio, slug size (PV) injection, crude oil viscosity, and core absolute permeability on the WAG performance are studied. By changing the WAG ratio in the model from 0.5 to 1 and to 2, it is noticed that the optimal operating condition is achieved at the WAG ratio of 1. The results also show that a higher absolute permeability increases the production rate, while the ultimate recovery of the system does not alter remarkably. For the same system, we also employ data-driven sub-models, including least square support vector machine (LSSVM) and adaptive neuro-fuzzy inference system (ANFIS) in series with an empirical model (EM) and a first principle model (FPM) to study three-phase flow in porous media. The LSSVM and ANFIS sub-models predict the two-phase water-oil, gas-oil, and gas-water relative permeabilities. The outputs from these models are supplied to the empirical models (EMs) to estimate the three-phase relative permeabilities for oil, gas, and water phases. Among the proposed hybrid models, the LSSVM-EM-FPM model significantly removes the non-linearity of the two-phase relative permeabilities. The absolute maximum error in estimating the ultimate oil RF is 1.7%, 2.5%, and 11.4% for the EM-FPM, LSSVM-EM-FPM, and ANFIS-EM-FPM hybrid models in the testing phase, respectively.

Forecasting WAG flooding performance using fast and robust models is important to obtain a better understanding of the WAG process, optimize the operational condition, and lower capital and operating costs at laboratory to field scales. In the last phase of this thesis, we introduce a

novel correlation to predict the performance of near-miscible WAG injection and develop an accurate model using gene expression programming (GEP) technique. Based on the error analysis, the GEP-based correlation is able to generate the target values with high accuracy. For instance, the training step leads to R^2= 92.85 % and *MSE*=1.38e-3, while R^2= 91.93 % and *MSE*=4.30e-3 are obtained for the testing phase.

7.3 CFD Simulation of Immiscible WAG Injection in a Fractured Porous Medium (Chapter 4)

The implementation of WAG injection in NFRs features inherent complexities not only related to the three-phase flow, saturation history, and cycle-dependent hysteresis of the individual phases, but also the fracture-matrix communication, fingering and early breakthrough of injecting phases in system and fracture medium specially during gas injection processes. Moreover, the experimental evaluation of WAG injection in a fractured system is expensive and time-consuming, if not impractical. This research phase provides details on the computational fluid dynamic (CFD) simulation of WAG injection in a fractured system. We evaluate the impacts of hysteresis, fracture characteristics (aperture, orientation, and fracture density in the network), and the three-phase relative permeability of phases during the WAG injection using a CFD modeling approach. The model simulates an immiscible WAG injection and the modeling results are compared to the experimental data in a strong water-wet sand-pack. Similar to the experiments, we simulate Maroon crude as the oil phase, and synthetic brine, and pure CO_2 at 100^{o}C and atmospheric pressure. The results from our model are in excellent agreement with the experimental data. The absolute relative error is less than 12 % for estimating the ultimate oil recovery factors (*RF*) in water flooding (WF) and gas injection (GI) cycles. The main outcomes of this simulation study are as follows:

- During the water flooding cycles, the mobility of water and oil in the matrix dominates the overall fluid mobility while in the gas injection cycles, the mobility of the gas and oil in the fracture dominates overall fluid mobility.
- The hysteresis effects result in higher ultimate oil recovery after 2.5 PVI. With and without hysteresis, the ultimate oil recovery factor values are 0.53 and 0.49 HCPV fraction, respectively.

- The hysteresis effects are mostly due to the gas trapping in the larger pores (such as those in fracture).
- Having a vertical fracture connected to a horizontal fracture in the system enhances the oil recovery through improving the matrix-fracture flow communication.
- Increasing the fracture aperture in the case in which the fracture is a high permeable porous medium leads to an increase in oil recovery at a fixed slug size and PVI.
- Increasing the fracture aperture increases the recovery factor and recovery rate of the oil phase. However, at later cycles, the early gas breakthrough reduces the incremental recovery.
- Fracture inclination angle does not remarkably change the ultimate *RF*; by changing the inclination angle from 30^{o} to 90^{o}, the *RF* is increased only by 2%.
- Including the gravity forces in vertical systems causes an overall improvement in *RF* through engaging both matrix and fracture media in all cycles. It increases the *RF* by 9%, compared to the horizontal model where no gravity force is applied to the system.
- As the permeability contrast between matrix and fracture media decreases, the flow communication between the two regions increases and improves the recovery performance of the WAG process.
- Lowering the IFT between phases significantly increases the oil recovery by providing more contact between phases.
- At a WAG ratio of 1, the highest oil recovery is obtained, while by lowering the WAG ratio, the fluid front is not stable, and less oil is recovered from the system.

Overall Main Outcomes of the Study:

- A comprehensive literature review study covers the application of the WAG injection at various scales and scenarios.
- The proposed mathematical model can accurately simulate three cycles of near-miscible WAG injection in a strongly water-wet system.
- Sensitivity analysis is conducted to further understand effect of WAG ratio, fluid and rock properties, and process conditions on WAG performance.
- The CFD model is able to successfully simulate the WAG injection in a fractured medium.

- The impact of hysteresis on the performance of WAG injection in a fractured system is highly significant.
- Gravity drainage mechanism is dominant over production from NFRs under WAG injection.
- The LSSVM exhibits better performance in predicting ultimate RF.
- The GEP model shows a very good match with the target data and successfully predicts the intermediate cycles RF and the final RF with the relative error of 3.48 %.

7.4 Recommendations for Future Work

The following suggestions and recommendations are given for future studies:

- The effect of the gravity on WAG recovery performance and mechanisms in homogeneous and heterogeneous porous systems can be studied.
- The influence of other wettability states (e.g., oil-wet and/or water-wet) on recovery of near-miscible WAG injection processes in porous media with various characteristics can be investigated.
- We recommend conducting further experimental and modeling studies on WAG in fractured media at the near-miscible and miscible conditions where broad thermodynamic conditions and fracture properties are examined.
- It would be also interesting if the WAG process is implemented for underground remediation to clean soil and water from oil spills and contaminations through both laboratory and modeling phases.
- It is believed that pore scale modeling and lattice Boltzmann simulation studies can help us to further understand the oil recovery and fluid displacement mechanisms over WAG operation.
- Investigation of mass transfer and fluid phase equilibria during WAG process can show better the component exchange between the phases, particularly while dealing with gas mixture. This will provide more effective tips and guidelines for design and operation of WAG processes.
- We also recommend using heterogeneous porous systems in terms of both wettability and permeability with various distributions in experimental and modeling WAG studies.

Appendix A

Governing Equations and Correlations Used in This Study.

Three-phase capillary pressure correlation used in this study proposed by Neshat et al.:

$$p_{co\alpha,m} = \sigma_{o\alpha} co\, s(\theta_{o\alpha}) \sqrt{\frac{\phi}{K}} \times \left[\frac{c_o}{\left(\frac{s_o - s_{or}}{1 - s_{or}}\right)^{a_o}} + \frac{c_\alpha}{\left(\frac{s_\alpha - s_{\alpha r}}{1 - s_{\alpha r}}\right)^{a_\alpha}} \right] \qquad \alpha \in \{w, g\} \tag{A- 1}$$

where $p_{co\alpha,m}$ is the three-phase capillary pressure between phase oil (o) and phase α (w or g); the subscript m refers to the matrix domain; $\sigma_{o\alpha}$ and $\theta_{o\alpha}$ are the interfacial tension and contact angle between phases o and α, respectively; c_o and c_α are the entry capillary pressure for the phases o and α, respectively; s stands for the phase saturation; and a_o and a_α symbolize the capillary exponent of phase oil and phase α, respectively [1].

Three-phase relative permeability model proposed by Shahverdi et *al.* [2].

$$k_{ro,m}^{3ph}(s_w, s_g) = \frac{\overline{s_o}}{(1-\overline{s_g})(1-\overline{s_w})} [k_{row} k_{rwg} + k_{rog} k_{rgw}] \tag{A- 2}$$

$$k_{rw,m}^{3ph}(s_o, s_g) = \frac{\overline{s_w}}{(1-\overline{s_g})(1-\overline{s_o})}[k_{rwo}k_{rog} + k_{rwg}k_{rgo}] \quad \text{(A- 3)}$$

$$k_{rg,m}^{3ph}(s_w, s_o) = \frac{\overline{s_g}}{(1-\overline{s_o})(1-\overline{s_w})}[k_{rgo}k_{row} + k_{rgw}k_{rwo}] \quad \text{(A- 4)}$$

where $k_{r\,\alpha\beta,m}$ is the two-phase relative permeability of phase α in the presence of phase β in the matrix; and $\overline{s_\alpha}$ introduces the normalized saturation of phase α that depends on the flow direction (imbibition/drainage) and the initial state of the grid block, as given below [3]:

$$\overline{s_\alpha} = \frac{s_\alpha - s_\alpha^*}{1-s_w^*-s_o^*-s_g^*} \qquad \alpha \in \{o, w, g\} \quad \text{(A- 5)}$$

In Eq. (A- 5), the s_α^* values are defined based on different injection fluid scenarios, as listed in Table Table ***0***.

Table 0: The parameters used in the three-phase relative permeability model in matrix medium.

Three-phase relative permeability	Model parameters	WAG injection cycle		
		Gas	Oil	Water
$k_{rg,m}^{3ph}$	s_g^*	s_g^{start}	s_{gt}	s_{gt}
	s_w^*	s_{wc}	s_{wc}	s_w^{start}
	s_o^*	0	s_o^{start}	s_{ot}
$k_{ro,m}^{3ph}$	s_g^*	0	s_{gt}	s_{gt}
	s_w^*	s_{wc}	s_{wc}	s_w^{start}
	s_o^*	s_{org}	s_o^{start}	s_{ot}
$k_{rw,m}^{3ph}$	s_g^*	0	0	0
	s_w^*	s_{wc}	s_{wc}	s_{wc}
	s_o^*	0	0	0

In Table ***0***, s_{α}^{start} is the saturation of phase α at the beginning of phase α injection process; and s_{gt} and s_{ot} denote the trapped/residual saturations of gas and oil, respectively. Eqs. (A- 2)-(A- 5) are used for the matrix domain.

-Three-phase relative permeability correlations in the fracture medium:

$$k_{rw,f}^{3ph} = \frac{{s_w}^3}{2}(3 - s_w) \tag{A- 6}$$

$$k_{rg,f}^{3ph} = {s_g}^2\left({s_g}^2 + \frac{\mu_g}{\mu_w}\left(3s_w - \frac{3}{2}{s_w}^2\right) + \frac{\mu_g}{\mu_o}\left(3s_g s_o + \frac{3}{2}{s_o}^2\right)\right) \tag{A- 7}$$

$$k_{ro,f}^{3ph} = {s_o}^2\left({s_o}^2 + \frac{\mu_o}{\mu_w}\left(3s_w - \frac{3}{2}{s_w}^2\right) + \frac{3}{2}s_g s_o\right) \tag{A- 8}$$

where $k_{r\alpha,f}^{3ph}$ is the three-phase relative permeability of phase α (i.e. oil, water, and gas) in the fracture domain; s_α is the saturation of phase α; and μ_α resembles the viscosity of phase α in the fracture.

According to the Brooks and Corey model, the capillary pressure of the phase oil-α reads as:

$$p_{co\alpha,f} = p_{d\alpha}(s_{e\alpha})^{-\frac{1}{\lambda}} \qquad \alpha \in \{w, g\} \tag{A- 9}$$

$$s_{e\alpha} = \frac{s_\alpha - s_{r\alpha}}{1 - s_{r\alpha}} \qquad \alpha \in \{w, g\} \tag{A- 10}$$

where $p_{d\alpha}$ denotes the entry capillary pressure of phase α, which is the minimum pressure for the non-wetting phase to displace the wetting phase from the largest pore accessible. The parameter λ is a measure of pore size distribution and describes the uniformity of the sand particles; and $s_{r\alpha}$ represents the residual saturation of the wetting phase α.

Two-phase relative permeability correlation proposed by Hirasaki [4]:

$$k_{rw} = k_{rw}^0 S_D^{n_w} \tag{A- 11}$$

$$k_{rnw} = k_{rnw}^0 (1 - S_D)^{n_{nw}} \tag{A- 12}$$

$$S_D = \frac{s_w - s_{wi}}{1 - s_{wi} - s_{nwr}} \tag{A- 13}$$

where the k_{rw} and k_{rnw} are the two-phase relative permeabilities of the wetting phase and non-wetting phase, respectively. The k_{rw}^0 and k_{rnw}^0, are the end point relative permeability values of

the wetting and non-wetting phases, respectively. The n_w, and n_{nw} are the wetting phase and non-wetting phase exponents, respectively.

Mualem's model (Eqs. (A-14)-(A-16)), which is a modified version of Van Genuchten model:

$$k_{rw}(s_w) = \overline{s_w}^{0.5}\left(1-\left(1-\overline{s_w}^{\frac{1}{m}}\right)^{m}\right)^{2} \tag{A-14}$$

$$k_{rn}(s_n) = \overline{s_n}^{\frac{1}{3}}\left(1-\left(1-\overline{s_n}^{\frac{1}{m}}\right)\right)^{2m} \tag{A-15}$$

$$\overline{s_\alpha} = \frac{s_\alpha - s_{\alpha r}}{1-\sum_\alpha s_{\alpha r}} \tag{A-16}$$

where the subscription *w* denotes the wetting phase; *n* refers to the non-wetting phase; $s_{\alpha r}$ symbolizes the residual saturation of the phase α; k_{rn} and k_{rw} denotes the two-phase relative permeability of the non-wet and wetting phase, respectively; and *m* is the model parameter which is obtained through optimization.The endpoint relative permeability and relative permeability exponents of both wetting phase and non-wetting phase for all three systems i.e. oil-water, water-gas, and oil-gas systems are tuned using the experimental data from literature and using the Pattern search optimization technique.

References

1. Neshat, S. S.; Pope, G. A. In *Compositional Three-Phase Relative Permeability and Capillary Pressure Models Using Gibbs Free Energy*, SPE Reservoir Simulation Conference, Society of Petroleum Engineers: 2017.
2. Shahverdi, H.; Sohrabi, M. In *Three-phase relative permeability and hystresis model for simulation of water alternating gas (WAG) injection*, SPE Improved Oil Recovery Symposium, Society of Petroleum Engineers: 2012.
3. Shahverdi, H.; Sohrabi, M., An improved three-phase relative permeability and hysteresis model for the simulation of a water-alternating-gas injection. *Spe Journal* **2013,** *18* (05), 841-850.
4. Hirasaki, G. J., Sensitivity coefficients for history matching oil displacement processes. *Society of Petroleum Engineers Journal* **1975,** *15* (01), 39-49.